MATHEMATICAL MODELS FOR HEAT TRANSFER IN HUMAN BODY

A THESIS SUBMITTED TO THE

CENTRAL DEPARTMENT OF MATHEMATICS
INSTITUTE OF SCIENCE AND TECHNOLOGY
TRIBHUVAN UNIVERSITY
NEPAL

FOR THE AWARD OF
DOCTOR OF PHILOSOPHY
IN MATHEMATICS

BY

KABITA LUITEL

DECEMBER 2022

MATHEMATICAL MODELS FOR HEAT TRASNFER IN HUMAN BODY

A THESIS SUBMITTED TO THE

CENTRAL DEPARTMENT OF MATHEMATICS
INSTITUTE OF SCIENCE AND TECHNOLOGY
TRIBHUVAN UNIVERSITY
NEPAL

FOR THE AWARD OF
DOCTOR OF PHILOSOPHY
IN MATHEMATICS

BY

KABITA LUITEL

DECEMBER 2022

EXTERNAL EXAMINERS

The Title of Ph.D. Thesis: " Mathematical Models for Heat Transfer in Human Body"

Name of Candidate: Mrs. Kabita Luitel

External Examiners:

(1) Prof. Dr. Jivandhar Jnawali
     Ratna Rajyalaxmi Campus
     Tribhuvan University, NEPAL

(2) Prof. Dr. Kapil Sharma
     South Asian University
     New Delhi, INDIA

(3) Prof. Dr. Frederique Drullion
     Department of Mathematics
     Embry-Riddle Aeronautical University
     Florida, USA

June 14, 2023

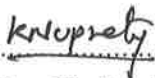(Dr. Surendra Kumar Gautam)
Asst. Dean

DECLARATION

Thesis entitled "**Mathematical Models for Heat Transfer in Human Body**" which is being submitted to the Central Department of Mathematics, Institute of Science and Technology (IOST), Tribhuvan University, Nepal for the award of the degree of Doctor of Philosophy (Ph.D.), is a research work carried out by me under the supervision of Prof. Dr. Kedar Nath Uprety, Central Department of Mathematics, Tribhuvan University, Nepal and co-supervised by Prof. Dr. Harihar Khanal, Department of Mathematics, Embry-Riddle Aeronautical University, Daytona Beach, Florida, USA and Prof. Dr. Dil Bahadur Gurung, Department of Mathematics, Kathmandu University, Kavre, Dhulikhel, Nepal. This research is original and has not been submitted earlier in part or full in this or any other form to any university or institute, here or elsewhere, for the award of any degree.

Kabita Luitel

i

RECOMMENDATION

This is to recommend that **Kabita Luitel** has carried out research entitled "**Mathematical Models for Heat Transfer in Human Body**" for the award of Doctor of Philosophy (Ph.D.) in **Mathematics** under my supervision and the co-supervision of Prof. Dr. Harihar Khanal and Prof. Dr. Dil Bahadur Gurung. To our knowledge, this work has not been submitted for any other degree. She has fulfilled all the requirements laid down by the Institute of Science and Technology (IOST), Tribhuvan University, Kirtipur for the submission of the thesis for the award of Ph.D. degree.

Prof. Dr. Kedar Nath Uprety
Supervisor
Central Department of Mathematics,
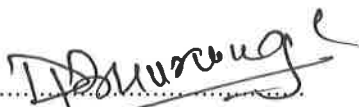**Tribhuvan University, Kirtipur, Kathmandu, Nepal**

Prof. Dr. Harihar Khanal
Co-Supervisor
Department of Mathematics,
Embry-Riddle Aeronautical University, Daytona Beach, Florida, USA

Prof. Dr. Dil Bahadur Gurung
Co-Supervisor
Department of Mathematics,
Kathmandu University, Kavre, Dhulikhel, Nepal

December, 2022

TRIBHUVAN UNIVERSITY
CENTRAL DEPARTMENT OF MATHEMATICS
OFFICE OF THE HEAD OF DEPARTMENT

KIRTIPUR, KATHMANDU
NEPAL

Date: Dec 29, 2022

Ref

Letter of Approval

On the recommendation of Supervisor **Prof. Dr. Kedar Nath Uprety**, Co-Supervisors **Prof.Dr. Harihar Khanal and Prof.Dr. Dil Bahadur Gurung,** this Ph.D. thesis submitted by **Mrs. Kabita Luitel**, entitled **"Mathematical Models for Heat Transfer in Human Body"** is forwarded by Central Department Research Committee (CDRC) to the Dean, IOST, T.U.

Dr. Tanka Nath Dhamala
Professor,
Head,
Central Department of Mathematics
Tribhuvan University
Kirtipur, Kathmandu
Nepal

ACKNOWLEDGEMENTS

ABSTRACT

The work is focused on human thermal comfort, which depends not only on physical, biological, and environmental heat transfer mechanisms but also on clothing parameters. In excessively hot or cold climatic conditions, the physiological imbalance and overall human thermal comfort can be maintained through the proper management of well-designed protective clothing. We have developed both linear and nonlinear mathematical models for heat transfer in the human body. For the linear case, Pennes' model is extended incorporating clothing thermal conductivity, the thickness of cloth, and clothing area factors. The extended model attempted to use the interface condition between the human body and cloth. The usual Robin's boundary condition is modified by incorporating effective clothing area factor and convective heat transfer coefficient as two important factors. Where the effective clothing area factor includes clothing insulation, air insulation, and clothing area factor. The convective heat transfer coefficient includes air velocity and the walking speed of a person. The interface between two non-homogeneous materials and the radiation-induced nonlinearity in Robin's boundary condition makes the problem difficult and intricate to solve analytically even in a simple geometry except for the steady state case. As such, we investigated the thermal responses of clothing insulation, air velocity and walking speed, metabolic and sweating effect, using numerical methods to the extended transient model and in varying spatial dimensions in cylindrical coordinates: one-dimensional radial, two-dimensional axisymmetric, and three-dimensional. First, we solved the one-dimensional model in radial direction numerically employing an implicit finite difference method. Solvability, consistency, stability, and convergence of the numerical scheme are established. Numerical simulation results exhibited that the light garment system would be comfortable and easy for sweat drainage. To address more realistic problems of finding both radial and longitudinal variations of the temperature profile in human limbs, we extended our model to two-dimensional axisymmetric case with time-dependent metabolism, temperature-dependent sweating, and clothing effects during physical exercise. In the radial direction, the numerical simulation results agree with the one-dimensional model whereas in the longitudinal direction there seem no remarkable variations observed which were also expected as the ratio of radial and axial length scales are significantly different. Finally, we further extended the model to three-dimension with temperature-dependent thermophysical parameters to address non-symmetric temperature variations in the abnormal tissue. The simulated results using Finite Volume (FV) energy conservation techniques

showed the nonlinear behavior of temperature in an abnormal tissue with an initial high temperature. Numerical tests with different lateral boundary conditions exhibit some non-symmetric variations in temperature in the cross-section. Various simulations for the axisymmetric model in (r, z)-direction were performed with zero flux at the inner, bottom, and top of the limb and Robin's boundary condition at the lateral surface to reveal an axially symmetric temperature profile. While implementing Robin's boundary condition at the top and the lateral surface of the limb, non-symmetric temperature variation in the skin surface and the top of the longitudinal cross-sectional slice is obtained. Additionally, numerical experiments have shown that various coefficients of temperature-dependent parameters, thermal conductivity $K(T)$, metabolic heat generation $q_m(T)$, and blood perfusion $w_b(T)$, are directly proportional to the temperature of abnormal tissue.

LIST OF ABBREVIATIONS

1D , 2D, 3D	One-dimension, Two–dimension, Three–dimension
e.g.	For Example
et al.	And others
etc.	And so on
i.e.	That is
n.d	Nondimensional
ANSI	American National Stansards Institute
ASHRAE	American Society of Heating, Refrigerating and Air-Conditioning Engineers
ISO	International Organization for Standardization
PDE	Partial Differencial Equation
CFL	Courant–Friedrichs–Lewy
CN	Crank–Nicolson
exp	Expontial
FD	Finite Difference
FV	Finite Volume
W	Watt
sec	Second
min	Minute
max	Maximum

LIST OF SYMBOLS

A	cross-sectional area
K	thermal conductivity
A_{cl}	clothing surface area
K_{cl}	thermal conductivity of clothing
K_t	thermal conductivity of tissue
I_{cl}	clothing insulation
I_a	air insulation
I_T	total insulation
δx	thickness or length
ΔT	temperature difference
∇T	temperature gradient
T_t	tissue temperature
T_{cl}	temperature of cloth surface
T_{sk}	temperature of skin surface
f_{cl}	clothing area factor
F_{cl}	effective clothing area factor
T_s	surface temperature
h_{conv}	convective heat transfer coefficient
T_∞	ambient temperature
E	rate of sweat evaporation
E_{sk}	sweat evaporation at skin
$\widetilde{E}$	error vector
L_v	latent heat of vaporization
T_a	arterial temperature

T_v	temperature of venule blood
c_b	specific heat of blood
w_b	blood perfusion rate
A_D	nude body surface area (Dubois surface area)
w	weight (mass) of the body
h	height of the body
q_m	metabolic heat generation per unit volume
q_b	basal metabolic rate
q_A	activity threshold metabolism
q_e	external heating source
t_m	sigmois midpoint
α_c	activity control parameter per unit time
m	mass
c	specific heat
$P_{w,air}$	vapor pressure of air
h_r	radiative heat transfer coefficient
h_c	combined heat transfer coefficient due to convection and radiation
h_A	heat transfer coefficient due to convection, radiation and clothing
$\tilde{r}$	dimensionless radial length
$\tilde{T}$	dimensionless temperature
$\tilde{M}$	dimensionless perfusion term
$\tilde{S}$	dimensionless source term
$\tilde{h}$	dimensionless heat transfer coefficient
Δr	radial distance between two gride points
Δt	temporal thickness
$\tilde{N}$	dimensionless evaporative term
M_t	metabolic rate per unit area
V_{air}	total relative air velocity
v_a	air velocity
W_s	walking speed
$\square$	completion of the proof of theorem

Greek Symbols

ρ	density
ρ_t	density of tissue
ρ_b	blood density
ρ_c	density of cloth
α	thermal diffusivity
α_c	activity control parameter per unit time
λ_l	eigenvalues
σ	proportionality constant
ϵ	emissivity
η	unit outward pointing normal vector
θ	weighted average
ϕ_a	arterial blood flow per unit volume
ϕ_v	venule blood flow per unit volume
Φ	flow rate
ϑ	increment in time period
τ	truncation error
$\mathcal{O}$	order of truncation error
Ω_L	computational domain
∇	gradient

LIST OF TABLES

LIST OF FIGURES

TABLE OF CONTENTS

CHAPTER 1

INTRODUCTION

The principles of heat transfer are the fundamental properties widely used in many fields of science and engineering. Biological and therapeutic aspects of the linear and nonlinear bioheat transfer equations have led the subject into one of the most diverse and emerging areas of mathematics in the twenty-first century. Many problems related to heat and mass transfer such as blood flow within the vessels, heat transfer through clothes, and their mathematical treatment for linear and nonlinear situations governed by a partial differential equation with appropriate initial and boundary conditions is combined and performed for a realistic numerical solution to the bioheat transfer models.

The study of heat transfer in the human body is one of the deserving areas of research for biomedical researchers, environmental scientists, and clothing designers as well. A human body with a complex vascular structure has multiple features of physical and physiological behaviors. Different environmental conditions as well as the body's personal heat transfer mechanisms are responsible for keeping the person in a comfort zone with an equilibrium core temperature, 37°C, within a narrow range (±0.6°C). Additionally, clothing protects the body from extreme climatic conditions and physical exercise helps maintain the person physically fit and healthy [38, 74]. Besides, some climatic factors such as air temperature, air movement, humidity in the air, and radiant heat are the basic components of the thermal environment. Thermal comfort not only relies upon how an individual responds to those climatic factors but also is affected by medication, the health condition of a person, the quantity of alcohol used, the level of physical activity and metabolic power of the person, and the types of clothes worn by an individual. It is a tedious to comprise all these factors and develop a new model for thermal comfort.

Clothes, the mediator between the human body and the environment, act as a cor-

nerstone in the study of human thermal comfort in the field of heat transfer in living organs. The presence of clothing, indeed, makes a vital difference in that system and the thermal comfort of living entities. Therefore, the thermal performance of clothing for human comfort has appeared as the center of research excellence in current years emphasizing the extension of existing Pennes' bioheat transfer model in the human body including the protective layer.

Because of the interface between two non-homogeneous matters-skin surface and cloth-having different physical and physiological behaviors, the complex radiation-induced nonlinearity in Robin's boundary condition makes not only the problem more challenging but also rear to handle it analytically. The numerical technique is a key building block for many current and upcoming computational efforts since it is the primary approach for solving partial differential equations of complexity in biological systems. These computational approaches may, therefore, be the best ways to avoid such complexity, and still have a great interest in the field of clothing science, textile industries, biological research as well as hyperthermia treatment of cancer in the medical field.

1.1 Motivation and Context

Human body physiology is the study of the functioning of the organisms in the human body. The two most crucial physiological components for human thermoregulation are blood flow and metabolism. Perfusion is the process of delivery of arterial and venous blood to a capillary in intricate vascular anatomy the biological tissue especially, human body which is crucial for the transportation of oxygen and nutrients throughout all organs and tissues. The volumetric blood flow per tissue with enough capillaries varies widely and is dependent on processes such as mass transfer to sustain metabolism, systemic blood pressure regulation, and heat transfer for thermoregulation. Depending on the temperature of the nearby tissues, blood can either be a sink or a source. Blood is typically sent from the heart to the body's remaining warm parts throughout the winter. Additionally, blood flow can help keep the body's internal organs warmer and cooler areas at a comfortable temperature. Individual differences exist in metabolism, which varies in response to physical activities such as cleaning, running, swimming, etc. In addition, as the body's metabolism speeds up during exercise, the temperature rises as activity duration lengthens. In such a situation, the person's metabolism speeds up, raising the tissue temperature close to the core. Due to the vapor pressure of the water on the skin and the air, sweating

starts, and the temperature at the skin's surface drops after a while. Moreover, in unusual circumstances, external heating devices might reduce the effectiveness of the treatment by causing cold tracks in the tissue during hyperthermia therapy for cancer or tumors at a point of increased tissue temperature of nearly 45°C. It is necessary to keep in mind that the primary goals of the study of thermal comfort are: firstly, physiological and physical heat transfer mechanism the body uses to maintain a stable internal temperature, and secondly, an equally important component is to learn how to safeguard the body against harmful surroundings and minor skin-surface wounds.

The consequence of wearing suitable clothing can be a significant impact on overall thermal comfort, keeping a person fully satisfied with the environment together with his/her equilibrium core temperature. Pennes' developed the experimental-based model incorporating the blood perfusion term in heat balance equation for the nude human forearm [93]. As the human being always appears with clothing, without including the effect of clothes does not provide an accurate result for perfecting human thermal comfort. The abnormal condition of a person due to the fluctuation of body temperature in extreme cold or hot climatic conditions can only be overcome by wearing sufficient clothing in winter and only light cloth in summer. When a person feels fully comfortable in his/her workplace, he/she can properly devote and concentrate to work and is able to do better performance.

This research work focuses not only on the extension of the model by adding the clothing parameters in the existing Pennes' model but also redefines the usual Robin's boundary condition by incorporating the insulation of air, insulation of cloth, clothing area factors as well as time-dependent metabolism, temperature-dependent sweating and the clothing parameters taken into consideration, which are lacking contexts in the models previously developed by Pennes' and other researchers in literatures [3, 8, 52, 64, 77, 78, 99, 102, 109, 122]. On the other hand, the presence of clothing is important for preserving thermal comfort at the equilibrium between body heat generation and heat loss. Clothing acts as an insulator and a medium for heat transfer from the body to the world outside of us. It is the interface between the surface of the skin and the environment. The main determinants of thermal comfort can be divided into two categories: human characteristics and environmental influences.

The change in metabolic rate because of several other factors, including age, sex, and health, is what determines thermal comfort. In addition, clothing is a significant aspect that influences thermal comfort. Small adjustments in the layers of clothing can make a significant difference in thermal comfort. Wearing a sweater and socks for

example, during the winter months improves comfort, whereas wearing light clothing during the summer months improves comfort at work. The environmental elements that contribute to thermal comfort by maintaining a comfortable environment in the room include air temperature, moving air, radiant temperature, and relative humidity correspondingly. Depending on the fabric's structure, the radiation heat flux passes through the fabric entirely at a particular depth, whereas the convection phenomenon of the heat source does not. Suitable management of personal factors along with these environmental influences provide better comfort at home, workplace (business, office, study rooms etc).

The capacity of analyzing various types of bioheat transfer processes has been pursuaded with the development of advanced computational techniques for complex mathematical models. Though many researchers [59, 125] utilized modern computing power solving, complicated mathematical problems, and studies focusing on thermal comfort and clothing system are not sufficient. Because of the adjustment which depends upon the energy exchange with body-environment, physiological, emotional, cultural, and social aspects of people makes cumbersome to evaluate thermal comfort. It is customarily important to have a deep understanding of heat transfer in the human body and the effect of clothing properties on the perceptivity of thermoregulatory and physiological conditions of a person with full satisfaction to the thermal environment.

Clothing is a key factor that plays a crucial role in the thermal capacity of the body to protect from external injury and to adapt to this thermal environment. So, a thermal model with protective clothing is needed to predict the temperature in a biological tissue together with a clothing layer. Despite the fact that numerous experiments on heat transfer related to clothing and fabric materials have been conducted in a well-equipped lab, the main internal physiological factor, the blood perfusion terms; has yet to be integrated into these models [28, 30, 46, 47, 48, 49, 54, 55, 85]. Therefore, a novel approach to minimize a remarkable gap in Pennes' model as well as clothing thermal comfort models, is the mathematical model for heat transport in the human body in conjunction with protective layer. Furthermore, the proposed two-dimensional axisymmetric bioheat transfer model in the human anatomic system with the basic physiological properties of the tissue material as well as time-dependent metabolism, temperature-dependent sweating, and the clothing parameters have to be taken into account. Finally, three-dimensional nonlinear (temperature-dependent thermophysical parameter) model with volumetric external heating source has been

develoed through which the temperature profiles in an abnormal tissue organ is observed in radial, r-direction, axial, z-derection, axisymmetric, (r, z)-direction, and angular symmetric, (r, θ)-direction. These models may be applicable in aerospace, textile industries, metrology, clinical, and biomedical fields.

1.2 Heat Transfer in Human Body

The area of biomedical science that examines the discoveries of the rate of energy transmission in the human body is known as heat transfer. Due to temperature differences, heat and energy can be transferred from one system to another. It moves from a medium with a higher temperature to one with a lower temperature until both have the same temperature. Humans have a core temperature of 37°C. This core temperature if rises up to $\geq$ 42°C and drop down to $\leq$ 27°C, might cause thermal damage. So, it is important to maintain a body temperature closely 37°C ($\pm$ 0.6°C). In addition to using clothing, the body continuously releases heat through metabolic processes, convection, radiation, respiration, and evaporation [38, 42, 78, 69].

The presence of a temperature difference, the basic requirement of heat transfer mechanism of normal clothed body can be seen in Figure 1.1.
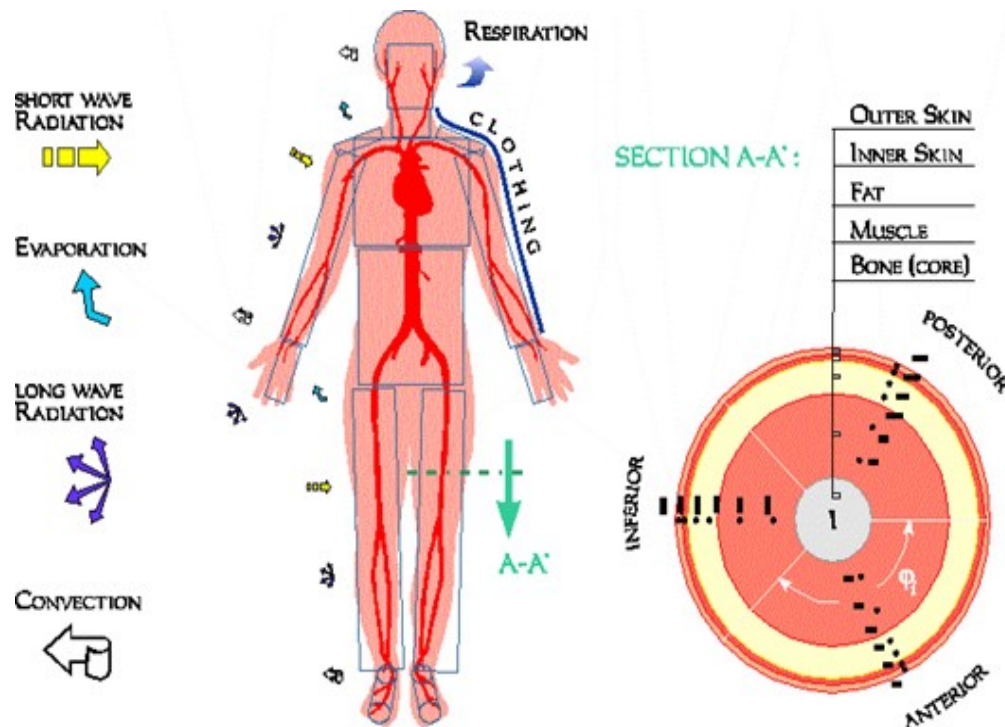
Figure 1.1: Heat transfer mechanisms [Havenith] [46].

1.2.1 Thermoregulation and Human Physiology

The discipline of human body physiology researches the operations of the human body organism. It involves the complicated heat transfer process brought on various mutually reinforcing phenomena, including the respiratory system, the thermoregulatory system, and the sense systems: the eye, receptor for sight, the ear, receptor for sound, and the skin, receptor for the sense. The human body has an extremely intelligent thermoregulatory system that uses thermo-receptors, which activate in response to too-hot or too-cold weather, to maintain a heat-balanced condition with a normal body core temperature [42]. In extreme climatic conditions, two cases might occur,

1. In an extremely hot atmosphere, the core temperature will be maintained at 37°C if enough heat is transferred from the body to the environment through perspiration. When the body's temperature rises above the thermo-neutral zone, which is around 38°C in a hot climate [42], the body emits more heat into the atmosphere. Most of the mechanisms only result in perspiration, which may be comfortably managed provided sweat can be adequately drained. Furthermore, blood vessels expand when the body's core temperature rises, increasing the volume of blood that reaches the skin and promoting heat loss from the body. The body will produce more heat for heat liberation and an increase in core temperature that results in hyperthermia (beyond 41°C) if the heat loss is insufficient.

2. In a very cold environment, if the body's heat is continuously released, the core temperature falls, and as a consequence it causes hypothermia in which heat loss continues and the temperature steadily declines until it reaches $\leq 32°C$. If the temperature falls below $\leq 27°C$, the person loses consciousness, and the heart stops beating [42]. People can, however, be brought back to awareness by rewarming, even from the shallow core temperature if they can prepare properly by wrapping themselves in a suitable warm cloth.

The human thermoregulatory system is depicted in Figure 1.2
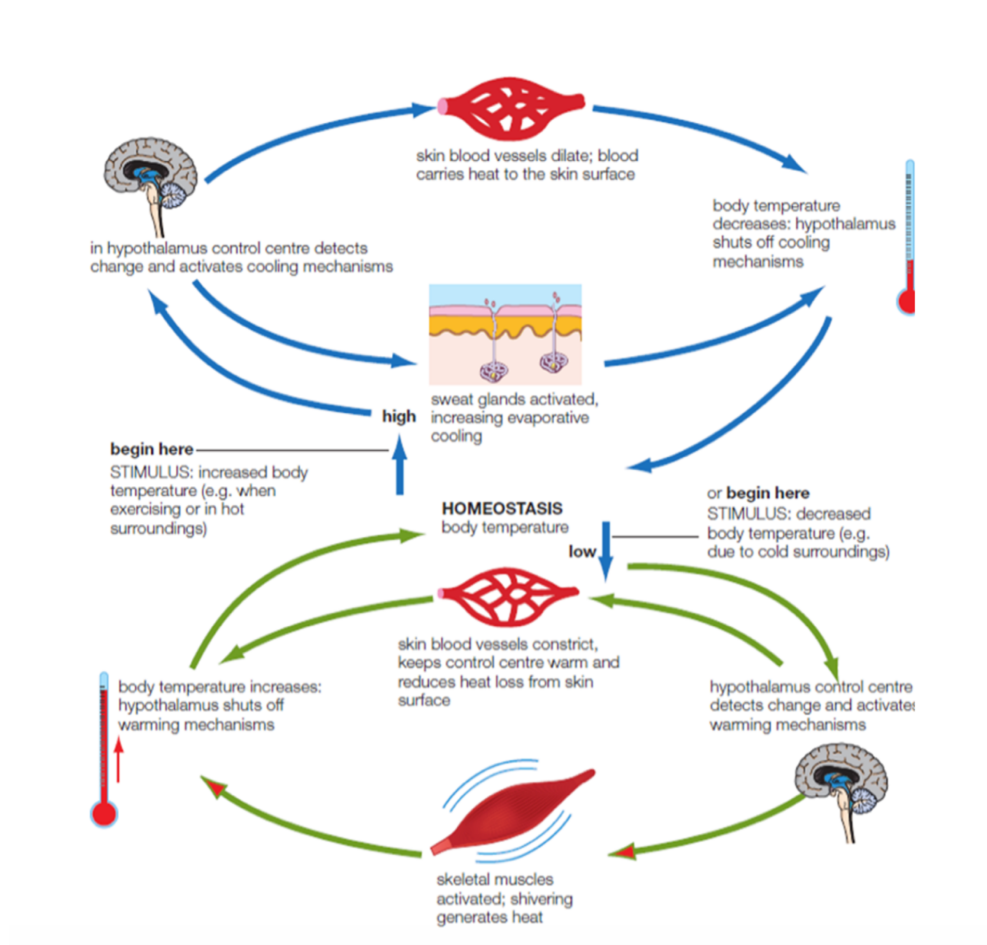
Figure 1.2: Schemetic view of human thermoregulatory system [51].

1.2.2 Human Thermal Comfort

Thermal refers to a person's experience of heat or cold, and comfort refers to how he/she is feeling. Having a comfortable body temperature is a subjective phenomenon known as human thermal comfort. According to ASHRAE (American Society of Heating, Refrigerating, and Air Conditioning Engineering) [49], human comfort is the mental state that communicates a person's sense of happiness with their thermal surroundings. A person's comfort is not only affected by his/her physical state, psychological state, and environmental impact, but also by his/her physiological response to the weather and the amount of liquid moisture present. Another important issue is how well the body regulates its temperature [46].

Every day, humans must deal with a variety of indoor, outdoor, and occasionally unusual circumstances. These performance-based settings determine the thermally comfortable zone. Workers in factories and other places of employment may get un-

comfortable or ill as a result of poor workplace conditions. The occurrence of thermal damage, a rare condition, is brought on by the body's core temperature fluctuating significantly above and below the normal range. If it rises, we refer to it as a hot injury, and if it falls, we refer to it as a cold injury. Figure 1.3 depicts a schematic view of the human thermal pleasant zone (hot and cold injury).
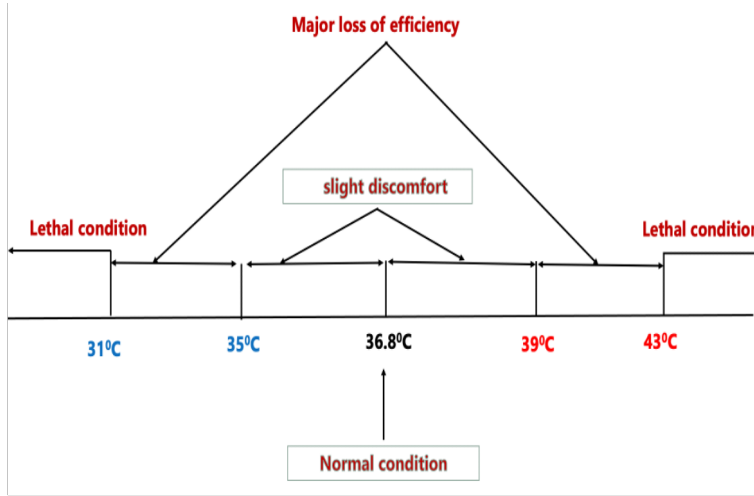
Figure 1.3: Human comfort zone.

1.2.3   Heat Transfer in Clothing System

Clothes serve as a shield between the body and the environment, protecting the body from both hot and cold conditions. The body seeks to release much heat in a cooler environment, but clothing also slows heat loss and keeps the body in a comfortable position, as seen in Figure 1.3. The overall heat transmission and human thermal comfort are influenced by a number of individual characteristics, including metabolism and clothing, as well as environmental elements, including radiant temperature, air temperature, relative humidity, and long and short wave solar-radiation absorption.

1.2.4   Clothing Insulation

The rate of heat exchange between the layers of trapped air and the environment is known as thermal insulation whose measurement is taken as Clo value. The clothing thermal insulation is determined by fabric structure, types of materials and its

layers [54, 74]. ASHARE 55, ISO 7730, and ISO (International Organization of Standardization) 9920 defines and measured the insulation of clothing ensemble using a static, standing thermal manikin. Clothing heat exchange, however, depends upon the movement of limb, posture, and moisture accumulation [49, 54]. Clo, the measurement unit, is the thermal insulation of overall clothing worn by a person which has 0.1 m/s air velocity at air temperature 21°C and a relative humidity of less than 50%. Among the total heat produced by the metabolic reaction, 24% of heat is lost through evaporation and respiration. Since

$$1 \text{ met} = 50 \, \text{kcal/m}^2 \, \text{hr},$$

the evaporative and respiratory heat loss $= 1 \text{ met} \times 24\% = 50 \text{ kcal/m}^2 \text{ hr} \times 0.24 = 12 \text{ kcal/m}^2 \text{ hr}.$

The rest of the energy $(50 - 12) \text{ kcal/m}^2 \text{ hr} = 38 \text{ kcal/m}^2 \text{ hr}$

This remaining is transmitted through the clothing system by conduction, convection, and radiation. The total insulation I_T, the sum of clothing insulation I_{cl} and air insulation I_a. Here $(I_T = I_{cl} + I_a)$ is calculated on the basis of the comfortable skin temperature $33^0 C$ as [74, 75]

$$I_T = \frac{(33 - 21)^\circ \text{ C}}{38 \text{ kcal/m}^2 \text{hr}} = 0.32 m^2 \, ^\circ\text{C(hr/kcal)}$$

With the help of these values together with 1 kcal/hr = 1.163 watt (W),
1 Clo unit is defined as

$$I_{cl} \, (\text{Clo}) = 0.18 \, \text{m}^2 \, ^\circ\text{C} \, (\text{hr/kcal }) = \frac{0.18 \, \text{m}^2 \, ^\circ\text{C}}{1.163 \text{W}} = 0.1550 \, \text{m}^2 \, ^\circ\text{C/W}.$$

Hence,

$$1 \text{ Clo} = 0.1550 \, \text{m}^2 \, ^\circ \text{ C/W}.$$

1.3   Objectives of the Study

1.3.1   General Objectives

- To develop mathematical models for heat transfer through a human body with and without clothing, and to ascertain the thermal reactions.

- To examine its response in the human thermoregulatory system, the appropriate linear and nonlinear mathematical models for axisymmetrical bioheat transfer in

9

higher dimensions with time-dependent metabolism and temperature-dependent thermo-physical parameters will be constructed and solved.

1.3.2 Specific Objectives

- To obtain the governing bioheat transfer equation using the cylindrical coordinate system based on the Fick's law of perfusion and the fundamental principle of thermodynamics.

- Use the implicit Finite Difference (FD) approach to solve the bioheat transfer equation for naked and expanded covered systems.

- To implement the extended model's validity and stability analysis by establishing a lemma and some theorems.

- To solve the axisymmetrical linear model by crank-Nicolson (CN) Scheme and apply solution for the thermal response during different physical activities.

- To solve the three-dimensional nonlinear model by Finite Volume Method (FVM) for analyzing temperature distribution in an abnormal tissue in radial, r-direction, axial, z-direction, axisymmetric, (r, z)-direction, and angular symmetric, (r, θ)-direction.

1.4 Rationale and Outline of Thesis

The analysis of temperature change and thermal responses in the human body because of numerous internal and external occurrences, as well as an essential component, the clothing factor, have been carried out in this research work. One-dimensional steady-state and transient Pennes' bioheat transfer models, mathematical models with protective clothing, axisymmetric models with time-dependent metabolism and sweating effects, and nonlinear axisymmetric models with temperature-dependent thermophysical parameters are some of the mathematical models that have been studied. In this thesis, the numerical computation for the linear mathematical models has been carried out with the finite difference (FD) approach. Another significant and of relevance in the study of a nonlinear mathematical model is the Finite Volume (FV) approximation of the transient bioheat transfer equation taking temperature-dependent thermophysical factors into consideration.

The preliminaries are covered in Chapter 2 along with several heat transmission processes in the human body, formulation, and development of a mathematical model. This chapter also includes the one-dimensional steady-state model with its analytical solution, the transient Pennes bioheat transfer model with its numerical solution using the implicit Finite Difference Method (FDM), and the impact of various parameters.

In Chapter 3 we describe the clothing heat transfer mechanism for human thermal comfort in detail. A mathematical model with a protective clothing layer, the extension of Pennes' bioheat model, has been developed. The numerical computation of the model with the clothing parameters at the boundary as well as the bioheat equation with protective layer have been separately treated and solved by using FDM. The special care is taken for heat flow within the human body and clothes, and also the special treatment is followed for validity and stability of the developed model by introducing some lemmas and theorems. The impact of various fiber parameters, including thermal conductivity, density, the specific heat of fiber, clothing insulation, air insulation, etc., has been examined by numerical simulation.

The study of two dimensional axisymmetrical bioheat transfer model with time- dependent metabolism and sweating effect is the key focus of Chapter 4, where the developed model and its computational results will have been obtained from the Crank-Nicolson FD scheme. The sweating and metabolic effect are studied as one of the applications to the real world problems during the physical activities of a person.

Special attention is given to develop a three-dimensional nonlinear bioheat transfer model in Chapter 5. Such models have verities of applications in physical and biological problems. So, we developed the models for one-dimensional radial (r-direction), axial, (z-derection), two-dimensional axisymmetric, $((r, z)$-direction), and angular symmetric,$((r, \theta)$-direction) from the three-dimensional nonlinear model in the cylindrical coordinate system. The constant external heating source has also been applied in the model. The computational resuts have been obtained by using Finite Volume (FV) method, observe the temperature profile with it's nonlinear behavior in an abnormal tissue.

The major outcomes of the research findings, discussions, conclusions, and recommendations are offered in the summary and conclusion, which is in Chapter 6.

CHAPTER 2

BIOHEAT TRANSFER MODEL

2.1 Introduction

This chapter overviews fundamental ideas of various heat transfer mechanisms. They are crucial in the development of the heat transfer equation, the standard parabolic equation. Two different aspects, analytical and numerical approaches, to solve the initial-value and/or boundary-value issues related to Pennes' kind of linear bioheat equation [93], each of which demonstrates a completely different technique of solutions in the cylindrical geometry are particular attention. These approaches are essential components of the complex heat transport and blood flow processes in a living tissue, which presents challenges and opportunities for computational advancement. First, the Modified Bessel function is useful for one-dimensional steady-state problems to achieve the analytical technique in the solution procedure. The bioheat transfer equation is converted into the form of a Modified Bessel equation, introducing the dimensionless parameters [77, 123]. For the numerical part, the Finite Difference (FD) scheme has been used for the one-dimensional transient situation where the differential equation is transformed into a system of difference equations for each of the nodes, and the cylindrical domain is discretized into a finite number of nodes. Before solving the model, it is, therefore, crucial to establish certain conceptual frameworks concerning the Bessel function and FD scheme.

Section 2.2 covers the fundamental concepts of heat transport processes, which are crucial components of the human thermoregulatory system. The exact formulation of the bioheat transfer equation in a cylindrical coordinate system, which typically relies upon the heat transfer phenomena in conjunction with the basic idea of thermodynamics, is covered in section 2.3. A brief overview of development of bioheat transfer model is presented in section 2.4. Section 2.5 discusses the one-dimensional

steady-state model and its analytical solution using the modified Bessel function. The various finite difference methods for unsteady-state models are described in section 2.6, and section 2.7 provides additional details on the implicit FD scheme for the solution of one dimensional transient bioheat transfer model with its stability and validity. The last section, 2.8, includes the conclusion of this chapter.

2.2 Heat Transfer Mechanisms

Heat transfer is energy transfer between two systems brought on by temperature variations. In thermodynamic system analysis, the quantity of energy transferred as a system transitions from one equilibrium system to another is of interest.

The science of thermodynamics focuses on calculating the rates of energy transmission, including heat transfer. Heat is always transported from a hotter medium to a cooler one, and it stops when the temperatures of the two media are equal. There must be a temperature difference from a high-temperature medium to a lower-temperature one for all three heat transfer mechanisms: conduction, convection, and radiation [16, 50, 86, 97].

2.2.1 Thermal Conduction

Thermal conductivity is the property of a material that has an ability to conduct heat through it. Conduction, the movement of heat through a stationary solid or liquid media is one of the important heat transfer mechanisms in a living tissue. Heat is transferred from a location with a higher temperature to a region with a lower temperature by the atomic and molecular action known as heat conduction.

In the overall heat exchange system, for nude persons, around 3% of heat transfer occurs through conduction. Fourier's Law of Conduction serves as the foundation for the thermal conduction-related heat transfer, which states that the quantity of thermal energy transferred by conduction through a medium is inversely proportional to the length across the medium, cross-sectional area, and temperature difference [16, 42]. Now,

$$\text{Rate of heat conduction} \propto \frac{(\text{area})(\text{temperature difference})}{\text{thickness}}$$

$$\dot{Q}_{cond} = -KA\frac{\Delta T}{\Delta x}, \tag{2.1}$$

13

where
$\dot{Q}_{cond}$:   rate of heat conduction (W)
K :   thermal conductivity of the material (W/m °C)
A :   cross-sectional area (m²)
ΔT :   temperature difference (°C)
Δx :   thickness or length (m).

The second law of thermodynamics mandates the minus sign in Fourier's law, as thermal energy transfer resulting from a thermal gradient must be from a warmer to a colder zone.

The temperature gradient in the direction normal to the area of the medium is the limiting case of the equation 2.1 as $\Delta x \to 0$. So

$$\dot{Q}_{cond} = -KA\frac{dT}{dx}. \tag{2.2}$$

The two/three-dimensional form of the Fourier's law is given as:

$$\dot{Q}_{cond} = -K\nabla T. \tag{2.3}$$

T :   tissue temperature (° C)
∇T :   temperature gradient (°C/m)
K :   constant, for an isotropic medium.

The geometry, thickness, and material of a medium, as well as the temperature difference across the medium affects the rate of heat conduction through it.

2.2.2 Convection

Convection is a process through which energy causes motion in the molecules of the fluid. In our context of blood flow in the body, the cell transfers heat due to the surrounding air, and convection also takes place. The process of convection from heated sources such as human skin is classified as "free convection" and "forced convection". Free convection due to density differences in the fluid associated with temperature gradient and forced convection due to external forces such as wind. Approximately 15% of the body heat is lost through convection [12, 16, 42, 67]. Newton's law of cooling states that the rate of a body's temperature change is directly proportional to the difference in temperature between the body and its surroundings under the influence of mild wind, has an impact on this. The rate of convection heat transfer $\dot{Q}_{conv}$ (W) is given by

$$\dot{Q}_{conv} \propto (T_s - T_\infty).$$

14

After inserting the proportionality constant h_{conv}, the convective heat transfer coefficient (W/m^2 ° C, the rate by Newton's law of cooling is expressed as

$$\dot{Q}_{\text{conv}} \;=\; h_{conv} A \left(T_s - T_\infty \right), \tag{2.4}$$

where
  A :   area of the surface (m^2) through which convective heat transfer occurs.
  T_s :   surface temperature (°C)
  T_∞ :   ambient temperature (°C).

Heat transfer coefficient h_{conv} is the experimentally determined parameter, not the property of the fluid but it depends upon the fluid's property and other mediums such as surface geometry, the nature of the fluid motion, air velocity, etc. [15]

Now, the energy balance equation at the surface boundary is

Energy inflow into the system = Energy outflow from the system,

or

(Energy conducted into the boundary) = (Energy convected from the boundary).

$$-K \frac{\partial T}{\partial \eta}\bigg|_{\text{at skin surface}} \;=\; h_{\text{conv}} A \left(T_s - T_\infty \right), \tag{2.5}$$

  where η :   outward pointing unit normal vector.

2.2.3   Thermal Radiation

The transmission of heat without any medium or any physical contact between two objects is called radiation. A primary cause of heat loss is the emission of heat from a body into the environment as well as the diffusion of heat via the air from a warm body to comparatively cold objects. When the temperature in the surrounding environment drops below the body's core temperature, thermal radiation from the body's surface is produced. The body surface emits thermal radiation in the range of 0.1,m to 100 m wavelengths. The middle infrared spectra range, between 5000 nm and 10000 nm, has strong absorptivity in the human skin, animal fur, and many non-metallic biological surfaces.

The surface of human body continuously radiates heat in the form of electromagnetic waves. The rate of emission depending on the absolute temperature of the radiating surface. This electromagnetic wavelength ranges from $10^{-10}\,\mu$m to $10^{10}\,\mu$m with

different rays, such as cosmic rays, γ rays, X rays, ultraviolet, thermal infrared, microwaves, radio waves, and TV waves, having varying values [4, 16, 125].

The emissivity in the middle infrared is also close to 100% due to high absorptivity in this region. So, heat loss from the surface of the human body via radiation is virtually the same as a black body, the perfect emitter and absorber of radiation [16, 66].

Josef Stefan in 1879 determined experimentally and Ludwig Boltzmann verified theoretically in 1884 that the radiation energy emitted by a black body per unit area per unit time is proportional to the fourth power of the absolute temperature and expressed as

$$\dot{Q}_{\text{black body}} = \sigma A T^4, \tag{2.6}$$

where

$\dot{Q}_{\text{black body}}$: black body emissive power (W)
σ : proportionality constant (W/m^2 K^4)
A : area of surface (m^2).

This proportionality constant σ is called the Stefan - Boltzmann constant with the value 5.67×10^{-8} (W/m^2 K^4).

Equation (2.6) is the Stefan-Boltzmann law of thermal radiation, according to which the net radiant exchange between two surfaces is proportional to the fourh power of the difference in absolute temperature and is expressed as [98]

$$\dot{Q}_{\text{black body}} = \sigma A \left(T_1^4 - T_2^4\right). \tag{2.7}$$

Approximately 60% of body heat is lost through radiation. The amount of radiated energy between two surfaces at a given wavelength depends upon the emissivity of the surface. According to same law, the radiation with emissivity of the surface, ϵ depends on the material and the structure of the corresponding surface given by [55, 97]

$$\dot{Q}_{\text{rad}} = \sigma \epsilon A \left(T_1^4 - T_2^4\right), \tag{2.8}$$

where

$$\epsilon = \frac{\dot{Q}_{\text{rad}}}{\dot{Q}_{\text{black body}}},$$

such that

$$\begin{cases} \epsilon = 1, & \text{for black body.} \\ 0 < \epsilon < 1, & \text{non-black body.} \end{cases} \tag{2.9}$$

16

The radiation from the human body surface increases when it is exposed to the environment, and the associated energy balance equation for radiation is determined by

$$-K \frac{\partial T}{\partial \eta}\bigg|_{\text{at skin surface}} = \sigma \epsilon A \left(T_s^4 - T_\infty^4 \right),\tag{2.10}$$

where
T_s : surface temperature
T_∞ : ambient temperature.

2.2.4 Evaporation

Evaporation is the process of transforming liquid into vapor. The high heat of vaporization is a very efficient cooling process, for attaining thermal equilibrium. Perspiration, a cooling process, can be viewed as a good example of evaporation. Insensible loss of fluids or perspiration happens at about $600\,\text{gm/day}$. The skin begins to perspire insensibly at $37°C$, and as the skin's temperature rises, so does the amount of sweat produced. According to Guyton and Hall [42], in a tropical climate, the natural maximum perspiration rate is at 1.5 Lt/h, but after 4 to 6 weeks of acclimatization, it can reach 3.5 Lt/h. The liquid's mass, the surrounding temperature, and the relative humidity influence the evaporative energy loss during latent heat change. The difference between the water vapor pressure at the skin, ambient air, and skin wetness determine the moisture on the skin through evaporative or latent heat loss from the skin. Approximately 22% of the body's heat loss occurs due to evaporation. However, by controlling the rate of sweating, it is possible to prevent the loss of heat caused by sweat evaporation [42]. The energy which changes a gram of a liquid into the gaseous state at the boiling point is called the latent heat of vaporization, L_v. For pure water, $L_v = 2.25106\text{J/kg}$, but sweat, which is 99% water with sodium chloride as solute, is an electrolyte with $L_v = 2.43106\,\text{J/kg}$. The evaporation of 1 gram of sweat removes 580 kcal or 2426 kJ of heat energy [4].

The formula for evaporation cooling rate is expressed as

$$\dot{Q}_{\text{evap}} = E L_v,\tag{2.11}$$

where
$\dot{Q}_{\text{evap}}$: rate of heat exchange due to evaporation (W)
E : rate of sweat evaporation (kg/sec) Lt/h. $[1\,\text{Lt/h} = 0.00020\,\text{kg/sec}]$

The metabolic rate rises as an individual engages in physical activity. The body's metabolism is speeding up, which results in extra heat energy. Energy lost by conduction, convection, and radiation is insufficient for maintaining a constant body core temperature. Evaporation, then, represents the fourth way that the body loses, energy. The energy balance equation owing to evaporation at a surface boundary is provided by

$$-K\frac{\partial T}{\partial \eta}\bigg|_{\text{at skin surface}} = EL_v. \tag{2.12}$$

The surface medium, ambient air humidity, and air convection are the key determinants of the evaporative heat exchange. Before evaporating into the air, evaporated perspiration may condense in a certain state, delivering heat to the layer of clothing. This will be covered in detail in Chapter 3.

2.2.5   Combined Heat Exchange Between Skin Surface and Environment

If the body is exposed to the environment and the thickness of the human limb is thought to be measured from the inner core towards the outer skin surface, then heat loss between the outer skin surface and environment (boundary) happens as a result of convection, radiation, and evaporation. If heat is escaping from the body, then the relationship between the combined heat exchange of the skin's surface with the environment is

$$-K\frac{\partial T}{\partial \eta}\bigg|_{\text{at skin surface}} = h_{\text{conv}}A\left(T_s - T_\infty\right) + \sigma\epsilon A\left(T_s^4 - T_\infty^4\right) + EL_v. \tag{2.13}$$

2.2.6   Blood Perfusion

Another crucial heat transmission technique that uses arteries and veins with countercurrent flow is blood perfusion, the heat exchange process that occurs in a living thing, the complicated channels inside the tissue. The rate of blood perfusion in various human tissues varies greatly based on a variety of physiological and environmental factors as well as physical activities [78, 109]. Based on Fick's law of perfusion, Harry Pennes' first proposed a concise expression for the term "blood perfusion" in 1948. He proposed that the rate of heat transfer from blood to tissue per unit volume, $\dot{Q}_{\text{Perfusion}}$ is proportional to the volumetric blood flow per unit time and the difference between the blood temperature entering small capillaries at an arterial, T_a and the outflow of

substance via the venule blood, T_v [93].

In order to maintain a comfortable position and a steady body core temperature, blood circulation plays a crucial function in either dispersing or warming the cooled area. The perfusion term expressed by Pennes' for the exchange of thermal energy between the blood and surrounding tissue is given by

$$\dot{Q}_{\text{Perfusion}} \quad = \quad \rho_b \, c_b \left(\phi_a \, T_a - \phi_v \, T_v \right), \tag{2.14}$$

where
$\rho_b :$ blood density
$c_b :$ specific heat of blood
$\phi_a :$ arterial blood flow per unit volume
$\phi_v :$ venule blood flow per unit volume.
$T_a :$ arterial temperature
$T_v :$ venulel temperature.

Even though the values of ϕ_a, ϕ_v, T_a and T_v will be different from each other for the deeper tissues of various organs of human body, there is hardly any difference between these values under normal conditions. The tissue temperature T always dominates the value of T_v.

So, by assuming $w_b = \phi_a = \phi_v$, the perfusion term in equation (2.14) can be rewritten as

$$\dot{Q}_{\text{Perfusion}} \quad = \quad \rho_b \, c_b w_b \left(T_a - T \right). \tag{2.15}$$

2.2.7   Metabolic Heat Generation

The chemical process known as metabolism that occurs when energy is moved between different chemical molecules in the body, leading to the production of heat energy. This involves a sequence of chemical adjustments that occur within an organism and allow for the production, consumption, and elimination of waste. Metabolism includes two phases: catabolism and anabolism.

- Catabolism
  Catabolism, the process of breaking down organic matter, produces heat energy in the body. By breaking down big complex molecules into smaller ones, the process makes it easier to absorb molecules and as a consequence, potential energy changes into kinetic energy. In this process, food consumed is transformed into various necessary acids that the body requires.

19

- Anabolism

  Anabolism, the process of forming molecules that are essential for the body's functionality, requires energy which is absorbed from the catabolic process. The anabolic process conversely transforms kinetic energy into potential energy.

Metabolism rises over time as a person's level of activity increases and varies from layer to layer, with the bone producing the least amount of heat $(0\,\mathrm{W/m^3})$ and the brain producing the greatest heat $(13400\,\mathrm{W/m^3})$. These metabolic values are related to body volume and are therefore calculated using the unit $\mathrm{W/m^3}$ [48, 78]. The Thermal Environmental Condition for Human Occupancy, ANSI (American National Standards Institute) 2017, referenced the Met unit to indicate the rate of transmission of energy into heat by individual metabolic processes, typically connected to skin surface area (A_D) of a person or body mass. The nude body surface area proposed by D. DuBois in 1916 [49] is

$$A_D = 0.202\,\mathrm{w}^{0.425}\,\mathrm{h}^{0.725},$$

where
$A_D:$ body surface area $(\mathrm{m^2})$
$w:$ weight (mass) of the body (kg)
$h:$ height of the body (m).

For an average size man, $173\,\mathrm{cm}$ and 70 kg, $A_D = 1.8\,\mathrm{m^2}$.

The rate of production of the energy of an average person seated at rest is given by [49]

$$1\ \mathrm{Met} = 50\ \mathrm{k\,cal/m^2\,hr} = 58.2\ \mathrm{W/m^2}.$$

Monitoring the rate of respiratory oxygen consumption, which varies from roughly $0.2\,\mathrm{L/\,min}$ at rest to $\geq 2\ \mathrm{L/\,min}$ during vigorous exercise, can provide a more precise estimate of metabolism. The additional resistance that clothing offers to dissipate heat will be discussed later in Chapter 3, but generally, as metabolic rate increases, garment surface temperature decreases. The following equation can be used to allow for the rate of change of heat in tissue medium caused by metabolic heat generation.

$$\dot{Q}_{\mathrm{metabolic}} \;=\; q_m, \tag{2.16}$$

where q_m is the rate of metabolic heat generation per unit volume.

2.3 Bioheat Transfer Equation

The foundation for heat transmission is derived from the basic idea of thermodynamics, which is concerned with the equilibrium state of the body's temperature as a result of the energy balance. The relationship between heat loss and gain perceived by the body is represented by the heat balance equation [78].

$$\text{Heat gain} = \text{Heat Loss},$$
$$(\text{ Net heat input rate }) + (\text{Heat generation rate}) = (\text{Change in internal energy}) . \quad (2.17)$$

The diffusion equation due to heat conduction in the system from equations (2.2) using the cylindrical coordinates (r, θ, z) is given by [16, 86]

$$\rho\, c \frac{\partial T}{\partial t} = K \left[\frac{\partial^2 T}{\partial r^2} + \frac{1}{r}\frac{\partial T}{\partial r} + \frac{\partial^2 T}{\partial z^2} + \frac{1}{r^2}\frac{\partial^2 T}{\partial \theta^2} \right]. \quad (2.18)$$

ρ : density
c : specific heat(kg).

All of the heat transfer mechanisms described in above section 2.2 are responsible for the derivation of bioheat transfer equation suggested by Harry Pennes' in 1948 [93, 119].

The rule of conservation of energy, which explains the diffusion of thermal energy in a homogeneous medium, is a prerequisite for this heat balancing equation to work. It can be used to simulate steady-state and unsteady-state diffusion equations, solid tumour growth, and heat transport. All of the heat transfer mechanisms described in above section 2.2 are responsible for the derivation of bioheat transfer equation suggested by Harry Pennes' in 1948.

Energy conservation with volumetric perfusion and source term within the living tissue ΔV are shown in schematic diagram Figure 2.1.
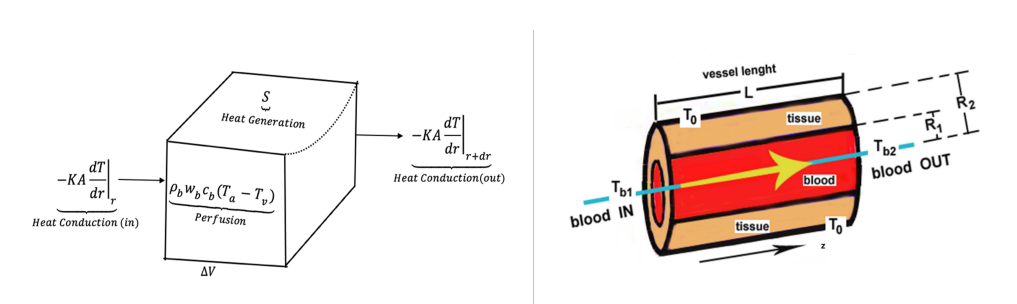
Figure 2.1: Schematic diagram of (left) energy balance inside small tissue element ΔV and (right) mechanistic representations of single blood vessel-tissue heat transfer[51].

The heat balance equation, obtained in (2.18), has been combined by adding energy conservation term via blood perfusion from equation (2.15) as shown in Figure 2.1, and metabolic term from equation (2.16) gives rise to the modified form of bioheat equation in human tissue element ΔV, considered as computational domain Ω_r

$$\rho\, c\frac{\partial T}{\partial t} \;=\; K\left[\frac{\partial^2 T}{\partial r^2} + \frac{1}{r}\frac{\partial T}{\partial r} + \frac{1}{r^2}\frac{\partial^2 T}{\partial \theta^2} + \frac{\partial^2 T}{\partial z^2}\right] + \rho_b w_b c_b\left(T_a - T\right) + q_m. \qquad (2.19)$$

The equation (2.19) with the total amount of heat stored in the body per unit of time is typically represented as

$$\underbrace{\rho c\frac{\partial T}{\partial t}}_{\text{Heat Storage}} \;=\; \underbrace{\nabla\cdot(K\nabla T)}_{\text{Diffusion}} + \underbrace{\rho_b w_b c_b\left(T_a - T\right)}_{\text{Perfusion}} + \underbrace{q_m}_{\text{Metabolism}}. \qquad (2.20)$$

The left hand side of this equation (2.20), is the total heat storage; the first and second terms of the right hand side are, respectively, diffusion and perfusion, whereas the third term is the rate of metabolic heat production. This well-known bioheat equation is called Pennes' bioheat transfer equation and was suggested by Harry Pennes' in 1948.

2.4   A Brief Overview of Development in Bioheat Transfer Models

Pennes' pioneering work from 1948 resulted in the well-known bioheat transfer model (2.20), which is based on experimental observation and includes the blood perfusion term for the heat movement within the tissue. He conducted research at Columbia University's College of Physicians and Surgeons [93]. His concept of a perfusion heat source is a realistic approximation of the thermal effect of blood under certain circumstances. Blood flow in a large vessel is perpendicular to the temperature gradient of the human tissue element. The bioheat transfer equation was then run successively by several researchers. Perl in 1962 [94] performed Fick's law and combined it with heat conduction and source term. The basic example of the equation for a spherically symmetric heat source embedded in an infinite tissue medium was finally solved by Perl after a ten-year period.

Further, Keller and Seiler in 1971 [63], Wulff in 1974 [120], Chen and Holmes in 1980 [18], and Weinbaum and Jiji Model in 1985 [117] modified the Pennes' model with major criticism that Pennes' model was centered on the idea that blood flow is a non-directional heat source or sink [8].

In 1972, Cooper and Trezek [20] discovered a mathematical solution to the heat diffusion equation for brain tissue that negligibly took blood flow and metabolic heat

production into account. An instrumental method for the direct measuring of heat loss from a man in his usual working mode was developed by Hodgson in 1974 [53]. Chao and Yang 1975 [17] applied steady- state and unsteady-state models to the issue of heat flow in the skin and sub-dermal tissues by keeping all the parameters constant. Patterson in 1976 [91] made an experimental attempt to ascertain the temperature profiles in the skin and subcutaneous tissue. These experimental findings only offer scant details, where a model is created to represent the temperature effects of blood flow in human skin. This model accurately accounted for the intricate mechanism of heat convection within the tissue. A paper about the case of intradermal temperature profiles under transitory thermal conditions was also published in 2018 [40].

Rubinsky and Pegg [99] proposed a mathematical model in 1988 that used the concept of a repeating structure made up of a tissue cylinder with an axial blood artery to study the freezing processes in biological tissues. The model was examined using irreversible thermodynamics, and the results of the experiments were contrasted with the mathematical findings in liver tissue [8]. In the clinical treatment of cancers with local hyperthermia, the paper further emphasizes thermal dose equivalence and the level of thermal damage or destruction of tissue. Despite numerous thermophysical criticism of Pennes' model and suggestions for alternate bioheat transport models, it is still commonly utilized because of its flexibility, and computational simplicity.

Saxena launched a study to investigate the problem of heat transfer in the skin and subcutaneous tissues. The 1980s are responsible for these significant contributions. In 1981, Saxena and Arya, in 1983 [100], Saxena and Bindra in 1986 [101], Rubinski and Pegg in 1988 utilized the well-known Pennes' model, and Saxena and Yadav in 1988 made a significant addition to the field of biomathematics [7, 8, 40]. Later, in 1999 Liu et al. [71] developed a model in a skin structure with a composition of three layers namely, the epidermis, dermis and subcutaneous layer, to investigate the behaviour of bioheat equation occurred in the thermal injury in the skin subjected to instantaneous heating. Throughout a couple of decades, 1990s and 2000s, other scholars, including Shih et al. in 2005, Rubinsky in 2003, Kai Yue Xinxin Zhang Fan Yu in 2004, Pardasani and Shakya in 2005, Yildirim in 2005, Zhao Zenifer 2005, Gurung 2007, Gustavo Gutierrez in 2007, Gurung and Saxena 2009, and Gurung and saxena 2010 [8, 39, 40, 41, 87, 105, 123, 124] analyzed Pennes' bioheat equation for thermal interaction between the tissue and perfused blood with a point heat source of constant density at the center of the spherical domain using analytical and numerical methods.

Lv et al. [79] purposed a new approach to evaluation of the physiological comfort of biological tissue in correlation with the thermal effect on neuron response and the thermal environment and investigated thermal sensory responses of human skin under various environmental conditions with major variables are air temperature, air velocity, metabolism, level of physical activities, and health condition. Effective temperature $T_e = 25°$C, widely accepted comfort temperature, just passes the comfort zone, has been selected as the average value of the variables in the Pennes model to reduce the uncertainty.

Zhao et al. [124] developed new two-level finite difference scheme for one dimensional Pennes' bioheat equation assuming the continuity of thermal conductivity across the domain boundaries of a three-layered skin model and proved that the stability criteria for the scheme. The constant physiological characteristics utilized in many models, such as Gurung in 2010, Luitel et al. in 2018, and Wissler in 1998 [38, 77, 119] are not adequately given for the hyperthermia therapy of cancer because of the non-uniform inner body structure of humans. Furthermore, Acharya et al. extended the Pennes' triple-layered skin model up to five-layered model in 2014 and 2015 [3, 4] to evaluate sex-related perfusion and metabolic effect in thermoregulation on human male and female skin, respectively. Gokul et al. [34] studied the transient heat transfer model in the human eye, where the thermal impacts of blinking are examined with different blinking rates, lid closures, and lid openings imitate. In 2020, Shrestha et al. studied a one-dimensional model in cartesian coordinate system with time-dependent metabolism during different physical activities. Most researchers have concentrated on using the finite element method [3, 4, 34, 37, 107].

With the abundance of research conducted throughout the 2010s, including techniques such as applying the fractional derivative and optimal control theory, the applications of the bioheat transfer model have quickly been expanded for the hyperthermia treatment against cancer [6, 27, 64, 69, 83]. Szasz et al. in 2016 used the bioheat transfer model to observe the connection between the Specific Absorption Rate (SAR) and the local temperature [111].

Rashkovska, Iljavz et al., Sharma and Kumar [59, 96, 103] presented the model taking blood perfusion and metabolic heat generation rate based on Van't Hoff Q_{10} [19] which speculates the reaction rate of perfusion and metabolic heat generation is doubled when the temperature increases by $10°C$. Its effects with sensitivity coefficient have been used in the literature of Davidson et al., Gupta and Shakya, Selmi et al. [25, 36, 102] model the temperature change of basal metabolic heat generation rate

in the living tissue.

Within these two years period in 2019, Iljaz et al.[59] developed the numerical modeling of tumor tissue at the skin with dynamic thermography as the function of temperature. Zomordikhami et al. in 2020 [126] analyzed the nonlinear bioheat heat transfer equation in magnetic hyperthermia. They also examined the role of temperature-dependent blood perfusion in by the delivery of drugs during hyperthermia. Hobiny et al. in 2020 [52] studied the nonlinear analysis of the bioheat model in living tissues induced by laser irradiation by using the finite elemant method where they obtained a numerical solution of the thermal damage of such tissue using the dual phase lag model. In the same year Farahat [31], Sharma and Kumar [103], and Selmi et al. [102] developed a model describing the heat transfer in the tumor tissue element by applying the external heating source during hyperthermia treatment in the different parts of the human body. Recently, Wust et al. in 2021 [121] critically analyzed the non-thermal membrane effects of electromagnetic fields and therapeutic applications in oncology especially in radio frequency (RF) and microwave (EMF). The nonlinearity of the model is referred to in Chapter 5.

2.5   One Dimensional Steady-State Bioheat Transfer Model

Though the investigators have developed alternative models for describing the perfusion rate and the difference between arterial blood and the local tissue temperature, no general thermal model suitable for anyone has so far been developed, especially for the description of convection heat transfer by blood in perfused tissue. The bioheat equation of Pennes' model still has acceptable results to predict the transient temperature due to its simplicity and flexibility. The governing differential equation is used as the basic mathematical model (2.20) for the heat transfer suggested by H. Pennes' in cylindrical form for radial direction is given by [93]

$$\rho c \frac{\partial T}{\partial t} = K \left[\frac{1}{r} \frac{\partial}{\partial r} \left(r \frac{\partial T}{\partial r} \right) \right] + \rho_b w_b c_b (T_a - T) + q_m. \qquad (2.21)$$

This section analyzes the Pennes bioheat equation for a one-dimensional steady-state case with suitable boundary conditions. To get precise answer, one of the most powerful analytical methods—the modified Bessel function approach—was applied. So, we introduce the Bessel differential equation and Bessel's function in the modified version, along with the boundary conditions. Generally, the solutions of governing equations provide information on the temperature inside the domain. The informa-

tion on the temperature at the boundary $\partial\Omega_r$ is equally important to get the complete temperature profile within the tissue element. Basically, three types of boundary conditions, namely Dirichlet (constant), Neumann (flux), and Robin's (Mixed) boundary conditions, are encountered in the solution of boundary value problems.

Left Boundary (Inner Boundary)

As the body core temperature is approximately 37°C, the flux boundary (Neumann boundary), the inner boundary condition of the living tissue; is taken as

$$\left.\frac{dT}{dr}\right|_{r=0} = 0. \tag{2.22}$$

Right Boundary (Outer Boundary)

As the outermost part of the human body, the skin, is exposed to the nearby the environment, where the heat flux occurs from the skin surface to environment and vice versa. So, Robin's boundary conditions (The mixed boundary condition) due to convection, radiation together with sweat evaporation guided by Newton's law of cooling is given by

$$-K\left.\frac{dT}{dr}\right|_{\text{at skin surface}} = h_{\text{conv}}A\left(T_s - T_\infty\right) + \sigma\epsilon\,A\left(T_s^4 - T_\infty^4\right) + EL_v, \tag{2.23}$$

where h_{conv}, E, L_v, and T_∞ represent the heat transfer coefficient due to convection W/m^2°C, rate of sweat evaporation kg/sec, L_v is latent heat vaporization J/kg, and ambient temperature °C respectively.

The appearance of the nonlinear radiation factor in the boundary condition causes the bioheat issue to become nonlinear. For such complexity, we employ the reduced form of the boundary condition:

$$
\begin{aligned}
-K\left.\frac{dT}{dr}\right|_{\text{at skin surface}} &= (T_s - T_\infty)\left[h_{\text{conv}} + \sigma\epsilon A\left(T_s + T_\infty\right)\left(T_s^2 + T_\infty^2\right)\right] + EL_v \\
&= (h_{\text{conv}} + h_r)\left(T_s - T_\infty\right) + EL_v \\
&= h_c\left(T_s - T_\infty\right) + EL_v.
\end{aligned} \tag{2.24}
$$

26

where h_c is the combined heat transfer coefficient due to convection and radiation given as

$$h_c = h_{\text{conv}} + h_r \qquad \text{and} \qquad h_r = \sigma \epsilon A \left(T_s + T_\infty \right) \left(T_s^2 + T_\infty^2 \right).$$

2.5.1 Bessel Differential Equation and Bessel Function

One of the most significant classes of special functions is the Bessel function. By changing the boundary conditions and applying the appropriate number of zeros and coefficient values to the Bessel function argument, the system equation can be reduced to Bessel's differential or modified equation [72, 123]. Bessel's equation and Bessel function occur in connection with many problems of physics and engineering. The Bessel function is presented as a power series solution to a second-order differential equation and appears in many diverse scenarios, particularly in situations involving cylindrical symmetry. So, we use the Bessel function as a tool to get the analytical solution of the cylinderical form of Pennes' bioheat equation.

The second order partial differential equation of the form

$$x^2 \frac{d^2y}{dx^2} + x \frac{dy}{dx} + \left(x^2 - p^2 \right) y \;\; = \;\; 0 \tag{2.25}$$

is called the Bessel's equation of order p, where p is any real number.

Bessel Function

The solution of equation (2.25) yields Bessel Function of the first kind $J_p(x)$ and second kind $Y_p(x)$ of order p as given by

$$y(x) \;\; = \;\; A J_p(x) + B Y_p(x), \tag{2.26}$$

where A and B are arbitrary constants to be determined from boundary conditions,

$$J_p(x) \;\; = \;\; \sum_{n=0}^{\infty} \frac{(-1)^n}{\Gamma(n+1)\,\Gamma(n+p+1)} \left(\frac{x}{2} \right)^{2n+p},$$

$$Y_p(x) \;\; = \;\; \frac{\cos p\pi\, J_p(x) - J_{-p}(x)}{\sin p\pi}.$$

2.5.2 Modified Bessel Differential Equation

The general form of the standard Modified Bessel equation is

$$x^2 \frac{d^2y}{dx^2} + x \frac{dy}{dx} - \left(\beta^2 x^2 + p^2 \right) y \;\; = \;\; 0. \tag{2.27}$$

Modified Bessel Function

The solution of Modified Bessel equation (2.27) is called Modified Bessel function of first kind with $I_p(\beta x)$ and Bessel function of second kind with $K_p(\beta x)$ of order p which is given by

$$y(x) \;=\; C I_p(\beta x) + D K_p(\beta x), \tag{2.28}$$

where C and D are arbitrary constants to be determines from the boundary conditions,

$$I_p(\beta x) \;=\; i^{-p} J_p(i\beta x),$$

and

$$K_p(\beta x) \;=\; \frac{\pi}{2 \sin p\pi} \left[I_{-p}(\beta x) - I_p(\beta x) \right].$$

2.5.3 Assumptions of the Steady State Model

In the model (2.21), we primarily assume that the computational domain is cylindrically symmetric, and we ignore the angular and axial directions of heat flow. The thermal conductivity and all other control parameters are considered in Table 2.1. From the computational viewpoint, nondimensionalization of the equation (2.21) and the boundary conditions (2.22) and (2.24) are performed by introducing the following characteristic quantities [77]

$$\widetilde{r} = \frac{r}{R} \qquad \text{and} \qquad \widetilde{T} = \frac{T - T_\infty}{T_a - T_\infty}. \tag{2.29}$$

2.5.4 Analytical Approach for Solution of the Model

One dimensional steady-state model is obtained from equation (2.21) is

$$\frac{d^2 T}{dr^2} + \frac{1}{r}\frac{dT}{dr} + M(T_a - T) + S \;=\; 0, \tag{2.30}$$

where

$$M = \frac{\rho_b w_b c_b}{K} \qquad \text{and} \qquad S = \frac{q_m}{K}.$$

Differentiation of equation (2.29) yields

$$\frac{d\tilde{r}}{dr} = \frac{1}{R}$$

$$\frac{dT}{dr} = \frac{d}{d\tilde{r}}[(T_a - T_\infty) + T_\infty]\frac{d\tilde{r}}{dr}$$

$$= (T_a - T_\infty)\frac{d\tilde{T}}{d\tilde{r}}\frac{1}{R}$$

$$\frac{dT}{dr} = \frac{(T_a - T_\infty)}{R}\frac{d\tilde{T}}{d\tilde{r}}$$

$$\frac{d^2T}{dr^2} = \frac{(T_a - T_\infty)}{R^2}\frac{d^2\tilde{T}}{d\tilde{r}^2} \tag{2.31}$$

Simplification and differentiation of equation (2.30) yields

$$\frac{(T_a - T_\infty)}{R^2}\frac{d^2\tilde{T}}{d\tilde{r}^2} + \frac{1}{R\tilde{r}}\frac{(T_a - T_\infty)}{R}\frac{d\tilde{T}}{d\tilde{r}} + M(T_a - T_\infty)\left(1 - \tilde{T}\right) + S = 0$$

$$\frac{d^2\tilde{T}}{d\tilde{r}^2} + \frac{1}{\tilde{r}}\frac{d\tilde{T}}{d\tilde{r}} + MR^2\left(1 - \tilde{T}\right) + \frac{R^2S}{(T_a - T_\infty)} = 0,$$

$$\frac{d^2\tilde{T}}{d\tilde{r}^2} + \frac{1}{\tilde{r}}\frac{d\tilde{T}}{d\tilde{r}} + \widetilde{M}\left(1 - \tilde{T}\right) + \tilde{S} = 0,$$

$$\frac{d^2\tilde{T}}{d\tilde{r}^2} + \frac{1}{\tilde{r}}\frac{d\tilde{T}}{d\tilde{r}} + \widetilde{M}\left(1 - \tilde{T}\right) + \tilde{S} = 0, \tag{2.32}$$

where, $\widetilde{M} = MR^2$, and $\tilde{S} = \dfrac{R^2S}{(T_a - T_\infty)}$

Equation (2.31) with the use of equation (2.32) and (2.39) reduces to

$$\frac{d^2\tilde{T}}{d\tilde{r}^2} + \frac{1}{\tilde{r}}\frac{d\tilde{T}}{d\tilde{r}} - M\tilde{T} + \left(\widetilde{M} + \tilde{S}\right) = 0. \tag{2.33}$$

Again we replace $\widetilde{M} + \tilde{S}$ by U, $\widetilde{M}$ by V and $(U - VT)$ by ϕ in equation (2.33) to make calculation easier, then we get

$$\tilde{r}^2\frac{d^2\phi}{d\tilde{r}^2} + \tilde{r}\frac{d\phi}{d\tilde{r}} - V\tilde{r}^2\phi = 0 \tag{2.34}$$

which is in Modified Bessel's equation of the form (2.27). The solution of equation (2.34) for ϕ is

$$\phi = C_1 I_0(\sqrt{V}\tilde{r}) + C_2 K_0(\sqrt{V}\tilde{r}), \tag{2.35}$$

where C_1 and C_2 are arbitrary constants to be determined from the boundary conditions.

$I_0(\sqrt{V}\tilde{r})$ and $K_0(\sqrt{V}\tilde{r})$ are the Modified Bessel function of first and second kind of

29

order 0, respectively.

Differentiating equation (2.35) we get

$$\frac{d\phi}{d\widetilde{r}} = C_1\sqrt{V}I_1(\sqrt{V}\widetilde{r}) + C_2\sqrt{V}K_1(\sqrt{V}\widetilde{r}).$$

Also, we have

$$\widetilde{T} = \frac{U}{V} - \frac{1}{V}\phi,$$

$$or\frac{d\widetilde{T}}{d\widetilde{r}} = -\frac{1}{V}\frac{d\phi}{d\widetilde{r}},$$

$$\text{therefore}: \frac{d\widetilde{T}}{d\widetilde{r}} = -\frac{1}{V}\left[C_1\sqrt{V}I_1(\sqrt{V}\widetilde{r}) + C_2\sqrt{V}K_1(\sqrt{V}\widetilde{r})\right]. \tag{2.36}$$

In terms of dimensionless parameters, the inner boundary condition (2.22) at the body core is

$$\left.\frac{d\widetilde{T}}{d\widetilde{r}}\right|_{\widetilde{r}=0} = 0. \tag{2.37}$$

The use of dimensionless parameters leads to the outer boundary condition (2.24) as

$$-K\left.\frac{d\widetilde{T}}{d\widetilde{r}}\right|_{\text{skin surface}} = R\,h_c\widetilde{T} + \frac{REL_v}{T_a - T_\infty} \tag{2.38}$$

Again introducing the dimensionless parameters,

$$\widetilde{h} = \frac{Rh_c}{K} \quad \text{and} \quad \widetilde{N} = \frac{EL_vR}{K\left(T_a - T_\infty\right)}.$$

$$\left.\frac{d\widetilde{T}}{d\widetilde{r}}\right|_{\text{skin surface}} = -\widetilde{h}\widetilde{T} - \widetilde{N} \tag{2.39}$$

From equation (2.36) and (2.37) we get,

$$C_2\sqrt{V}K_1(\sqrt{V}\widetilde{r}) = 0, \quad \text{since} \quad K_1(\sqrt{V}\widetilde{r}) \neq 0, \, C_2 = 0 \text{ gives}$$

$$\frac{d\widetilde{T}}{d\widetilde{r}} = -\frac{1}{V}\left[C_1\sqrt{V}I_1(\sqrt{V}\widetilde{r})\right].$$

Right Boundary at skin surface is also given as

$$\frac{d\widetilde{T}}{d\widetilde{r}} = -\widetilde{h}\widetilde{T} + \widetilde{N} \qquad \text{at } \widetilde{r} = R, \, \widetilde{r} = 1,$$

30

$$\text{so, } -\widetilde{h}\widetilde{T} + \widetilde{N} = -\frac{1}{V}\left[C_1\sqrt{V}I_1(\sqrt{V})\right],$$

$$\text{or, } -\widetilde{h}\left[\frac{U}{V} - \frac{1}{V}\phi\right] + \widetilde{N} = -\frac{1}{V}\left[C_1\sqrt{V}I_1(\sqrt{V})\right],$$

$$\text{therefore, } -\widetilde{h}\left[\frac{U}{V} - \frac{1}{V}\left(C_1 I_0(\sqrt{V}\widetilde{r}) + 0.K_0(\sqrt{V}\widetilde{r})\right)\right] + \widetilde{N} = -\frac{1}{V}\left[C_1\sqrt{V}I_1(\sqrt{V})\right].$$

The calculation yields the value of constant C_1 as

$$C_1 = \left[\frac{\widetilde{h}U + \widetilde{N}V}{\widetilde{h}I_0(\sqrt{V}) + \sqrt{V}I_1(\sqrt{V})}\right].$$

Afrer calculation the solution for $\widetilde{T}$ is

$$\widetilde{T} = \frac{U}{V} - \frac{1}{V}\left[\frac{\left(\widetilde{h}U + \widetilde{N}V\right)I_0(\sqrt{V}\widetilde{r})}{\widetilde{h}I_0(\sqrt{V}) + \sqrt{V}I_1(\sqrt{V})}\right].$$

Finally a solution for T is

$$T = (T_a - T_\infty)\widetilde{T} + T_\infty$$

$$= T_\infty + (T_a - T_\infty)\left[\frac{U}{V} - \frac{1}{V}\left\{\frac{\left(\widetilde{h}U + \widetilde{N}V\right)I_0(\sqrt{V}\widetilde{r})}{\widetilde{h}I_0(\sqrt{V}) + \sqrt{V}I_1(\sqrt{V})}\right\}\right]. \tag{2.40}$$

2.5.5 Analytical Results and Discussion

To determine the impact of these variables on the distribution of body temperature, the values of physical and physiological parameters from various works of literature are summarized in Table 2.1. Simulated results with and without sweat evaporation have been exihibted in Figures 2.2 – 2.6 to observe the effect of different atmospheric temperatures, thermal conductivities, blood perfusion rates, and metabolic heat generation.

Graphs in Figure 2.2 show the body temperature decreasing from the body core towards the skin surface in the case of lower environmental temperature than the body core temperature. The graphs in right-hand Figure 2.2 reveal that the body temperature decreases more quickly towards the skin surface than in left-hand Figure 2.2, this is due to the evaporation effect. On the contrary, in the case of high atmospheric temperature, the body temperature increases from the core of the body towards the skin surface, the graphs in right-hand Figure 2.3 show that the temperature increases

Table 2.1: Thermophysical parameters [77, 78, 123]

Parameters	Symbols	Values	Units
Thermal Conductivities	K	0.48	W/m$\,°CC$
Blood specific heat	c_b	3850	J/kg$\,°CC$
Blood density	ρ_b	1000	kg/m^3
Blood perfusion rate	w_b	3	kg/m$^3\,s$
Metabolism	q_m	1085	W/m^3
Arterial temperature	T_a	37	°C
Convectional heat transfer coefficient	h_c	10.023	W/m$^2\,°$C
Latent heat of vaporization	L_v	2400000	J/kg
Evaporation rate	E	0.00004	kg/s
Environmental temperature	T_s	28	°C
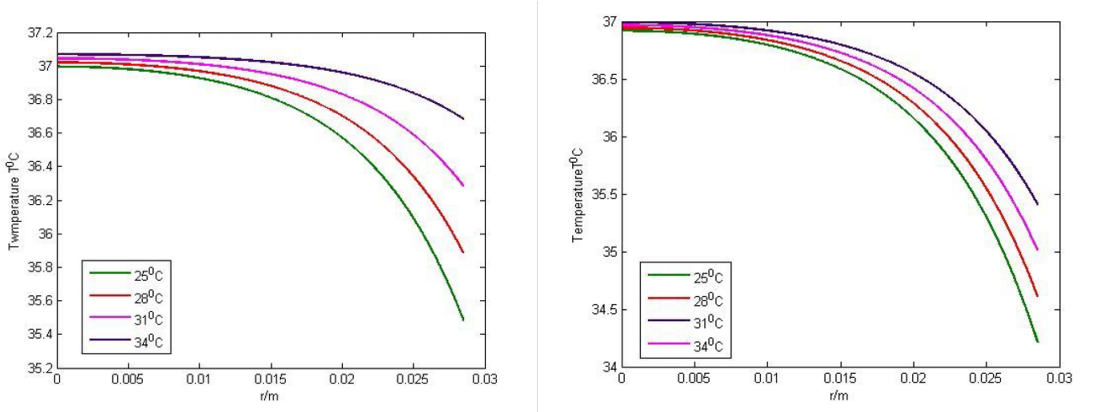
Figure 2.2: Temperature profile along radial direction with $T_\infty \leq 37°$C when (left) evaporation $(E = 0)$ and (right) evaporation $(E \neq 0)$.

more slowly towards the skin surface than in the graphs in left-hand Figure 2.3. This is due to the presence of sweat, which helps cool down the body temperature. According to left-hand Figure 2.4, the temperature of the body inside rises as thermal conductivity grows, whereas the temperature of the body's surface falls rapidly in right-hand Figure 2.4, due to the impact of sweat evaporation. The graphs in the left and right halves of Figure 2.6 show that the temperature in the radial direction decreases as blood perfusion rises. In the right-hand Figure 2.5 in comparison with the left-hand Figure 2.6, the temperature decreases sharply as it approaches the body's surface because of the evaporation effect and blood perfusion.

As seen in the graphs on the left-hand and right-hand Figure 2.6, the values of metabolic heat generation have a slight impact on the distribution of body temperature. The change in metabolic heat from $542\,$W/m^3 to 1085 W/m^3 make the
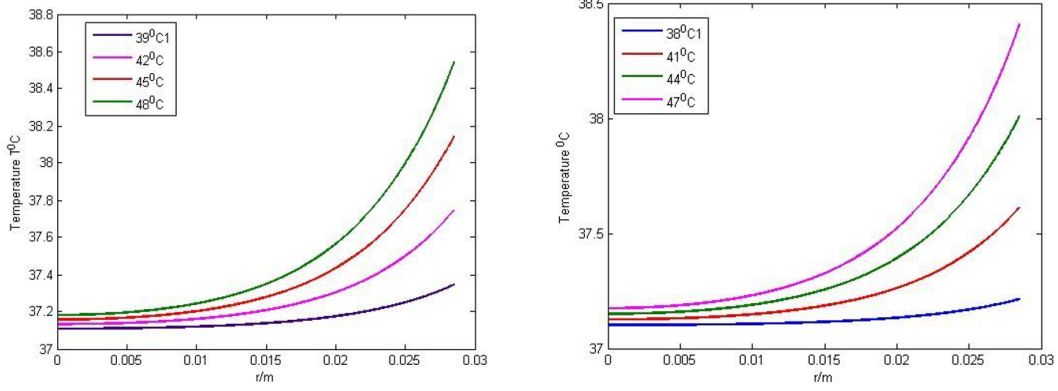
Figure 2.3: Temperature profile along radial direction with $T_\infty \leq 37°C$ when (left) evaporation ($E = 0$) and (right) evaporation ($E \neq 0$).
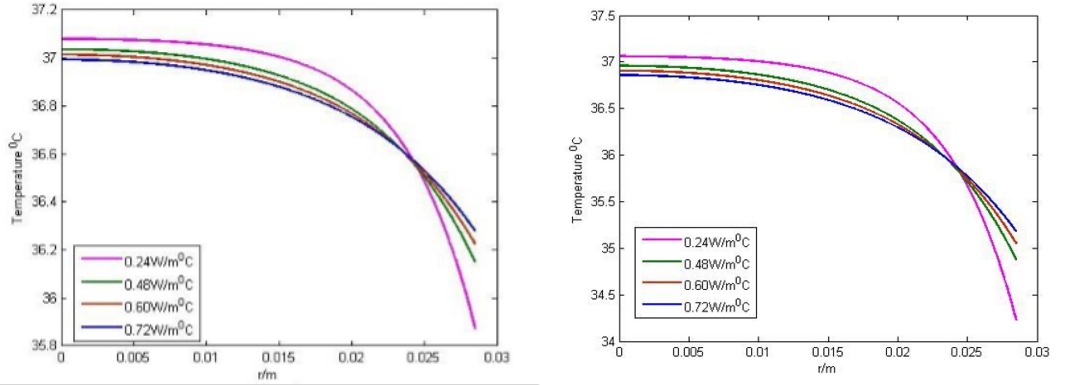
Figure 2.4: Temperature profile for different values of thermal conductivities when (left) evaporation ($E = 0$) and evaporation ($E \neq 0$).

small change in body temperature almost 0.1°C whereas its effect on the skin surface is negligible. This happens due to the negligible concentration of blood vessels toward the skin surface. The impact of metabolic heat is essentially nonexistent when sweat evaporation is present, as seen in the right-hand Figure 2.6.

2.6 One Dimensional Transient Bioheat Transfer Model

The bioheat transfer problem changes into a transient state or unsteady condition when the temperature T is a function of both the spatial variable r and the time variable t. Equation (2.21) is the Pennes model's one-dimensional transient bioheat equation. We use the Finite Difference (FD) approach in achieving the numerical solution of Pennes' one-dimensional model after obtaining an analytical solution for
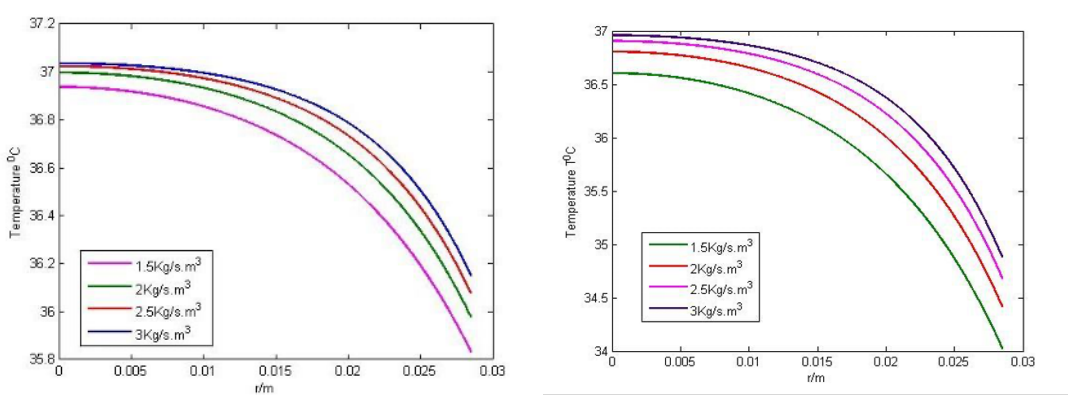
Figure 2.5: Temperature profile for different rates of blood perfusion when (left) evaporation ($E = 0$) and (right) evaporation ($E \neq 0$).
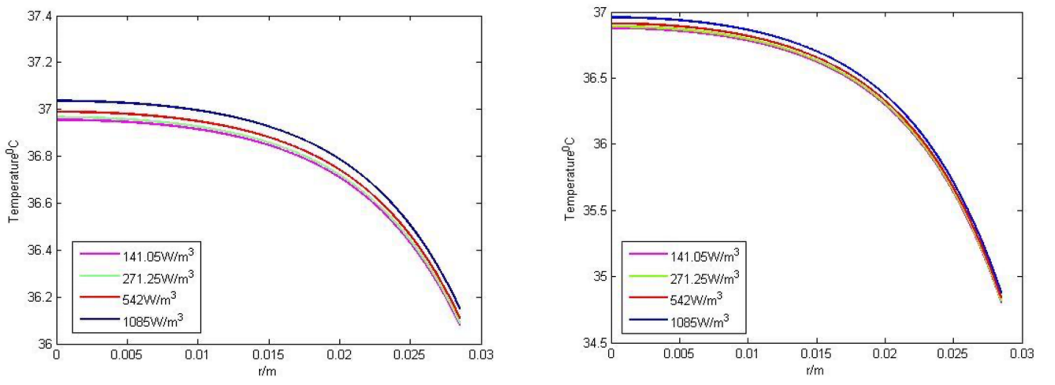
Figure 2.6: Temperature profile for different metabolic rates when (left) evaporation ($E = 0$) and (right) evaporation ($E \neq 0$).

the steady state case. Rewriting (2.21)

$$\rho c \frac{\partial T}{\partial t} = K \left[\frac{1}{r} \frac{\partial}{\partial r} \left(r \frac{\partial T}{\partial r} \right) \right] + \rho_b w_b c_b (T_a - T) + q_m, \qquad \text{in } \Omega_r. \qquad (2.41)$$

The primary assumption of this model is that the temperature depends on both the spatial variable r and the time variable t. The computational domain is cylindrical symmetry and heat flow always occurs in the radial direction, not only in the steady state-case but also in various time steps. The thermal conductivity and all other control parameters are taken into account and tabulated in Table 2.1. The spatial domain is discretized into a finite collection of points for computing purposes, as shown in Figure 2.7.
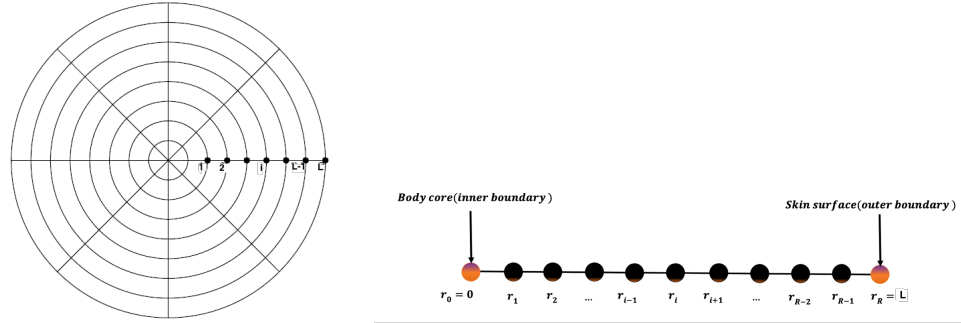
Figure 2.7: (left) Circular limb of the human body part and (right) spatial discretization in radial direction.

2.6.1 Numerical Approach for Bioheat Transfer Equation

Even though an analytical approach is a powerful tool for solving a PDE, the actual problem with complicated geometry cannot be solved using this approach. The numerical simulation methodology turns into an alternative method for obtaining an approximation of the answer to such a challenging problem. The two main components of numerical systems are accuracy and stability. In the subject of biomathematics, a number of methods have been created and are frequently used to find solutions to such heterogeneous problems. These methods include the finite difference method (FDM), the finite element method (FEM), and the finite volume method (FVM). The linear equation in this thesis work has been solved using FDM, in Chapter 2 – 4, while the nonlinear bioheat transport equations have been solved using FVM, later in Chapter 5.

2.6.2 Finite Difference Scheme

L. Euler employed the Finite Difference Method (FDM) for the first time in 1768. Additionally, C. Runge expanded it in the case of two dimensions in 1908. The foundational theoretical article by Courant, Friedrichs, and Lewy from 1928 contain the solution to the mathematical physics issues using finite differences. Before the 1960s, numerical applications and theoretical findings regarding the accuracy, stability, and convergence of finite-difference techniques had been published [10, 22, 86, 90]. In the field of physics and engineering, the FDM has recently emerged as one of the most popular methods for the numerical solution of partial differential equations. In the year 1999, Liu et al. [71] used the FDM to simulate and study the Pennes' bioheat equation in a triple-layered skin structure made up of the epidermis, dermis, and sub-

cutaneous tissues.

Euler's explicit method, Euler's implicit method, and Crank-Nicolson (CN) [21] methods are the three main schemes for the finite difference method. The implicit and CN schemes are more stable than the explicit system. In numerical computations, the implicit technique has been used to obtain better results. In this method, the derivative at each grid point is approximated by difference equations at nearby grid points by discretizing the computational domain into a uniform collection of intervals in each spatial coordinate. Compared to an explicit scheme, an implicit scheme is unconditionally more stable. The accuracy of the numerical solution is determined by the increase in the number of points [10, 22, 70, 81]. Harfash A.J. in 2008 [43] developed a high accuracy finite difference scheme for a three-dimensional micoscale heat transport equations. They have used a fourth order compact Finite Difference scheme with Crank-Nicolson technique to prove the unconditional stability and computationally more accurate than second order in Zhao et.al. [124].

2.6.2.1 Finite Difference Framework

The computing cylindrical domain, $(0 \leq r \leq L)$, is discretized into uniform intervals in each spatial coordinate having total R numbers of steps in r direction to create a grid in the finite difference framework, where $\Delta r = L/R$. In the center of the computing area, central finite difference techniques can be applied; however, near the boundaries, special boundary stencils are required. The employment of a boundary stencil that is equally accurate as the inner stencil is preferred from the perspective of accuracy. However, due to stability issues, the boundary stencil's accuracy is frequently reduced [45, 81, 90, 116].

The discretized finite number of points in space $[0, L]$ and time $[0, N]$ are shown in Figure 2.8. The open squares stand for known initial values, closed squares for known boundary values, and open circles for interior nodes to be filled by this method.

2.6.2.2 Taylor's Series Expansion

The key technique of FD approximation is the consequence of Taylor series expansion. Recalling Taylor series expansion for T(r) about the point r_0 is

$$\frac{\partial T}{\partial r} = \lim_{\Delta r \to 0} \frac{T(r_0 + \Delta r) - T(r_0)}{\Delta r}. \tag{2.42}$$
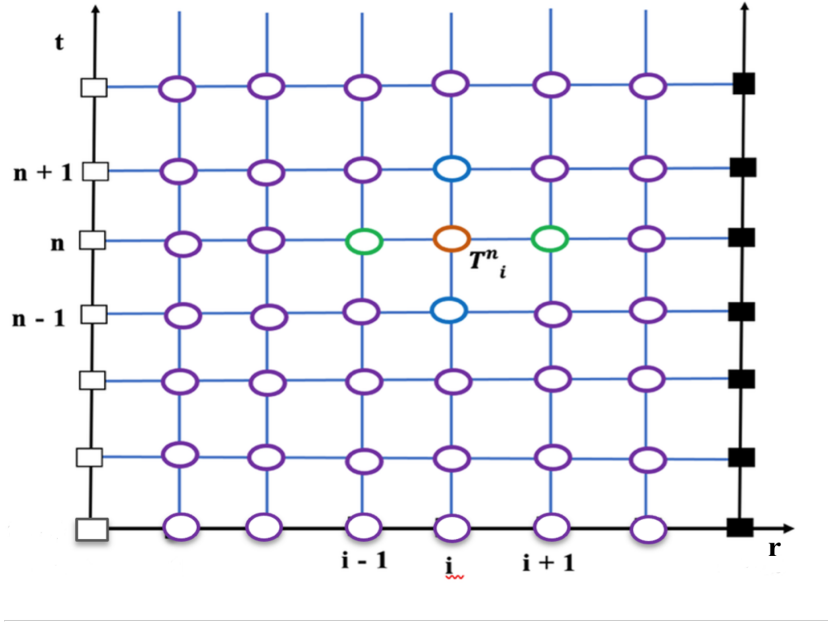
Figure 2.8: Discretization of mesh in FD scheme with open square for flux boundary, closed square for Robin's boundary with known values and open circles for interior nodes

The reasonable approximation of $\dfrac{\partial T}{\partial r}$ for a sufficiently small but finite Δr.

Forward Difference Scheme

The Taylor series expansion for $T(r)$ about the point r_i (positive r) is given by

$$T(r_i + \Delta r) \;=\; T(r_i) + \Delta r \left.\frac{\partial T}{\partial r}\right|_{r_i} + \frac{\Delta r^2}{2}\left.\frac{\partial^2 T}{\partial r^2}\right|_{r_i} + \frac{\Delta r^3}{3!}\left.\frac{\partial^3 T}{\partial r^3}\right|_{r_i} + \cdots \qquad (2.43)$$

Backward Difference Scheme

The Taylor series expansion for $T(r)$ about the point r_i (negative r) is given by

$$T(r_i - \Delta r) \;=\; T(r_i) - \Delta r \left.\frac{\partial T}{\partial r}\right|_{r_i} + \frac{\Delta r^2}{2}\left.\frac{\partial^2 T}{\partial r^2}\right|_{r_i} - \frac{\Delta r^3}{3!}\left.\frac{\partial^3 T}{\partial r^3}\right|_{r_i} + \cdots \qquad (2.44)$$

The basis for developing finite difference approximations for the first derivative $\dfrac{\partial T}{\partial r}$, at r_0 can be formed from the rearrangement of these two expressions (2.43) and (2.44) for forward and backward respectively

$$\left.\frac{\partial T}{\partial r}\right|_{r_i} \;=\; \frac{T(r_i + \Delta r) - T(r_i)}{\Delta r} - \frac{\Delta r}{2}\left.\frac{\partial^2 T}{\partial r^2}\right|_{r_i} - \frac{\Delta r^2}{3!}\left.\frac{\partial^3 T}{\partial r^3}\right|_{r_i} + \cdots \qquad (2.45)$$

$$\frac{\partial T}{\partial r}\bigg|_{r_i} = \frac{T(r_i) - T(r_i - \Delta r)}{\Delta r} - \frac{\Delta r}{2}\frac{\partial^2 T}{\partial r^2}\bigg|_{r_i} + \frac{\Delta r^2}{3!}\frac{\partial^3 T}{\partial r^3}\bigg|_{r_i} - \cdots \quad (2.46)$$

higher-order derivatives, as well as nodal values of T, are present in the first derivative expression, as expected. We cannot achieve our goal by including these higher-order derivatives in the approximation because they are obviously unknown. Since there is no better representation, we create an error term to stand in for all higher-order derivatives in equations (2.45) and (2.46) containing the following terms:

$$\frac{\partial T}{\partial r}\bigg|_{r_i} = \frac{T(r_0 + \Delta r) - T(r_0))}{\Delta r} + \mathcal{O}(\Delta r), \quad (2.47)$$

$$\frac{\partial T}{\partial r}\bigg|_{r_i} = \frac{T(r_0) - T(r_0 - \Delta r))}{\Delta r} + \mathcal{O}(\Delta r), \quad (2.48)$$

where $\mathcal{O}(\Delta r)$ is the order of truncation error or discretization error associated with the finite difference approximation. This represents the difference between the derivative and its finite difference representation. The infinite Taylor series was terminated after a few terms in order to get the expression for the derivative that is being approximated, hence the name "truncation error."

$$\mathcal{O}(\Delta r) = \frac{\partial T}{\partial r}\bigg|_{r_i} - \frac{T(r_i + \Delta r) - T(r_i)}{\Delta r} - \frac{\Delta r}{2}\frac{\partial^2 T}{\partial r^2}\bigg|_{r_i} - \frac{\Delta r^2}{3!}\frac{\partial^3 T}{\partial r^3}\bigg|_{r_i} + \cdots \quad (2.49)$$

Central Difference Scheme

The central difference approximation is obtained by subtracting equation (2.48) from equation (2.47)

$$\frac{\partial T}{\partial r}\bigg|_{r_i} = \frac{T(r_0 + \Delta r) - T(r_0 - \Delta r))}{2\Delta r} + \mathcal{O}[(\Delta r)^2] \quad (2.50)$$

where

$$\mathcal{O}[(\Delta r)^2] \equiv \frac{(\Delta r)^2}{3!}\frac{\partial^3 T}{\partial r^3}\bigg|_{r_i} + \frac{(\Delta r)^4}{5!}\frac{\partial^5 T}{\partial r^5}\bigg|_{r_i} + \cdots \quad (2.51)$$

The truncation error in central difference approximation approaches zero very faster than that in the case of backward and forward given in expression (2.51).

After removing the error terms $\mathcal{O}[(\Delta r)]$, from equation (2.47) and (2.48), $\mathcal{O}[(\Delta r)^2]$

from equation (2.50), and the use of $T_i \approx T(r_i)$, $T_{i+1} \approx T(r_i + \Delta r)$ and $T_{i-1} \approx T(r_i - \Delta r)$, the approximate solution for the exact solution in the corresponding equations, respectively yield

$$\left. \frac{\partial T}{\partial r} \right|_{r_i} \approx \frac{T_{i+1} - T_i}{\Delta r}. \tag{2.52}$$

$$\left. \frac{\partial T}{\partial r} \right|_{r_i} \approx \frac{T_i - T_{i-1}}{\Delta r}. \tag{2.53}$$

$$\left. \frac{\partial T}{\partial r} \right|_{r_i} \approx \frac{T_{i+1} - T_{i-1}}{2\Delta r}. \tag{2.54}$$

2.6.2.3 Second Order Central Difference Scheme

We again manipulate the Taylor series expansion about $T(r)$ of the equation (2.50) to get the central difference approximation for second order derivative.

$$\left. \frac{\partial^2 T}{\partial r^2} \right|_{r_i} = \frac{T(r_0 + \Delta r) - 2T(r_0) + T(r_0 - \Delta r)}{(\Delta r)^2} + \mathcal{O}[(\Delta r)^2], \tag{2.55}$$

where
$$\mathcal{O}[(\Delta r)^2] \equiv \frac{(\Delta r)^2}{12} \left. \frac{\partial^4 T}{\partial r^4} \right|_{r_i} + \cdots,$$

after removing the error term $\mathcal{O}\left[(\Delta r)^2\right]$, second order in space from equation (2.55), approximate the derivative as follows:

$$\left. \frac{\partial^2 T}{\partial r^2} \right|_{r_i} \approx \frac{T_{i-1} - 2T_i + T_{i+1}}{(\Delta r)^2.} \tag{2.56}$$

2.6.3 Different Forms of Finite Difference Scheme for Transient Case

In the transient case, the equation includes both derivatives with respect to time and space. If R and J be the total number of steps in r and t directions, $\Delta r = L/R$ and $\Delta t = N/J$ be the step sizes in r and t directions, respectively. In the limit, the answer using such a numerical technique converges to the true value with the exact solution as the mesh spacing (Δr and Δt) in the cylindrical version of the equation goes to zero. As mentioned above, there is a brief description of the three distinct systems in the transient condition with time domain ($0 \leq t \leq N$) and the space domain ($0 \leq r \leq L$).

2.6.3.1 Euler's Explicit Method

The first order time derivative in forward scheme of equation (2.41) is

$$\frac{\partial T}{\partial t} = \frac{[T(r, t + \Delta t) - T(r, t)]}{\Delta t} + \mathcal{O}(\Delta t). \tag{2.57}$$

With truncation error $\mathcal{O}(\Delta t) = \frac{\Delta t}{2} \frac{\partial T}{\partial t}$. We approximate first order time derivative with forward scheme at the point at (r_i, t_n) is given by

$$\left. \frac{\partial T}{\partial t} \right|_{t_n, r_i} \approx \frac{T_i^{n+1} - T_i^n}{\Delta t} \tag{2.58}$$

Using central difference approximation for first and second order derivative of T at r_i for all terms at time step t_n, we get

$$\left. \frac{\partial T}{\partial r} \right|_{t_n, r_i} \approx \frac{T_{i+1}^n - T_{i-1}^n}{2\Delta r} \tag{2.59}$$

$$\left. \frac{\partial^2 T}{\partial r^2} \right|_{t_n, r_i} \approx \frac{T_{i-1}^n - 2T_i^n + T_{i+1}^n}{(\Delta r)^2}. \tag{2.60}$$

2.6.4 Euler's Implicit Method

The first order time derivative in backward scheme of equation (2.41) is

$$\frac{\partial T}{\partial t} = \frac{[T(r, t) - T(r, t - \Delta t)]}{\Delta t} + \mathcal{O}(\Delta t). \tag{2.61}$$

With truncation error $\mathcal{O}(\Delta t) = \frac{\Delta t}{2} \frac{\partial T}{\partial t}$. We approximate first order time derivative with forward scheme at the point at (r_i, t_{n+1}) is given by

$$\left. \frac{\partial T}{\partial t} \right|_{t_{n+1}, r_i} \approx \frac{T_i^{n+1} - T_i^n}{\Delta t}. \tag{2.62}$$

Using central difference apprroximation of first and second order derivative of T at r_i for all terms at time step t_{n+1}, we get

$$\left. \frac{\partial T}{\partial r} \right|_{t_{n+1}, r_i} \approx \frac{T_{i+1}^{n+1} - T_{i-1}^{n+1}}{2\Delta r} \tag{2.63}$$

$$\left. \frac{\partial^2 T}{\partial r^2} \right|_{t_{n+1}, r_i} \approx \frac{T_{i-1}^{n+1} - 2T_i^{n+1} + T_{i+1}^{n+1}}{(\Delta r)^2}. \tag{2.64}$$

2.6.5 Crank-Nicolson Scheme

For the purpose of improving the temporal accuracy, two Taylor series expansions must be employed for the time derivative. Though the Crank-Nicolson scheme is the combination of Euler's Explicit method and Euler's Implicit method, in this method the governing equation is satisfied neither at time index n in Explicit nor at time index $n+1$ in Implicit. It is satisfied at $n+\frac{1}{2}$.

We first think about the time step size $\frac{\Delta t}{2}$ in the Crank-Nicolson approach in an analogous manner. The time instant $t+\frac{\Delta t}{2}$ is represented by the time index $n+\frac{1}{2}$. We won't actually use these time instants or time indices. They are just inserted to facilitate derivation, and they will be removed in the course of that process. The extension of Taylor's series is then carried out in two steps: first, the solution at $t+\Delta t$ is extended about the solution at $t+\frac{\Delta t}{2}$, followed by the solution at $t+\frac{\Delta t}{2}$, and last, the solution at t. The following is a description of the processes:

$$T_i^{n+1} \;=\; T_i^{n+\frac{1}{2}} + \frac{\Delta t}{2}\left.\frac{\partial T}{\partial t}\right|_{i,n+\frac{1}{2}} + \frac{1}{2}\left(\frac{\Delta t}{2}\right)^2\left.\frac{\partial^2 T}{\partial t^2}\right|_{i,n+\frac{1}{2}} + \frac{1}{6}\left(\frac{\Delta t}{2}\right)^3\left.\frac{\partial^3 T}{\partial t^3}\right|_{i,n+\frac{1}{2}} + \cdots \quad (2.65)$$

$$T_i^{n} \;=\; T_i^{n+\frac{1}{2}} - \frac{\Delta t}{2}\left.\frac{\partial T}{\partial t}\right|_{i,n+\frac{1}{2}} + \frac{1}{2}\left(\frac{\Delta t}{2}\right)^2\left.\frac{\partial^2 T}{\partial t^2}\right|_{i,n+\frac{1}{2}} - \frac{1}{6}\left(\frac{\Delta t}{2}\right)^3\left.\frac{\partial^3 T}{\partial t^3}\right|_{i,n+\frac{1}{2}} + \cdots \quad (2.66)$$

Subtracting and rearranging, we get

$$\frac{T_i^{n+1} - T_i^{n}}{\Delta t} \;=\; \frac{\partial T}{\partial t} + \frac{(\Delta t)^2}{24}\left.\frac{\partial^3 T}{\partial t^3}\right|_{i,n+\frac{1}{2}} + \cdots$$

$$\frac{T_i^{n+1} - T_i^{n}}{\Delta t} \;=\; \frac{\partial T}{\partial t} + \mathcal{O}\left[(\Delta t)^2\right]. \qquad (2.67)$$

After removing the error term $\mathcal{O}\left[(\Delta t)^2\right]$, second order in time from equation (2.67), approximate the derivative as follows:

$$\frac{\partial T}{\partial t} \;\approx\; \frac{T_i^{n+1} - T_i^{n}}{\Delta t}. \qquad (2.68)$$

The second derivative term in spacial direction with eliminating the second order error term can be written in similar manner

$$\frac{\partial^2 T}{\partial r^2} \;\approx\; \frac{T_{i-1}^{n+\frac{1}{2}} - 2T_i^{n+\frac{1}{2}} + T_{i+1}^{n+\frac{1}{2}}}{(\Delta r)^2}. \qquad (2.69)$$

In reality, the quantities on the right-hand side of (2.69) must be further approxima-tions because there is no temporal node at $n + \frac{1}{2}$.

$$T_i^{n+1} \approx \frac{T_i^n + T_i^{n+1}}{2} - \frac{1}{8}\frac{\partial^2 T}{\partial r^2}. \tag{2.70}$$

When the corresponding value from equation (2.70) is substituted into equation (2.69), we obtain

$$\frac{\partial^2 T}{\partial r^2} \approx \frac{1}{2}\left[\frac{T_{i-1}^n - 2T_i^n + T_{i+1}^n}{(\Delta r)^2} + \frac{T_{i-1}^{n+1} - 2T_i^{n+1} + T_{i+1}^{n+1}}{(\Delta r)^2}\right]. \tag{2.71}$$

2.7 Finite Difference Scheme for Bioheat Equation

In the one-dimensional spatial domain ($0 \leq r \leq L$) and the time domain ($0 \leq t \leq N$), we consider the temperature, T as a function of r and t. We then use the FD scheme to obtain a discrete difference equation that approximates the continuous partial differential equation for $T(r, t)$ at a finite set of r in Ω_r. By increasing the number of meshes, the numerical solution can be made more accurate. Central difference methods are employed in the interior of the computational domain, while special boundary stencils are required at the boundary to make it as accurate as an interior stencil.

2.7.1 Euler Explicit Method for Bioheat Equation

Using the corresponding difference approximations (2.58), (2.59) and (2.60) into the bioheat transfer equation (2.41) yields

$$\rho c \frac{T_i^{n+1} - T_i^n}{\Delta t} = K\left[\frac{T_{i-1}^n - 2T_i^n + T_{i+1}^n}{(\Delta r)^2} + \frac{1}{r_i}\frac{T_{i+1}^n - T_{i-1}^n}{2\Delta r}\right] + W_b c_b\left(T_a - T_i^{n+1}\right) + q_m.$$

$$T_i^{n+1} = T_i^n + \frac{D\Delta t}{(\Delta r)^2}\left[T_{i-1}^n - 2T_i^n + T_{i+1}^n + \frac{\Delta t}{2r_i}\left(T_{i+1}^n - T_{i-1}^n\right)\right]$$

$$+ M\Delta t\left(T_a - T_i^{n+1}\right) + S\Delta t, \tag{2.72}$$

$$\text{where,}\quad D = \frac{K}{\rho c},\quad \lambda = \frac{D\Delta t}{(\Delta r)^2},\quad \text{and}\quad \mu = D\frac{\Delta t}{\Delta r}$$

$$\text{and}\quad M = \frac{W_b c_b}{\rho c},\quad S = \frac{q_m}{\rho c},\quad \text{and}\quad F = \Delta t\left(MT_a + S\right).$$

$$T_i^{n+1} = \left(\lambda - \frac{\mu}{2r_i}\right)T_{i-1}^n + \left(1 - 2\lambda - M\Delta t\right)T_i^n + \left(\lambda + \frac{\mu}{2r_i}\right)T_{i+1}^n + F, \tag{2.73}$$

$$\text{with } i = 1, 2 \cdots, R - 1.$$

2.7.1.1 Stability Criteria for Explicit Method

The condition for numerically stable of explicit scheme (2.73) is

$$1 - 2\lambda - M\Delta t \geq 0,$$

$$\text{or } 1 \geq (2\lambda + M\Delta t),$$

$$\text{or } \lambda \leq \frac{1 - M\Delta t}{2},$$

$$\text{therefore } \lambda \leq \frac{1 - M\Delta t}{2} = \frac{1}{2} - \frac{M\Delta t}{2} \leq \frac{1}{2}.$$

The explicit scheme is only stable and the approximations in this scheme iterate to steady-state only for the suitable small time step size which is ≤ 0.5. The explicit scheme, therefore, is conditionally stable. This criteria is called CFL stability criteria (after Courant–Friedrichs–Lewy (CFL)).

2.7.2 Euler Implicit Method for Bioheat Equation

Finite difference equation for (2.41) using Implicit scheme, we get as

$$\frac{\rho c}{\Delta t} \left[T_i^{n+1} - T_i^n \right] = K \left[\frac{T_{i-1}^{n+1} - 2T_i^{n+1} + T_{n+1}^{n+1}}{(\Delta r)^2} \right] + \frac{K}{r_i} \left[\frac{T_{n+1}^{n+1} - T_{n-1}^{n+1}}{2\Delta r} \right]$$
$$+ W_b c_b \left(T_a - T_i^{n+1} \right) + q_m, \qquad i = 1, 2 \cdots, R - 1, \qquad (2.74)$$

Further simplification yields

$$\left(-\lambda + \frac{\mu}{2r_i} \right) T_{i-1}^{n+1} + (1 + 2\lambda + M\Delta t) T_i^{n+1} + \left(-\lambda - \frac{\mu}{2r_i} \right) T_{i+1}^{n+1} - F = T_i^n, \qquad (2.75)$$
$$i = 1, 2 \cdots, R - 1.$$

Equation(2.75) is the Finite difference (FD) approximation for interior nodes of the equation (2.41).

2.7.3 FD Scheme for Inner Boundary (at Body Core) $r_0 = 0$

The radial distance is measured from the body core towards the skin surface in the cylindrical human body as shown in Figure 2.7. At the body core, both r and the

heat flux $\dfrac{\partial T}{\partial r}$, are zero, then $\dfrac{1}{r}\left(\dfrac{\partial T}{\partial r}\right)$ approaches to indeterminate form $\dfrac{0}{0}$ as $r \to 0$. Using L'Hospital rule,

$$\frac{1}{r}\frac{\partial T}{\partial r}\bigg|_{r=0} = \frac{\dfrac{\partial}{\partial r}\left(\dfrac{\partial T}{\partial r}\right)}{\dfrac{\partial}{\partial r}(r)}\bigg|_{r=0} = \frac{\partial^2 T}{\partial r^2}\bigg|_{r=0}.$$

In this case, FD approximation of equation (2.41) at $r = 0$ is

$$-2\lambda T_{-1}^{n+1} + (1 + 4\lambda + M)\, T_0^{n+1} - 2\lambda T_1^{n+1} - F \;=\; T_0^n. \tag{2.76}$$

The FD scheme for left boundary $\dfrac{\partial T}{\partial r} = 0$ at $r = 0$ is

$$T_{-1}^{n+1} \;=\; T_1^{n+1}. \tag{2.77}$$

Using equation (2.77) in equation (2.76), we obtain

$$(1 + 4\lambda + M\Delta t)T_0^{n+1} - 4\lambda T_1^{n+1} - F \;=\; T_0^n. \tag{2.78}$$

2.7.4   FD Scheme for Outer Boundary (Skin Surface) $r_R = L$

The central difference approximation is

$$T_{R+1}^{n+1} \;=\; T_{R-1}^{n+1} - \frac{2\Delta r h_c}{K}\left(T_R{}^{n+1} - T_\infty\right). \tag{2.79}$$

Then FD approximation at $r = R$ is

$$-2\lambda T_{R-1}^{n+1} + \left[(1 + 2\lambda + M\Delta t) - \left(-\lambda - \frac{\mu}{2r_R}\right)\frac{2h_c\Delta r}{K}\right] T_R^{n+1} + F_R - F = T_R^n, \tag{2.80}$$

where

$$F_R = \frac{2\Delta r B_R}{K}\left(h_c T_\infty\right).$$

Writing the equations (2.78), (2.75), and (2.80) in the matrix equation form

$$A\,T^{n+1} \;=\; T^n + B, \tag{2.81}$$

where

$$T^n = \begin{bmatrix} T_0^n & T_1^n & T_2^n & \cdots & T_R^n \end{bmatrix}',$$

A is the corresponding tridiagonal matrix of order $(R+1) \times (R+1)$, $T^{(n+1)}$ and B are of column vectors of order $(R+1) \times 1$.

$$A = \begin{bmatrix} E_0 & -4\lambda & 0 & 0 & \cdots & & 0 \\ D_1 & E_1 & B_1 & 0 & \cdots & & 0 \\ 0 & D_2 & E_2 & B_2 & \cdots & & 0 \\ \vdots & \vdots & \vdots & \ddots & \ddots & & \vdots \\ 0 & 0 & \cdots & \cdots & -2\lambda & \left(E_R - B_R \dfrac{2h_c \Delta r}{K} \right) \end{bmatrix},$$

$$T^{n+1} = \begin{bmatrix} T_0^{n+1} \\ T_1^{n+1} \\ T_2^{n+1} \\ \vdots \\ T_R^{n+1} \end{bmatrix}, \qquad \text{and} \qquad B = \begin{bmatrix} F \\ F \\ F \\ \vdots \\ F \\ F - F_R \end{bmatrix},$$

where

$$E_0 = (1 + 4\lambda + M\Delta t), \quad E_i = (1 + 2\lambda + M\Delta t), \qquad \text{for } i = 1, 2, \cdots . R$$

$$D_i = \left(-\lambda + \frac{\mu}{2r_i} \right), B_i = \left(-\lambda - \frac{\mu}{2r_i} \right), \qquad \text{for } i = 1, 2, \cdots, R.$$

2.7.5 Stability Analysis of Transient Model

To perform the solvability, consistency, stability, and convergence of FD scheme for T^{n+1}, we introduce a column vector T^n of size $(R+1) \times 1$ which represents the numerical solutions at time step t^n as

$$T^n = [T_0{}^n\ T_1{}^n \cdots T_N{}^n \cdots T_R{}^n]'.$$

Since the matrix A in equation (2.81) is invertible and diagonally dominant, the system is solvable. We have matrix $A = [a_{l,j}]_{(R+1)\times(R+1)}$

$$|a_{jj}| \ \geq \ \sum |a_{lj}| \quad \forall l, j.$$

Hence the system (2.81) is unconditionally solvable for each time step n.

To show the consistency of the model, we have approximated our model (2.41) by FD scheme in (2.78), (2.75), and (2.80), which has truncation error $\tau(\Delta r, \Delta t) =$

$\mathcal{O}\left[(\Delta r)^2 + \Delta t\right].$

So

$$\tau(\Delta r, \Delta t) = \mathcal{O}\left[(\Delta r)^2 + \Delta t\right],$$

as

$$\Delta r, \Delta t \to 0, \tau(\Delta r, \Delta t) \to 0,$$

therefore

$$\lim_{\Delta r, \Delta t \to 0} \tau(\Delta r, \Delta t) = 0.$$

So the model is consistent.

Theorem 2.7.1 (Gershgorin). *For each λ, the eigenvalues of a square matrix $A = [a_{l,j}]$ with size $(R+1) \times (R+1)$, for $j = 0, 1, 2, \cdots, R$.*

$$|\lambda - a_{l,j}| \leq \sum_{l=0,\, l \neq j} |a_{l,j}|. \tag{2.82}$$

As the consequence of the Gershgorin theorem 2.7.1, we have the following two inequalities.

(i)

$$|\lambda| \leq |\lambda - a_{j,j}| \leq \sum_{l=0,\, l \leq j} |a_{l,j}|.$$

(ii)

$$|\lambda| \geq |a_{j,j}| - |\lambda - a_{j,j}| \geq |a_{j,j}| - \sum_{l=0,\, l \leq j} |a_{l,j}|.$$

Lemma 2.7.1. *If λ_l for $l = 1, 2, \cdots, R$ represents the eigenvalues of the square matrix A and $\|.\|_2$ represents the second matrix norm $(\|A\|_2 = \max_l |\lambda_l|)$, then we have following results.*

(i)

$$|\lambda_l| \geq 1 + M\Delta t, \qquad \text{for } 1 \leq l \leq R.$$

(ii)

$$\left\|A^{-1}\right\|_2 \leq \frac{1}{1 + M\Delta t} \leq 1 - M^*\Delta t \leq 1, \qquad \text{for } 1 \leq l \leq R.$$

where M^* is the positive constant.

Proof. (i) For $l = 0$, We have

$$|a_{j,j}| = |1 + 4\lambda + M\Delta t|, \qquad \text{and} \qquad \sum_{l=0,\, l\neq j} |a_{l,j}| = |-4\lambda|,$$

$$|a_{j,j}| - \sum_{l=0,\, l\neq j} |a_{l,j}| = |1 + 4\lambda + M\Delta t| - |-4\lambda| \geq 1 + M\Delta t.$$

For $l = 1, 2, \cdots, R-1$, we have

$$|a_{j,j}| = |1 + 2\lambda + M\Delta t|,$$

and

$$\sum_{l=0,\, l\neq j} |a_{l,j}| = \left|-\lambda + \frac{\mu}{2r_l}\right| + \left|-\lambda - \frac{\mu}{2r_l}\right|,$$

$$|a_{j,j}| - \sum_{l=0,\, l\neq j} |a_{l,j}| = |1 + 2\lambda + M\Delta t| - \left|-\lambda + \frac{\mu}{2r_l}\right| + \left|-\lambda - \frac{\mu}{2r_l}\right| \geq 1 + M\Delta t.$$

Now from Gershgorin theorem 2.7.1 for each eigenvalues λ_l for $l = 0, 1, 2, \cdots, R$ of square matrix A in equation (2.81)

$$|\lambda_l| \geq |a_{j,j}| - \sum_{l=0,\, l\leq j} |a_{l,j}| \geq 1 + M\Delta t.$$

Hence,

$$|\lambda_l| \geq 1 + M\Delta t.$$

(ii)   We have

$$|\lambda_l| \geq 1 + M\Delta t.$$

$$\|A\|_2 = \max_{1\leq l\leq R} \{|\lambda_l|\}. \tag{2.83}$$

Without loss of generality, we can assume at least one value of A, satisfy (2.83), then A is diagonally dominant, so, A^{-1} exists, then

$$AA^{-1} = A^{-1}A = I.$$

We obtain,

$$A^{-1} = \frac{1}{A}I,$$

where, I is $(R+1) \times (R+1)$ unit matrix.

Now, taking norm on both sides,

$$\left\|A^{-1}\right\|_2 = \frac{1}{\|A\|} \|I\|,$$

47

or

$$\left\|A^{-1}\right\|_2 \leq \frac{1}{\max_{1 \leq l \leq R}} \left\{\|\lambda_l\|\right\}.$$

Therefore

$$\left\|A^{-1}\right\|_2 \leq \frac{1}{1 + M\Delta t} \leq 1 - M^*\Delta t \leq 1, \qquad \text{for } l = 0, 1, 2, \cdots, R.$$

□

Theorem 2.7.2. *The Finite Difference (FD) scheme* (2.81) *is stable with respect to initial data if*

$$\left\|E^{n+1}\right\|_2 \leq \left\|E^0\right\|_2, \qquad \text{for } n \geq 1, \tag{2.84}$$

where, E^{n+1} *is the error equation, obtained from difference between exact solution* $T^{*(n+1)}$ *and solution* $T^{(n+1)}$ *from FD scheme at time level* $(n+1)$.

Proof. We have error equation of (2.81) in the form of

$$E^{n+1} = A^{-1}E^n. \tag{2.85}$$

Using above relation (2.85) repeatedly, we get

$$E^{n+1} = (A^{-1})E^{n-1} = \cdots = [(A^{-1})^n E^\circ C], \qquad \text{for } n = 1, 2, \cdots, N. \tag{2.86}$$

The relation with second norm is

$$\left\|E^{n+1}\right\|_2 \leq \left\|A^{-1}\right\|_2^n \left\|E^0\right\|_2. \tag{2.87}$$

Using Lemma 1.1, we get

$$\left\|E^{n+1}\right\|_2 \leq \left\|E^0\right\|_2. \tag{2.88}$$

This shows that FD scheme (2.81) is uncondinally stable with respect to initial data.

□

In the limit as the mesh spacing Δr and Δt in the cylindrical form of bioheat transfer equation goes to zero, the solution from such numerical method converges to the true value with the exact solution as shown in next theorem.

Theorem 2.7.3 (Convergence)**.** *Finite difference schemes* (2.78)*,* (2.75)*, and* (2.80)*, are unconditionally convergence.*

Proof. Let us consider the error vector $\tilde{E}^{n+1}$ such that

$$\tilde{E}^{n+1} = \tilde{T}^{n+1} - T^{n+1}. \tag{2.89}$$

Where we have introduced the vector $\tilde{T}$ of size $(R+1) \times 1$ that represents the exact solution at the time step t^n such that

$$\tilde{T}^n = \left[T(r_0, t^n), T(r_1, t^n), T(r_2, t^n), ..., T(r_R, t^n) \right], \tag{2.90}$$

then, the matrix form with exact solution be

$$A\tilde{T}^{n+1} = \tilde{T}^n + B + \tau^{n+1}, \tag{2.91}$$

where τ^{n+1} is the vector of truncation error at level t^n. Now, the vector $\tilde{E}$ in (2.89) on the substraction of (2.81) from (2.91) gives the relation

$$
\begin{aligned}
\tilde{E}^{n+1} &= A^{-1}\tilde{E}^n + A^{-1}\tau^{n+1} \\
&= A^{-1}\left(A^{-1}\tilde{E}^{n-1} + A^{-1}\tau^n \right) + A^{-1}\tau^{n+1}.
\end{aligned}
$$

Using above relation (2.91) repeatedly, we get

$$\tilde{E}^{n+1} = (A^{-1})^n \tilde{E}^{\circ}C + \sum_{k=0} \left(A^{-1} \right)^k \tau^{n-k}. \tag{2.92}$$

Taking second norm on (2.92) we get,

$$\left\| \tilde{E}^{n+1} \right\|_2 \leq \left\| A^{-1} \right\|^n \left\| \tilde{E}^{\circ}C \right\|_2 + \left(\sum_{k=0}^{n} \left\| A^{-1} \right\|_2^k \right) \max_{1 \leq k \leq R} \left\{ \left\| \tau^k \right\|_2 \right\}.$$

As initially no error occurs at $t = 0$, we take $T^{\circ}C = 0$ and get $\tilde{E} = 0$
Applying $\|A^{-1}\|_2 \leq 1$ from lemma 1.1, we have

$$\left\| \tilde{E}^{n+1} \right\|_2 \leq \left(\sum_{k=o}^{n} \left\| A^{-1} \right\|_2^k \right) \max_{1 \leq k \leq R} \left\{ \left\| \tau^k \right\|_2 \right\}.$$

The truncation error $\tau(\Delta r, \Delta t)$ gives

$$\left\| \tau^k \right\|_2 \to 0 \text{ as } \Delta r \to 0, \ \Delta t \to 0.$$

Which implies

$$\left\| \tilde{E}^{n+1} \right\|_2 \to 0, \ \text{ as } 1 \leq k \leq R.$$

Hence the system is unconditionally convergent. $\qquad \square$

2.7.6   Numerical Results and Discussion

The different biological and thermophysical characteristics listed in Table 2.1 affect the numerical outcomes of the heat transfer model in living tissue. A cylindrical limb is evenly discretized into a certain number of nodes in the domain along the radial direction of heat flow from the body's core toward the skin surface. Figure 2.9 displays temperature profile for low (left) and high (right) heat transfer coefficients, while Figure 2.10 calculates temperature profiles for heat loss through lower (left) and greater (right) thermal conductivities at various time steps. The space domain's (tissue thickness') measurement is $L = 0.03$ m. The parameter values have been considered as [78, 123]

$$K = 0.48 \text{ W/m}^\circ\text{C}, \quad c_b = 1000 \text{ J/kg}^\circ\text{C}, \quad w_b = 3.5 \text{ kg/m}^3 \text{ sec}, \quad T_a = 37^\circ\text{C},$$
$$L_v = 24 \times 10^5 \text{J/kg}, \quad E = 4 \times 10^{-5} \text{ kg/s}, \quad \text{and } T_\infty = 22^\circ\text{C}.$$

The temperature profile for the two different values of thermal conductivity K, and heat transfer coefficients h_c are considered, respectively as

$$K = 0.24 \text{ W/m}^\circ\text{C}, \quad K = 0.24 \text{ W/m}^\circ\text{C},$$
$$h_c = 10.023, \text{W/m}^2 \,^\circ\text{C}, \quad h_c = 30.23 \text{ W/m}^2 \,^\circ\text{C},$$

and are represented by the graphs in Figures 2.9 and 2.10, from the system of equation (2.81).
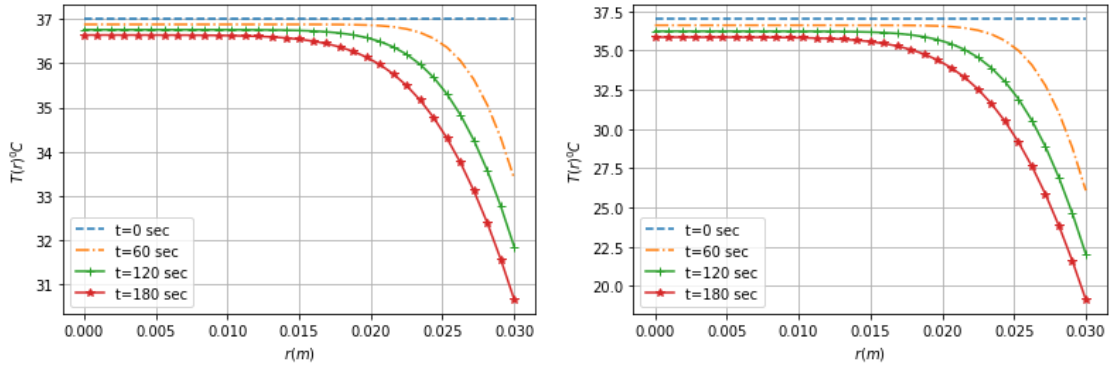
Figure 2.9:   Radial temperature profile at (left) $h_c = 10.023 \text{ W/m}^2 \,^\circ\text{C}$ and (right)$h_c = 30.023 \text{ W/m}^2 \,^\circ\text{C}$.

The surface of naked human body directly interacts with the outside environment, where the convection and radiation heat transfer coefficients are present. The striking impact of varied heat transfer coefficients for temperature distribution with temper-
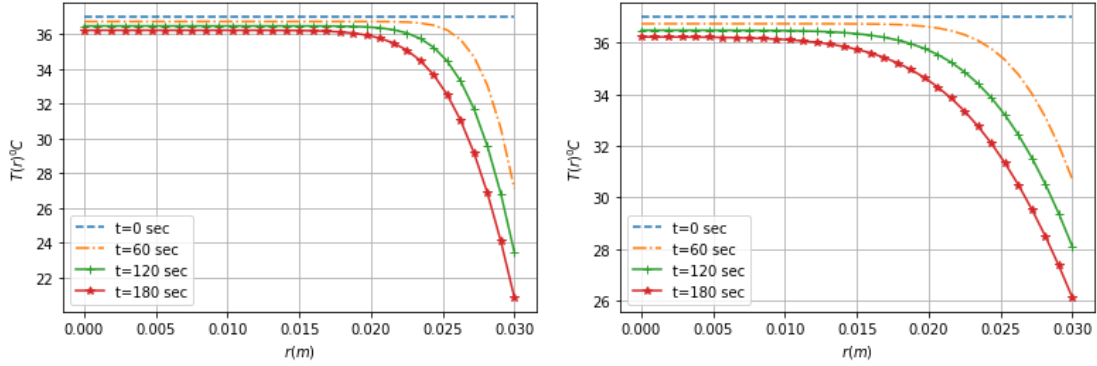
Figure 2.10: Radial temperature profile at (left) $K = 0.24 \, \text{W/m} \, ^\circ\text{C}$ and (right) $K = 0.72 \, \text{W/m} \, ^\circ\text{C}$.

ature profile at rest, 60 sec, 120 sec, and 180 sec is depicted in Figure 2.9. After reaching a specific radial distance from the body's center, the temperature in the skin is steady state and gradually decreases as it approaches the skin's surface. In the left-hand Figure, 2.9 the temperature at the skin's surface is 33°C after 60 sec, 31°C after 120 sec, and 29°C after 180 sec. On the other hand, in the right-hand Figure 2.9, the rate at which the body's core heats up the skin as it approaches the skin's surface slows noticeably.

The graphs in the picture illustrate how various thermal conductivities affect the skin's temperature, which up to a given radial distance is uniform like in the case of heat transfer coefficients or steady-state. The temperature at the skin's surface then rapidly drops to 31°C in 60 sec, 29°C in 120 sec, and 27°C in 180 sec, as in the left-hand Figure 2.10. In the right-hand Figure 2.10, it is found that the temperature profile in the skin drops smoothly downward from the body's center to the skin's surface. The temperature reaches 33.7°C in 60 sec, 32°C in 120 sec, and goes up to 29°C in 180 sec. The result shows that skin surface temperature increases with the increase in thermal conductivities.

2.8 Conclusion

In order to analyze the heat transfer coefficient and conduction effect in the cylindrical shape of the human body, the analytical solution of the one-dimensional Pennes bioheat equation in cylindrical form with mixed boundary conditions and the latent heat of sweat evaporation in a steady-state case has been obtained. This has been followed by a numerical solution using the implicit finite difference method. Using

the analytical and numerical solutions produced in this model, the effects of the temperature changes in different air temperatures, thermal conductivities, metabolic heat generation rates, blood perfusion rates, and heat exchange coefficients have been individually observed. In order to investigate the derived numerical FD scheme for the transient model, various theorems with justifications for its consistency, stability, and convergence have been established.

The analytical investigation reveals that factors such as air temperature, blood perfusion rates and heat transfer coefficients have a greater impact on skin surface temperature than that on the body core. As the ambient temperature, blood perfusion rates, and heat transfer coefficients rise, the temperature in the radial direction falls. It is possible to detect a very small change in body core temperature as well as a slight rise in metabolic heat production, both of which have very little impact on the skin's surface. In comparison to the scenario proposed by Luitel et al. and Yue K. et al. [73, 77, 123], the various parameters utilized in this model certainly have a notable impact on the temperature distribution in the human body. The numerical results verify that as the heat transfer coefficient increases in the various time steps, the temperature at the skin surface goes down significantly. The temperature on the skin surface rises as thermal conductivity increases. The graphs demonstrate that a major portion of the heat loss from the skin surface is due to heat transfer coefficients. This Chapter provides an essential and comprehensive overview of the body's thermoregulatory system as well as information about the physiological disturbance caused by a variety of circumstances.

CHAPTER 3

MATHEMATICAL MODEL FOR HEAT TRANSFER IN HUMAN BODY WITH PROTECTIVE LAYER

3.1 Introduction

This Chapter aims to develop a mathematical model that combines the ideas of heat transport within the human body with the characteristics of clothes. Special focus is given to incorporating the protective layer in the well-known bioheat transfer model by adding the clothing parameters into that of Pennes' equation. Starting with the fundamentals of clothing heat transfer phenomena in section 3.2, a brief overview of some developments in clothing and human thermal comfort in section 3.3, we establish the main model in section 3.4. Decoupling the model equation, implementing the fully implicit finite difference method with Neumann boundary conditions, modifying Robin's boundary condition by adding clothing parameters in the usual one, and combining the separate solution of decoupled equation by using interface condition, is the major task of this Chapter given in section 3.5. In section 3.6, we analyze the existence, validity, stability, and convergence of the implicit scheme via some theorems. Using the model with modified Robin's boundary conditions, we also observe the effect of garment insulation, air insulation, air velocity, and walking speed which have a significant impact on the temperature variation in the human body.

3.2 Clothing Heat Transfer Mechanisms

Heat transfer through the cloth mainly depends upon the clothing insulation, radiant temperature, clothing area factor, the thermal conductivity of clothes, the thickness of clothes, convective heat transfer coefficient, walking speed, air velocity, and ambient temperature. These clothing heat transfer mechanisms together with physical and

physiological elements mentioned in Chapter 2 provide better comfort for human thermoregulatory system than that of the nude body.

3.2.1 Clothing Insulation for Human Thermal Comfort

Clothing, an important insulator for the human body and a mean that maintains thermal comfort, strongly influences the heat exchange phenomena and hence controls body temperature. American Society for Heating, Refrigerating and Air Conditioning Engineering (ASHRAE) [29, 49] in thermal environmental conditions for human occupancy, has mentioned that the thermal comfort is the individual's feeling that expresses the satisfaction with the thermal environment, and the insulation of clothing is the resistance to sensible heat transfer by garments. Thermal insulation of clothing systems is determined by the properties and the construction of fabric materials, the air layers between them, and also the layers of trapped air [55]. Generally clothing insulation expressed by the Clo unit (1 Clo $= 0.155\,\mathrm{m^2\,^\circ C/W}$) [74, 75]. The total insulation I_T is the sum of clothing insulation I_{cl}, and air insulation I_a, as shown in left-hand Figure of 3.1, where, $I_T = I_{cl} + I_a$. For the active occupant who is moving
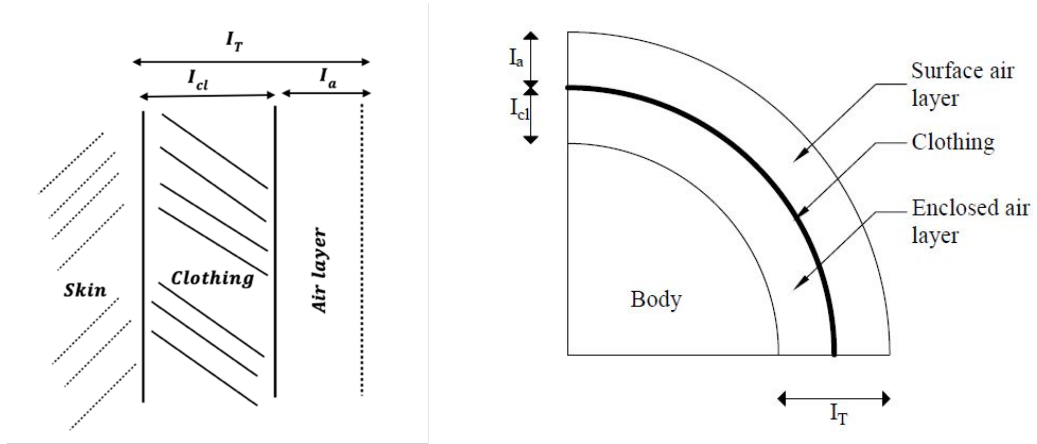
Figure 3.1: Schematic view of (left) total insulation I_T and (right) I_T in the circular limb [74, 75].

or involved in some activities, the clothing insulation can be determined as follows [49].

$$I_{\mathrm{cl,\ active}} = I_{\mathrm{cl,rest}} \times (0.6 + 0.4/M_t),$$

where
M_t : metabolic rate
$I_{cl,rest}$: clothing insulation $(\mathrm{m^2\,^\circ C/W})$ without movement.

ASHRAE in the same project; specified the two zones accordingly Clo values of clothing insulation, 0.5 Clo for one and 1.0 Clo for the other. The linear interpolation between these two Clo values determines the comfort zones for the intermediate value of I_{cl} by the relation

$$T_{\min,I_{cl}} = \frac{1}{0.5} \left[(I_{cl} - 0.5\,\text{Clo})\, T_{\min,1.0\,\text{Clo}} + (1.0\,\text{Clo} - I_{cl})\, T_{\min,0.5\,\text{Clo}} \right].$$

$$T_{\max,I_{cl}} = \frac{1}{0.5} \left[(I_{cl} - 0.5\,\text{Clo})\, T_{\max,1.0\,\text{Clo}} + (1.0\,\text{Clo} - I_{cl})\, T_{\max,0.5\,\text{Clo}} \right].$$

Clothing area factor, f_{cl}, the ratio of clothed human body surface area, A_{cl} and Dubois (nude body) surface area, A_D, according to ISO-9920 (International Organization for Standardization), ASHARE standard 55, ISO 7730, [49, 75] has been calculated as

$$f_{cl} = \frac{A_{cl}}{A_D}.$$

The clothing area factor can also be estimated in terms of clothing insulation, as suggested by McCullough and Jones in 1984 [115] is

$$f_{cl} = 1 + 0.31 I_{cl}. \tag{3.1}$$

When 1 Clo $= 0.155\,\text{m}^2\,^\circ\text{C/W}$, mentioned in ASHRAE standard 55 and ISO 9920, which provides a database on the clothing area factor and intrinsic clothing thermal resistance of many non-Western and Western, Gulf region and Korean clothing ensembles [49, 115], are given as

$$f_{cl} = 1 + 1.977 I_{cl}. \tag{3.2}$$

The clothing efficiency factor F_{cl} (dimensionless quantity), as shown in Figure 3.1 with total insulation and clothing area factor f_{cl} is given by [48, 49]

$$F_{cl} = \frac{I_a}{I_T} = \frac{I_a}{I_{cl} + I_a/f_{cl}}. \tag{3.3}$$

3.2.2 Insulation for Entire Clothing ($I_{cl} = \sum i_{cl}$)

Clo is a unit of thermal insulation of overall clothing, total garment including tops, bottoms innerwear and everything (including even socks, gloves, etc), each of which is indicated by i_{cl}. The total clothing and its insulation for a person in summer and winter is given in Table 3.1.

Table 3.1: Total clothing insulation for a person [49, 75].

Cloth item (Summer)	Clo value (m^2 °C/W) (i_{cl})	Cloth item (Winter)	Clo Value (m^2 °C/W) (i_{cl})
Half shirt	0.19	Full shirt	0.28
Underware	0.04	Underware	0.04
Pant	0.11	Pant	0.25
Shocks	0.02	Thick shocks	0.05
Shoes	0.02	Shoes	0.04
		Sweater	0.28
Total (I_{cl})	$\Sigma i_{cl} = 0.38$	Total (I_{cl})	$\Sigma i_{cl} = 0.91$

3.2.3 Radiant Temperature in Clothing System

The heat exchange between body and environment by radiation is the energy emitted by a black body per unit area per unit time is proportional to the fourth power of the absolute temperature [3, 38]. As most of the human body parts are always wrapped with appropriate clothes, the radiative heat losses from the outer surface of the cloth to the environment is expressed in this case by

$$\dot{Q}_{\text{rad}} = \sigma \epsilon A_{cl} \left(T_{cl}^4 - T_\infty^4 \right). \tag{3.4}$$

The energy balance equation due to radiation in the clothing system now is provided as

$$-K_{cl} \frac{\partial T_{cl}}{\partial \eta} \bigg|_{\text{at cloth surface}} = \sigma \epsilon A_{cl} \left(T_{cl}^4 - T_\infty^4 \right), \tag{3.5}$$

where
K_{cl} :   thermal conductivity of cloth (W/ m°C)
T_{cl} :   temperature of cloth (°C)
A_{cl} :   surface area of human body including cloth (m^2).

3.2.4 Convective Heat Exchange with Air Velocity and Walking Speed

In general, walking speed is the measurement of the person's basic walking ability in which a person travels a certain distance in a specific direction in a time. Air velocity directly comes into contact in the human body and makes the body immediately cool. Moving air in warm or humid conditions can increase heat loss through convection without any change in air temperature. If there is no movement of air, humid conditions increase, and if increase in air movement, the body will be cooler because of

convective heat loss. Air velocity may be corrected to account for a person's level of physical activity because it also increases air movement. According to ISO-7933 the convective heat transfer also depends upon the walking speed W_s and relative air velocity V_{air} is given by [54, 74]

$$h_{\text{conv}} = 8.7 \, V_{air} \qquad \text{and} \qquad V_{air} = v_a + W_s, \tag{3.6}$$

and

$$W_s \;=\; 0.0052(M_t - 58), \tag{3.7}$$

where
  V_{air} : total relative air velocity (m/s)
  v_a : air velocity (m/s)
  W_s : walking speed (m/s)
  M_t : metabolic heat generation rate (W/m^2).

The air velocity has a significant impact on the amount of overall heat loss from the body. This is affected by Newton's law of cooling, which states that, in the presence of a light breeze, the rate at which a body's temperature changes is proportional to the difference in temperature between the surface of the body and its surroundings. The formula for the convective heat transfer rate is

$$-K_t \frac{dT_t}{dr}\bigg|_{\text{at skin surface}} = h_{\text{conv}} A \left(T_s - T_\infty\right), \tag{3.8}$$

where
  K_t : thermal conductivuty of tissue (W/m°C)
  T_t : tissue temerature (temerature for body part) (°C)

In the clothing system, the sensible heat loss from skin to clothing and then from clothing to environment. So, the boundary condition of Robin type due to convection guided by Newton's Law of cooling for convection is given by [48, 49]

$$-K_{cl} \frac{dT_{cl}}{dr}\bigg|_{\text{at cloth surface}} = h_{\text{conv}} A_{cl} \left(T_{cl} - T_\infty\right). \tag{3.9}$$

Though many researchers [28, 30, 46, 48, 49, 54, 85, 88] have played a major role for a significant turn in the field of thermal comfort through protective clothing by taking the heat balance equation and focusing on the heat transfer only through clothing. There is still lacking for the study of energy and heat balance in the internal human body part and clothing as well. Our area of interest is, therefore, to extend the

bioheat transfer equation. The investigation of human thermal comfort in garment systems has benefitted greatly from the work of numerous researchers. The majority of researchers [3, 40, 59, 61, 62, 65, 77, 78] studying the temperature distribution in the human body using Pennes' model, however, have not included the boundary conditions of clothing insulation, walking speed, and air velocity. Therefore, one of the focuses of this research effort is the modification of the typical boundary condition of the Robin type, incorporating a connection to these characteristics.

3.3 A Brief Overviews of Studies in Clothing and Human Thermal Comfort

Initial knowledge regarding to clothing insulation was used for military applications. Soldiers wearing garments with proper insulation were mobilized to put out the fire. For protection against thermal risks, Liu et al. [71] have created thermal protective clothing that can convey heat in the $20W/m^2$-$160W/m^2$ range through radiation, conduction, or convection.

In ISO-1986, a number of techniques are provided for figuring out clothing's thermal characteristics. It also includes a database of dry, intrinsic garment insulation values, I_{cl}, based on readings from a heated thermal manikin, primarily for indoor clothing worn [89]. The air gap and thermal insulation have a significant impact on skin burn injuries. Thermal insulation shields the body from the cold and also protects against burn damage at the skin's surface. The air gap offers thermal insulation that restricts heat transmission to the skin when exposed to fire, preventing burn injuries. It's still worthwhile to think about issues with bioheat transfer and thermal comfort in clothing. A number of researchers [48, 49, 54, 57, 114] have made significant advancements for the understanding of thermal comfort in clothing system considering the linear equation only for cloth with clothing area factor. The experiment was done within the various human manikins including a database of non-Western ensembles' static apparel thermal insulation and vapor permeability values for ASHARE standard 55, ISO-7730 (International Organization for Standardization) ISO-9920 [49].

The UC Berkeley Comfort Model was recommended by Holmer in 2006 [55] and Voelker in 2009 [114] for heat and moisture transmission through clothing. To examine how moisture affected Nomex materials' heat resistance, and water vapor permeability, Baczek and Hes [9] utilized seven ensembles as test subjects and measured them in a lab. In their experimental work measuring the thermal conductivity of wet

fabric, Slavinec et al. in 2016 [110] investigated the effect of moisture on the thermal conductivity of fabric, compared their linear model with the estimation of a theoretical model, and focused on measuring the thermal conductivity of cotton fabrics for increasing relative amounts of water.

Shen et al. in 2018 [104] developed the heat transfer model along the longitudinal and transverse directions in the fabric to show that the high thermal conductivity causes the heat transfer significantly faster along the longitudinal direction than along the transverse direction of the fabric. For the purpose of improving the safety and production efficiency of workers in very hot environments, Dung and Anh in 2019 [26] proposed the thermal protective design for industrial working at high temperature, and further investigated the degree of skin burn, the effect of fabric and air-gap thickness and compared the simulated results concluding both, fabric thickness, and air gap to improve the thermal protective properties.

The study of the human body's thermal comfort in such non-uniform environments is insufficient unless clothing properties are incorporated. In real life situations about $(75-90)\%$ of the human body's surface area is always covered with protective clothing system as shown in Figure 1.1. Pennes' bioheat equation (2.21), has been, therefore, extended for the clothing system in this Chapter. Despite numerous improvements that have been made in the bioheat transfer model as mentioned in the previous Chapter 2 [3, 4, 40, 77, 93, 107, 109, 123, 124], the application in clothing science is still limited because clothing has not been taken into account in these models. Various studies [30, 33, 46, 49, 55, 82, 84, 85, 118] have been done by utilizing dry and sweating thermal manikins in an advanced laboratory to assess the thermal qualities of clothes, such as insulation and evaporative resistance. These studies, however, continued ignoring the blood perfusion concept. So, our work combines both subject areas (bioheat transfer in human tissue and clothing), has the potential to have a significant impact on biomedicine as well as clothing and environment designers.

3.4   Mathematical Model of Heat Transfer with Protective Clothing

The extension of Pennes' bioheat equation (2.20) with protective clothing system is given by [75, 76]

$$\underbrace{\rho c \frac{\partial T}{\partial t}}_{\text{Heat Storage}} = \underbrace{\nabla \cdot (K \nabla T)}_{\text{Diffusion}} + \underbrace{\rho_b w_b c_b (T_a - T)}_{\text{Perfusion}} + \underbrace{q_m}_{\text{Metabolism}} + \underbrace{P_{cl} (T_s - T_{cl})}_{\text{Clothing}} \text{ in } \Omega_L \quad (3.10)$$

Where the total heat storage on the left-hand side is the combination of the first, second, and third terms of the right-hand side, respectively diffusion, perfusion, and metabolic heat generation. The additional term $P_{cl}(T_s - T_{cl})$ is the protective clothing, where

$$P_{cl} = \frac{K_{cl}}{A_{cl}}(\text{W/m}^3\,^\circ\text{C}). \tag{3.11}$$

L : final point of the radial length of human tissue element with cloth(m)
Ω_L : computational domain
K_{cl} : thermal conductivity of cloth$(\text{W/m}^\circ\text{C})$
A_{cl} : surface area of clothed human body (m^2)
T_s : skin surface temperature $(^\circ\text{C})$
T_{cl} : surface temperature of cloth$(^\circ\text{C})$.

3.4.0.1 One Dimensional Extended Bioheat Equation in Cylindrical Form

The overall goal of the thesis is to investigate the temperature distributions throughout the human body's cylinderical structure. The cylindrical form of this bioheat equation in a radial direction is, therefore, performed here

$$\rho c \frac{\partial T}{\partial t} = K\left[\frac{1}{r}\frac{\partial}{\partial r}\left(r\frac{\partial T}{\partial r}\right)\right] + \rho_b c_b w_b(T_a - T) + q_m + P_{cl}(T_s - T_{cl}), \quad \text{in } \Omega_L. \tag{3.12}$$

3.4.0.2 Initial Condition

The initial condition for the time-dependent boundary value problem is given by

$$T(r,0) = T_0(r). \tag{3.13}$$

where

$$T = \begin{cases} T_t, & \text{for body part} \quad 0 \leq r \leq N. \\ \\ T_{cl}, & \text{for clothes part} \quad N \leq r \leq R. \end{cases} \tag{3.14}$$

3.4.0.3 Neumann Condition at the core (Inner Boundary)

As the body core temperature is constant, the Neumann boundary condition, flux boundary for the interior part of the living tissue; is considered uniform as in equation

$$\text{at } r = 0, \qquad \left.\frac{\partial T_t}{\partial r}\right|_{\text{at body core}} \quad = \quad 0. \qquad \text{in } \partial\Omega_L \qquad (3.15)$$

3.4.0.4 Robin Boundary Condition at Clothing Surface (Outer Boundary)

The right side is fitted with clothes and directly exposed to the environment. The continuous heat flux occurs between clothes surface and the atmosphere, and as a consequence, the body losses heat to the surroundings via clothes. So, the boundary condition of Robin type, due to the convection and radiation is guided by Newton's Law of cooling and Stefan Boltzmann law separately for convection and radiation along with effective clothing area factor is given by [48, 49, 75]

$$-K_{cl}\left.\frac{\partial T_{cl}}{\partial r_{cl}}\right|_{\text{at clothes surface}} \quad = \quad F_{cl}\left[h_{\text{conv}}\left(T_{cl} - T_\infty\right) + \epsilon\sigma\left(T_{cl}^4 - T_\infty^4\right)\right],$$

$$\text{at } R = L, \text{ in } \partial\Omega_L, \qquad (3.16)$$

where
F_{cl} :   effective clothing area factor given in equation (3.3) (dimensionless)
h_{conv} :   convective heat transfer coefficient (W/m^2 °C)
ϵ :   emissivity ($0 \leq \epsilon \leq 1$)
σ :   Stefan Boltzmann constant (W/m^2 K^4) = 5.57×10^{-8}
T_{cl} :   temperature of cloth (°C)
T_∞ :   ambient temperature (°C)
r_{cl} :   thickness of the clothes (m).

The appearance of nonlinear radiation term in the boundary condition makes the bioheat transfer problem nonlinear. In this case, we minimize this complexity by simplifying and introducing a suitable iterative procedure if $(T_{cl} + T_\infty)(T_{cl}^2 + T_\infty^2)$ is known, then equation (3.16) becomes linear and can be treated as a convective boundary condition.

$$-K_{cl}\left.\frac{\partial T_{cl}}{\partial r_{cl}}\right|_{\text{at clothes surface}} \quad = \quad F_{cl}\left[h_{\text{conv}}\left(T_{cl} - T_\infty\right) + \epsilon\sigma\left(T_{cl} - T_\infty\right)\left(T_{cl} + T_\infty\right)\left(T_{cl}^2 + T_\infty^2\right)\right]$$

$$= \quad F_{cl}\left(T_{cl} - T_\infty\right)\left[h_{\text{conv}} + \epsilon\sigma\left(T_{cl} + T_\infty\right)\left(T_{cl}^2 + T_\infty^2\right)\right]$$

$$-K_{cl}\left.\frac{\partial T_{cl}}{\partial r_{cl}}\right|_{\text{at clothes surface}} \quad = \quad F_{cl}\left(h_{\text{conv}} + h_r\right)\left(T_{cl} - T_\infty\right),$$

$$-K_{cl}\left.\frac{\partial T_{cl}}{\partial r_{cl}}\right|_{\text{at clothes surface}} \quad = \quad h_A\left(T_{cl} - T_\infty\right), \qquad (3.17)$$

where

$$F_{cl} = \frac{I_a}{I_{cl} + I_a/f_{cl}}$$

$$h_r = \epsilon\sigma\left(T_{cl} + T_\infty\right)\left(T_{cl}^2 + T_\infty^2\right)$$

$$h_A = F_{cl}\left(h_{\text{conv}} + h_r\right).$$

At time step $t_n = n$

$$-K_{cl}\left.\frac{\partial T_{1cl}}{\partial r_{cl}}\right|_{\text{at clothes surface}} = F_{1cl}\left(h_{\text{conv}} + h_r\right)\left(T_{1cl}^n - T_\infty\right)$$

$$-K_{cl}\left.\frac{\partial T_{1cl}}{\partial r_{cl}}\right|_{\text{at clothes surface}} = F_{1cl}\left(h_{\text{conv}} + h_r\right)\left(T_{1cl}^n - T_\infty\right) \tag{3.18}$$

$$h_r = \epsilon\sigma\left(T_{1cl}^{n-1} + T_\infty\right)\left((T_{1cl}^{n-1})^2 + T_\infty^2\right), \tag{3.19}$$

where
T_{1cl}^n :   the temperature sequences for $n = 1, 2, 3, \cdots$
T_{1cl}^0 :   initial guess of temperature.

The iteration will continue until the convergent condition is reached.

$$\left\|T_{1cl}^n - T_{1cl}^{n-1}\right\| \le \delta,$$

where δ is iteration tolerance.

It is extremely difficult to investigate heat transport in such nonhomogeneous materials, including the human body and clothing. The equation (3.12), therefore, has been decoupled into two parts, body, and clothes.

3.4.1   Model with Interface

The mathematical model in cylindrical form with clothing at the boundary is taken in the case of a negligible air gap or tight-fitting clothing. The main assumption in this model is the heat flows from the body core toward the skin surface, in the radial direction. N^{th} node is considered as the interface between the skin surface and clothes, and the clothing appears in the boundary as shown in Figure 3.2, where R^{th} node represents the clothes surface that expose to the environment. The computational domain and its discretization can be seen in Figure 3.2.

Basically, we perform the following five steps.
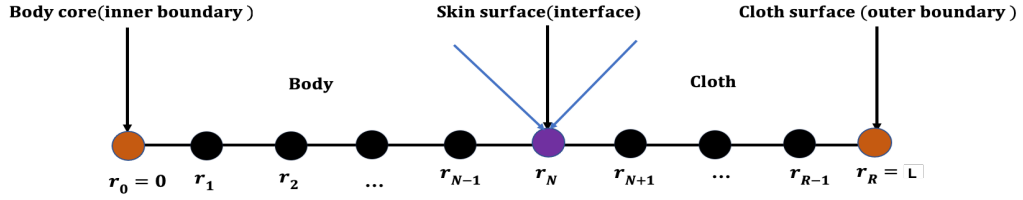
Figure 3.2: Discretization of mesh in the radial direction from core to the skin surface with the interface.

1. Decoupling of model (3.12) into two separate parts, for human tissue, and cloth.

2. Separate construction of Finite Difference (FD) schemes for each of both parts.

3. Use of the interface and boundary conditions, and combining the solutions of each part to obtain a solution of the model (3.12)

4. Proof of solvability, consistency, stability, and convergence of the FD scheme.

5. Display numerical results graphically.

3.4.2 Model for Body Part (Absence of Clothing)

In the absence of clothing, from the model (3.12), $P_{cl} = 0$, we have

$$\rho c \frac{\partial T_t}{\partial t} = K_t \left[\frac{1}{r} \frac{\partial}{\partial r} \left(r \frac{\partial T_t}{\partial r} \right) \right] + \rho_b c_b w_b (T_a - T_t) + q_m, \qquad \text{in } \Omega_N, \qquad (3.20)$$

where
$\Omega_N :$ computational domain for human tissue including N nodes
$T_t :$ tissue temperature (temperature for body part)(°C).

3.4.3 Model for Clothing Part (Absence of Perfusion and Metabolism)

In the absence of perfusion and metabolism from the model (3.12), $w_b = 0$, and $q_m = 0$, we have

$$\rho c \frac{\partial T_{cl}}{\partial t} = K_{cl} \left[\frac{\partial^2 T_{cl}}{\partial r^2} + \frac{1}{r} \frac{\partial}{\partial r} \left(\frac{\partial T_{cl}}{\partial r} \right) \right] + P_{cl} (T_s - T_{cl}), \qquad \text{in } \Omega_{L-N}, \quad (3.21)$$

where
$\Omega_{L-N} :$ computational domain for human tissue including $L - N$ nodes
$T_{cl} :$ cloth temperature (temperature for clothing part) (°C).

3.5 Numerical Method for the Model

The solution procedure is followed by applying the fully implicit Finite Difference Method (FDM) to both of the decoupled equations (3.20) and (3.21). We discretize the bioheat Equation (3.12) having R points altogether in the domain, taking N points in the body part, equation (3.20), and $R - N$ points in the clothing part, equation (3.21) as shown in Figure 3.2.

3.5.1 Constructions of Finite Difference Scheme

As the foundation of our model, we first create a one-dimensional form of cylindrical tissue for a body part that is separated into N discrete points that are each individually characterized by spatial indices, with the assumption that $r_i = i\Delta r$ in the radial direction. Figure 3.2 illustrates the discretization of a circular cross-section of the peripheral human limb where axial temperature flow is considered uniform.

3.5.2 FD Scheme for Body part

We use the FD scheme by writing equation (3.20) using an implicit finite difference scheme.

$$
\rho c \frac{T_i^{n+1} - T_i^n}{\Delta t} = K_t \left[\frac{T_{i-1}^{n+1} - 2T_i^{n+1} + T_{i+1}^{n+1}}{\Delta r^2} + \frac{T_{i+1}^{n+1} - T_{i-1}^{n+1}}{2i\Delta r} \right]
$$
$$
+ \rho_b c_b w_b \left(T_a - T_i^{n+1} \right) + q_m. \tag{3.22}
$$

The construction in equation (3.22) implies that of FD scheme for the interior grid has the truncation error of order $\mathcal{O}\left(\Delta r^2 + \Delta t\right)$ for each interior point (t^n, r_i), $n \geq 1$, $0 < i < N$.
when
$$
D = \frac{K_t}{\Delta r^2}, \quad \alpha = D\frac{\Delta t}{\Delta r^2}, \quad M = \frac{w_b c_b}{\rho c}, \quad S = \frac{q_m}{\rho c}, \quad \text{and } F = \Delta t \left(MT_a + s \right).
$$
Equation (3.22) becomes

$$
D_i T_{i-1}^{n+1} + E_i T_i^{n+1} + B_i T_{i+1}^{n+1} - F = T_i^n \tag{3.23}
$$

where $D_i = \left(-\alpha + \frac{\alpha}{2i}\right)$, $E_i = (1 + 2\alpha + M\Delta t)$, and $B_i = \left(-\alpha - \frac{\alpha}{2i}\right)$.

3.5.2.1 FD Scheme at Boundary $r = 0$ (Body core)

The cylindrical thickness r is measured from body core as shown in Figure 3.2. At the body core, both r and the heat flux $\frac{\partial T_t}{\partial r}$, are zero, then $\frac{1}{r}\left(\frac{\partial T_t}{\partial r}\right)$ approaches

to indeterminate form $\dfrac{0}{0}$ as $r \to 0$. The use of the L'Hospital rule then gives

$$\frac{1}{r}\frac{\partial T_t}{\partial r}\bigg|_{r=0} = \frac{\dfrac{\partial}{\partial r}\left(\dfrac{\partial T_t}{\partial r}\right)}{\dfrac{\partial}{\partial r}(r)}\bigg|_{r=0} = \frac{\partial^2 T_t}{\partial r^2}\bigg|_{r=0}.$$

Now equation (3.7) becomes

$$\frac{\partial T_t}{\partial t} = 2D\left(\frac{\partial^2 T_t}{\partial r^2}\right) + M(T_a - T_t) + S. \tag{3.24}$$

The FD scheme of equation (3.24) at $r = 0$ is

$$-2\alpha T_{-1}^{n+1} + (1 + 4\alpha + M\Delta t)\,T_0^{n+1} - 2\alpha T_1^{n+1} - F = T_0^n.$$

$$E_0 T_0^{n+1} - 4\alpha T_1^{n+1} - F = T_0^n. \tag{3.25}$$

3.5.2.2 Right Boundary for Skin Surface (Interface Condition at $i = N$)

The skin surface is covered by clothing. So, At $i = N$, the interface between body and clothes, we take the rightmost Dirichlet boundary condition at this point as

$$T_c\bigg|_{i=N} = T_{cl}\bigg|_{i=N} = T_{int}.$$

FD scheme at $i = N$

$$D_N T_{N-1}^{n+1} + E_N T_N^{n+1} + B_N T_{int} - F = T_N^n. \tag{3.26}$$

The system of equations (3.25), (3.23) and (3.26) can be written in the matrix form as

$$A_1\,T_t^{n+1} = T_t^n + B_1, \tag{3.27}$$

where A_1 is the corresponding tridiagonal matrix of order $(N+1) \times (N+1)$,

$$A_1 = \begin{bmatrix} E_0 & -4\alpha & 0 & 0 & \cdots & 0 \\ D_1 & E_1 & B_1 & 0 & \cdots & 0 \\ 0 & D_2 & E_2 & B_2 & \cdots & 0 \\ \vdots & \vdots & \vdots & \ddots & \ddots & \vdots \\ 0 & 0 & \cdots & D_{N-1} & E_{N-1} & B_{N-1} \\ 0 & 0 & \cdots & \cdots & D_N & E_N \end{bmatrix}$$

T_t^{n+1} and B_1 are column vector of order $(N+1) \times 1$ as

$$T_t^{n+1} = \begin{bmatrix} T_0^{n+1} & T_1^{n+1} & T_2^{n+1} & \cdots & T_N^{n+1} \end{bmatrix}',$$

and

$$B_1 = \begin{bmatrix} F & F & F & \cdots & F - B_N T_{int} \end{bmatrix}',$$

3.5.3 FD Scheme for Clothing Part

3.5.3.1 Left Boundary at Cloth $i = N$

As we have mentioned above, the skin surface is the interface between the body and clothing part at $i = N$, the left boundary for cloth whose FD scheme is given by

$$D_N T_{N-1}^{n+1} + E_N T_N^{n+1} + B_N T_{N+1}^{n+1} = T_N^n, \qquad (3.28)$$

where

$$D_N = \left(-\alpha_1 + \frac{\alpha_1}{2N}\right), B_N = \left(-\alpha_1 - \frac{\alpha_1}{2N} + P_1\right)$$

$$E_N = (1 + 2\alpha_1 + P_1), \text{ and } \alpha_1 = \frac{D_{cl}\Delta t}{(\Delta r_c)^2}.$$

3.5.4 Interface Condition at $i = N$ (Between Skin and Cloth)

It is vital to assess the interface thermal conductivity K_N before taking the temperature at the point where the skin's surface and clothing meet. The thermal conductivity of non-homogeneous materials, such as the body and clothing, which contains a variety of physiological qualities, is not consistent. So it is highly desirable to have the correct formulation for nonuniform K_N. According to Luitel et al. [75] and Patankar [90], the interface conductivity K_N is to be assumed to vary linearly between two points N and $N + 1$. The interfaces between the adjacent blocks must in this situation be subject to appropriate interface conditions. As a result, numerical interface treatments become challenging, even though they are supposed to ensure stability and maintain the high accuracy of the numerical scheme.

$$K_N = f_N K_t + (1 - f_N)K_{cl},$$

where
f_N : interpolation factor, $= \Delta r_c/\Delta r$
Δr_c : spatial length between the adjacent nodes in the clothing part.

For the interface gridpoint N, we consider the control volume surrounding N is filled with the uniform conductivity K_t of body tissue, one around $N+1$ with a conductivity K_{cl} of clothes. The good representation of heat flux over the composite domain between N and $N + 1$ leads to [90]

$$q_N = -K \frac{T_{N+1} - T_N}{\left(\dfrac{\Delta r}{K_t} + \dfrac{\Delta r_c}{K_{cl}}\right)}.$$

3.5.4.1 Interface Conditions at $i = N$ (Left Boundary for Cloth Part)

The heat flux occurs at the skin surface, and the leftmost boundary of clothes at $i = N$ is given by

$$-K_t \frac{\partial T_t}{\partial r}\bigg|_{i=N} \quad = \quad q_N. \tag{3.29}$$

FD formulation for (3.29),

$$\frac{T_{N+1}^{n+1} - T_{N-1}^{n+1}}{2\Delta r} \quad = \quad -K \frac{T_{N+1} - T_N}{\left(\dfrac{\Delta r}{K_t} + \dfrac{\Delta r_c}{K_{cl}}\right)}.$$

$$T_{N-1}^{n+1} \quad = \quad T_{N+1}^{n+1} - 2R_c q_N. \tag{3.30}$$

Now equation (3.28) with left boundary condition (3.30) can be written as

$$E_N T_N^{n+1} + \left(-2\alpha_1 - P_1\right) T_{N+1}^{n+1} - F_N \quad = \quad T_N^n, \tag{3.31}$$
$$\text{where} \qquad F_N = D_N 2 R_c q_N.$$

3.5.4.2 FD Scheme for Interior Node

FD scheme for each interior gride point (t^n, r_i), with $i = N + 1, \cdots, R - 1$
in the clothing part is given by

$$D_i T_{i-1}^{n+1} + E_i T_i^{n+1} + B_i T_{i+1}^{n+1} \quad = \quad T_i^n. \tag{3.32}$$

where $D_i = \left(-\alpha_1 + \dfrac{\alpha_1}{2i}\right)$, $E_i = (1 + 2\alpha_1 + M\Delta t)$, and $B_i = \left(-\alpha_1 - \dfrac{\alpha_1}{2i}\right)$.
As in the previous case (3.23), the construction in (3.32) implies that of FD scheme have the truncation error of order $\mathcal{O}\left(\Delta r^2 + \Delta t\right)$ for each interior point (t^n, r_i), $n \geq 1$, $N < i < R$.

3.5.4.3 Boundary Conditions at $i = R$ (At Surface of Cloth)

The heat flux occurs at the outer surface of the rightmost boundary of clothes at $i = R$ with the modified heat transfer coefficient h_A due to convection, radiation along with clothing parameters in relation (3.17) is given by

$$-K_{cl} \frac{\partial T_{cl}}{\partial r_c}\bigg|_{i=R} \quad = \quad h_A(T_{cl}^{n+1} - T_\infty).$$

$$T_{R+1}^{n+1} = T_{R-1}^{n+1} - 2h_A R_c \left(T_R^{n+1} - T_\infty\right).$$

FD scheme at $i = R$ is now given by

$$(-2\alpha_1 - P_1) T_{R-1}^{n+1} + (E_R - B_R 2h_A R_c) T_R^{n+1} - F_R = T_R^n. \tag{3.33}$$

The system of equations (3.31), (3.32), and (3.33) can be written in the matrix form as

$$A_2 \, T_{cl}^{n+1} = T_{cl}^n + B_2, \tag{3.34}$$

where A_2 is the corresponding tridiagonal matrix of order $(R - N) \times (R - N)$,

$$A_2 = \begin{bmatrix} E_N & -2\alpha_1 - P_1 & 0 & 0 & \cdots & & 0 \\ D_{N+1} & E_{N+1} & E_{N+1} & 0 & \cdots & & 0 \\ 0 & D_{N+2} & E_{N+2} & B_{N+2} & \cdots & & 0 \\ \vdots & \vdots & \vdots & \ddots & \ddots & & \vdots \\ 0 & 0 & \cdots & D_{N-1} & E_{N-1} & & B_{N-1} \\ 0 & 0 & \cdots & \cdots & -2\alpha_1 - P_1 & E_R - 2h_A R_c B_R \end{bmatrix},$$

and T_{cl}^{n+1} and B_2 are column vector of order $N + 1 \times 1$ as

$$T_{cl}^{n+1} = \begin{bmatrix} T_N^{n+1} & T_{N+1}^{n+1} & T_{N+2}^{n+1} & \cdots & T_{R-1} & T_R^{n+1} \end{bmatrix}',$$

$$B_2 = \begin{bmatrix} F_N & 0 & 0 & \cdots & -F_R \end{bmatrix}'.$$

3.6   Analysis of the Model

We perform the solvability, consistency, stability, and convergence of the FD scheme for T^{n+1} by introducing a vector T^n of size $(R + 1) \times 1$ as a piecewise function that represents the numerical solutions at time step t^n as

$$T^n(T_t^n, T_{cl}^n) = \begin{bmatrix} T_0^n & T_1^n & T_2^n & \ldots T_N^n & \cdots & T_{R-1}^n & T_R^n \end{bmatrix}',$$

such that

$$T^n = \begin{cases} T_t^n = \begin{bmatrix} T_1^n & T_2^n & T_3^n & \cdots & T_{N-1}^n & T_N^n \end{bmatrix}', & \text{for} \quad 1 \leq l \leq N. \\ \\ T_{cl}^n = \begin{bmatrix} T_N^n & T_{N+1}^n & T_{N+2}^n & \cdots & T_{R-1}^n & T_R^n \end{bmatrix}', & \text{for} \quad N \leq l \leq R. \end{cases} \tag{3.35}$$

and the FD Scheme for both body and clothes part can be combinedly written as

$$T^{n+1} = A^{-1} T^n + B, \tag{3.36}$$

where

$$A = \begin{cases} A_1, & \text{for} \quad 1 \leq l \leq N \text{ (Body part)}. \\\\ A_2, & \text{for} \quad N \leq l \leq R \text{ (Cloth part)}. \end{cases}$$

$$B = \begin{cases} B_1, & \text{for} \quad 1 \leq l << N \text{ (Body part)}. \\\\ B_2, & \text{for} \quad N \leq l \leq R \text{ (Cloth part)}. \end{cases}$$

For the continuity condition $T_t = T_{cl}$ at the interface $l = N$. The solvability result can be stated in the next theorem.

Theorem 3.6.1 (Solvability). *The equation (3.36) is solvable unconditionally for each time step n.*

Proof. To show the solvability of equation (3.36), we need to prove that the matrix A is invertible, that is the matrix A is diagonally dominant. We show A_1 and A_2 both are diagonally dominant.

For matrix A_1

$R_1(1^{st}$ row):

$$|a_{jj}| \geq \sum |a_{lj}| \quad \text{since} \quad |1 + 4\alpha + M\Delta t| > |-4\alpha|.$$

$R_i(i^{th}$ row):

$$|a_{jj}| \geq \sum_{l=0,\, l \neq j}^{R-2} |a_{lj}|,$$

since

$$|1 + 2\alpha + M\Delta t| > \left| -\alpha + \frac{\alpha}{2i} \right| + \left| -\alpha - \frac{\alpha}{2i} \right| > |-2\alpha|.$$

$(N-1)^{th}$ row):

$$|a_{jj}| \geq \sum |a_{lj}|,$$

since

$$|E_{N-1} + B_{N-1}| > |D_{N-1} - \beta B_{N-1}| + |B_{N-1}|,$$

$$|(1 + 2\alpha + M\Delta t)| > \left| (-\alpha + \frac{\alpha}{2(N-1)}) + (-\alpha - \frac{\alpha}{2(N-1)}) \right| = |-2\alpha|.$$

69

$R_N(N^{th}$ row):

$$|a_{jj}| \ge \sum |a_{lj}|, \quad \text{since} \quad |E_N| > |D_N|.$$

Since each row is diagonally dominant, matrix A_1 is invertible. Hence (3.27) is un-conditionally solvable. For matrix A_2

$R_N(N^{th}$ row:

$$|(1 + 2\alpha_1 + P_1)| > |-2\alpha_1 + P_1|,$$

therefore

$$|a_{jj}| \ge \sum |a_{lj}|.$$

R_i^{th} row:

$$|a_{jj}| \ge \sum_{l=N+1, \, l \ne j}^{R-1} |a_{lj}|,$$

since

$$|1 + 2\alpha + P_1| > \left|-\alpha_1 + \frac{\alpha_1}{2(N+1)}\right| + \left|-\alpha_1 - \frac{\alpha_1}{2(N+1)} + P_1\right| > |-2\alpha_1 + P_1|.$$

R_R (R^{th} row):

$$\left|(1 + 2\alpha_1 + P_1) + 2h_A R_{cl}\left(\alpha_1 + \frac{\alpha_1}{2(R)}\right)\right| > |-2\alpha_1 + P_1|.$$

Hence

$$|a_{jj}| \ge \sum |a_{lj}|, \quad \text{for} l = N+1, N+2, \cdots, R.$$

Since each row is diagonally dominant, matrix A_2 is invertible. Hence the system (3.34) is unconditionally solvable. Being each row in A_1 and A_2 is diagonally domi-nant, they are invertible. So is matrix A. Hence the system (3.36) is unconditionally solvable. $\qquad \square$

Lemma 3.6.1. *If λ_l for $l = 0, 1, 2, ..., R$ represents the eigenvalues of the square matrix A and $\|.\|_2$ represents the second matrix norm (i.e. $\|A\|_2 = \max_l |\lambda_l|$) then we have the following results*

1.

$$|\lambda_l| \ge \begin{cases} 1 + M\Delta t, & for \quad 1 \le l \le N-1. \\ \\ 1 + P_1, & for \quad N \le l \le R. \end{cases} \tag{3.37}$$

70

2.

$$|\lambda_l| \quad \geq \quad \begin{cases} 1 + M\Delta t, & for \quad 1 \leq l \leq N - 1. \\ \\ 1 + P_1, & for \quad N \leq l \leq R. \end{cases} \qquad (3.38)$$

where M^* and P_1^* are some positive constants.

Proof. The lemma is the direct consequence of Gershgorin Theorem 2.7.1 as the matrices A_1 and A_2 are invertible.

$\square$

Theorem 3.6.2 (Consistency). *A Finite Difference(FD) scheme for model (3.12) with truncation error $\tau(\Delta r, \Delta t)$ is consistent if*

$$\tau(\Delta r, \Delta t) \to 0 \quad as \quad \Delta r, \Delta t \to 0.$$

Proof. We have approximated our model (3.12) by FD scheme in (3.23) and (3.32), which has truncation error $\tau(\Delta r, \Delta t) = \mathcal{O}\left((\Delta r)^2 + \Delta t\right)$.
So,

$$\lim_{\Delta r, \Delta t \to 0} \tau\left(\Delta r, \Delta t\right) = 0,$$

so as $\Delta r, \Delta t \to 0$,

$$\tau(\Delta r, \Delta t) \to 0.$$

Hence the model is consistent. The stability result will be obtained in next theorem.

$\square$

Theorem 3.6.3 (Stability). *The FD scheme of equation (3.12) is stable with respect to initial data if*

$$\left\| E^{n+1} \right\|_2 \quad \leq \quad \left\| E^0 \right\|_2. \qquad (3.39)$$

Proof. For the stability of (3.36), it is sufficient to prove that both of T_t^{n+1} and T_{cl}^{n+1} are stable.
For T_t^{n+1}

$$A_1 \, T_t^{n+1} \quad = \quad T_t^n + B_1. \qquad (3.40)$$

Premultiplying to the system (3.40) by A_1^{-1} we obtain

$$T_t^{n+1} \quad = \quad A_1^{-1} \, T_t^n + A_1^{-1} \, B_1.$$

Take $T_t^{*(n+1)}$ be small perturb in T_t^{n+1}, then

$$A_1 \, T_t^{*(n+1)} \;=\; T_t^{*(n)} + B_1.$$

Assume the error equation

$$E_1^{n+1} = T_t^{n+1} - T_t^{*(n+1)},$$

then

$$
\begin{aligned}
E_1^{n+1} &= \left(A_1^{-1}T_t^n + A_1^{-1}B_1\right) - \left(A_1^{-1}T_t^{*n} + A_1^{-1}B_1\right) \\
E_1^{n+1} &= A_1^{-1}(T_t^n - T_t^{*n}) \\
&= A_1^{-1}E_1^n \\
&= A_1^{-1}(A_1^{-1}E_1^{n-1}) \\
&= (A_1^{-1})^2(E_1^{n-1}) \\
&= (A_1^{-1})^2(A_1^{-1}E_1^{n-2}) \\
&= (A_1^{-1})^3(E_1^{n-2}) \\
&\;\;\vdots \\
&= (A_1^{-1})^n E_1^0, \qquad \text{for} \quad n = 1, 2, \cdots, N.
\end{aligned}
$$

So we have

$$E_1^{n+1} \;=\; (A_1^{-1})^n E_1^0 \qquad \text{for} \qquad n = 1, 2, \cdots, N.$$

With respect to the second norm

$$\left\| E_1^{n+1} \right\|_2 \;\leq\; \left\| A_1^{-1} \right\|_2^n \left\| E_1^0 \right\|_2.$$

From Lemma 3.6.1 we have $\qquad \left\| A_1^{-1} \right\|_2 \leq 1,$
so

$$\left\| E_1^{n+1} \right\|_2 \;\leq\; \left\| E_1^0 \right\|_2.$$

Also

$$\left\| E_1^{n+1} \right\|_2 \;\leq\; C_1 \left\| E_1^0 \right\|_2, \qquad \text{for} \quad C_1 = 1. \tag{3.41}$$

Similar process can be followed for the system (3.34) to get

$$\left\| E_2^{n+1} \right\|_2 \;\leq\; C_2 \left\| E_2^0 \right\|_2, \qquad \text{for} \quad C_2 = 1. \tag{3.42}$$

where $E_2^{n+1} = T_{cl}^{n+1} - T_{cl}^{*(n+1)}$ be the error equation and $T_{cl}^{*(n+1)}$ is small perturb in T_{cl}^{n+1}

We, then see that (3.41) and (3.42) both are bounded. Therefore

$$||E^{n+1}||_2 \leq C||E^0||_2. \tag{3.43}$$

Hence by the Lax-Richtmyer theorem both systems are unconditionally stable with respect to initial data. Hence the system (3.36) is unconditionally stable. $\square$

3.6.1 Convergence

A system (3.36) is said to be convergent to the exact solution of partial differential equation (3.12) if

$$\lim_{\Delta r, \Delta t \to 0} \left| E^{n+1} \right| = 0.$$

Theorem 3.6.4 (Convergence)**.** *The FD schemes of equation* (3.12) *is unconditionally convergent.*

Proof. Let us introduce the vector $\widetilde{T}^n$ of size $(R+1) \times 1$ which represents the exact solution at the time step t^n such that

$$\widetilde{T}^n = \begin{cases} \widetilde{T_t}^n = \begin{bmatrix} T(r_0, t^n) & T(r_1, t^n) & \dots & T(r_N, t^n) \end{bmatrix}', & \text{for } 1 \leq l \leq N. \\ \\ \widetilde{T_{cl}}^n = \begin{bmatrix} T(r_N, t^n) & T(r_{N+1}, t^n) & \dots & T(r_R, t^n) \end{bmatrix}', & \text{for } N \leq l \leq R. \end{cases} \tag{3.44}$$

where

$$A\widetilde{T}^{n+1} = \widetilde{T}^n + B = \begin{cases} \widetilde{T_t}^n + B_1 + \tau_1^{n+1}, & \text{for } 1 \leq l \leq N. \\ \\ \widetilde{T_{cl}}^n + B_2 + \tau_2^{n+1}, & \text{for } N \leq l \leq R. \end{cases} \tag{3.45}$$

where, τ_1^{n+1} and τ_2^{n+1} are the vectors of truncation error at level t^n and satisfying continuity at interface condition at $l = N$ that is, $T_t = T_{cl}$, and $\widetilde{T}_t = \widetilde{T}_{cl}$. We have the numerical solution in T as

$$T^n \left(T_t^n, T_{cl}^n \right) = \begin{bmatrix} T(r_0, t^n) & T(r_1, t^n) & \dots & T(r_N, t^n) & \dots & T(r_R, t^n) \end{bmatrix}',$$

where

$$A\,T^{n+1} = T^n + B = \begin{cases} T_t^n + B_1, & \text{for } 1 \leq l < N. \\ \\ T_{cl}^n + B_2, & \text{for } N \leq l \leq R. \end{cases} \tag{3.46}$$

73

Equation (3.46) is based on the construction of discretization schemes.

Now substracting (3.46) from (3.45) we get

$$
\begin{aligned}
A(\tilde{T}^{n+1} - T^{n+1}) &= (\tilde{T}^n - T^n) + \tau^{n+1} \\
A\tilde{E}^{n+1} &= \tilde{E}^n + \tau^{n+1}
\end{aligned}
$$

where the error vector $\tilde{E}^{n+1}$ is given by

$$
\begin{aligned}
\tilde{E}^{n+1} &= \tilde{T}^{n+1} - T^{n+1} \\
\tilde{E}^{n+1} &= A^{-1}\tilde{E}^n + A^{-1}\tau^{n+1} \\
E^{n+1} &= A^{-1}E^n + A^{-1}\tau^{n+1} \\
&= A^{-1}(A^{-1}\tilde{E}^{n-1} + A^{-1}\tau^n) + A^{-1}\tau^{n+1} \\
&= (A^{-1})^2(A^{-1}\tilde{E}^{n-2} + A^{-1}\tau^{n-1}) + (A^{-1})^2\tau^n + A^{-1}\tau^{n+1} \\
&= (A^{-1})^3\tilde{E}^{n-2} + (A^{-1})^3\tau^{n-1} + (A^{-1})^2\tau^n + A^{-1}\tau^{n+1} \\
&\vdots \\
&= (A^{-1})^n\tilde{E}^0 + \sum_{k=0}^{n}(A^{-1})^k\tau^{n-k} \quad\quad (3.47) \\
\tilde{E}^{n+1} &= (A^{-1})^n\tilde{E}^0 + \sum_{k=0}^{n}(A^{-1})^k\tau^{n-k} \quad\quad (3.48)
\end{aligned}
$$

Taking second norm on (3.48), we obtain the following result

$$
\left\|\tilde{E}^{n+1}\right\|_2 \leq \left\|A^{-1}\right\|_2^n \left\|\tilde{E}^0\right\|_2 + \left(\sum_{k=0}^{n}\left\|A^{-1}\right\|_2^k\right) \max_{1\leq k\leq R}\left\{\left\|\tau^k\right\|_2\right\}.
$$

Initially we take $T^0 = 0$, since initially no error occurs at $t = 0$, so $\tilde{E}^0 = 0$.

From Lemma 3.6.1 1, $\left\|A^{-1}\right\|_2 \leq 1$, we have

$$
\left\|\tilde{E}^{n+1}\right\|_2 \leq \left(\sum_{k=0}^{n}\left\|A^{-1}\right\|_2^k\right) \max_{1\leq k\leq R}\left\{\left\|\tau^k\right\|_2\right\}.
$$

The construction of $\tau(\Delta r, \Delta t)$, gives

$$
\left\|\tau^k\right\|_2 \rightarrow 0 \text{ as } \Delta r \rightarrow 0, \Delta t \rightarrow 0.
$$

This implies

$$
\left\|E^{n+1}\right\|_2 \rightarrow 0, \text{ for } 1 \leq k \leq R.
$$

Hence the system is unconditionally convergent. $\qquad\square$

3.7 Numerical Results, Graphical Verification, and Discussion

The bioheat equation (3.12) has been decoupled into equations (3.20) and (3.21) to yield the numerical solution for heat transmission in the human body with the protective layer. The temperature obtained from the solution of equation (3.20) for the skin surface has been used to calculate the temperature for the protective clothing layer. So far the effect of cloth is concerned, the thickness of clothes $0.005\,\mathrm{m}$ is added to the tissue thickness $0.03\,\mathrm{m}$ and the new thickness $L = (0.03\,\mathrm{m} + 0.005\,\mathrm{m}) = 0.035\,\mathrm{m}$. For the numerical experiment, the physical and physiological parameters in Table 2.1 (for the body part) and in Table 3.2 (for the clothing part) have been considered.

Table 3.2: Physical parameters related to clothing properties [1, 38, 49, 55, 114]

Parameters	Symbols	Values	Units
Thermal conductivities of body	K_t	0.48	W/m°C
Thermal conductivity of cloth	K_{cl}	0.305	W/m°C
Thickness of clothes (Domain)	L_{cl}	0.0050	m
Density of clothes	ρ_{cl}	1550	kg/m^3
Specific heat of clothes	c_{cl}	1340	J/ kg °C
Clothing Insulation	I_{cl}	0.17	m^2 °C/W
Air insulation	I_a	0.0992	m^2 °C/W
Area of nude body	A_b	1.7	m^2
Clothing area factor	f_{cl}	1.75	dimensionless

3.7.1 Effect of Clothing Insulation

The effect of clothing and air insulation has been observed at the different time steps. The temperature profile with these effects is also compared with the temperature profile in the nude body. The tissue thickness $0.03\,m$ is taken as the size of the space domain. The solution of the system of equation (3.25) with these parametric values and the additional values [48, 49] in left-hand Figure 3.3 illustrates the graphs for the time-dependent temperature profiles with clothing insulation I_{cl} and air insulation I_a. The parametric values from Table 3.1 without additional parameters are used to plot the graph of the temperature variation within the nude body in right-hand Figure 3.3.

The results show that cloth keeps the body warm and comfortable by trapping a layer of air between the person's skin and the fabric. The presence of insulation in
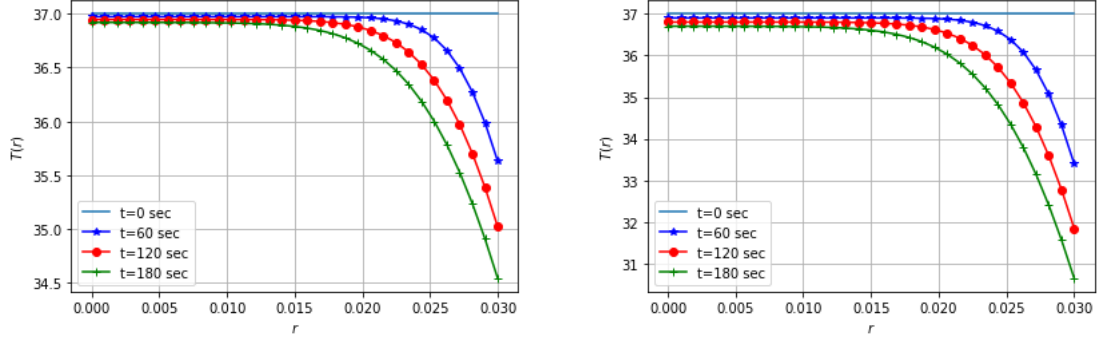
Figure 3.3: The variation of skin surface temperature (left) $I_{cl} = 0.172$ m$^2\,°$C/W, $I_a=$ 0.0992 m$^2\,°$C/W, $v_{air}=0$ m/s, and $w_s=0$ m/s (right) $I_{cl} = 0.172$ m$^2\,°$C/W, $I_a = 0.0992$ m$^2\,°$C/W, $v_a = 4.1$ m/s, $w_s = 0.42$ m/s

left-hand Figure 3.3 shows the rate of heat transfer from the body representing the temperature profiles at rest and different time steps. When a person removes clothing from his/her body, he/she starts to feel that the layer of trapped air dissipates and reacts to the cooler air around him/her. The rate of heat transfer from the body in this situation is higher than that of the clothing case. Except for rest (t = 0) in both cases (clothed and naked body), the temperature in the skin from the body core with a certain radial distance is uniform, that is, steady-state, and then in left-hand Figure 3.4, it goes down towards the skin surface and reaches 35.6°C in 60 sec, 35°C in 120 sec and 34.5°C in 180 sec. The results, in this case, are the consequences of the insulation of clothes as well as air insulation.

On the other hand, the temperature at the nude skin surface is 29°C in 60 sec, 26°C in 120 sec, and 24°C in 180 sec, respectively, represented in right-hand Figure 3.3. The result is due to the absence of protective cloth in the body.

3.7.2 Effect of Air Velocity and Walking Speed

The velocity of wind and person's walking speed have an important role in heat loss from the body. The values of thermophysical and clothing parameters have been calculated and assigned from Tables 2.1 and 3.2, respectively. Aditionally the parametric values related to air velocity and walking speed have been cited from [48, 54] to evaluate the variation of temperature within the body.

The graphs in Figure 3.4 stand for the temperature profile at the different time steps starting from 0 second up to 180 seconds. Even though the air velocity and walking speed occur, it results in a small variation in temperature at the skin surface than
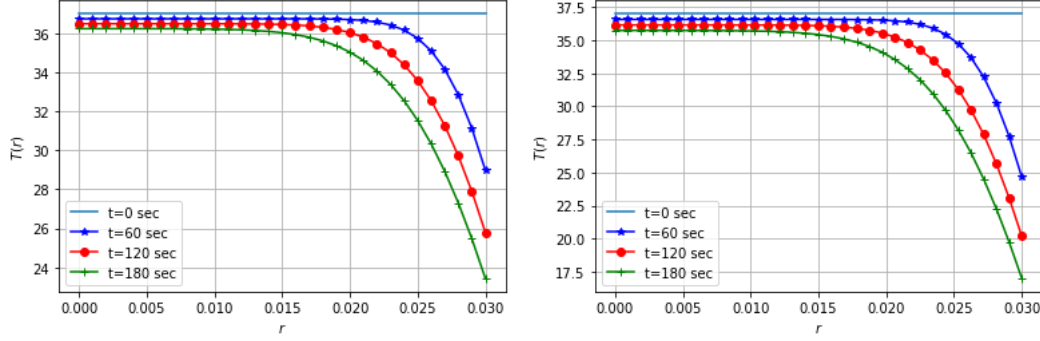
Figure 3.4: Variation in temperature with (left) $V_a = 0$ m/s $w_s = 0$ m/s , $I_{cl} = 0$ m^2 °C/W, $I_a = 0$ m^2 °C/W, and (right) $V_a = 4.1$ m/s, $w_s = 0.42$ m/s, $I_{cl} = 0$ m^2 °C/W, $I_a = 0$ m^2 °C/W.

that of the temperatures in left-hand Figure 3.4. This outcome is due to the presence of clothing insulation. Right-hand Figure 3.4 brings out the effects of wind velocity and walking speed without clothing insulation. These significant variations in temperatures in right Figure 3.4 at skin surface in different time steps are upshot of the relative velocity of air.

The graphs in a single Figure 3.5, with the colors red, green, pink, and purple, respectively, stand for the body temperature with the effect of air velocity and walking speed only, the body temperature including the effect of all parameters, and the body temperature with the effect of clothing parameters only. All of the results in Figures 3.3 and 3.4 have been accumulated in this Figure 3.5.

From all these Figures, there is no doubt that clothing insulation helps to decrease the rate of heat loss from the body whereas air velocity gives rise to heat loss from the body.

3.7.3 Temperature Profile of the Body with Clothing

The values of clothing and thermophysical parameters have been tabulated in Tables 2.1 and 3.2, then the temperature profile have been performed in the left-hand and right-hand Figure 3.6 in time step $\Delta t = 0.01$ sec, and 3.7 in time step $\Delta t = 0.4$ sec with different mesh sizes $\Delta r = 0.001$ m,, and 0.0005 m respectively. Similarly, the left-hand Figure and the right-hand Figure 3.8 show the temperature profile of the human body with the clothing layer in time steps $\Delta t = 0.01$ sec and $\Delta t = 0.4$ sec, respectively with mesh size $\Delta r = 0.00005$ m.

The curves in the left-hand Figures 3.6 and 3.7 slightly deviate when $r_N = N \Delta r_N$
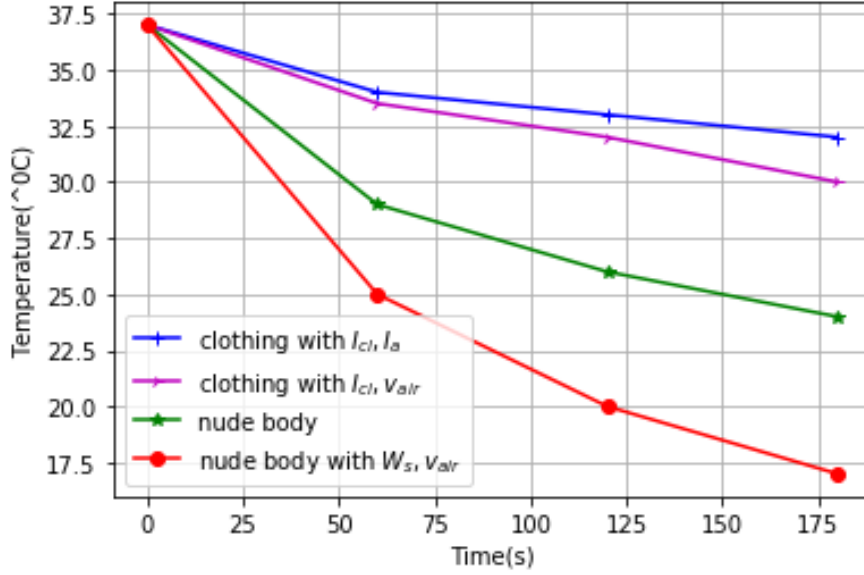
Figure 3.5: Temperatures at skin surface for nude body and clothed body with clothing insulation and air velocity, $R = 0.03\,\mathrm{m}$.

$= 0.030\,\mathrm{m}$, at the skin surface due to the interface condition between two materials having nonhomogeneous behavior. The curves in right-hand Figures 3.6 and 3.7 are less deviated than in left-hand Figures 3.6 and 3.7 while the graphs in left-hand and right-hand Figure 3.8 are smoother than in the previous four Figures 3.6 and 3.7. The comparison in graphs indicates that the increment in the number of grid points makes the graphs smoother, more accurate, reliable, and independent of mesh sizes as well. All the graphs in Figures 3.6, 3.7, and 3.8 show that the temperature remains steady up to a certain distance of $0.02\ m$ from the body core, then decreases towards the skin surface and further then towards clothes. The temperature profile obtained in 60 sec, 120 sec, and 180 sec, respectively remains the same regardless of the mesh sizes.

3.7.4 Graphical Verification

The stability of developed FD schemes (3.25) and (3.32) for one dimensional Pennes' bioheat equation (3.12) has also been verified by considering the body with protective clothing system at the boundary node and the effects of different parameters mentioned in Table 2.1 and in Table 3.2 have been investigated for different grid points 25, 40, and 55, and points 100, 500, and 1000 in both non-clothing and clothing cases are taken at the increment to demonstrate the validity and applicability of the developed

78
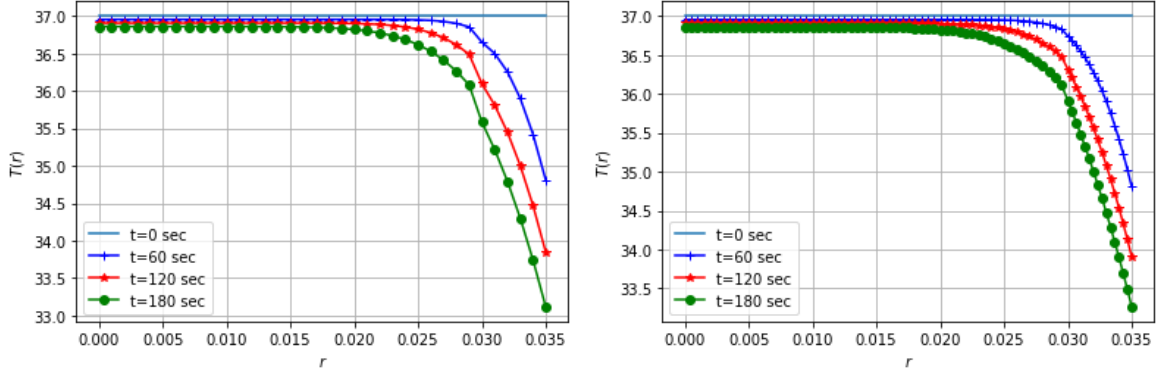
Figure 3.6: Temperature profile along radial direction in $\Delta t = 0.01$ sec (left) Mesh size $\Delta r = 0.001$ m (right) mesh size $\Delta r = 0.0005$ m.
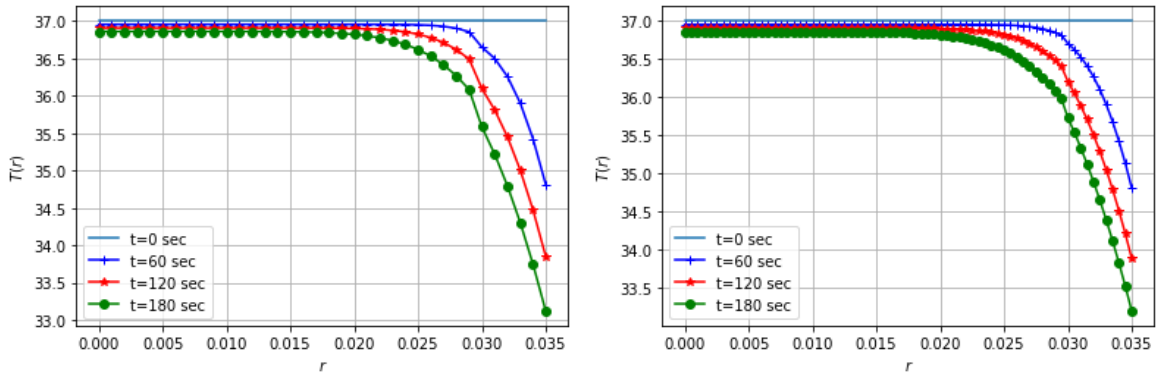
Figure 3.7: Temperature profile along radial direction in $\Delta t = 0.4$ sec (left) mesh size $\Delta r = 0.001$ m (right) mesh size $\Delta r = 0.0005$ m .
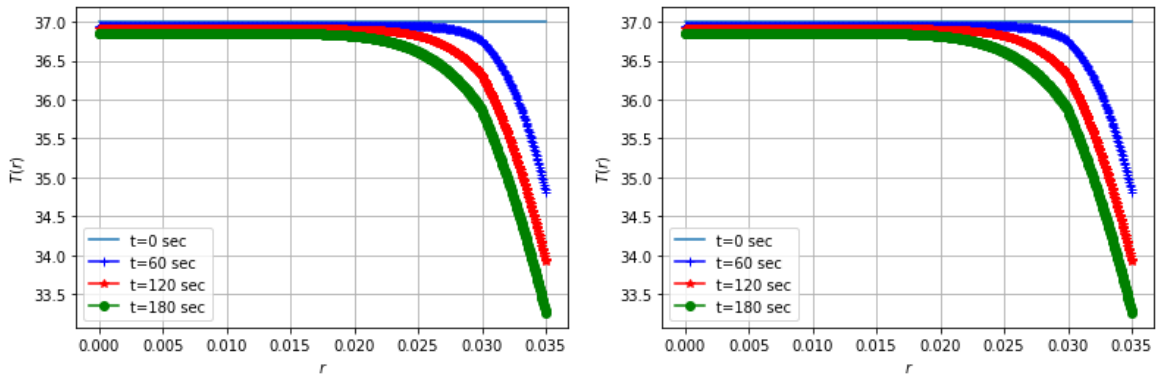
Figure 3.8: Temperature profile along radial direction with mesh size $\Delta r = 0.0005$ m at time step (left) $\Delta t = 0.01$ sec (right) $\Delta t = 0.4$ sec.

numerical implicit FD scheme at time increment in 0.01 sec in Figures 3.9 and 3.10. The tissue thickness of the human cylindrical limb in this model is taken $L= 0.03$ m [73, 123], from the body core to the skin surface in addition to the thickness of clothes

$0.005\,\text{m}$ [38], the results are calculated with the new thickness $L = 0.035\,\text{m}$.
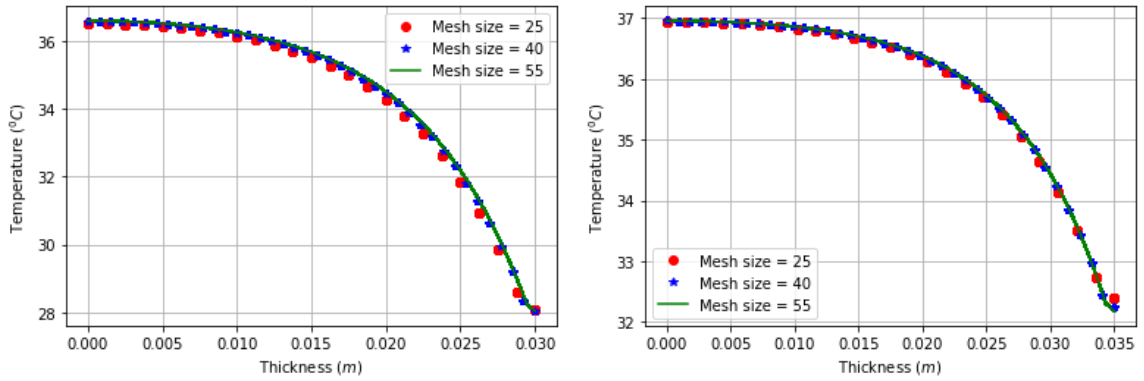
Figure 3.9: Temperature profile along radial direction in 180 sec with gride points 25, 40, and 55 (left) nude and (right) clothed body.
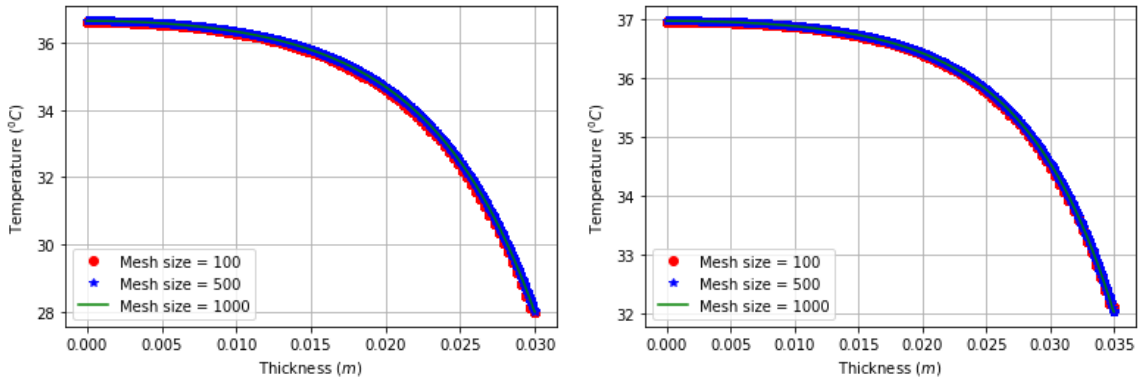
Figure 3.10: Temperature profile along the radial direction in 180 sec with gride points 100, 500, and 1000 (left) nude and (right) clothed body.
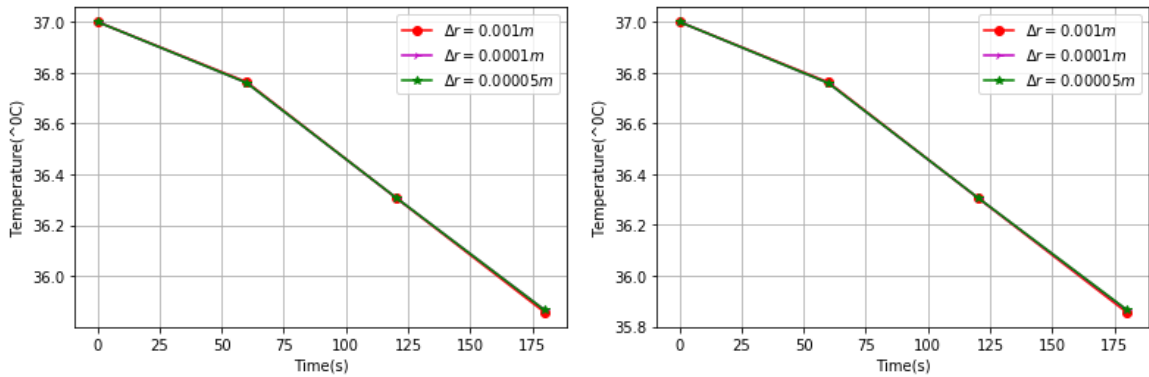
Figure 3.11: Temperature profile at the interface (skin surface) with different mesh sizes (left) at $\Delta t = 0.01$ sec and (right) at 0.4 sec.
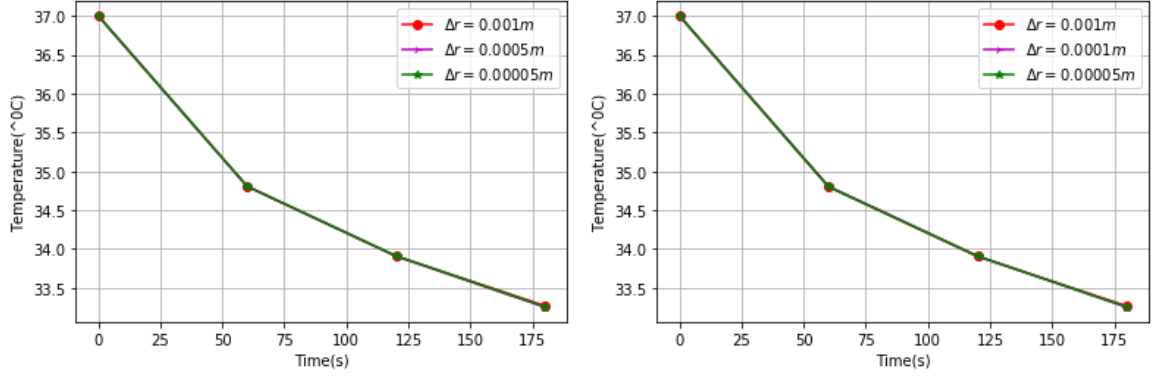
Figure 3.12: Temperature profile at the interface (clothes surface) with different mesh sizes (left) at $\Delta t = 0.01$ sec and (right) at 0.4 sec.
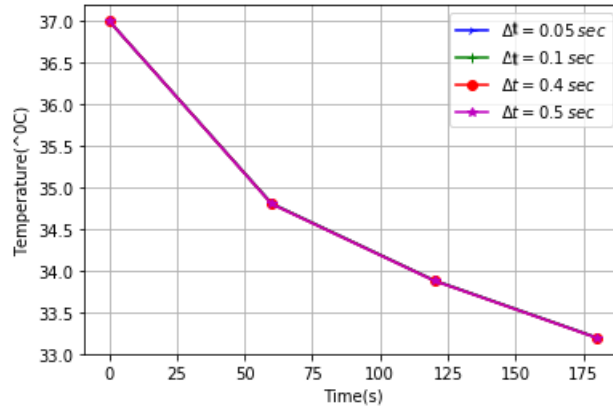
Figure 3.13: Temperature profile when $\Delta r = 0.0005$ m at different small time steps Δt.

The numerical verification has been performed in Figure 3.9 with three different mesh sizes (different grid points) 25, 40, and 55 at time increment $\Delta t = 0.01$ sec for non-clothing left-hand and clothing right-hand system of the human body. The temperature of the nude body (left) at the skin surface is 28°C. In the clothing state (right), on the contrary, the temperature rises up to 32°C. This result is because of the effect of clothing insulation and other parameters related to clothes in Table 3.2. A Similar outcome has appeared in Figure 3.10 with different grid points (mesh sizes) 100, 500, and 1000 at time increment (step) $\Delta t = 0.01$ sec. This observation has taken up to 3 min. The temperature in Figure 3.9 and in Figure 3.10 coincides on the same curve even though the mesh sizes are different for non-clothing, the nude body left-hand and the corresponding temperature for the clothed body right-hand are almost the same. In both cases, the Figures are independent no matter what the mesh sizes are. These results verify the stability of the implicit FD scheme for a newly developed model with clothing at the boundary.

81

In the case of the protective layer, the interface temperature (skin surface) obtained from results having different mesh sizes at time step 0.01 sec and 0.4 sec are represented in graphs of left-hand and right-hand Figure 3.11 and exhibited in Tables 3.3 and 3.4, respectively.

Similarly, the temperatures at the surface of cloth with different mesh sizes at time steps 0.01 sec and 0.4 sec are represented in graphs of left-hand and right-hand Figure 3.11 and exhibited in Tables 3.5 and 3.6, respectively. Furthermore, the temperature profile at different time steps 0.05 sec, 0.1 sec, 0.4 sec, and 0.5 sec when mesh size is 0.0005 m has been presented in Figure 3.13 and tabulated in Table 3.7.

Table 3.3: Temperature profile at the interface (skin surface) when $\Delta t = 0.01$ sec.

Δr (m)	Temperature in 60 sec	Temperature in 120 sec	Temperature in 180 sec
0.001	36.76374598	36.30866076	35.85715129
0.0001	36.76037207	36.30920285	35.86597663
0.00005	36.7602856	36.309688591	35.86747444

Table 3.4: Temperature profile at the interface (skin surface) when $\Delta t = 0.4$ sec.

Δr (m)	Temperature in 60 sec	Temperature in 120 sec	Temperature in 180 sec
0.001	36.76374598	36.30866076	35.85715129
0.0001	36.76037207	36.30920285	35.86597663
0.00005	36.7602856	36.309688591	35.86747444

Table 3.5: Temperature profile at the clothing surface when $\Delta t = 0.01$ sec.

Δr (m)	Temperature in 60 sec	Temperature in 120 sec	Temperature in 180 sec
0.001	34.8052701	33.88093058	33.19336681
0.0001	34.80522479	33.9068697	33.2500773
0.00005	34.80551148	33.91018652	33.25706422

As the graphs presented in Figure 3.11 with temperature profile in Tables 3.3 and 3.4 for body parts and in Figure 3.12 with temperature profile inTables 3.5 and 3.6 for clothes coincide respectively. It can be concluded that the numerical solution of the model is stable and convergence with respect to the grid.

The temperatures in Table 3.7 and graphs in Figure 3.13 at different time steps

Table 3.6: Temperature profile at the clothing surface when $\Delta t = 0.4$ sec.

$\Delta r(\text{m})$	Temperature in 60 sec	Temperature in 120 sec	Temperature in 180 sec
0.001	34.79948362	33.87632483	33.18921782
0.0001	34.80522479	33.9068697	33.2500773
0.00005	34.79994767	33.90584859	33.25312605

Table 3.7: Temperature profile when $\Delta r = 0.0005\,\text{m}$ at different time steps.

Δr (m)	Temperature in 60 sec	Temperature in 120 sec	Temperature in 180 sec
0.05	34.80467674	33.8804583	33.19294127
0.1	34.803935	33.87986792	33.19240934
0.4	34.79948362	33.87632483	33.18921782
0.5	34.79799948	33.8751435	33.18815399

$\Delta t = 0.05$ sec, $\Delta t = 0.1$ sec , $\Delta t = 0.4$ sec, and $\Delta t = 0.5$ sec with $\Delta r = 0.0005\,\text{m}$, coincide, respectively. So, all graphs are independent of the time step sizes.

These results help to verify the stability and convergence of the FD scheme for the model.

3.7.5 Validation of the Results

The solution of the bioheat transfer equation depends upon the feature of human body organs, blood flow, and environmental situation. The behavior of the solution procedure is also influenced by the specified initial and boundary conditions and the insulation values of the structure of the fabric. Both Neumann boundary condition—the flux boundary condition and the modified Robin boundary condition—a mixed boundary conditions are used in this work. The Differential equation is approximated into the systems of difference equations using Taylor's series method. Euler's implicit finite difference method is used with these initial and boundary conditions to solve the models independently for the human tissue element and the insulating layer, then combine the results with the interface condition. By constructing a lemma and a few theorems, it has also been proven that the proposed FD schemes for the cylindrical shape of the body with a protective garment system and its effects are solvable (existence), consistent, stable, and convergent. The developed model, therefore, is theoretically valid. Additionally, the numerical computational results in this work seem to agree with the similar values of experimentally tested and verified clothing

parameters by ISO-7730, ASHARE standard 55 [48, 49], and the results Figures 3.9 and 3.10 for clothing at the boundary have good agreement with the results of Zhao et al. [124].

3.8 Conclusion

The mathematical model of the Pennes type has been expanded by incorporating the clothing parameter as a protective layer. The model has been solved using a fully implicit, finite difference method. The body temperature decreases up to 17.5°C for the nude body after the addition of wind velocity and walking speed to the modified convective term, in the existing Robin's condition. On the contrary, the temperature of the body reaches 34.5°C while adding the effective clothing area factor in the usual Robin's boundary condition. Additionally, wearing clothing simultaneously prevents the body from a quick drop in skin temperature. Suitable management of clothing in harsh climatic conditions keeps the body at a highly satisfactory and comfort level. The lemma and theorems have been established for analyzing the solvability, consistency, stability, and convergence of the implicit FD scheme of the model. We conclude that the developed model with the clothing phenomena is stable, consistent, and convergent on the basis of grid points as well as time step sizes. The mathematically verified model is useful for clothing and environmental designers as well as biomedical researchers, who can be benefitted from the knowledge of microclimate temperature and can accordingly design workplace and functional clothing so that people can feel comfortable for better performance. The developed model also fosters advanced clothing systems to provide better comfort to the human body. The results seem to agree with the similar values of clothing parameters, which are experimentally verified in ASHRAE [49], and Figure 3.10 for clothing at the boundary has good agreement with the results by Zhao et al. [124].

CHAPTER 4

TWO-DIMENSIONAL AXISYMMETRIC MODEL WITH TIME-DEPENDENT METABOLISM AND PHYSICAL ACTIVITIES

4.1 Introduction

Previously developed models, especially based on one dimensional bioheat model, we have analyzed the temperature distribution only in the radial direction. In this Chapter, we develop a two-dimensional axisymmetrical bioheat transfer model in cylindrical coordinates, assuming symmetry in the angular direction incorporating a time-dependent metabolic heat generation during physical activities and the temperature-dependent sweating effect at boundary conditions.

Although there are considerable research articles available on the two-dimensional axisymmetrical bioheat model [5, 23, 58, 59, 80], we did not find any work which has incorporated clothing in their research. We have also included clothing parameters in the two-dimensional model. This model accounts for the basal physiological properties of the tissue material based on ASHRAE Standard 55-2017 and other literatures [38, 48, 49, 77, 84, 93, 124] as well as time-dependent metabolism and temperature-dependent sweating. The proper result cannot be recognized if the clothing system and its significance for preserving human thermal comfort are ignored. Thus, this chapter also covers garment parameters at boundary conditions. Sweating is an important mechanism of heat loss from the human body. Evaporation accounts for 22% of heat loss under typical resting settings. The body's primary method of heat dissipation is sweating, especially while exercising. Physical exercise leads to heat loss from the body and keeps the body in a comfortable condition. All these primary contexts are covered in section 4.2. Modifying the existing Robin's boundary condition by taking clothing and nonlinear sweating into account is the major focus in section

4.3. Development and implementation of the numerical methods, simulation results and discussion, and conclusion of the Chapter 4 are presented in sections 4.4, 4.5, and 4.6 respectively .

4.2 Role of Clothing, Physical Activities, Metabolism and Sweating

Clothing safeguards the body from extreme climatic conditions, and physical activity helps to keep a person physically fit and healthy. The human anatomical structure, which involves multiple heat transfer phenomena, is extensively responsible for maintaining the person in a comfort zone with an equilibrium core temperature [38, 42, 78]. One would be able to easily drain perspiration and feel comfortable in the light clothing system. In contrast, wearing thick, impermeable clothing will prevent the body from rapidly warming up in hot environments due to reduced evaporation and exercise maintains a person's physical health and fitness.

4.2.1 Physical Activities and Metabolism

The rate of production of energy due to the utilization of oxygen and food is known as the metabolic rate. $ISO\,8996$, $ANSI/ASHRAE$ standard $55-2017$ defines that the metabolic rate is the heat obtained from the transformation of chemical energy and mechanical work from personal activities [48, 49]. The amount of metabolic heat generation rate highly depends upon the various physical activities at the different time levels. The large amount of metabolic energy that produces more heat due to more physical activities may sometimes create a problem in blood circulation and lead to a heart attack if the storage metabolism cannot dissipate properly. The heat and vapor transfer properties of clothing worn by a person have a major role in his/her strength in the workplace. Many researchers Havenith, Lundgren, Kuklane, Van Hoof, Oĝulata [48, 49, 55, 85, 113] who got involved in the field of clothing thermal comfort, have used metabolism related to body surface area or body mass with its unit of W/m^2 mentioning the metabolism of seated person is 1 MET = 58.2 W/m^2. So far as research related to biomedical is concerned [29, 31, 65, 74, 123], the activity-based metabolic heat generation rate is generally considered as related to body volume with its unit W/m^3.

Healthy human tissue has $1114\,\mathrm{W/m^3}$ [108], the average basal metabolic rate (BMR), which is the metabolic heat generation rate in the rest condition of a person. The more blood flow, the more metabolic rate. It may change according to age, sex, and

the different activities. Shrestha and Acharya [106, 107] recently studied $1D$ mathematical model for thermoregulation in the human dermal part during sarcopenia and the metabolic differences during physical exercise. The finite element method for the cartesian coordinate system has been applied considering only the case for the non-clothing body. The metabolic rates $3266.67\,(\text{W}/\text{m}^3)$, $3889\,(\text{W}/\text{m}^3)$ and $7918\,(\text{W}/\text{m}^3)$ during cleaning, walking and running, respectively [48, 107] in 2000 seconds are taken and presented in the Figure 4.1.
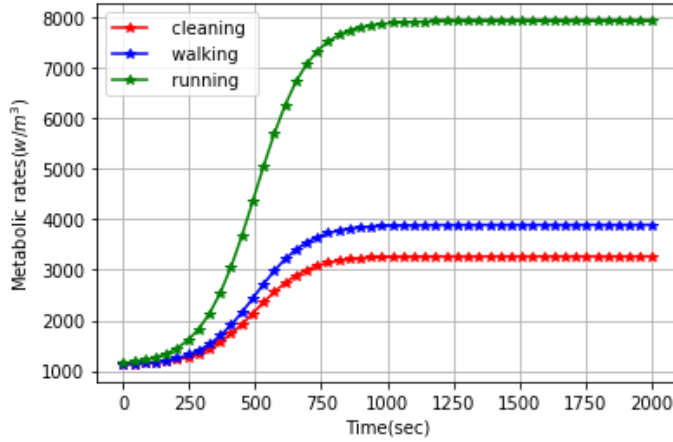
Figure 4.1: Metabolism in different activities.

.

The nature of this S-shaped graph in Figure 4.1 shows the logistic behavior of time-dependent metabolism in which a person's metabolic rate initially rises when he/she engage in various activities and then remains stable after a period of 750 seconds.

4.2.2 Physical Activities, Evaporation and Sweating

The human body regulates its temperature through perspiration by losing heat as tiny water drops from the skin's surface. The evaporative heat loss may be sensible and insensible. The sensible heat loss occurs by regulatory sweating and insensible heat loss by skin diffusion. The level of different physical activities determines the sweat evaporation in the body, which depends on skin temperature T_{sk}. The sweat evaporation rate E_{sk}, as the function of skin surface temperature, is given by [56, 78, 107]

$$E_{sk} = 8.47 \times 10^{-5} \left[(0.1 \times T_{sk} + 0.9 \times T_a + 0.9) - 36.6 \right]. \qquad (4.1)$$

87

Evaporative heat transfer coefficients
$17.008 \times 10^{-6} (\mathrm{W/m^2\,sec}), 24.792 \times 10^{-6} (\mathrm{W/m^2\,sec}), 33.190 \times 10^{-6} (\mathrm{W/m^2\,sec})$. at resting, cleaning and running are taken and presented in left-hand Figure 4.2.

The absorption of water vapor with anhydrous calcium chloride across a surface area of skin results in insensible perspiration, which is the water evaporation from the skin's surface without the presence of visible sweat droplets. At a high ambient temperature and high metabolic rate, the body produces more sweat than at a low ambient temperature and at rest.

The insensible perspiration from the surface of the skin E_{sk} that depends upon the level of activity and ambient temperature is given by [31, 60]

$$E_{sk} = \eta_e\, A_{\mathrm{sk}}(P_{w,sk} - P_{\mathrm{w,\,air}}) \tag{4.2}$$

$$\text{and} \qquad P_{\mathrm{w,sk}} = w\, T_{sk} - S \tag{4.3}$$

where
η_e : 0.35, evaporative coefficient ($\mathrm{W/m^2\,mm\,Hg}$)
$A_{\mathrm{sk:}}$ skin surface area ($\mathrm{m^2}$)
$P_{\mathrm{w,\,air:}}$ 14.69, vapor pressure of air (Kpa)
$P_{\mathrm{w,sk}}$: water vapor pressure at the skin with constant value S= 2.53.

The vapor pressure of water $P_{\mathrm{w,sk}}$, the function of the skin surface temperature with different values of w, is presented in right-hand Figure 4.2.
Both the evaporative heat transfer coefficient E_{sk} and the vapor pressure of water $P_{\mathrm{w,\,sk}}$ have a linear relationship with the skin surface temperature that can be seen in Figure 4.2.
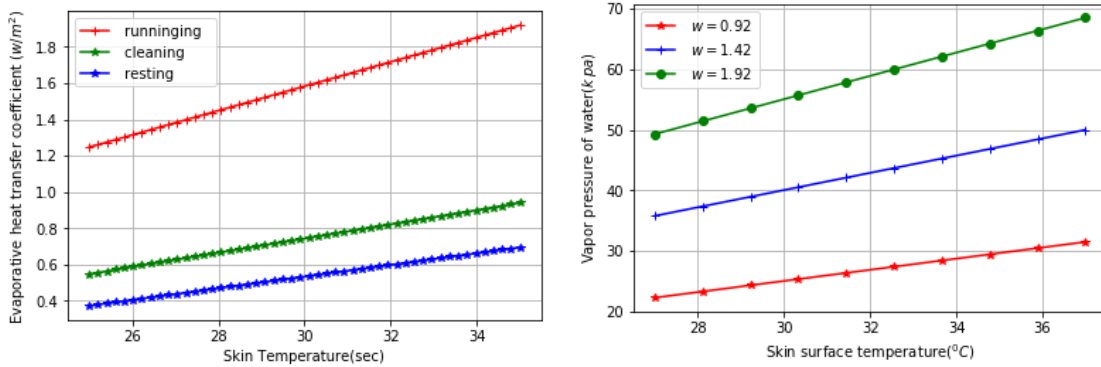
Figure 4.2: (left) Evaporative heat transfer and (right) water vapour pressure.

4.3 Two-Dimensional Axisymmetric Bioheat Transfer Model

The human body is shaped like a cylinder, including individual body parts. Therefore, we employed the cylindrical coordinate system for the course of this investigation. For computational purposes in this section, we prefer an axisymmetric two-dimensional bioheat transfer model that simulates a three-dimensional object in reality.

4.3.1 Assumptions of the Model

Cylindrical shapes are considered for numerical and analytical techniques in a variety of engineering and scientific computations. These forms are typically considered normal shapes for heat transfer. In Chapter 2, the bioheat transfer equation in a three-dimensional cylindrical coordinate system (r, θ, z) is presented. The general form of the equation (2.20) can be applied for the study of heat flow in radial, angular, and axial directions r, θ, and z, respectively. Keeping the angular direction constant in many situations, axisymmetric computations may now be performed with angular symmetry as shown in Figure 4.3. The transient bioheat transfer equation,
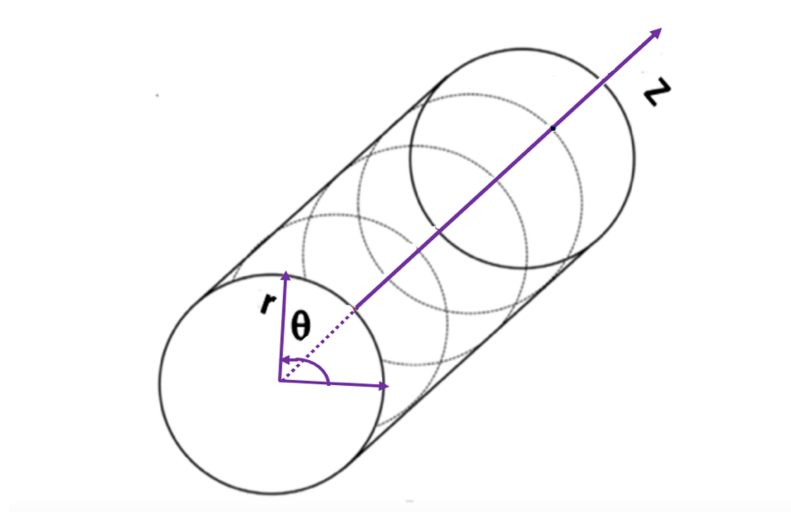
Figure 4.3: Cylindrical coordinate system.

formulated for the thermal response of the living tissue, incorporates the heat transfer mechanisms due to physical and physiological activities [93, 108] is given by

$$\rho c \frac{\partial T}{\partial t} \;=\; \nabla \cdot [K \nabla T] + \rho_b c_b \, w_b (T_a - T) + q_m(t), \qquad (4.4)$$

where

ρ : tissue density (kg/m³)

c : tissue specific heat (J/kg°C)

K : thermal conductivity of tissue(W/m°C)

$$\nabla \cdot [K\nabla T] \;=\; K\left(\frac{\partial^2 T}{\partial r^2} + \frac{1}{r}\frac{\partial T}{\partial r} + \frac{\partial^2 T}{\partial z^2}\right) \tag{4.5}$$

w_b : blood perfusion rate (kg/m³ sec)

c_b : blood specific heat (J/kg°C)

T_a : arterial blood temperature (°C)

$q_m(t)$: metabolic heat generation (W/m³) implemented as [107]

$$q_m(t) \;=\; \left[q_b + \frac{(q_A - q_b)}{1 + e^{-\alpha_c\,(t-t_m)}}\right] \tag{4.6}$$

where

q_b : basal metabolic rate (W/m³)

q_A : activity threshold metabolism (W/m³)

t_m : sigmoid midpoint

α_c : activity control parameter per unit time ($0 \le \alpha_c \le 1$).

The bioheat equation (4.4) is a modification of the bioheat equation suggested by Pennes' in 1948 with total heat storage on the left-hand side; the first, second, and third terms of the right-hand side are diffusion, perfusion, and metabolic heat generation, respectively. The modified term $q_m(t)$ expressed in (4.6) is the metabolic heat generation during physical exercise. The symbols r and z used in equation (4.5), be the radial and the axial distance from the core towards the boundaries, represented by OA and OC respectively in left-hand and right-hand Figure 4.4.

The shape of human body parts appears to be axially symmetric whose cylindrical limb and a cross-sectional slice are shown in Figure 4.4. So, two-dimensional axisymmetrical unsteady-state temperature profiles from the bioheat equation (4.4) have been performed in both the radial and axial directions by using a cylindrical coordinate system with temperature as the function of (r, z, t) only.

4.3.2 Boundary Conditions

The boundary conditions with inner boundary D_1 at the core, outer boundary D_2 at the skin surface (expose to the environment), bottom and top boundaries D_3 and D_4 in Figure 4.3 are given by

$$-K\frac{\partial T}{\partial r}\bigg|_{r=0} \;=\; 0, \qquad\qquad \text{for } t=0 \text{ in } D_1. \tag{4.7}$$
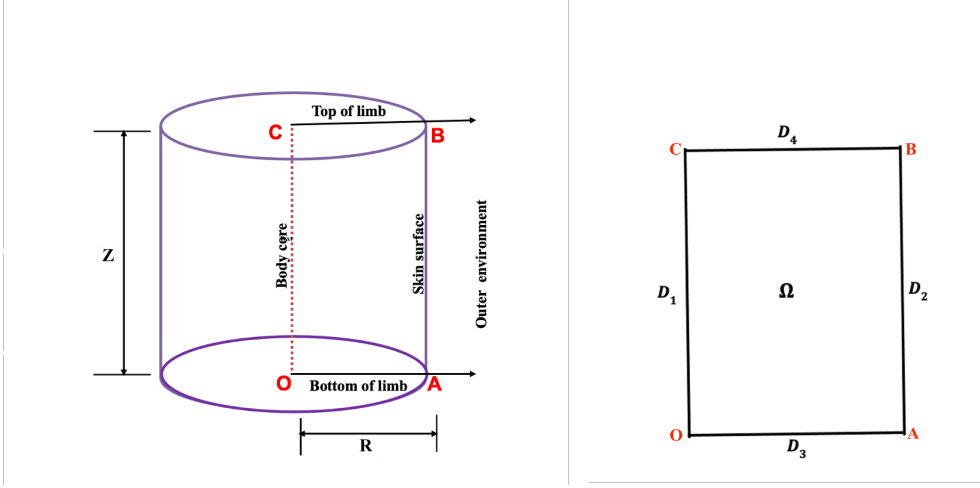
Figure 4.4: Cylindrical human body shape and Cross-sectional slice (Ω) with boundaries.

$$-K\frac{\partial T}{\partial r}\bigg|_{r=R} = h_A(T - T_\infty) + E_{sk}, \quad \text{for } t > 0 \text{ in } D_2. \tag{4.8}$$

$$-K\frac{\partial T}{\partial z}\bigg|_{z=0} = 0, \qquad \text{for } t > 0 \text{ in } D_3. \tag{4.9}$$

$$-K\frac{\partial T}{\partial z}\bigg|_{z=Z} = 0, \qquad \text{for } t > 0 \text{ in } D_4. \tag{4.10}$$

where E_{sk} is the sweat evaporation given in equation (4.1), and (4.2) for sensible and insensible perspiration, h_∞ be ambient temperature and h_A be the combined heat transfer coefficient due to convection and radiation along with clothing insulation which is given by

$$h_A = F_{cl}\left(h_{\text{conv}} + h_r\right) \qquad \text{and} \qquad F_{cl} = \frac{I_a}{I_{cl} + I_a/f_{cl}}.$$

4.3.3 Initial Condition

The initial condition at $t = 0$ in the model is

$$T(r, z, t = 0) = T_0(r, z).$$

As the irregular shape of the human body organs poses a challenge for obtaining the exact solution, the numerical scheme is chosen to provide a better approximation solution for a two-dimensional bioheat transfer model with sweating and clothing effect at the outer boundary.

4.4 Numerical Methods for Two-Dimensional Axisymmetric Bioheat Equation

Solving the bioheat transfer problems using numerical methods is of great interest in the field of physiological and biological research for observing the effect of the fluctuation in temperature due to various factors. In one dimensional case, as discussed in previous Chapters, the temperature is assumed to flow only along the radial (r)-direction whereas in the axisymmetric two-dimensional (r, z) case, it flows in both the radial and axial directions. Here we describe the finite difference discretization process and deduce the Euler's Explicit, Euler's Implicit, and Crank- Nicolson methods in such a cylindrical geometry as shown in Figure 4.5.
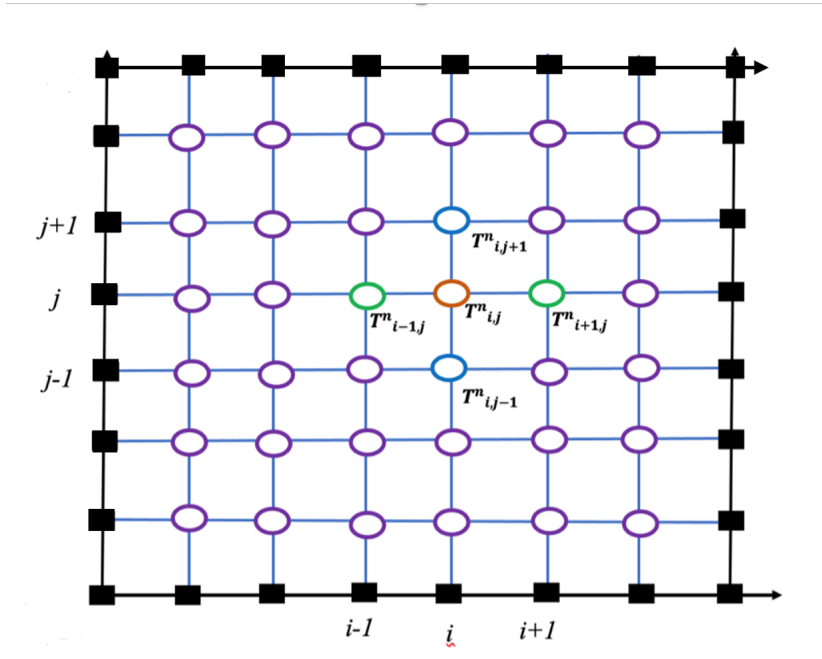
Figure 4.5: FD discretization of spatial domain (Ω) in radial and axial direction with time domain.

4.4.1 Finite Difference Discretization

We set up a two-dimensional (r, z) mesh on a cylindrical-shaped human limb by dividing the radial length $[0, R]$ into M_r sub intervals and the axial length $[0, Z]$ into M_z subintervals with $\Delta r = R/M_r$ and $\Delta z = Z/M_z$, respectively and construct a three-dimensional grid (r_i, z_j, t_n) with $r_i = i\,\Delta r$, $i = 0, 1, 2, \cdots, M_r$, $z_j = j\,\Delta z$, $j = 0, 1, 2, \cdots, M_z$ and $t_n = n\Delta t$, $n = 1, 2, \cdots, N$ as shown in Figure 4.5

Explicit Scheme

Consider that $T_{i,j}^n$ denotes $T(r_i, z_j, t_n)$.

The partial differential equation (4.4) can be approximated using explicit scheme as

$$\left.\frac{\partial T}{\partial t}\right|_{(r_i,z_j,t_n)} \approx \frac{T_{i,j}^{n+1} - T_{i,j}^n}{\Delta t} \tag{4.11}$$

$$\left.\frac{\partial T}{\partial r}\right|_{(r_i,z_j,t_n)} \approx \frac{T_{i+1,j}^n - T_{i-1,j}^n}{2\Delta r} \tag{4.12}$$

$$\left.\frac{\partial^2 T}{\partial r^2}\right|_{(r_i,z_j,t_n)} \approx \frac{T_{i-1,j}^n - 2T_{i,j}^n + T_{i+1,j}^n}{\Delta r^2} \tag{4.13}$$

$$\left.\frac{\partial^2 T}{\partial z^2}\right|_{(r_i,z_j,t_n)} \approx \frac{T_{i,j-1}^n - 2T_{i,j}^n + T_{i,j+1}^n}{\Delta z^2} \tag{4.14}$$

With the help of equations (4.11), (4.12), (4.13), and (4.14), the Explicit scheme for axisymmetric bioheat transfer equation (4.4) at time level t_n becomes

$$\begin{aligned}
\frac{T_{i,j}^{n+1} - T_{i,j}^n}{\Delta t} &= D\left[\frac{T_{i-1,j}^n - 2T_{i,j}^n + T_{i+1,j}^n}{\Delta r^2} + \frac{T_{i+1,j}^n - T_{i-1,j}^n}{2r_i\Delta r} + \frac{T_{i,j-1}^n - 2T_{i,j}^n + T_{i,j+1}^n}{\Delta z^2}\right] \\
&\quad + \beta\left(T_a - T_{i,j}^n\right) + \gamma_{m,i,j}^n,
\end{aligned} \tag{4.15}$$

where $D = \dfrac{K}{\rho c}$ and $\beta = \dfrac{w_b\, c_b\, \rho_b}{\rho\, c}$, $\gamma_m = \dfrac{q_m(t)}{\rho c}$.

The construction of grid for two-dimensional cylindrical geometry in Explicit scheme is shown in Figure 4.6.

4.4.1.1 Implicit Scheme

In the equation (4.5) we denote $T(r_i, z_j, t_{n+1})$ by $T_{i,j}^{n+1}$. The partial differential equation (4.5) can be approximated using an implicit scheme as

$$\left.\frac{\partial T}{\partial t}\right|_{(r_i,z_j,t_{n+1})} \approx \frac{T_{i,j}^{n+1} - T_{i,j}^n}{\Delta t} \tag{4.16}$$
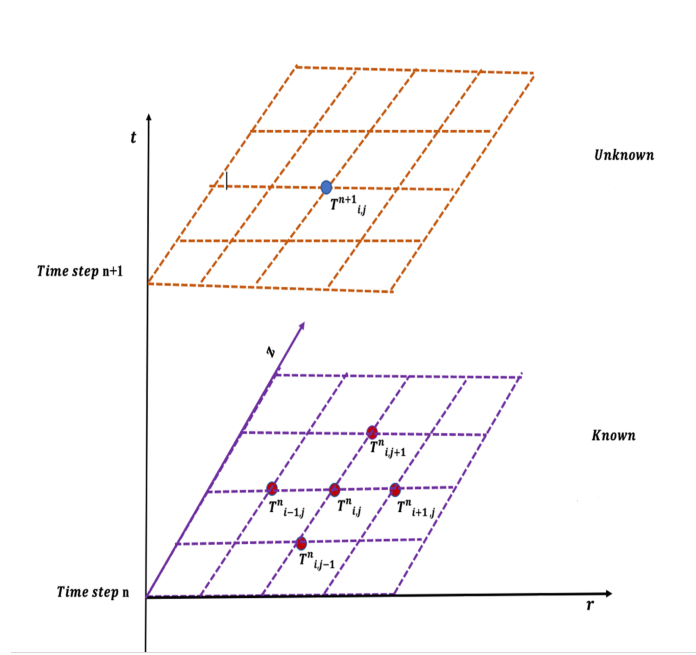
Figure 4.6: Schematic representation of the relationship between the variables at two successive time steps in Explicit method with 5 by 5 grid system.

$$\left. \frac{\partial T}{\partial r} \right|_{(r_i, z_j, t_{n+1})} \approx \frac{T_{i+1,j}^{n+1} - T_{i-1,j}^{n+1}}{2\Delta r} \tag{4.17}$$

$$\left. \frac{\partial^2 T}{\partial r^2} \right|_{(r_i, z_j, t_{n+1})} \approx \frac{T_{i-1,j}^{n+1} - 2T_{i,j}^{n+1} + T_{i+1,j}^{n+1}}{\Delta r^2} \tag{4.18}$$

$$\left. \frac{\partial^2 T}{\partial z^2} \right|_{(r_i, z_j, t_{n+1})} \approx \frac{T_{i,j-1}^{n+1} - 2T_{i,j}^{n+1} + T_{i,j+1}^{n+1}}{\Delta z^2}. \tag{4.19}$$

With the help of equations (4.16), (4.17), (4.18), and (4.19), the Implicit scheme for equation (4.4) at time level t_{n+1} becomes

$$\frac{T_{i,j}^{n+1} - T_{i,j}^n}{\Delta t} = D \left[\frac{T_{i-1,j}^{n+1} - 2T_{i,j}^{n+1} + T_{i+1,j}^{n+1}}{\Delta r^2} + \frac{T_{i+1,j}^{n+1} - T_{i-1,j}^{n+1}}{2r_i \Delta r} + \frac{T_{i,j-1}^{n+1} - 2T_{i,j}^{n+1} + T_{i,j+1}^{n+1}}{\Delta z^2} \right]$$
$$+ \beta \left(T_a - T_{i,j}^{n+1} \right) + \gamma_{m,i,j}^{n+1} \tag{4.20}$$
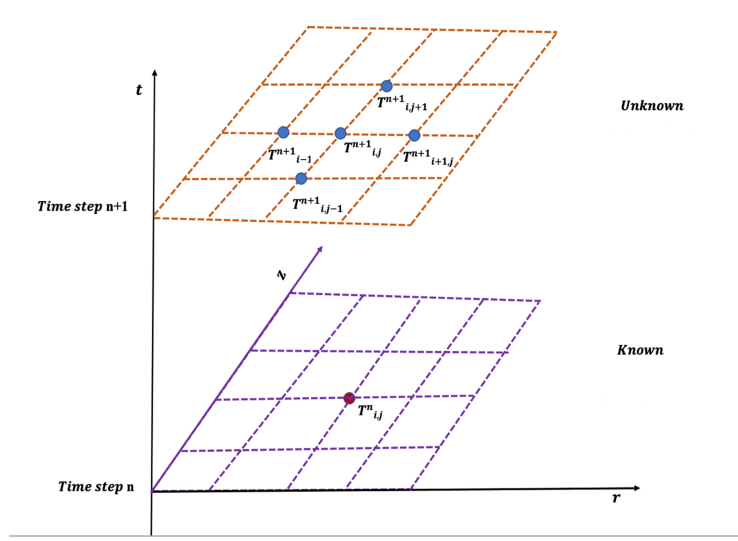
Figure 4.7: Schematic representation of the relationship between the variables at two successive time steps in Implicit method with 5 by 5 grid system.

Crank-Nicolson Scheme

FD scheme using a weighted average θ ($0 \le \theta \le 1$) of the derivatives $\dfrac{\partial T}{\partial r}, \dfrac{\partial^2 T}{\partial r^2}$, and $\dfrac{\partial^2 T}{\partial z^2}$ at two times label t_n and t_{n+1} is given by [21]

$$\frac{1}{\Delta t}\left[T_{i,j}^{n+1} - T_{i,j}^{n}\right] - \theta\left[D\left(\frac{T_{i-1,j}^{n+1} - 2T_{i,j}^{n+1} + T_{i+1,j}^{n+1}}{(\Delta r)^2} + \frac{1}{2r_i\Delta r}\left(T_{i+1,j}^{n+1} - T_{i-1,j}^{n+1}\right)\right)\right]$$

$$+\theta\left[D\left(\frac{T_{i,j-1}^{n+1} - 2T_{i,j}^{n+1} + T_{i,j+1}^{n+1}}{(\Delta z)^2}\right) + \left(\beta T_{i,j}^{n+1} - \gamma_{m,i,j}^{n+1}\right)\right]$$

$$= (1-\theta)\left[D\left(\frac{T_{i-1,j}^{n} - 2T_{i,j}^{n} + T_{i+1,j}^{n}}{(\Delta r)^2} + \frac{1}{2r_i\Delta r}\left(T_{i+1,j}^{n} - T_{i-1,j}^{n}\right)\right)\right]$$

$$+ (1-\theta)\left[D\left(\frac{T_{i,j-1}^{n} - 2T_{i,j}^{n} + T_{i,j+1}^{n}}{(\Delta z)^2}\right) + \beta T_{i,j}^{n} + \gamma_{m,i,j}^{n}\right]$$

$$\text{or } (1 - \Delta t\theta\beta)T_{i,j}^{n+1} - \theta\left[F_r\left(T_{i-1,j}^{n+1} - 2T_{i,j}^{n+1} + T_{i+1,j}^{n+1}\right) + \frac{F_{r1}}{2r_i\Delta r}\left(T_{i+1,j}^{n+1} - T_{i-1,j}^{n+1}\right)\right]$$

$$+\theta\left[F_z\left(T_{i,j-1}^{n+1} - 2T_{i,j}^{n+1} + T_{i,j+1}^{n+1}\right) + \Delta t\gamma_{m,i,j}^{n+1}\right]$$

$$= (1-\theta)\left[F_r\left(T_{i-1,j}^{n} - 2T_{i,j}^{n} + T_{i+1,j}^{n}\right) + \frac{F_{r1}}{2r_i\Delta r}\left(T_{i+1j}^{n} - T_{i-1,j}^{n}\right)\right]$$

$$+ (1-\theta)\left[F_z\left(T_{i,j-1}^{n} - 2T_{i,j}^{n} + T_{i,j+1,j}^{n}\right) + \left(1 - \Delta t\beta\right)T_{i,j}^{n} + \Delta t\gamma_{m,i,j}^{n}\right]. \quad (4.21)$$

Equation 4.21 is difference scheme having truncation error of order $\mathcal{O}\left(\Delta t^2 + \Delta z^2 + \Delta r^2\right)$,

where $F_r = \dfrac{D\Delta t}{(\Delta r)^2}$, $F_{r_1} = \dfrac{D\Delta t}{(\Delta r)}$, and $F_z = \dfrac{D\Delta t}{(\Delta z)^2}$.

The construction of a grid for two-dimensional cylindrical geometry in the Crank-Nicolson scheme is shown in Figure 4.8.
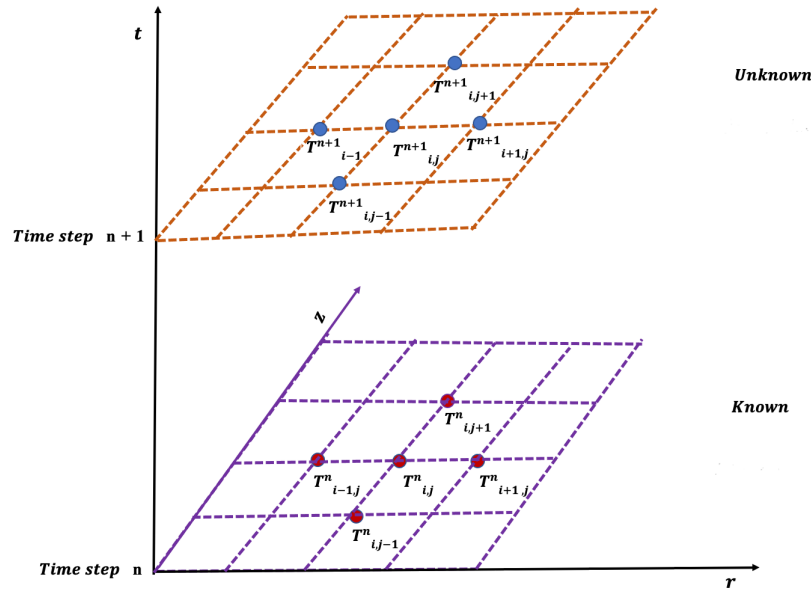
Figure 4.8: Schematic representation of the relationship between the variables at two successive time steps in the Crank-Nicolson method with 5 by 5 grid system.

According to the value of weighted average $'\theta'$, we can decide whether the finite scheme is explicit, implicit, or Crank-Nicolson method as follows

$$\theta = \begin{cases} 0 & \text{Scheme is explicit} \\ 0.5 & \text{Scheme is Crank-Nicolson} \\ 1 & \text{Scheme is implicit} \end{cases}$$

Mesh Points Numbering

A system of the algebraic equation (4.21), coupled at the new time level $n + 1$, has been organized as a structured matrix system of time-dependent metabolism. We must solve a system of (linear) algebraic equations, given below

$$AT = b, \tag{4.22}$$

where A is the coefficient matrix that is sparse, T is the vector of unknowns, and b is the vector on the right-hand side. Let p be the single index corresponding to the position of the mesh point (i, j). Then we have a two-dimensional nodal arrangement as shown in Figure 4.9
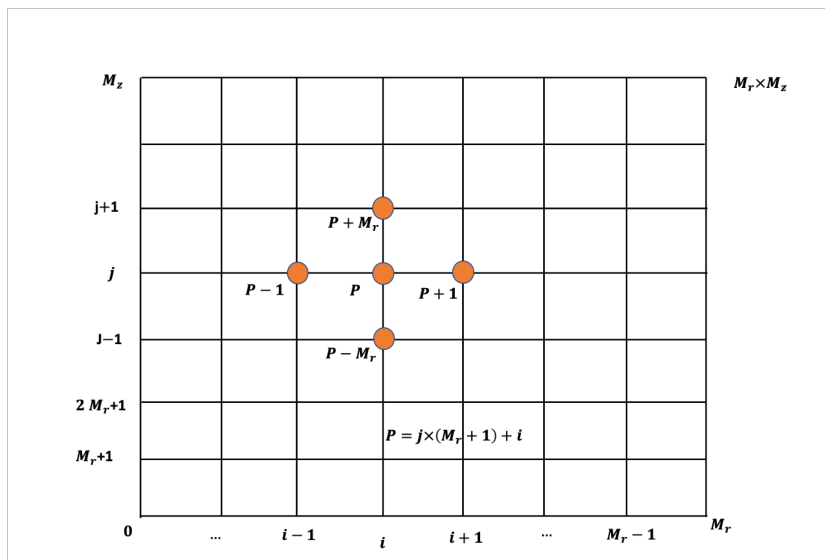
Figure 4.9: 2D mesh discretization with boundaries.

Now introducing a mapping $m(i, j)$ from a mesh point with indices (i, j) to the corresponding unknown position p in Figure 4.9 from the equation system

$$p \;=\; \text{pos}(i, j) = j \times (M_r + 1) + i.$$

For the interior points of the left-hand side in equation (4.21)

$$A_{\text{pos}(i,j),\text{pos}(i,j)} = A_{p,p} = 1 + 2\theta \left(F_r + F_z \right) + \beta \Delta t$$

$$A_{p,\text{pos}(i-1,j)} = A_{p,p-1} = \theta \left(-F_r + \frac{F_{r_1}}{r_i} \right)$$

$$A_{p,\text{pos}(i+1,j)} = A_{p,p+1} = \theta \left(-F_r - \frac{F_{r_1}}{r_i} \right)$$

$$A_{p,\text{pos}(i,j-1)} = A_{p,p-(M_z+1)} = -\theta F_z$$

$$A_{p,\text{pos}(i,j+1)} = A_{p,p+(M_z+1)} = -\theta F_z$$

The corresponding right-hand side vector in the equation system has the entries b_p where p represents the corresponding number of the equations. We have from the right-hand side of equation (4.21)

$$
\begin{aligned}
b_p[i,j] &= T_{i,j}^n + (1-\theta)\left[\frac{F_{r_1}(T_{i+1,j}^n - T_{i-1,j}^n)}{r_i} + F_r\left(T_{i-1,j}^n - 2T_{i,j}^n + T_{i+1,j}^n\right)\right] \\
&+ F_z\left(T_{i,j-1}^n - 2T_{i,j}^n + T_{i,j+1}^n\right) + (1-\Delta t\beta)\,T_{i,j}^n + \Delta t\,\gamma_m\left(r_i, z_j, t_n\right) \\
&+ \Delta t\,\theta\,\gamma_m\left(r_i, z_j, t_{n+1}\right),\text{for } j = 1,\cdots, M_z, \text{ for } i = 1,\cdots, M_r. \qquad (4.23)
\end{aligned}
$$

4.4.1.2 FD Scheme of Boundary Conditions

FD scheme for Neumann boundary with zero flux at inner D_1, bottom D_3, and top D_4 in equations (4.7), (4.9), and (4.10) are boundaries of the computational domain Ω, respectively. These fluxes at corresponding boundaries are implemented for time steps n and $n+1$ as follows.

$$T_{-1,j}^n = T_{1,j}^n, \quad T_{i,-1}^n = T_{i,1}^n, \quad T_{i,M_z+1}^n = T_{i,M_z-1}^n$$

and

$$T_{-1,j}^{n+1} = T_{1,j}^{n+1}, \quad T_{i,-1}^{n+1} = T_{i,1}^{n+1}, \quad T_{i,M_z+1}^{n+1} = T_{i,M_z-1}^{n+1}$$

The outer body surface D_2, covered by clothing, is exposed to a hot and cold environment. So, Robin boundary condition (4.8) due to convection, radiation, as well as the effective clothing area factor and sweat evaporation, is implemented for the outer boundary. The FD scheme in this outer boundary is given by

$$T_{Mr+1,j}^n = T_{Mr-1,j}^n - \frac{2h_A\Delta r}{k}\left[\left(T_{Mr,j}^n - T_\infty\right) + E_{\text{sk}}\right]$$

$$T_{Mr+1,j}^n = T_{Mr-1,j} - 2Bi\left[\left(T_{Mr,j}^n - T_\infty\right) + E_{\text{sk}}\right], \qquad (4.24)$$

and

$$T_{Mr+1,j}^{n+1} = T_{Mr-1,j}^{n+1} - \frac{2h_A\Delta r}{k}\left[\left(T_{Mr,j}^{n+1} - T_\infty\right) + E_{\text{sk}}\right]$$

$$T_{Mr+1,j}^{n+1} = T_{Mr-1,j}^{n+1} - 2Bi\left[\left(T_{Mr,j}^{n+1} - T_\infty\right) + E_{sk}\right], \qquad (4.25)$$

where $Bi = \dfrac{h_A \Delta r}{K}$ be the Biot number.

After implementation of the above FD scheme of inner, bottom, top and outer boundary conditions for the corresponding (scheme) of the expression $b_p[i,j]$ in equation (4.23) for each boundary respectively prescribes the discretized equations as follows

$$
\begin{aligned}
b_p[0,j] \;=\;& T_{0,j}^n + (1-\theta)\left[\frac{F_{r_1}(T_{0+1,j}^n - T_{0-1,j}^n)}{r_i} + F_r\left(T_{0-1,j}^n - 2T_{0,j}^n + T_{0+1,j}^n\right)\right] \\
+\;& F_z\left(T_{0,j-1}^n - 2T_{0,j}^n + T_{0,j+1}^n\right) + (1-\Delta t\beta)\,T_{0,j}^n + \Delta t\,\gamma_m\left(r_0, z_j, t_n\right) \\
+\;& \Delta t\,\theta\,\gamma_m\left(r_0, z_j, t_{n+1}\right), \;\text{for } j=1,\cdots,M_z, \qquad \text{for } i=0. \qquad (4.26)
\end{aligned}
$$

$$
\begin{aligned}
b_p[i,0] \;=\;& T_{i,0}^n + (1-\theta)\left[\frac{F_{r_1}(T_{i+1,0}^n - T_{i-1,0}^n)}{r_i} + F_r\left(T_{i-1,0}^n - 2T_{i,0}^n + T_{i+1,0}^n\right)\right] \\
+\;& F_z\left(T_{i-1,0}^n - 2T_{i,0}^n + T_{i+1,0}^n\right) + (1-\Delta t\beta)\,T_{i,0}^n + \Delta t\,\gamma_m\left(r_i, z_0, t_n\right) \\
+\;& \Delta t\,\theta\,\gamma_m\left(r_i, z_0, t_{n+1}\right), \;\text{for } i=1,...,M_r \quad \text{for } j=0. \qquad (4.27)
\end{aligned}
$$

$$
\begin{aligned}
b_p[i,M_z] \;=\;& T_{i,M_z}^n + (1-\theta)\left[\frac{F_{r_1}(T_{i+1,M_z}^n - T_{i-1,M_z}^n)}{r_i} + F_r\left(T_{i-1,M_z}^n - 2T_{i,M_z}^n + T_{i+1,M_z}^n\right)\right] \\
+\;& F_z\left(T_{i,M_z-1}^n - 2T_{i,M_z}^n + T_{i,M_z+1}^n\right) + (1-\Delta t\beta)\,T_{i,M_z}^n + \Delta t\,\gamma_m\left(r_i, z_{M_z}, t_n\right) \\
+\;& \Delta t\,\theta\,\gamma_m\left(r_i, z_{M_z}, t_{n+1}\right), \;\text{for } i=1,\cdots,M_r, \;\text{for } j=M_z. \qquad (4.28)
\end{aligned}
$$

$$
\begin{aligned}
b_p[M_r,j] \;=\;& (1-\theta)\left[F_r\left(2T_{Mr-1,j}^n - 2(1+Bi)T_{Mr,j}^n\right) + \frac{F_{r1}}{2r_{Mr}\Delta r}\left(-2BiT_{Mr,j}^n\right)\right] \\
+\;& (1-\theta)\left[F_z\left(T_{Mr,j-1}^n - 2T_{Mr,j}^n + T_{Mr,j+1,j}^n\right) + (1-\Delta t\beta)\,T_{Mr,j}^n\right] \\
+\;& (1-\theta)\left[\Delta t\gamma_m + 2BiFr\left(1 + \frac{F_{r1}}{2r_{Mr}}\right)T_\infty\right], \qquad (4.29) \\
& \text{for } j=1,\cdots,M_z, \;\text{for } i=M_r.
\end{aligned}
$$

4.5   Numerical Results and Discussions

The rate of metabolic heat generation increases when a person is doing some housework and other activities. With the help of the sparse matrix in equation (4.22), as well as the initial condition $T(r,z,t=0) = T_0(r,z)$ and boundary conditions for each in equations (4.7), (4.8), (4.9), and (4.10), their effects on body temperature are revealed. In these circumstances, the sweating case's axial and radial temperature profiles are compared to those for the non-sweating case. Meanwhile, we should be

conscious of the nature of fabric throughout the physical activity period [88]. The activity-based metabolic rate during running, the evaporation coefficient, the activity control parameter, and the basal metabolic rate are cited from [31, 107] and tabulated in Table 4.1. The material properties of the human tissue and clothes have already been summarized in Table 2.1 of Chapter 2 and in Table 3.2 of Chapter 3 for the numerical verification of the results. The results obtained from the Crank-Nicolson scheme of the equation (4.4) are presented in Figures 4.10–4.13.

Table 4.1: Physical parameters related to metabolism and vapor pressure [31, 108]
.

Parameters	Symbols	Values	Units
Basal metabolism	q_b	1114	W/m^3
Activity based metabolism (running)	q_A	7918	W/m^3
Activity control parameter	α	$0 \leq \alpha \leq 1$	/ sec
Sigmoid midpoint		300	
Evaporation coefficient	β	4.66628	W/m^2 Pkpa
Surface area of body part	A_{sk}	0.09990	m^2
Vapor pressure of water at air	$P_{w,air}$	14.69	Pkpa
Environmental temperature	T_∞	24	°C

In the case of non-sweating at $t = 150$ sec in left-hand Figure 4.10, the temperature of a runner increases at a distance of 0.002 m is 37.2°C . The temperature is approximately equal to 37.3°C at a distance from 0.005 m to 0.020 m. After then, the temperature decreases slightly in the radial direction and it becomes 36.90°C at the skin surface due to the convective and radiative heat transfer at the boundary. The same nature of the remaining graphs is depicted in the same Figure 4.10 at 300 sec, 450 sec, 600 sec, where the temperature also decreases slowly from the core towards the skin surface up to 37.01°C, 37.2°C and 37.4°C respectively. These radial temperature profile in Table 4.1, have been observed at the middle of the length in the longitudinal direction at $z = 0.25$ m.

Table 4.2: Radial temperature profile at body core to the skin surface at various lengths in the (left) non-sweating case at $z_j = 0.25$ m.

Time(s)	0.002(m)	0.005(m)	0.010(m)	0.015(m)	0.020(m)	0.025(m)	0.030(m)
150	37.20°C	37.30°C	37.30° C	37.30°C	37.30°C	37.18°C	36.90°C
300	37.40°C	37.55°C	37.60° C	37.59°C	37.50°C	37.32°C	37.01°C
450	37.55°C	37.75°C	37.85° C	37.85°C	37.81°C	37.70°C	37.20°C
600	37.70°C	37.95°C	38. 10°C	38.75°C	37.90°C	37.70°C	37.40°C

When sweat evaporation of a runner is taken into consideration, the graphs in the
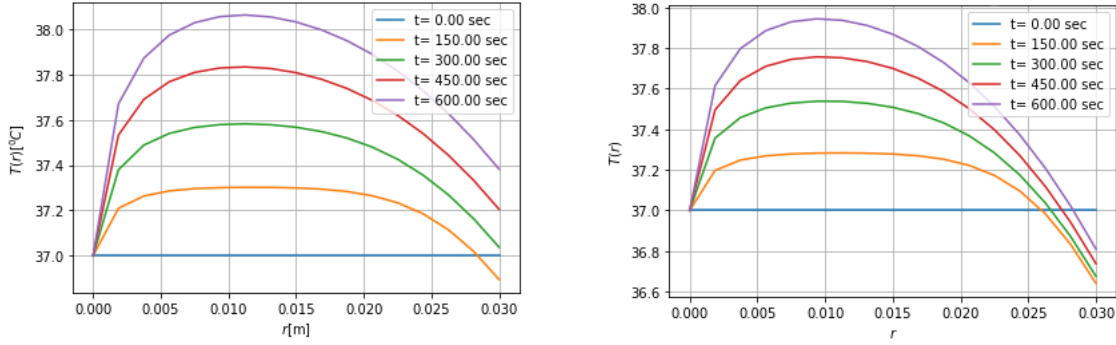
Figure 4.10: Radial temperature profile of a runner in the case of (left) non-sweating and (right) sweating.

right-hand Figure 4.10 depict the temperature profile at 150 sec the equivalent temperatures at distances of 0.002 m to 0.005 m as in the left-hand Figure 4.10, shown in Table 4.3. In 300 sec, 450 sec, 600 sec the temperature increases near core and reaches up to 37.39°C, 37.50°C, and 37.60°C, again increasing slightly from core to the radial distance 0.015 m then drops sharply when it approaches the skin's surface, where it hits 36.63°C, 36.63°C 36.63°C, and 36.63°C in 150 sec, 300 sec, 450 sec, 600 sec, respectively. It occurs because sweat evaporation is the major cause of heat loss through the skin. The details of its impacts on temperature distribution are shown in Table 4.3 at axial distance $z = 0.25$ m from the bottom or middle of the height of the limb.

Table 4.3: Radial temperature profile at body core to the skin surface at various lengths in the sweating case at $z_j = 0.25$ m.

Time (s)	0.002(m)	0.005(m)	0.010(m)	0.015(m)	0.020(m)	0.025(m)	0.030(m)
150	37.20°C	37.30°C	37.30° C	37.30°C	37.21°C	37.05°C	36.63°C
300	37.39°C	37.50°C	37.57° C	37.50°C	37.40°C	37.10°C	36.75°C
450	37.50°C	37.70°C	37.77° C	37.70°C	37.50°C	37.20°C	36.78°C
600	37.60°C	37.88°C	37. 95°C	37.90°C	37.62°C	37.30°C	36.80°C

Table 4.4: Longitudional temperature profile at body core to the skin surface at various length in non-sweating case at $r = 0.01$ m.

Time (s)	0 (m) 0.025(m)	0.1(m)	0.2(m)	0.25(m)	0.3(m)	0.4(m)	0.475(m)
150	35.50°C	36.50°C	37.25°C	37.27°C	37.25°C	36.50°C	35.50°C
300	35.75°C	36.75°C	37.50°C	37.51°C	37.50°C	36.75°C	35.75°C
450	36.01°C	37.00°C	37.70°C	37.75°C	37.70°C	37.00°C	36.01°C
600	36.25°C	37.25°C	37.78°C	38.00°C	37.78°C	37.25°C	36.25°C
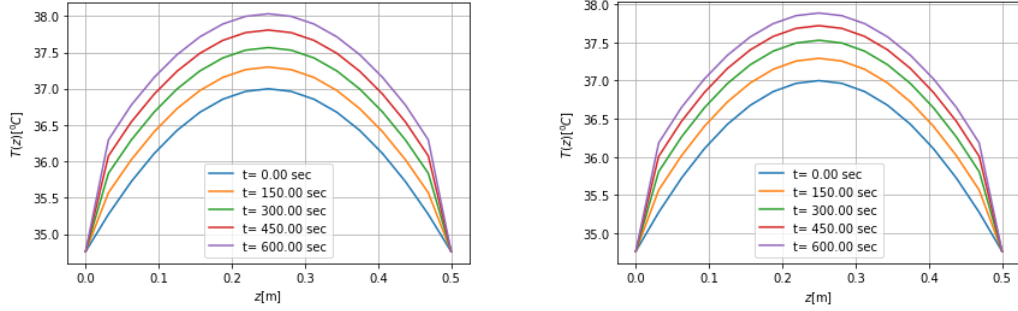
Figure 4.11: Longitudinal temperature profile of runner in the case of (left) non-sweating and (right) sweating.

Table 4.5: Longitudional temperature profile at body core to the skin surface at various length in sweating case at $r = 0.01$ m.

Time (s)	0 (m) 0.025(m)	0.1(m)	0.2(m)	0.25(m)	0.3(m)	0.4(m)	0.475(m)
150	35.50°C	36.50°C	37.25°C	37.27°C	37.25°C	36.50°C	35.50°C
300	35.75°C	36.75°C	37.48°C	37.50°C	37.48°C	36.75°C	35.75°C
450	36.00°C	36.80°C	37.60°C	37.65°C	37.60°C	36.80°C	36.00°C
600	36.20°C	37.25°C	37.75°C	37.80°C	37.75°C	37.25°C	36.20°C

Longitudinal temperature profile at different time levels up to 600 sec at 0.01 m, the radial distance from body core is observed and presented in Figure 4.11. The symmetrical graphs in Figure 4.11 during running have a time-dependent metabolism. These axial temperature increase as exercise time increases and reaches up to 37.27°C, 37.51°C, 37.75°C, and 38.00°C, at 150 sec, 300 sec, 450 sec, 600 sec, respectively in the left-hand Figure 4.11 for the non-sweating case. There is only a slight variation in temperature with similar nature of graphs in the left-hand side of Figure 4.11 and these temperature reach up to 37.27°C, 37.50°C, 37.65°C, and 37.80°C, in 150 sec, 300 sec, 450 sec, 600 sec respectively in sweating case. These results can be seen in the right-hand Figure 4.11. This is because of the presence of water vapor pressure on skin and air during perspiration. All the graphs in Figure 4.11 and the corresponding values of temperature in Tables 4.4 and 4.5 ensure the axially symmetric temperature profile with clothing and sweating effect in the human limb during physical activities special in running cases.

Heat maps (contour and surface plots) for the temperature profile with the same parameter values as in radial and longitudinal case at 600 sec are shown in Figures 4.10 and 4.11 for the non-sweating and sweating case. Both contour and surface plots are also axially symmetrical and both, core and skin temperatures in the right-hand plots of Figures 4.12 and 4.13 are less than that of the temperatures in the left-hand plots

of Figures 4.10 and 4.11. These results are again due to the effect of sweat evaporation. On the other hand, the presence of clothing at the outer boundary works as an insulator and prevents the body from losing heat quickly. So, only a slight variation in temperature at right-hand plots in Figures 4.10 and 4.11 can be seen even though sweat evaporation occurs.
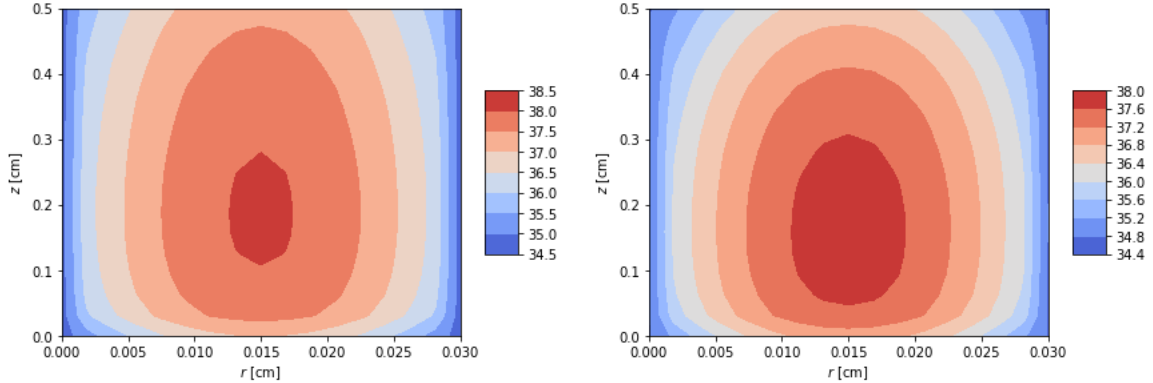
Figure 4.12: Contour Plot of a runner in the case of (left) non-sweating and (right) sweating.
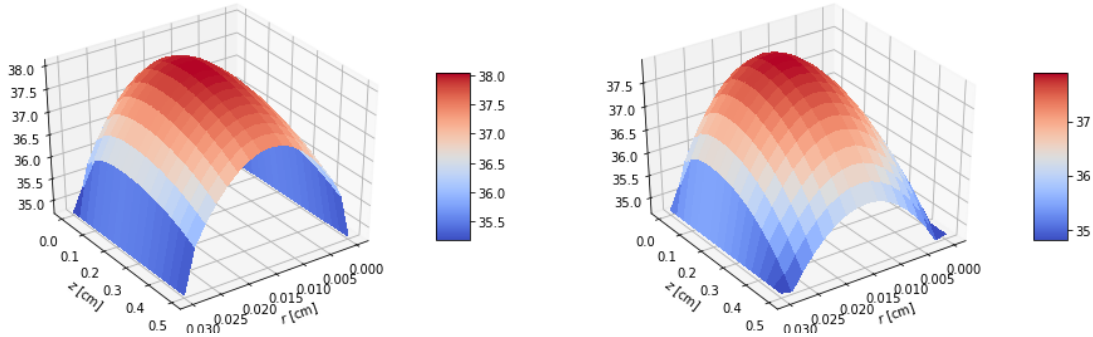
Figure 4.13: Surface Plot of a runner in the case of (left) non-sweating and (right) sweating.

4.6 Conclusion

A two-dimensional axisymmetric bioheat transfer model with a time-dependent metabolic rate has been developed with a modification to Pennes' bioheat transfer model. The effect of clothing and perspiration has been considered while assigning the modified Robin boundary condition. The temperature-dependent sweating term in (4.8) makes the axisymmetric problem nonlinear with the modified boundary condition of mixed type. To get a more precise estimate of thermal responses during physical activity,

the Crank-Nicolson FD technique has been implemented. From the perspective of implementation, explicit systems are incredibly straightforward and practical. The limitation on time step size imposes a cost on the scheme's numerical stability. Although implicit schemes are unconditionally stable, they have a significant computational cost. So, in this study, the bioheat equation is solved using the Crank-Nicolson method.

Changing the mixed boundary flux at the curved surface of the limb and the top, bottom, and inner flux boundaries at the core, we fix a two-dimensional grid and carry out the task using the axial direction as the height of the limb and the radial direction as the radius of the circular section extending from the core to the outside.

The effect of time-dependent metabolic heat generation at various time steps has been demonstrated to cause an increase in body core temperature as time passes. The goal of this Chapter is to draw the conclusion that a runner with a high metabolic rate raises his/her body temperature as the running period increases. The sweat gland begins to produce perspiration immediately after a predetermined period of time, and as the sweat evaporates, the radial temperature drops. Clothing, additionally, prevents rapid loss of skin temperature at the same time. There is minimal variation in body core temperature in the axial direction while changes in metabolic rate and insensible sweat evaporation which is due to flux boundaries at the inner, bottom, and top.

We discovered that the outcomes from the one-dimensional model agree with the numerical simulation findings for the same experiment as in one dimension imposing the flux and modified mixed boundary conditions in the outer surface. Therefore, the longitudinal profile and the one-dimensional model agree. Thus the model may have a significant contribution in the field of bioheat transfer as well as sports science and clothing design.

CHAPTER 5

THREE-DIMENSIONAL NONLINEAR MATHEMATICAL MODEL

5.1 Introduction

The heat transmission in living tissue is no longer linear in abnormal (tumor) tissue organs and extreme environmental conditions (laser ablation) the heat transmission in living tissue is not necessarily linear. The biomedical sector primarily uses the revolutionary nonlinear PDE technology for cryosurgery, hypothermia, burn injury treatment, and hyperthermic cancer treatment. The human thermoregulatory system behaves in a highly nonlinear manner due to the complicated internal vasculature architecture and multiple sensors. There are additional mathematical and computing challenges brought when switching from a linear to a nonlinear model. There is currently no general theory that can solve all nonlinear problems analytically. On the other hand, when attainable, analytical approaches are beneficial since they establish the key aspects of the issue and give insight into different system characteristics that affect heat transport [2, 24, 68, 69]. Heat transmission in the living organ is greatly influenced by various temperature-dependent thermophysical factors, including thermal conductivity, blood perfusion, metabolism, and heat transfer coefficient. This is especially the case in abnormal tissues. Analyzing how biological phenomena react to temperature gradients is essential to improving the efficacy of thermal techniques. Tissues undergoing hyperthermic and ablative treatments may experience structural and mechanical changes as a result of a number of thermally induced processes, including protein denaturation, dehydration, shrinkage, and mechanical stiffening [6, 14, 32, 44, 83, 112]. The linear PDE bioheat equation served as the foundation for the mathematical models that were created in the previous chapters. The temperature-dependent thermophysical parameters are important avenues for heat transport in complicated geometries, especially human tissue organs [92].

In Chapter 4 we considered a two-dimensional axisymmetric model with time-dependent metabolism during physical activity for the linear case. In complex geometry, nonlinearity still becomes more crucial to obtain a more consistent temperature distribution. In this Chapter, we discuss the nonlinear behavior and method of obtaining the numerical solution of the nonlinear bioheat equation. The nonlinearity is adopted by the use of the relationship between thermo-physical parameters and temperature. A nonlinear model with an external heating source has been prescribed in section 5.2. The numerical procedure, based on the Finite Volume (FV) discretization of PDE, simulation results and discussion, and conclusion of the Chapter have been included in section 5.3, 5.4, and 5.5, respectively.

The physical and physiological parameters may be linearly, quadratically, cubically, or exponentially [6, 11, 13, 24, 35, 65] depending upon the temperature.

5.2   Nonlinear Bioheat Transfer Model

To study the nonlinear behavior of heat transfer in a cylindrical-shaped abnormal tissue organ, we express the Pennes bioheat transfer equation using time-dependent /temperature-dependent physiological parameters $c(t), K(T), w_b(T), q_m(T)$ [11, 13] along with the external heating source q_e in the cylindrical coordinates as

$$\rho c \frac{\partial T}{\partial t} = \left[\frac{1}{r} \frac{\partial}{\partial r} \left(K(T) r \frac{\partial T}{\partial r} \right) + \frac{1}{r^2} \frac{\partial^2 T}{\partial \theta^2} + \frac{\partial^2 T}{\partial z^2} \right] + c_b \rho_b w_b(T)(T_a - T) + q_m(T) + q_e, \quad (5.1)$$

where
K :   temperature-dependent thermal conductivity
w_b :   temperature dependent blood perfusion
q_m :   temperature dependent metabolic heat generation
q_e :   external heating source (W/m^3).

We consider a cylindrical-shaped small limb of the human forearm with a tumor in the specific location as shown in Figure 5.1.

Initial and Boundary Conditions

We prescribe the initial temperature distribution as some known function of position $T(r, z, \theta, 0) = T_0(r, z, \theta)$ and the boundary conditions are prescribed as follows.

$$-K \frac{\partial T}{\partial r} \bigg|_{r=0} = 0, \qquad \qquad \text{in } D_1 \qquad \qquad (5.2)$$

$$-K \frac{\partial T}{\partial r} \bigg|_{R} = h_c(T - T_\infty) + E_{sk}, \qquad \text{in } D_2 \qquad \qquad (5.3)$$
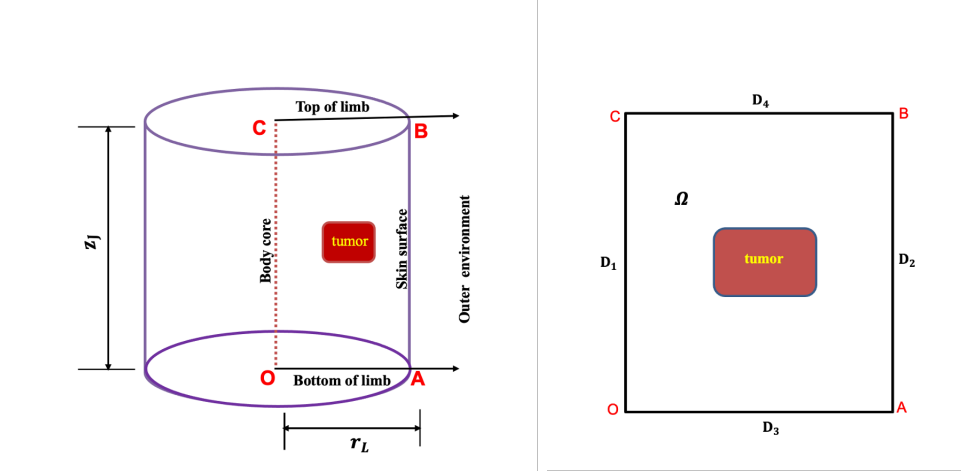
Figure 5.1: Schematic view of the cylindrical limb with the location of tumor tissue at $r_i = 0.015\,m$ and $z_j = 0.21\,m$.

$$-K\frac{\partial T}{\partial z}\bigg|_{z=0} \quad = \quad 0, \qquad\qquad \text{in } D_3 \qquad\qquad (5.4)$$

$$-K\frac{\partial T}{\partial z}\bigg|_Z \quad = \quad \begin{cases} 0, & \text{for Neumann,} \\ h_c(T - T_\infty) + E_{sk}, & \text{for Robin,} \end{cases} \quad \text{in } D_4. \qquad (5.5)$$

5.3   Finite Volume Discretization for Bioheat Transfer Equation

In the Finite Volume Method (FVM), we discretize the domain into a finite number of control volumes, that's why called the Finite Volume. A local energy balance equation (5.1) is written on each "finite volume" and an integral formulation of the fluxes over the boundary (faces) of the finite volume is then obtained using the Divergence Theorem. Then the fluxes are approximated in terms of the discrete unknowns. The best feature of the finite volume method is that it maintains the conservation law at the discrete level because it is based on the "balance" approach.

Let $M_r \in \mathbb{N}$, $M_z \in \mathbb{N}$, and $M_t \in \mathbb{N}$, then we set up a three dimensional (r, z, θ) mesh of the cylindrical domain $0 < r < R$, $0 < z < Z$, $0 \leq \theta < 2\pi$ with $M_r \times M_z \times M_t$ nodes

$$\mathcal{M} = V_{i,j,m} \quad \text{for } i = 1, 2, \cdots, M_r;\; j = 1, 2, \cdots, M_z;\; m = 1, 2, \cdots, M_t.$$

Let us consider the uniform grid with

$$\Delta r = R/M_r,\; \Delta z = Z/M_z,\; \text{ and } \; \Delta\theta = 2\pi/M_t.$$

For $i = 1, \cdots, R$, let $r_{1/2} = 0$, $r_{i+1/2} = r_{i-1/2} + \Delta r$, $r_{M_r+1/2} = R$,

for $j = 1, \cdots, Z$, let $z_{1/2} = 0$, $z_{j+1/2} = z_{j-1/2} + \Delta z$ and $z_{M_z+1/2} = Z$,

for $m = 2, \cdots, M_{t-1}$, let $\theta_{1/2} = \theta_{M_t+1/2} = 2\pi - \frac{\Delta\theta}{2}$, $\theta_{\frac{3}{2}} = \frac{\Delta\theta}{2}$, $\theta_{m+1/2} = \theta_{m-1/2} + \Delta\theta$

and the control volume

$$V_{i,j,m} = \int_{r_{i-1/2}}^{r_{i+1/2}} \int_{z_{j-1/2}}^{z_{j+1/2}} \int_{\theta_{m-1/2}}^{\theta_{m+1/2}} r \, d\theta \, dz \, dr. \tag{5.6}$$

The areas of the radial $(Ar_{i-1/2,j,m})$, axial $(Az_{i,j-1/2,m})$, and angular $(A\theta_{i,j,m-1/2})$ faces are respectively

$$\int_{z_{j-1/2}}^{z_{j+1/2}}\int_{\theta_{m-1/2}}^{\theta_{m+1/2}} r \, d\theta \, dz, \quad \int_{r_{i-1/2}}^{r_{i+1/2}}\int_{\theta_{m-1/2}}^{\theta_{m+1/2}} r \, d\theta \, dr, \quad \text{and} \quad \int_{r_{i-1/2}}^{r_{i+1/2}}\int_{z_{j-1/2}}^{z_{j+1/2}} dz \, dr. \tag{5.7}$$

Let $(r_i)_{i=0,1,\cdots,M_r+1}$, $(z_j)_{j=0,1,\cdots,M_z+1}$, and $(\theta_m)_{m=0,1,\cdots,M_t+1}$, such that

$$\begin{array}{ll}
r_{i-1/2} < r_i < r_{i+1/2}, & \text{for } i = 1, 2, \cdots, M_r, \, r_0 = 0, \, r_{M_r+1} = R, \\
z_{j-1/2} < z_j < z_{j+1/2}, & \text{for } j = 1, 2, \cdots, M_z, \, z_0 = 0, \, z_{M_z+1} = Z, \\
\theta_{m-1/2} < \theta_m < \theta_{m+1/2}, & \text{for } m = 1, 2, \cdots, M_t, \, \theta_0 = \theta_{M_t}, \, \theta_1 = \theta_{M_t} + 1 = 0,
\end{array} \tag{5.8}$$

and let $x_{i,j,m} = (r_i, z_j, \theta_m)$, for $i = 1, 2, \cdots, M_r; j = 1, 2, \cdots, M_z; m = 1, 2, \cdots, M_t$. We also define $r_b = M_r + 1$, $z_b = M_z + 1$, $t_b = M_t + 1$ for the indices at the boundary nodes.

Time discretization is performed with variable time steps.

Let $T > 0$ be the time, $\{t_0 \cdots, t_{N_{\max}}\}$, a partition of $[0, T]$, and $\Delta t_n = t_{n+1} - t_n$ is the time step size.

Let $U_{i,j,m}^n$ denote the mean value of T over the control volume $V_{i,j,m}$. The value of $U_{i,j,m}^n$ is also the numerical approximations of $T(r_i, z_j, \theta_m, t_n)$. Consider the PDE in divergence form:

$$\frac{\partial T}{\partial t} + \nabla \cdot \mathbf{\Phi} = s_1 + s_2(T), \tag{5.9}$$

where

$$\mathbf{\Phi} = \left\langle D\frac{\partial T}{\partial r}, \frac{D}{r}\frac{\partial T}{\partial \theta}, D\frac{\partial T}{\partial z} \right\rangle, \quad D = \frac{K(T)}{\rho c(t)}, \quad s_1 = \frac{\rho_b c_b w_b T_a}{\rho c(t)}, \quad s_2(T) = \frac{\rho_b c_b w_b(T) + q_m(T)}{\rho c(t)}.$$

In order to obtain the numerical scheme, we integrate formally equation (5.9) over each control volume $V_{i,j,m}$ and time interval $[t_n, t_n + \Delta t_n]$, $n = 0, 1, \cdots, N_{\max}$

$$\int_{V_{i,j,m}} (T(t_{n+1}) - T(t_n)) \, dV + \int_{t_n}^{t_n+\Delta t_n} \int_{\partial V_{i,j,m}} \Phi \cdot \mathbf{n}_{i,j,m} \, dA \, dt$$

$$= \int_{t_n}^{t_n+\Delta t_n} \int_{V_{i,j,m}} [s_1 + s_2(T)] \, dV \, dt, \tag{5.10}$$

108

where

$\mathbf{n}_{i,j,m}$:   the outward unit normal to the control volume $V_{i,j,m}$.

Let us define $t_{n+\vartheta} := t_n + \vartheta \, \Delta t_n = (1 - \vartheta) \, t_n + \vartheta \, t_{n+1}$, with $0 \leq \vartheta \leq 1$ to be some intermediate time. Then (5.10) takes the form:

$$\frac{1}{\Delta t_n} \int_{V_{i,j,m}} (T(t_{n+1}) - T(t_n)) \ dV + \int_{\partial V_{i,j,m}} \Phi(t_{n+\vartheta}) \cdot \mathbf{n}_{i,j,m} \ dA \ dt$$

$$= \int_{V_{i,j,m}} [s_1 + s_2(T(t_{n+\vartheta}))] \ dV \qquad (5.11)$$

From this we get

$$U_{i,j,m}^{n+1} = U_{i,j,m}^n + \frac{\Delta t_n}{V_{i,j,m}} \left[(A\Phi)_{i-1/2,j,m}^{n+\vartheta} + (A\Phi)_{i+1/2,j,m}^{n+\vartheta} + (A\Phi)_{i,j-1/2,m}^{n+\vartheta} \right.$$

$$\left. + (A\Phi)_{i,j+1/2,j,m}^{n+\vartheta} + (A\Phi)_{i,j,m-1/2}^{n+\vartheta} + (A\Phi)_{i,j,m+1/2}^{n+\vartheta} \right]$$

$$+ \Delta t_n \left[s_1 + s_2(T_{i,j,m}^{n+\vartheta}) \right] \qquad (5.12)$$

for $i = 1, \cdots, M_r$, $j = 1, \cdots, M_z$, $m = 1, \cdots M_t$, $n = 0, 1, \cdots, N_{\max}$.

The flow rates for equation (5.12) are given by

$$(A\Phi)_{i-1/2,j,m}^{n+\vartheta} = -\alpha_{i-1/2,j,m} \, K_{i,j,m} \left(\frac{U_{i,j,m}^{n+\vartheta} - U_{i-1,j,m}^{n+\vartheta}}{r_i - r_{i-1}} \right), \qquad (5.13)$$

$$i = 1, \cdots, M_r + 1, \ j = 1, \cdots, M_z, \ m = 1, \cdots M_t,$$

$$(A\Phi)_{i+1/2,j,m}^{n+\vartheta} = \alpha_{i+1/2j,m} \, K_{i,j,m} \left(\frac{U_{i+1,j,m}^{n+\vartheta} - U_{i,j,m}^{n+\vartheta}}{r_{i+1} - r_i} \right), \qquad (5.14)$$

$$i = 1, \cdots, M_r + 1, \ j = 1, \cdots, M_z, \ m = 1, \cdots M_t,$$

$$(A\Phi)_{i,j-1/2,m}^{n+\vartheta} = -\alpha_{i,j-1/2,m} \, K_{i,j,m} \left(\frac{U_{i,j,m}^{n+\vartheta} - U_{i,j-1,m}^{n+\vartheta}}{z_j - z_{j-1}} \right), \qquad (5.15)$$

$$i = 1, \cdots, M_r, \ j = 1, \cdots, M_z + 1, \ m = 1, \cdots M_t,$$

$$(A\Phi)_{i,j+1/2,m}^{n+\vartheta} = \alpha_{i,j+1/2,m} \, K_{i,j,m} \left(\frac{U_{i,j+1,m}^{n+\vartheta} - U_{i,j,m}^{n+\vartheta}}{z_{j+1} - z_j} \right), \qquad (5.16)$$

$$i = 1, \cdots, M_r, \ j = 1, \cdots, M_z + 1, \ m = 1, \cdots M_t,$$

$$(A\Phi)_{i,j,m-1/2}^{n+\vartheta} = -\alpha_{i,j,m-1/2} \, \frac{K_{i,j,m}}{r_i} \left(\frac{U_{i,j,m}^{n+\vartheta} - U_{i,j,m-1}^{n+\vartheta}}{\theta_m - \theta_{m-1}} \right), \qquad (5.17)$$

$$i = 1, \cdots, M_r, \ j = 1, \cdots, M_z, \ m = 1, \cdots M_{t+1},$$

$$(A\Phi)_{i,j,m+1/2}^n = \alpha_{i,j,m+1/2} \, \frac{K_{i,j,m}}{r_i} \left(\frac{U_{i,j,m+1}^{n+\vartheta} - U_{i,j,m}^{n+\vartheta}}{\theta_{m+1} - \theta_m} \right), \qquad (5.18)$$

$$i = 1, \cdots, M_r, \ j = 1, \cdots, M_z, \ m = 1, \cdots M_{t+1},$$

Both explicit and implicit scheme can be obtained by using $\vartheta = 0$ and $\vartheta = 1$, respectively in (5.12).

Using one-dimensional, and two-dimensional control volumes $V_i = \left(r_{i+1/2} - r_{i-1/2}\right)$, $V_j = \left(z_{j+1/2} - z_{j-1/2}\right)$, $V_{i,j} = \left(r^2_{i+1/2} - r^2_{i-1/2}\right)\left(z_{j+1/2} - z_{j-1/2}\right)$, and $V_{i,m} = \left(r^2_{i+1/2} - r^2_{i-1/2}\right)\left(\theta_{m+1/2} - \theta_{m-1/2}\right)$ in equation (5.12), we can derive the Finite Volume numerical algorithms for one-dimensional radial (r-direction), one-dimensional longitudinal (z-direction), two-dimensional axisymmetric ((r, z)-direction), and two-dimensional angular symmetric ((r, θ)-direction) models.

Explicit Finite Volume schemes for one-dimensional cases are

In radial (r-direction)

$$
\begin{aligned}
U_i^{n+1} &= U_i^n + \frac{\Delta t_n}{V_i}\left[(\Phi)_{i-1/2}^{n+\vartheta} + (\Phi)_{i+1/2}^{n+\vartheta}\right] \\
&\quad + \Delta t_n\left[s_1 + s_2(T_i^{n+\vartheta})\right]
\end{aligned}
\tag{5.19}
$$

The flow rates in r-direction are:

$$
(\Phi)_{i-1/2}^{n+\vartheta} = -\alpha_{i-1/2}\,K_i\left(\frac{U_i^{n+\vartheta} - U_{i-1}^{n+\vartheta}}{r_i - r_{i-1}}\right),
\tag{5.20}
$$

$$
(\Phi)_{i+1/2}^{n+\vartheta} = \alpha_{i+1/2}\,K_i\left(\frac{U_{i+1}^{n+\vartheta} - U_i^{n+\vartheta}}{r_{i+1} - r_i}\right)
\tag{5.21}
$$

for $i = 1, \cdots, M_r + 1$, $n = 0, 1, \cdots, N_{\max}$.

In longitudinal (z-direction)

$$
\begin{aligned}
U_j^{n+1} &= U_j^n + \frac{\Delta t_n}{V_j}\left[(\Phi)_{j-1/2}^{n+\vartheta} + (\Phi)_{j+1/2}^{n+\vartheta}\right] \\
&\quad + \Delta t_n\left[s_1 + s_2(T_j^{n+\vartheta})\right]
\end{aligned}
\tag{5.22}
$$

The flow rates in z-direction are:

$$
(\Phi)_{j-1/2}^{n+\vartheta} = -\alpha_{j-1/2}\,K_j\left(\frac{U_j^{n+\vartheta} - U_{j-1}^{n+\vartheta}}{z_j - z_{j-1}}\right),
\tag{5.23}
$$

$$
(\Phi)_{j+1/2}^{n+\vartheta} = \alpha_{j+1/2}\,K_j\left(\frac{U_{j+1}^{n+\vartheta} - U_j^{n+\vartheta}}{z_{j+1} - z_j}\right)
\tag{5.24}
$$

for $j = 1, \cdots, M_z + 1$, $n = 0, 1, \cdots, N_{\max}$.

Explicit Finite Volume schemes for two-dimensional cases are:

In axisymmetric ((r, z)-directions)

$$U_{i,j}^{n+1} = U_{i,j}^n + \frac{\Delta t_n}{V_{i,j}} \left[(A\Phi)_{i-1/2,j}^{n+\vartheta} + (A\Phi)_{i+1/2,j}^{n+\vartheta} + (A\Phi)_{i,j-1/2}^{n+\vartheta} + (A\Phi)_{i,j+1/2}^{n+\vartheta} \right]$$

$$+ \Delta t_n \left[s_1 + s_2(T_{i,j}^{n+\vartheta}) \right] \tag{5.25}$$

$$\text{for } i = 1, \cdots, M_r, \ j = 1, \cdots, M_z, \ n = 0, 1, \cdots, N_{\max}.$$

Flow rates in (r, z)-directions are:

$$(A\Phi)_{i-1/2,j}^{n+\vartheta} = -\alpha_{i-1/2,j} K_{i,j} \left(\frac{U_{i,j}^{n+\vartheta} - U_{i-1,j}^{n+\vartheta}}{r_i - r_{i-1}} \right), \tag{5.26}$$

$$(A\Phi)_{i+1/2,j}^{n+\vartheta} = \alpha_{i+1/2,j} K_{i,j} \left(\frac{U_{i+1,j}^{n+\vartheta} - U_{i,j}^{n+\vartheta}}{r_{i+1} - r_i} \right), \tag{5.27}$$

$$i = 1, \cdots, M_r + 1, \ j = 1, \cdots, M_z.$$

$$(A\Phi)_{i,j-1/2}^{n+\vartheta} = -\alpha_{i,j-1/2} K_{i,j} \left(\frac{U_{i,j}^{n+\vartheta} - U_{i,j-1}^{n+\vartheta}}{z_j - z_{j-1}} \right), \tag{5.28}$$

$$(A\Phi)_{i,j+1/2}^{n+\vartheta} = \alpha_{i,j+1/2} K_{i,j} \left(\frac{U_{i,j+1}^{n+\vartheta} - U_{i,j}^{n+\vartheta}}{z_{j+1} - z_j} \right), \tag{5.29}$$

$$i = 1, \cdots, M_r, \ j = 1, \cdots, M_z + 1.$$

In angular symmetric ((r, θ)-directions)

$$U_{i,m}^{n+1} = U_{i,m}^n + \frac{\Delta t_n}{V_{i,m}} \left[(A\Phi)_{i-1/2,m}^{n+\vartheta} + (A\Phi)_{i+1/2,m}^{n+\vartheta} + (A\Phi)_{i,m-1/2}^{n+\vartheta} + (A\Phi)_{i,m+1/2}^{n+\vartheta} \right]$$

$$+ \Delta t_n \left[s_1 + s_2(T_{i,m}^{n+\vartheta}) \right] \tag{5.30}$$

$$\text{for } i = 1, \cdots, M_r, \ m = 1, \cdots, M_t, \ n = 0, 1, \cdots, N_{\max}.$$

Flow rates in (r, θ) directions are:

$$(A\Phi)^{n+\vartheta}_{i-1/2,m} = -\alpha_{i-1/2,m} K_{i,m} \left(\frac{U^{n+\vartheta}_{i,m} - U^{n+\vartheta}_{i-1,m}}{r_i - r_{i-1}} \right), \tag{5.31}$$
$$i = 1, \cdots, M_{r+1}, \ m = 1, \cdots, M_t.$$

$$(A\Phi)^{n+\vartheta}_{i+1/2,m} = \alpha_{i+1/2,m} K_{i,m} \left(\frac{U^{n+\vartheta}_{i+1,m} - U^{n+\vartheta}_{i,m}}{r_{i+1} - r_i} \right), \tag{5.32}$$
$$i = 1, \cdots, M_r + 1, \ m = 1, \cdots, M_t.$$

$$(A\Phi)^{n+\vartheta}_{i,m-1/2} = -\alpha_{i,m-1/2} K_{i,m} \left(\frac{U^{n+\vartheta}_{i,m} - U^{n+\vartheta}_{i,m-1}}{\theta_m - \theta_{m-1}} \right), \tag{5.33}$$
$$i = 1, \cdots, M_r, \ m = 1, \cdots, M_t + 1.$$

$$(A\Phi)^{n+\vartheta}_{i,m+1/2} = \alpha_{i,m+1/2} K_{i,m} \left(\frac{U^{n+\vartheta}_{i,m+1} - U^{n+\vartheta}_{i,m}}{\theta_{m+1} - \theta_m} \right), \tag{5.34}$$
$$i = 1, \cdots, M_r, \ m = 1, \cdots, M_t + 1.$$

The results in nonlinear heat transfer are calculated for an abnormal tissue, simulated in python, exhibited graphically, and discussed in the next section 5.4.

5.4   Numerical Results and Discussion

The Initial condition for two-dimensional (r, z)-direction is $T(r, z, t) = T_0(r, z)$, and for three-dimensional (r, z, θ) is $T(r, z, \theta, t) = T_0(r, z, \theta)$ at time $t = 0$. Imposing the boundary conditions given in equations (5.2) - (5.5), in radial and axial faces of the control volume, effects on the aberrant tissue temperature in the body have been observed. Figures 5.2–5.9 show the corresponding outcomes of the equation (5.1), θ with continuous periodicity, for one-dimensional radial direction, one-dimensional axial direction, two-dimensional axisymmetric (r, z)-direction, and the cross-section profile in angular symmetric (r, θ)-direction, respectively, for which the used parametric values are given in the Table 5.1 for abnormal tissues.   The graphs in Figures 5.6 –5.8, on the left up to 2 min and on the right up to 10 min, respectively, demonstrate the nonlinear temperature profiles of $K(T)$, $w_b(T)$, and $q_m(T)$ with their corresponding coefficients for constant, linear, and quadratic cases, respectively. The choice of corresponding coefficients makes the results more accurate and reliable. We, therefore, need to be aware of the choice of coefficients throughout the nonlinear investigation. To observe the temperature in an aberrant cell, an external heating source of 250 W/m^3 has also been provided [64], which is important.

112

Table 5.1: Thermophysical parameters related to abnormal tissue [31, 59, 95].

Parameters	Symbols	Units	Values (tumor)
Thermal conductivities	k_0	W/m°C	0.642
Blood specific heat	c_b	J/kg°C	3850
Blood density	ρ_b	kg/m³	1040
Blood perfusion rate	w_b	kg/s m³	7×10^{-4}
Metabolism	q_m	W/m³	33800
Arterial temperature	T_a	°C	37
Total thickness of domain	L	m	0.03
The constant coefficient	ϵ	n. d.	1×10^{-7}
Convectional heat transfer coefficient	h_A	W/m²°C	30.035
Surrounding temperature	T_{air}	°C	28

The tumor is assumed to be located at 0.015m radial direction from the core of the body towards the skin surface and 0.22 m axial meters from the bottom of the limb towards the top. That is, the position of the target place is $(r_i, z_j) = (0.015\text{m}, 0.22\text{m})$, for which the tumour dimension, $4\,\text{mm} \times 4\text{mm}$ in size.

5.4.1 One-Dimensional Radial Temperature Profile (r-direction)

Graphs of left-hand and right-hand Figure 5.2 display the radial temperature profiles of malignant tissue up to 2 min and 10 min, respectively, which are tabulated in Table 5.2. The graphs in left-hand Figure 5.2 depict the radial temperature profiles at a
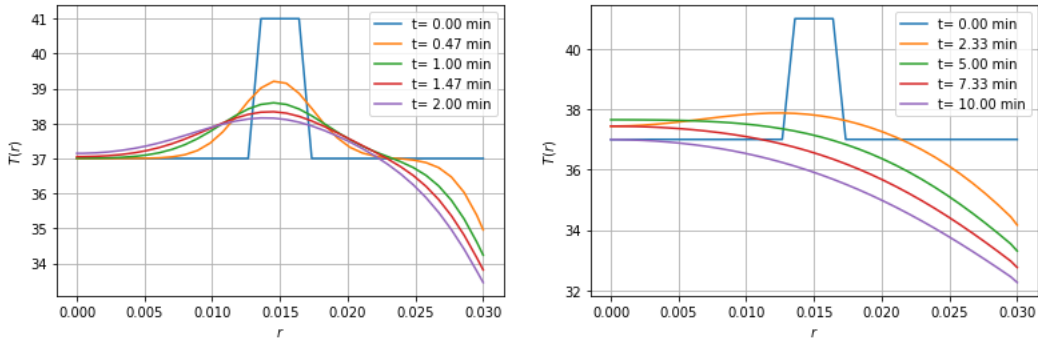
Figure 5.2: Radial temperature profiles when $z_j = 0.22\,\text{m}$ (left) at 2 min (right) at 10 min.

different time up to 2 min. The radial temperature is 37°C from 0 min up to 0.010 m then increases quickly and reaches 41°C in the interval $(0.13\,\text{m}, 0.117\,\text{m})$ in the initial phase, then smoothly decreases from pick at the point 0.015 m and reaches 39.20°C, 38.50°C, 38.25°C, and 38.15°C, in time 0.47 min, 1.00 min, 1.47 min, and 2.00 min,

Table 5.2: Radial temperature profile at body core to the skin surface at various lengths with tumor tissue at $z_j = 0.22\,\text{m}$.

Time (min)	0.00 (m)	0.005 (m)	0.007 (m)	0.010 (m)	0.013 (m)	0.015 (m)	0.017 (m)	0.020 (m)	0.025 (m)	0.030 (m)
0.00	37.00	37.00	37.00	38.00	41.00	41.00	41.00	37.00	37.00	37.00
0.47	37.00	37.00	37.00	37.50	38.00	39.20	38.00	37.50	37.00	35.00
1.00	37.00	37.10	37.50	38.00	38.40	38.50	38.40	37.50	36.70	34.40
1.47	37.00	37.20	37.50	38.00	38.20	38.25	38.20	37.50	36.50	33.98
2.00	37.00	37.50	37.80	38.00	38.05	38.15	38.05	37.50	36.10	33.50
5.00	37.00	37.00	37.60	37.50	37.25	37.00	36.90	36.50	35.00	33.50
10.00	37.00	37.00	36.75	36.50	36.25	36.00	36.75	36.50	33.90	32.50

respectively. On the contrary, the temperature at the distance of 0.005 m from the body core up to the heating point increases smoothly, and decreases smoothly from the heating point (0.015 m, 0.022 m) up to (0.022 m) and then again decreases sharply towards the skin surface and reaches 35°C, 34.40° C, 33.98°C, and 33.50°C, in times 0.47 min, 1.00 min, 1.47 min, and 2.00 min, respectively, as depicted in left-hand Figure 5.2 and Table 5.2. The behavior of curves in this left-hand Figure 5.2 are sinusoidal within the interval (0.008 m, 0.022 m), the neighborhood of the location of the tumor. These results show the nonlinear behavior of heat transfer within abnormal tissue. The curves in right-hand Figure 5.2 show the radial temperature profile at different time steps up to 10 min where the temperature at 2.33 min slightly increases up to 38°C within the radial interval (0.008 m, 0.022 m) then smoothly decreases towards the skin surface. The remaining curves indicate the smooth decrease in temperature towards the skin surface and reach 33.5°C, 33°C, and 32.5°C in 5 min, 7.33 min, and 10 min, respectively. The temperatures of 5 min and 10 min are also accumulated in the Table 5.2.

5.4.2 One-Dimensional Longitudinal Temperature Profile (z-direction) with Neumann Boundary Condition

The longitudinal temperature profiles of malignant tissue up to 2 min and 10 min, respectively, are shown in Figure 5.3. The relevant axial temperatures are tabulated in Table 5.3. The graphs in left-hand Figure 5.3 and Table 5.3 demonstrate the axial temperature profile at various time periods up to 2 min at 0.015 m radial distance from the body core. The heating point for an unhealthy type of tissue is the middle of the axial distance $z_j = 0.22\,\text{m}$. When the external heat source is applied to the tumor tissue for hyperthermic treatment of tumor cell initially, the temperature
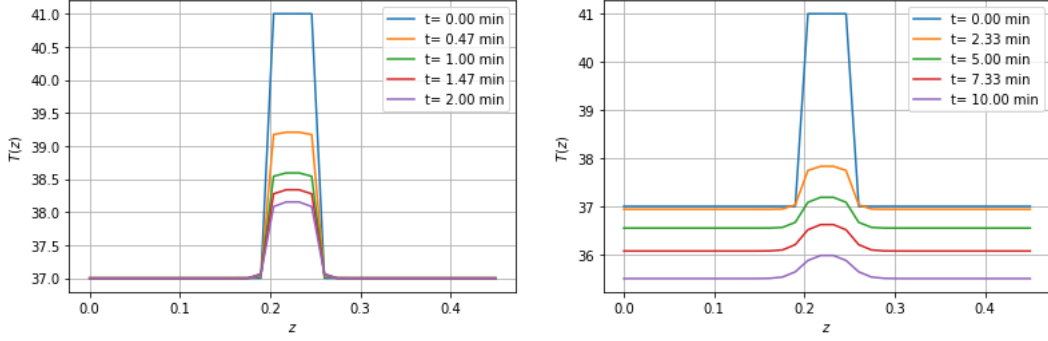
Figure 5.3: : Longitudinal temperature profile when $r_i = 0.015\,\text{m}$ (left) at $2\,\text{min}$ (right) at $10\,\text{min}$ with flux boundary.

Table 5.3: Longitudinal temperature profile at body core to the skin surface at various length in(right), abnormal tissue at $r_i = 0.015\,\text{m}$.

Time (min)	0.00 (m)	0.10 (m)	0.19 (m)	0.20 (m)	0.22 (m)	0.25 (m)	0.30 (m)	0.40 (m)	0.45 (m)
0.00	37.00	37.00	37.00	41.00	41.00	41.00	37.00	37.00	37.00
0.47	37.00	37.00	37.00	39.25	39.25	39.25	37.00	37.00	37.00
1.00	37.00	37.00	37.00	38.50	38.52	38.50	37.00	37.00	37.00
1.47	37.00	37.00	37.00	38.20	38.25	38.20	37.00	37.00	37.00
2.00	37.00	37.00	37.00	38.10	38.12	38.10	37.00	37.00	37.00
5.00	36.50	36.50	36.50	37.00	37.15	37.00	36.50	36.50	36.50
10.00	35.50	35.50	35.50	35.80	36.00	35.80	35.50	35.50	35.50

increases up to 41°C, and as time increase the temperature gradually decrease from 39.25°C, 38.52°C, 38.40°C, and 38.12°C up to 2.00 min, respectively, within the interval (0.19 m, 0.25 m) in the axial face as shown in left-hand Figure 5.3. Except for this interval, the axial temperature is steady state. From the observation, there is no large variation in the axial temperature in Figure 5.3 due to the zero flux boundary conditions at the bottom and top of the limb. As in the radial flow, the initial temperature in the axial direction is high because of the characteristic of tumor tissue as well as the external spatial heating source as shown in Figure 5.2 and Figure 5.3. All of these curves in the axial direction are also sinusoidal in nature within the axial interval (0.19 m, 0.25 m).

The curves in the right-hand Figure 5.3 exhibit the axial temperature profile with peak temperatures 41°C, 37.8°C, 37.15°C, 36.5°C, and 36°C at 0 min, 2.33 min, 5 min, 7.33 min, and 10 min, respectively within the axial interval (0.19 m, 0.25 m) and steady-state otherwise.

These results verify that the effect of external heating is initially high and lowers the

effects as time lengthens. Both radial and longitude temperature decreases in 10 min than in 2 min. After a certain period, the axial temperature becomes a steady-state in the entire domain due to the Neumann boundary condition applied and no repetition of external heating in the abnormal tissue. From these observations, we further claim that the temperature distribution is axially symmetrical while plugging the zero flux at both sides, bottom, and top.

5.4.3 One-Dimensional Longitudinal Temperature Profile (z-direction) with Neumann and Robin Boundary Conditions
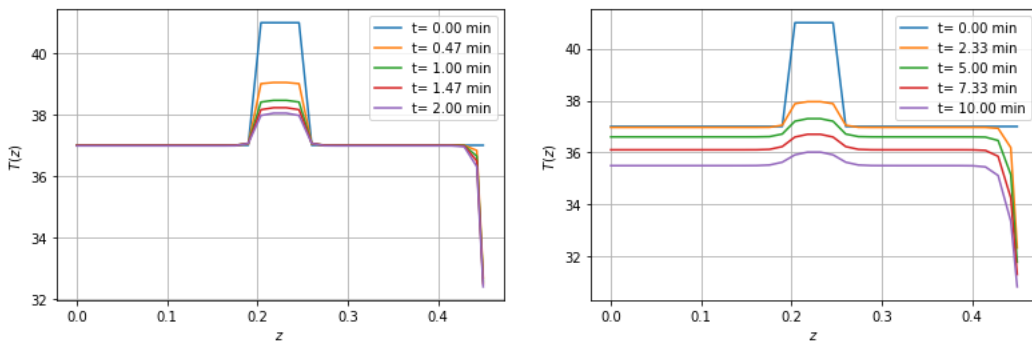
Figure 5.4: :Longitudinal temperature profile when $r_i = 0.015\,m$ (left) at $2\,\mathrm{min}$ (right) at $10\,\mathrm{min}$ with flux boundary at bottom and Robin at top.

The left-hand Figure 5.4 shows the temperatures of aberrant tissue within the axial interval (0.19m, 0.22m) for 41°C, 39°C, 38.5°C, 38.25°C, and 38°C in 0 min, 0.47 min, 1 min, 1.47 min, and 2 min, respectively, and the right-hand Figure 5.4 shows the decrease in temperature up to 36°C in 10 min. The temperature of the limb's apex suddenly drops to 32°C, in 2 min and 31°C, in 10 min. Additionally, Figure 5.4 shows that the axial temperature is constant from the bottom to 0.19 m and from 0.22 m to 0.42 m height, and declines gradually from 0.42 m to 0.44 m radial distance, and then drops sharply at the topmost of the limb. These outcomes show the nonlinear behavior of the temperature in the axial direction which is the consequence of the characteristic of the tumor cell, the Robin boundary conditions at top, zero flux at the bottom, and the external heat source.

5.4.4 Temperature Profiles of Nonlinear Thermophysical Parameters

In this section, we observe the effect of various temperature-dependent thermophysical parameters such as thermal conductivity, metabolic heat generation rate, blood

perfusion, and time-dependent specific heat for tumor tissues when $r_i = 0.015$ m and $z_j = 0.22$ m, and exhibited in Figure 5.5 – 5.8.   The thermal conductivity of abnormal
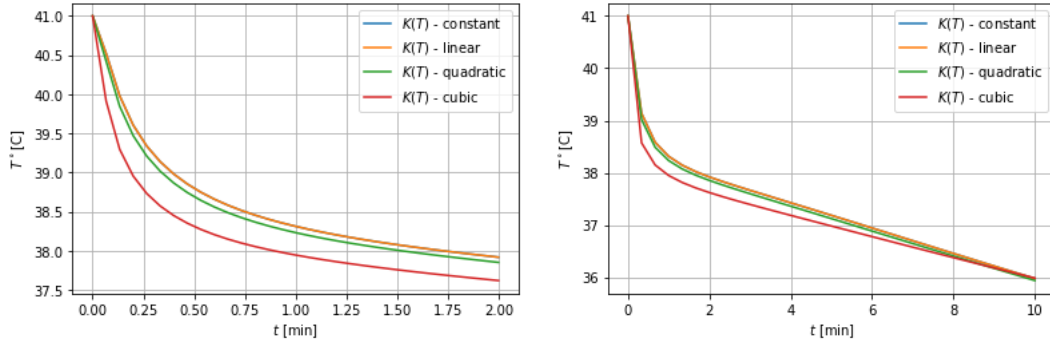
Figure 5.5: Temperature profile with various thermal conductivity coefficients upto (left) 2 min (right) 10 min.
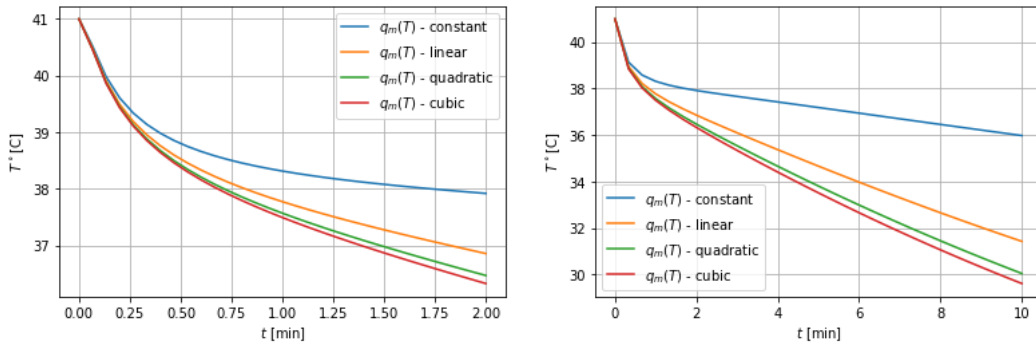
Figure 5.6: Temperature profile with various coefficients of metabolic heat generation upto (left) 2 min (right) 10 min.
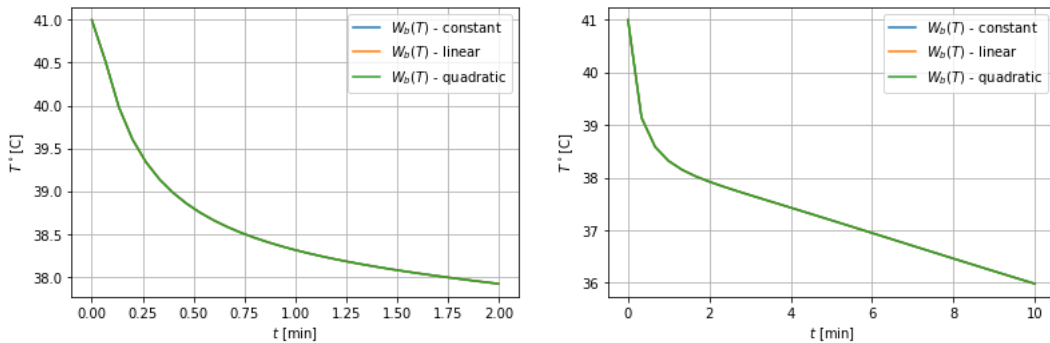
Figure 5.7: Temperature history with various blood perfusion coefficients upto (left) 2 min (right) 10 min.

tissue is 0.642 W/m°C, [95]. Choosing the linear, quadratic, and cubic coefficients

of values control thermal parameters, $k_0 = 0.4728$, $k_1 = 0.003$, and $k_2 = 0.0001$, $k_3 = 0.00001$, respectively [13], and graphically presented in Figure 5.5 in 2 min and 10 min. In the left-hand Figure 5.5 the tumour temperature decreases sharply from 41°C, to 39.4°C, 39.4°C, 39.25°C, and 38.75°C, in 0.25 min for constant, linear, quadratic, and cubic thermal conductivities, respectively. After then the graphs decrease slowly up to 38°C, 37.9°C, and 37.75°C in the case of constant, linear, quadratic, and cubic thermal conductivities, respectively. Similarly, in right-hand Figure 5.5 the temperature decreases and each curve reaches 36°C in 10 min. In the case of constant and linear thermal conductivity, the curves in both of the Figures coincide. This observation shows that with the decrease in coefficients of thermal conductivities the temperature decreases in the small range. The curve in the case of constant and linearly dependent thermal conductivity coincides with temperature 41°C initially, in 0 min in both of the Figure 5.5 for abnormal tissue. The extreme temperature is due to the initially applied constant heating source and also the high rate of thermal conductivity in the abnormal tissue. As the cubic coefficient of thermal conductivity decreases from 0.0001 to 0.00001 the temperature lowers to 37.75°C in 2 min and 36°C, in 10 min

For the computational purpose of the temperature history, we set up the different metabolic coefficients $q_{b1} = 10^5$, $q_{b2} = 10^3$, and $q_{b3} = 10$ with $q_b = 33800$ for tumour tissues. Temperature profiles with these values at various times up to 2 min can be seen in Figure 5.6 in the graphs of left-hand Figure 5.6. The observation of the temperature profile for tumour tissue shows that the temperature is high 41°C in the initial phase then decreases sharply from 41°C to 40°C, in 0.125 min and coincides with all categories, constant, linear, quadratic, and cubic metabolic rates. After then the temperature decreases slowly to 38°C, 36.98°C, 36.5°C, and 36.4°C in 2 min. The temperature reaches down to 36°C, 31.98°C, 30°C, and 29.98°C in 10 min for the case of constant, linear, quadratic, and cubic, respectively. As the coefficients of metabolism decrease and time lengthens, the temperature increases and the extreme temperature is the cause of the initially applied constant spatial heating source.

The temperature profiles for different coefficients of blood perfusion is observed at the same position at 0.015 m, the radial distance from the core, and 0.22 m, axial distance from the bottom. Various perfusion coefficients with $w_{b0} = 3$, basal perfusion rate, and $w_{b0} = 0.0007$, for tumour tissue, are chosen. Besides this, the coefficients $w_{b1} = 0.0005$, $w_{b2} = 0.0002$, and $w_{b3} = 0.0000001$ [59, 65] for constant, linear, and quadratic case are chosen and presented the temperature profile for the tumor in the Figure 5.7 with graphs in left-hand up to 2 min and right-hand up to 10 min. All

118

the graphs in both Figures coincide in the case of low values of constant and linear, and quadratic coefficients. Tissue temperature decreases from 41°C up to 38.0°C in 2 min in left-hand Figure 5.7 and reaches up to 36°C in 10 min. With the increase or decrease of blood perfusion coefficients in a small range, there is no remarkable change in temperature. This outcome is brought by the neglegible concentration of blood vessels at the skin's surface.

5.4.5 Axisymmetric Temperature Profile in (r, z)-direction (Contour and surface Plot)

The plots in the first row of Figures 5.8, 5.9, and 5.10 are obtained by using Robin boundary at the lateral and zero flux at the inner, bottom, and top. The plots in second row of the same Figures 5.8- 5.10 show the case, where the Robin boundary is used at the lateral surface and top, with zero flux in the inner and at bottom of the limb.

5.4.5.1 Initial Temperature Profile in contour and surface Plot

The initial temperature profiles at time $t = 0$ min is presented in Figure 5.8. Each of
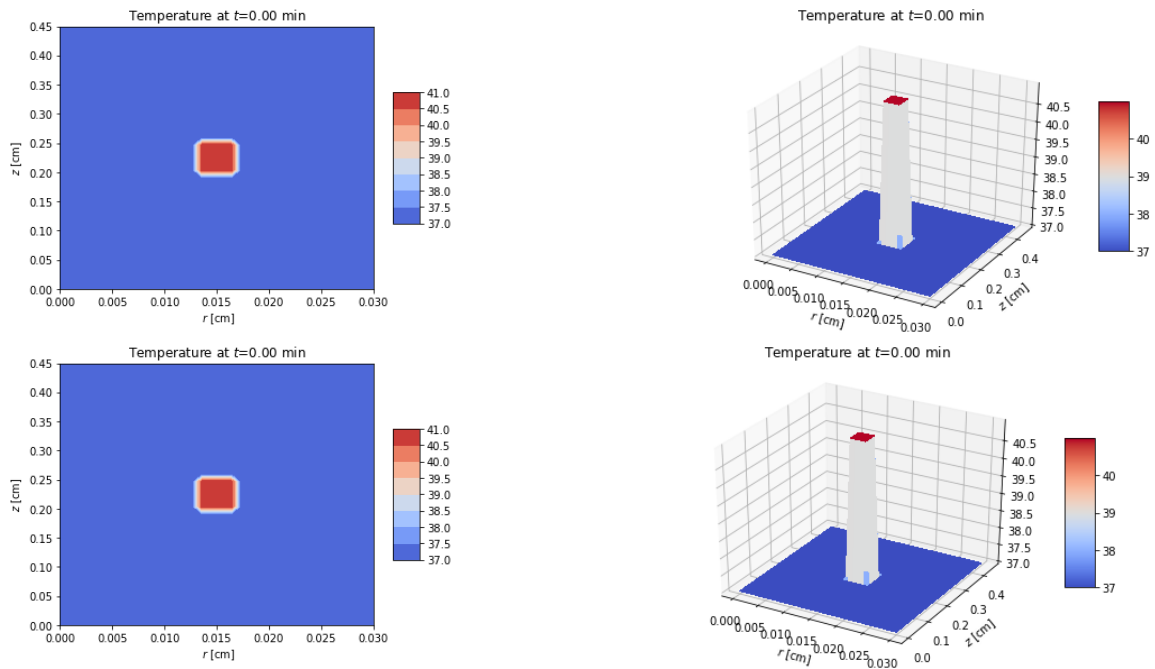
Figure 5.8: Initial temperature profiles when $r_i = 0.015\,\mathrm{m}$ and $z_j = 0.022\,\mathrm{m}$ for (left) contour plot and (right) surface plot.

the contour (left) and surface (right) plots in Figure 5.8 display the extreme temperature 41°C within the tumour tissue and 37°C elsewhere initially at $t = 0$, no matter which of the boundary conditions are used. Because of the external heat source used in the abnormal tissue, the initial temperature is much higher than that of the normal one.

5.4.5.2 Axisymmetric Temperature Profile in (r, z)-direction (Contour and surface Plot)

For the unsteady state, the contour and surface plots are shown in Figure 5.9 and Figure 5.10, respectively, simulated in 1 min, 2 min, and 10 min. The first row in both Figures is obtained by using the Robin boundary condition at the lateral surface with zero flux at the inner, bottom, and top.

The second row in both Figures are obtained by using the Robin boundary condition at the lateral surface and top, with zero flux at the inner and bottom. Each of the
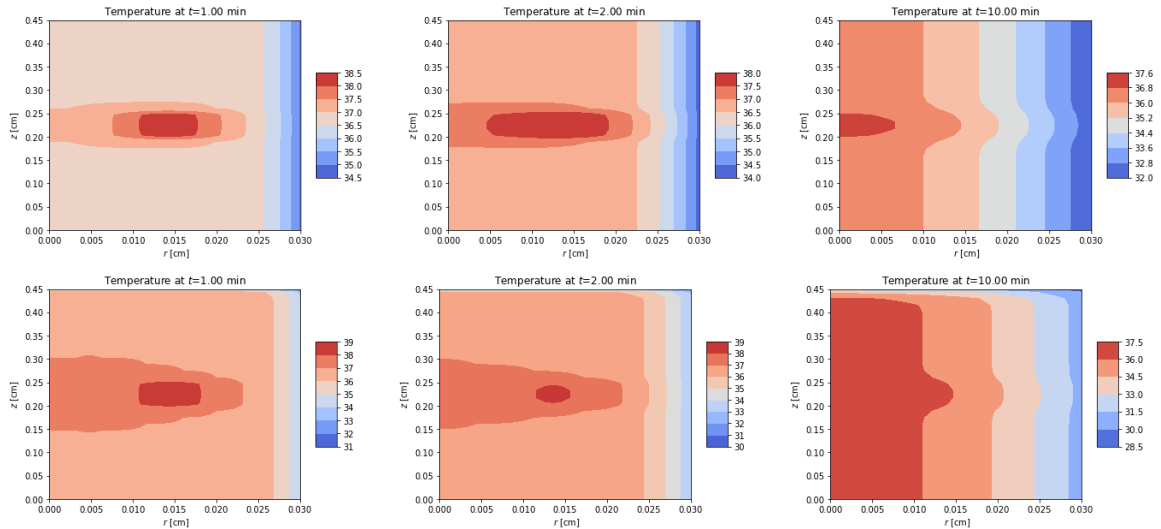
Figure 5.9: Contour plot for temperature profile in tumor tissue (first row) Robin boundary lateral and (second row) Robin boundary at lateral and top in 0 min, 1 min, 2 min, and 10 min when $r_i = 0.015$ m and $z_j = 0.022$ m.

contour and surface plots in Figures 5.9, and 5.10, with a red color and the peak in Figure 5.10 indicates high temperature in tumor tissue that was initially 41°C in 0 min in Figure 5.8. The temperatures in the first row of the Figure 5.9, contour and 5.10, surface, are axially symmetric with high temperature 38.5°C, 38°C, and 37.6°C at peak in 1 min, 2 min, and 10 min respectively. The temperature slows down to 37°C, 36.50°C, and 35°C, respectively in tumour area, and then drop down

to 34.5°C, 34°C, and 32°C, respectively in 1 min, 2 min, and 10 min, near the skin surface. The temperature flattens slowly and spreads within the peripheral region of the tumour in the radial direction as in a similar manner in left-hand Figure 5.2 and axially same as in the one-dimensional case of Figure 5.3. The same results are shown in the surface plots of the first row of Figure 5.10 which verifies the good agreement with one-dimensional results. These axially symmetrical results are due to the zero flux in the inner, at the bottom, and top of the limb. Except for the axial interval
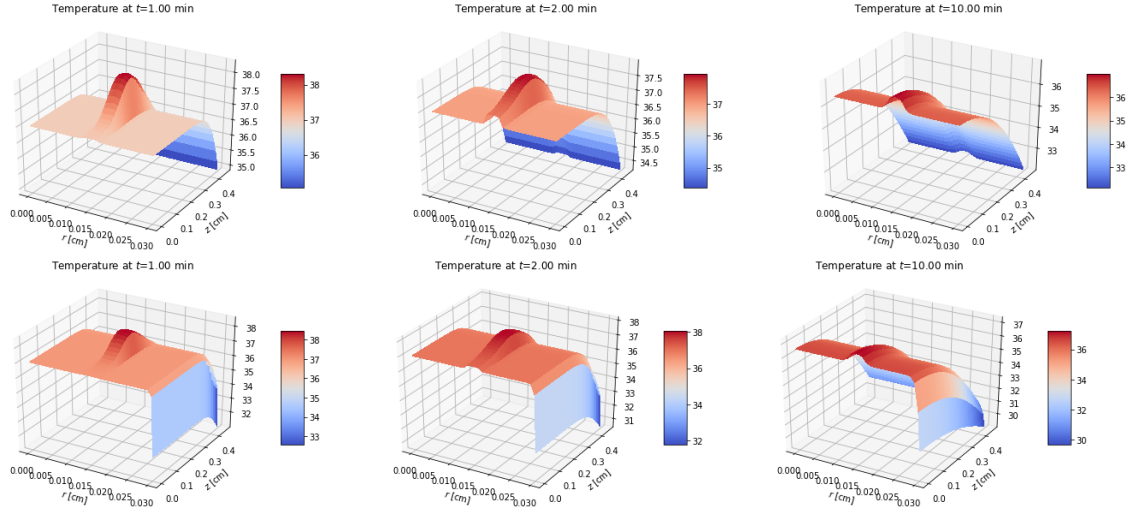
Figure 5.10: surface plot for temperature profile in tumor tissue (first row) Robin boundary lateral and (second row) Robin boundary at lateral and top in 0 min, 1 min, 2 min, and 10 min when $r_i = 0.015$ m and $z_j = 0.022$ m.

(0.42 m, 0.45 m) near the top, where the temperature declines in each slice over the course of 1 min, 2 min, and 10 min, respectively, the temperatures in the second row of the Figures 5.9 and 5.10 are axially symmetric. Low temperatures of 31°C, 30°C, and 28.5°C in 1 min, 2 min, and 10 min, respectively, and high temperatures of 39°C, 39°C, 37.5°C at peak have been observed. According to the first row of Figure 5.2, the temperature gradually flattens and spreads around the tumor's periphery in both radial direction and axial directions mostly similar to the one-dimensional scenario as shown in Figure 5.5. The same nature of diffusion is seen in the first row of Figure 5.9 as in each of the plots in the second row of Figure 5.10. These outcomes are due to the presence of Robin boundary conditions at the lateral surface and at the top of the limb.

5.4.6 Cross-Sectional Temperature Profile

Finally, we show the temperature in the cross-section of the limb from a three-dimensional simulation. We can apply these simulations for the observation of the temperature of slices at different points of interest. The boundary conditions, different locations, and different sizes of tumor cause variations in the temperature profile. The three plots in the first row of Figure 5.11 show the cross-sectional temperature of normal tissue with a viewpoint of the limb at $z = 0.11\,\mathrm{m}$, one-fourth of the limb height, with Robin boundary condition at the lateral and top surface, with a zero-flux boundary condition at the bottom. The three plots in the second row of Figure 5.11 indicate the cross-sectional temperature in the case of abnormal tissue with Robin boundary condition at the lateral and the top of the surface, and zero flux boundary condition for the inner and bottom.

In the first three plots of Figure 5.11, the temperature is uniformly diffused in all
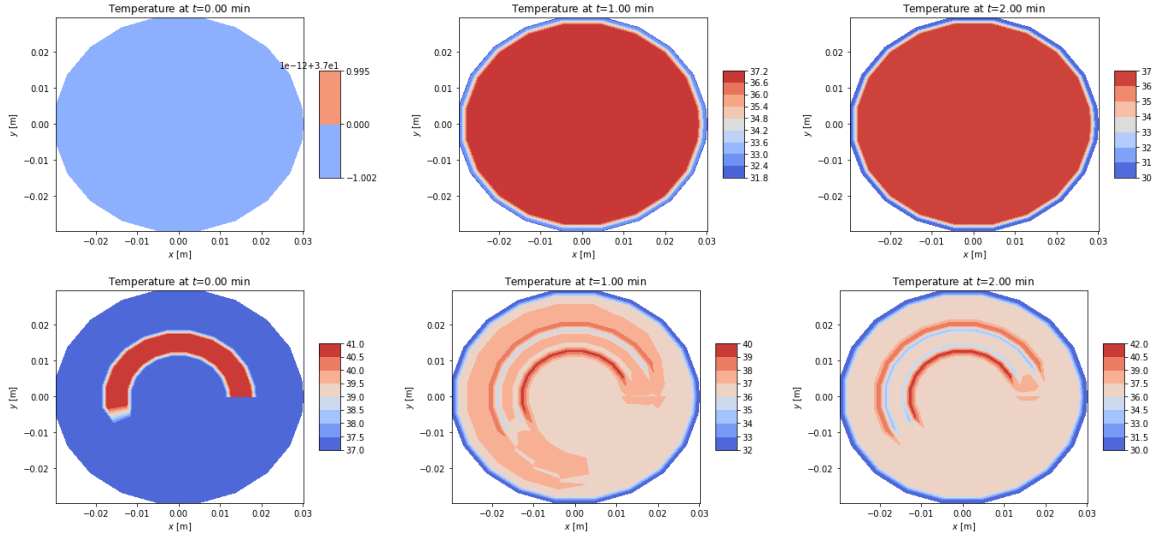
Figure 5.11: Cross-sectional temperature profile (first row) normal (second row) in tumour in 0 min, 1 min, and 2 min when $r_i = 0.015\,\mathrm{m}$, $z_j = 0.011\,\mathrm{m}$, and $\theta_m = 2\,\pi$ in (r, θ) direction.

directions and the overall temperature goes on decreasing and reaches to 34°C, 32°C, and 30°C in 0 min, 1 min, and 2 min, respectively in normal tissue. For the abnormal tissue, the initial temperature is high and the temperature within the cross-section drops generally, though not consistently as in the case of normal tissue. In a minute, the temperature of aberrant tissue drops from high temperatures down to 40°C in some areas, and temperature between 35°C, and 36°C within some other parts of the tumor then drops down to 32°C. The temperature rises in some areas of the abnormal

tissue reaching upto 42°C, and then falls in other areas of the abnormal tissue ranging from 34°C, to 36°C, reaching down to 34°C, in 2 min. In this way, the nonlinearity of the temperature profiles within the abnormal tissue are observed in the cross-section.

5.5 Conclusion

The three-dimensional bioheat transfer model with temperature-dependent thermo-physical parameters has been investigated, and numerically solved by applying the Finite Volume (FV) method, and computationally simulated numerical results have been obtained via python. These temperature-dependent thermophysical parameters make the model (5.1) highly nonlinear. The obtained results are applied to observe their effects in the variation of temperature, in tumor tissue at different times, 0 min, 0.47 min, 1 min, 1.47 min, and 2 min in the left-hand Figure 5.2, and 0 min, 0.33 min, 5 min, 7.33 min, and 10 min in the right-hand Figure 5.2. When the tumor tissue is continuously heated, the temperature at the heating point first rises, then starts to spread as the time period lengthens, the peak temperature decreases smoothly and the peripheral temperatures increase as related to the previous time step in the radial direction. That is, the peak of the curves flattens at different times. This outcome is the consequence of Robin's boundary condition which was applied to the outer surface of the body organ. In comparison to healthy tissues, the temperature at the skin's surface is noticeably high in aberrant tissue. Due to the application of the Neumann condition being applied to the bottom and top of the computational living organ, the longitudinal temperature in the axial direction decreases as time passes on but does not spread as much in the peripheral region as it does in the radial direction.

We found that the results for the one-dimensional model, obtained by using modified Robin boundary condition in the lateral surface agree with the results obtained from the numerical simulation for one-dimensional (r-direction), and one-dimensional (z-direction), nonlinear models. Though the implicit scheme is unconditionally stable, rare in the case of the nonlinear model. So, in this Chapter, the three-dimensional bioheat equation is explicitly solved by the Finite Volume method. The nonlinear behaviors of the one-dimensional models in r-direction, and z-direction, two-dimensional axisymmetric, (r, z)-directions, angular axisymmetric, (r, θ)-direction heat flow together temperature history with nonlinear thermal conductivities, metabolic rates, and blood perfusion rates are taken into account.

The numerical observation of all of these simulated results with obtained sinusoidal

curves within the radial (0.008 m, 0.022 m) and axial (0.19 m, 0.25 m) intervals for 2 min and the additional results for 10 min demonstrate the nonlinear behavior of thermophysical parameters with higher temperature in abnormal tissue due to the characteristics of the tumor and initially applied external heating source.

CHAPTER 6

SUMMARY AND CONCLUSION

The main objective of this work was to develop reliable, and efficient numerical solutions to the extended Pennes' linear and nonlinear mathematical models. One-dimensional with and without clothing, two-dimensional axisymmetric, and three-dimensional nonlinear are the major focuses of the work. We summarized the overall work, conclusions, and some research plans for future directions.

6.1 Summary

The basic terminologies and conceptual frameworks, along with information on the physiological disturbances in the human body under different circumstances, are concisely covered in Chapter 2. Also, the analytical approach for the one-dimensional steady-state model and the numerical approach for the one-dimensional transient model in the cylindrical nude body are also described in detail. In Chapter 3, Pennes' model is extended by incorporating the clothing phenomenon, and it is further extended to an axisymmetric two-dimensional bioheat transfer model with the clothing effect at the boundary in Chapter 4. In addition to these, the model is extended to the three-dimensional nonlinear form in Chapter 5 to observe the non-symmetry of temperature variation in the abnormal tissue. The developed transient models have been solved numerically and computationally simulated in Python.

6.2 Conclusion

The work consists of three parts: (a) the extension of the bioheat transfer model by incorporating clothing as a protective layer (b) the construction of an axisymmetric model with time-dependent metabolism, clothing, and sweating effect during physical

125

activities, and (c) the extension to a three-dimensional nonlinear model.

In the first part, we extended the model by adding the clothing parameters: thermal conductivity of cloth, clothing area factor, and thickness of the cloth as a protective layer. To reduce the computational complexity caused by the diverse physiological behaviors of two non-homogeneous materials, cloth, and the human body, the interface condition has been used. The usual Robin's boundary condition is modified by incorporating two important factors: the effective clothing area factor and the convective heat transfer coefficient. The effective clothing area factor includes clothing insulation, air insulation, and the clothing area factor. The convective heat transfer coefficient, on the other hand, includes air velocity and the walking speed of a person. The results obtained from the implicit finite difference method show that thermal comfort and thermal insulation depend on the properties of the fabric, and human physical, and physiological factors. The simulation results with two types of modified Robin's boundary conditions demonstrated that using clothing insulation with mild air velocity and walking speed provides better comfort than the case of using effective clothing area factor, only or using relative air velocity only. That is, clothing insulation helps decrease the rate of heat loss from the body whereas air velocity causes heat loss from the body, as described in Figure 3.5. Solvability, consistency, stability, and convergence of the implicit finite difference scheme are verified by a lemma and some theorems, based on grid points and time step sizes as well.

The second part of this work was to extend Pennes' model in an axisymmetric two-dimensional (2D) form with time-dependent metabolism, clothing, and sweating effects during physical activities. This extended 2D model has been solved by using the Crank-Nicolson FD technique and applied to observe the effect of time-dependent metabolism. It has been demonstrated that a high metabolic rate causes the body temperature increases during exercises and metabolic heat generation at various time steps causes an increase in body core temperature with time. The insulation of clothing material prevents a quick drop in skin temperature with the change in metabolic rate and maintains the body temperature even in the case of sweat evaporation during physical exercise. A minor symmetrical change has been noticed in the body core temperature in the longitudinal direction, due to the significantly different ratio of radial and axial length scales and the flux boundary at the inner, bottom, and top of the limb.

The third part of the work was to extend the model to a three-dimensional nonlinear model with temperature-dependent parameters and external heat sources in order

to understand the behaviors of the temperature variation in the abnormal tissue. This model consists of one-dimensional (radial r-direction), one-dimensional (axial, z-direction), two-dimensional axisymmetric (r, z)-direction, and angular symmetric (r, θ)-direction. The models have been solved by using the finite volume (FV) energy conservation law for the investigation of the temperature profile in 1D radial, 1D axial, 2D axisymmetric, and 2D angular symmetric, together with the nonlinear-thermal conductivity, blood perfusion rate, and metabolism having a linear, quadratic, and cubic relationship with temperature. It has been found that the temperature increases quickly and reaches 41°C in the interval (0.13 m, 0.17m) with external heat of 250 W/m^3, applied initially, and later drops quickly to normal conditions. The temperature profile goes on flattening with the lengthens of time, as described in Figures 5.2 -5.11, which happens with respect to the size of the tumor. The temperature spreads within the periphery and the curves flatten out over time, the skin's surface temperature is substantially high in aberrant tissue, and the longitudinal temperature in the axial direction drops over time but does not propagate as much in the peripheral area as it does in the radial direction. In the longitudinal direction, it is observed that there are no notable variations in temperature due to zero flux boundary at the bottom and top, which was also expected, as the ratio of radial and axial length scales is significantly different. However, switching from the zero-flux boundary to Robin's boundary condition at the top, non-symmetric and nonlinear behavior is observed in the longitudinal temperature profile. The numerical simulation results in the radial direction agree with the one-dimensional model. The numerical observation of all these simulated results with sinusoidal curves obtained within the radial (0.008m, 0.022m) and axial (0.19m, 0.25m) intervals for 2 min; and the results in additional time for 10 min revealed that the temperature decreases from the core to the skin surface in a similar manner as in the normal case of the radial temperature profile.

A further numerical investigation has been carried out for up to 2 min and then up to 10 min with linear, quadratic, and cubic coefficients of temperature-dependent parameters to perceive their effect on the temperature variation in abnormal tissue, which shows that these various coefficients of thermal conductivity $K(T)$, metabolic heat generation $q_m(T)$, and blood perfusion $w_b(T)$, are directly proportional to the temperature within the target tissue. Various simulations for an axisymmetric model in the (r, z)-direction have been performed with zero flux at the inner, bottom, and top of the limb and Robin's boundary condition at the lateral surface, which revealed an axially symmetric temperature profile. Imposing Robin's boundary condition at the top and lateral surfaces of the limb revealed non-symmetric temperature variation

in the skin surface and the top of the longitudinal cross-sectional slice. The simulation results for angular symmetric model (r, θ)-direction with various lateral boundary conditions demonstrate non-symmetric variations in the temperature in the cross-section of the tumor tissue.

6.2.1 Suggestions for Future Directions

Future work

- Consideration of the thermal transmission characteristic of textile for human thermal comfort.

- Consideration of the Specific Absorption Rate (SAR) into account hyperthermia treatment against cancer.

- Use of electromagnetic radiation for the hyperthermia treatment against cancer.

REFERENCES

[1] ABBAS, A., ZHAO, Y., ZHOU, J., WANG, X., AND LIN, T. Improving thermal conductivity of cotton fabrics using composite coatings containing graphene, multiwall carbon nanotube or boron nitride fine particles. *Fibers and Polymers 14*, 10 (2013), 1641–1649.

[2] ABD-EL MALEK, M. B., AND HELAL, M. M. Group method solution for solving nonlinear heat diffusion problems. *Applied mathematical modelling 30*, 9 (2006), 930–940.

[3] ACHARYA, S., GURUNG, D., AND SAXENA, V. Human males and females body thermoregulation: perfusion effect analysis. *Journal of thermal biology 45* (2014), 30–36.

[4] ACHARYA, S., GURUNG, D. B., AND SAXENA, V. P. Two dimensional finite element method for metabolic effect in thermoregulation on human males and females skin layers. *Journal of coastal life medicine 3*, 8 (2015), 623–629.

[5] ADAMOWICZ, A. Axisymmetric fe model to analysis of thermal stresses in a brake disk. *Journal of theoretical and applied mechanics 53* (2015).

[6] ANDREOZZI, A., BRUNESE, L., IASIELLO, M., TUCCI, C., AND VANOLI, G. P. Modeling heat transfer in tumors: a review of thermal therapies. *Annals of biomedical engineering 47*, 3 (2019), 676–693.

[7] ARAYA, G., AND GUTIERREZ, G. Analytical solution for a transient, three-dimensional temperature distribution due to a moving laser beam. *International Journal of Heat and Mass Transfer 49*, 21-22 (2006), 4124–4131.

[8] ARKIN, H., XU, L., AND HOLMES, K. Recent developments in modeling heat transfer in blood perfused tissues. *IEEE Transactions on Biomedical Engineering 41*, 2 (1994), 97–107.

[9] Baczek, M. B., and Hes, L. The effect of moisture on thermal resistance and water vapour permeability of nomex fabrics. *Journal of Materials Science and Engineering. A 1*, 3A (2011), 358.

[10] Baranowska, A., and Zdzisław, K. Finite difference approximations for nonlinear first order partial differential equations. *Zeszyty Naukowe Uniwersytetu Jagiellońskiego. Universitatis Iagellonicae Acta Mathematica 1258* (2002), 15–30.

[11] Bardati, F., and Gerosa, G. On the solution of the non-linear bio-heat equation. *Journal of biomechanics 23*, 8 (1990), 791–798.

[12] Belmiloudi, A. *Heat Transfer: Mathematical Modelling, Numerical Methods and Information Technology*. BoD–Books on Demand, 2011.

[13] Bhattacharya, A., and Mahajan, R. Temperature dependence of thermal conductivity of biological tissues. *Physiological measurement 24*, 3 (2003), 769.

[14] Bianchi, L., Cavarzan, F., Ciampitti, L., Cremonesi, M., Grilli, F., and Saccomandi, P. Thermophysical and mechanical properties of biological tissues as a function of temperature: A systematic literature review. *International Journal of Hyperthermia 39*, 1 (2022), 297–340.

[15] Cebeci, T. *Convective heat transfer*. Springer, 2002.

[16] Cengel, Y. A., and Ghajar, A. J. Heat and mass transfer. *A practical approach* (2007).

[17] Chao, K., and Yang, W. Response of skin and tissue temperature in sauna and steam baths. *Bio-Mech. syrup., ASME* (1975), 69–71.

[18] Chen, M. M., and Holmes, K. R. Microvascular contributions in tissue heat transfer. *Annals of the New York Academy of Sciences 335*, 1 (1980), 137–150.

[19] Cohen Stuart, C. A study of temperature-coefficients and van't hoff's rule. In *KNAW Proceedings* (1912), vol. 14, pp. 1159–73.

[20] Cooper, T. E., and Trezek, G. J. A probe technique for determining the thermal conductivity of tissue.

[21] Crank, J., and Nicolson, P. A practical method for numerical evaluation of solutions of partial differential equations of the heat-conduction type. *Advances in Computational Mathematics 6*, 1 (1996), 207–226.

[22] Croft, D. R., and Lilley, D. G. Heat transfer calculations using finite difference equations.

[23] da Silva, G., Lima, R., Lyra, P., de Carvalho, D., and Fernandes, A. The use of an axisymmetric formulation of the finite volume method for the thermal analysis of the retina and ocular tissues following implantation of retinal prosthesis. *Journal of the Brazilian Society of Mechanical Sciences and Engineering 34* (2012), 308–313.

[24] Dai, G., and Huang, J. Nonlinear thermal conductivity of periodic composites. *International Journal of Heat and Mass Transfer 147* (2020), 118917.

[25] Davidson, E. A., Janssens, I. A., and Luo, Y. On the variability of respiration in terrestrial ecosystems: moving beyond q10. *Global change biology 12*, 2 (2006), 154–164.

[26] Dung, L. T., and Ngoc Anh, L. T. Study on thermal protective clothing for working in the high temperature working environmental. *International Journal of Advanced Basic Science 7*, 1 (2019), 18–23.

[27] Erdmann, B., Lang, J., and Seebab, M. Adaptive solutions of nonlinear parabolic equations with application to hyperthermia treatments. In *CHT'97-Advances in Computational Heat Transfer. Proceedings of the International Symposium* (1997), Begel House Inc.

[28] Fabbri, K. A brief history of thermal comfort: from effective temperature to adaptive thermal comfort. In *Indoor thermal comfort perception*. Springer, 2015, pp. 7–23.

[29] Fabbri, K. Ergonomics of the thermal environment. human body and clothes. In *Indoor Thermal Comfort Perception*. Springer, 2015, pp. 25–74.

[30] Fanger, P. O., et al. Thermal comfort. analysis and applications in environmental engineering. *Thermal comfort. Analysis and applications in environmental engineering.* (1970).

[31] Farahat, A. E., Kahil, H. M., and Hussein, K. F. A. Microwave diathermy for deep heating therapy of knee joint. *Progress In Electromagnetics Research C 99* (2020), 15–33.

[32] Faure, S. A finite volume scheme for the nonlinear heat equation.

[33] GASPAR, A., OLIVEIRA, A., AND QUINTELA, D. Effects of walking and air velocity on convective heat transfer from a nude manikin. In *Winsdor Conference: Comfort and Energy Use in Buildings: Getting Them Right–International Conference, Windsor Great Park, UK* (2006), pp. 27–30.

[34] GOKUL, K., GURUNG, D. B., AND ADHIKARY, P. R. Fem approach for transient heat transfer in human eye.

[35] GUNTUR, S. R., AND CHOI, M. J. Influence of temperature-dependent thermal parameters on temperature elevation of tissue exposed to high-intensity focused ultrasound: numerical simulation. *Ultrasound in medicine & biology 41*, 3 (2015), 806–813.

[36] GUPTA, N., AND SHAKYA, M. One dimensional transient state finite element model to study thermal variations due to transient vasoconstriction followed by persistent vasodilation during inflammation in surgical wound of peripheral tissues of human limb. *Indian J of Sci and Tech 10*, 12 (2017), 1–15.

[37] GURUNG, D., GOKUL, K., AND ADHIKARY, P. Mathematical model of thermal effects of blinking in human eye. *International Journal of Biomathematics 9*, 01 (2016), 1650006.

[38] GURUNG, D., AND SAXENA, V. Transient temperature distribution in human dermal part with protective layer at low atmospheric temperature. *International Journal of Biomathematics 3*, 04 (2010), 439–451.

[39] GURUNG, D., SAXENA, V., AND ADHIKARY, P. Fem approach to one dimensional unsteady state temperature distribution in human dermal parts with quadratic shape functions. *Journal of applied mathematics & informatics 27*, 1_2 (2009), 301–313.

[40] GURUNG, D. B. *Mathematical study of abnormal thermo-regulation in human dermal parts*. PhD thesis, 2018.

[41] GUTIERREZ, G. Study of the bioheat equation with a spherical heat source for local magnetic hyperthermia. *Mecánica Computacional*, 42 (2007), 3562–3572.

[42] GUYTON, C., AND HALL, J. E. Pocket companion to textbook of medical physiology.

[43] HARFASH, A. J. High accuracy finite difference scheme for three-dimensional microscale heat equation. *Journal of computational and applied mathematics 220*, 1-2 (2008), 335–346.

[44] HARISH, S., ANNANTH, V. K., ABINASH, M., KANNAN, K., AGARWAL, S., AND MOHANA, N. A study on numerical methodologies in solving fluid flow and heat transfer problems. In *IOP Conference Series: Earth and Environmental Science* (2021), vol. 850, IOP Publishing, p. 012021.

[45] HASSANPOUR, S., AND SABOONCHI, A. Validation of local thermal equilibrium assumption in a vascular tissue during interstitial hyperthermia treatment. *Journal of Mechanics in Medicine and Biology 17*, 05 (2017), 1750087.

[46] HAVENITH, G. Heat balance when wearing protective clothing. *Annals of occupational Hygiene 43*, 5 (1999), 289–296.

[47] HAVENITH, G., AND FIALA, D. Thermal indices and thermophysiological modeling for heat stress. *Comprehensive Physiology 6*, 1 (2011), 255–302.

[48] HAVENITH, G., HOLMÉR, I., AND PARSONS, K. Personal factors in thermal comfort assessment: clothing properties and metabolic heat production. *Energy and buildings 34*, 6 (2002), 581–591.

[49] HAVENITH, G., KUKLANE, K., FAN, J., HODDER, S., OUZZAHRA, Y., LUNDGREN, K., AU, Y., LOVEDAY, D., ET AL. A database of static clothing thermal insulation and vapor permeability values of non-western ensembles for use in ashrae standard 55, iso 7730, and iso 9920. *Ashrae Trans 121*, 1 (2015), 197–215.

[50] HEWITT, G. F., SHIRES, G. L., AND BOTT, T. *Process heat transfer.* begell house, 1994.

[51] HIMME, B. https://www.pathwayz.org/tree/plain/thermoregulation.

[52] HOBINY, A. D., AND ABBAS, I. A. Nonlinear analysis of dual-phase lag bioheat model in living tissues induced by laser irradiation. *Journal of Thermal Stresses 43*, 4 (2020), 503–511.

[53] HODGSON, T. *The development of instrumentation for the direct measurement of heat loss from man in a normal working mode.* PhD thesis, 1974.

[54] HOLMÉR, I. Protective clothing and heat stress. *Ergonomics 38*, 1 (1995), 166–182.

[55] HOLMER, I. Protective clothing in hot environments. *Industrial health 44*, 3 (2006), 404–413.

[56] HÖPPE, P. R. Heat balance modelling. *Experientia 49*, 9 (1993), 741–746.

[57] HU, P., TANG, H., ZHENG, L., AND FANG, C. J. Optimal design of protective clothing based on difference equation. *Mathematical Models in Engineering 5*, 2 (2019), 48–55.

[58] HUNTER, B., AND GUO, Z. Comparison of the discrete-ordinates method and the finite-volume method for steady-state and ultrafast radiative transfer analysis in cylindrical coordinates. *Numerical Heat Transfer, Part B: Fundamentals 59*, 5 (2011), 339–359.

[59] ILJAŽ, J., WROBEL, L. C., HRIBERŠEK, M., AND MARN, J. Numerical modelling of skin tumour tissue with temperature-dependent properties for dynamic thermography. *Computers in biology and medicine 112* (2019), 103367.

[60] INOUE, T. Effect of relative humidity on heat loss of men exposed to environments of 80, 76, and 72f. *ASHVE Trans. 59* (1953), 329–346.

[61] JIANG, S., MA, N., LI, H., AND ZHANG, X. Effects of thermal properties and geometrical dimensions on skin burn injuries. *Burns 28*, 8 (2002), 713–717.

[62] KATIĆ, K., LI, R., AND ZEILER, W. Thermophysiological models and their applications: A review. *Building and Environment 106* (2016), 286–300.

[63] KELLER, K. H., AND SEILER JR, L. An analysis of peripheral heat transfer in man. *Journal of Applied Physiology 30*, 5 (1971), 779–786.

[64] KENGNE, E., LAKHSSASSI, A., AND VAILLANCOURT, R. Temperature distribution in living biological tissue simultaneously subjected to oscillatory surface and spatial heating: analytical and numerical analysis. In *International Mathematical Forum* (2012), vol. 7, Citeseer, pp. 2373–2392.

[65] KENGNE, E., MELLAL, I., HAMOUDA, M. B., AND LAKHSSASSI, A. A mathematical model to solve bio-heat transfer problems through a bio-heat transfer equation with quadratic temperature-dependent blood perfusion under

a constant spatial heating on skin surface. *Journal of Biomedical Science and Engineering 2014* (2014).

[66] KREITH, F., AND BLACK, W. Z. Basic heat transfer.

[67] KREITH, F., AND MANGLIK, R. M. *Principles of heat transfer.* Cengage learning, 2016.

[68] KUDRYASHOV, N. A., AND SHILNIKOV, K. E. Nonlinear bioheat transfer models and multi-objective numerical optimization of the cryosurgery operations. In *AIP Conference Proceedings* (2016), vol. 1738, AIP Publishing LLC, p. 230009.

[69] LAKHSSASSI, A., KENGNE, E., SEMMAOUI, H., ET AL. Investigation of nonlinear temperature distribution in biological tissues by using bioheat transfer equation of pennes' type. *Natural Science 2*, 03 (2010), 131.

[70] LARSSON, S., AND THOMÉE, V. *Partial differential equations with numerical methods*, vol. 45. Springer, 2003.

[71] LIU, J., CHEN, X., AND XU, L. X. New thermal wave aspects on burn evaluation of skin subjected to instantaneous heating. *IEEE transactions on biomedical engineering 46*, 4 (1999), 420–428.

[72] LUITEL, K. Bessel function for temperature distribution in cylindrical human body, 2013.

[73] LUITEL, K. Mathematical model for temperature distribution in cylindrical human body. In *2017 2nd International Conference on Man and Machine Interfacing (MAMI)* (2017), IEEE, pp. 1–5.

[74] LUITEL, K., GURUNG, D. B., KHANAL, H., AND UPRETY, K. N. Role of clothing insulation for thermal comfort: a numerical study using bio-heat transfer model. *Journal of Mathematics and Statistics 16*, 1 (2020), 224–232.

[75] LUITEL, K., GURUNG, D. B., KHANAL, H., AND UPRETY, K. N. Bioheat transfer equation with protective layer. *Mathematical Problems in Engineering 2021* (2021).

[76] LUITEL, K., GURUNG, D. B., KHANAL, H., AND UPRETY, K. N. Stability and convergence of implicit finite difference scheme for bioheat transfer equation

with clothing effect in human thermal comfort. *Structural Intregrity and Life, Special Issue 21* (2021), 23–28.

[77] LUITEL, K., GURUNG, D. B., AND UPRETY, K. N. Effect of various parameters for temperature distribution in human body: an analytical approach. *Advances in Science, Technology and Engineering Systems Journal, Special issue on Recent Advances in Engineering Systems Journal 3*, 5 (2018), 421–426.

[78] LUITEL, K., KHANAL, H., UPRETY, K. N., ET AL. Numerical study of transient bio-heat transfer model with heat transfer coefficient and conduction effect in cylindrical living tissue. *The Nepali Mathematical Sciences Report 36*, 1-2 (2019), 17–26.

[79] LV, Y.-G., DENG, Z.-S., AND LIU, J. 3-d numerical study on the induced heating effects of embedded micro/nanoparticles on human body subject to external medical electromagnetic field. *IEEE transactions on nanobioscience 4*, 4 (2005), 284–294.

[80] LYRA, P., LIMA, R., DE CARVALHO, D., AND DA SILVA, G. An axisymmetric finite volume formulation for the solution of heat conduction problems using unstructured meshes. *Journal of the Brazilian Society of Mechanical Sciences and Engineering 27* (2005), 407–414.

[81] MAZUMDER, S. *Numerical methods for partial differential equations: finite difference and finite volume methods.* Academic Press, 2015.

[82] NEVES, S., CAMPOS, J., AND MAYOR, T. Effects of clothing and fibres properties on the heat and mass transport, for different body heat/sweat releases. *Applied Thermal Engineering 117* (2017), 109–121.

[83] NOUR, M., BOUGATAYA, M., KENGNE, E., EL GUEMHIOUI, K., AND LAKHSSASSI, A. Framework of the bio-heat transfer for laser/cancer treatment. *International Journal of Pharma Medicine and Biological Sciences 5*, 4 (2016), 194–200.

[84] OF HEATING, A. S., REFRIGERATING, ENGINEERS, A.-C., AND INSTITUTE, A. N. S. *Thermal environmental conditions for human occupancy*, vol. 55. American Society of Heating, Refrigerating and Air-Conditioning Engineers, 2004.

[85] OĞULATA, R. T. The effect of thermal insulation of clothing on human thermal comfort. *Fibres & Textiles in Eastern Europe 15*, 2 (2007), 61.

[86] ÖZIŞIK, M. N., ORLANDE, H. R., COLACO, M. J., AND COTTA, R. M. *Finite difference methods in heat transfer.* CRC press, 2017.

[87] PARDASANI, K., AND SHAKYA, M. A two dimensional infinite element model to study temperature distribution in human dermal regions due to tumors. *Journal of Mathematics and statistics 1*, 3 (2005), 184–188.

[88] PARSONS, K. International standards for the assessment of the risk of thermal strain on clothed workers in hot environments. *Annals of Occupational Hygiene 43*, 5 (1999), 297–308.

[89] PARSONS, K., HAVENITH, G., HOLMÉR, I., NILSSON, H., AND MALCHAIRE, J. The effects of wind and human movement on the heat and vapour transfer properties of clothing. *Annals of Occupational Hygiene 43*, 5 (1999), 347–352.

[90] PATANKAR, S. V. *Numerical heat transfer and fluid flow.* CRC press, 2018.

[91] PATTERSON, J. Heat and matter transfer in body organs with special reference to skin blood flow and localised hyperthermia.

[92] PEAVY, B. A heat transfer note on temperature dependent thermal conductivity. *Journal of Thermal Insulation and Building Envelopes 20*, 1 (1996), 76–90.

[93] PENNES, H. H. Analysis of tissue and arterial blood temperatures in the resting human forearm. *Journal of applied physiology 1*, 2 (1948), 93–122.

[94] PERL, W. Heat and matter distribution in body tissues and the determination of tissue blood flow by local clearance methods. *Journal of Theoretical Biology 2*, 3 (1962), 201–235.

[95] RAGAB, M., ABOUELREGAL, A. E., ALSHAIBI, H. F., AND MANSOURI, R. A. Heat transfer in biological spherical tissues during hyperthermia of magnetoma. *Biology 10*, 12 (2021), 1259.

[96] RASHKOVSKA, A., TROBEC, R., DEPOLLI, M., AND KOSEC, G. 3-d numerical simulation of heat transfer in biomedical applications. In *Heat transfer phenomena and applications.* InTech, 2012, pp. 99–151.

[97] ROHSENOW, W. M., HARTNETT, J. P., CHO, Y. I., ET AL. *Handbook of heat transfer*, vol. 3. McGraw-Hill New York, 1998.

[98] ROHSENOW, W. M., HARTNETT, J. P., AND GANIC, E. N. Handbook of heat transfer fundamentals.

[99] RUBINSKY, B., PEGG, D., AND CALNE, R. Y. A mathematical model for the freezing process in biological tissue. *Proceedings of the Royal Society of London. Series B. Biological Sciences 234*, 1276 (1988), 343–358.

[100] SAXENA, V., AND ARYA, D. Steady state heat distribution in epidermis and subdermal tissue. *J. Theor. Biolo 102* (1983), 227–286.

[101] SAXENA, V., AND BINDRA, J. Temperature distribution in dermal regions of human body under variable physiological and atmospheric conditions. *Proc. Nat. Acad. Sci. India. A 56* (1986), 219–225.

[102] SELMI, M., BIN DUKHYIL, A. A., AND BELMABROUK, H. Numerical analysis of human cancer therapy using microwave ablation. *Applied Sciences 10*, 1 (2020), 211.

[103] SHARMA, S. K., AND KUMAR, D. A study on non-linear dpl model for describing heat transfer in skin tissue during hyperthermia treatment. *Entropy 22*, 4 (2020), 481.

[104] SHEN, H., YOKOYAMA, A., AND SUKIGARA, S. Modeling of heterogeneous heat transfer in fabrics. *Textile Research Journal 88*, 10 (2018), 1164–1172.

[105] SHIH, T.-C., KOU, H.-S., LIAUH, C.-T., AND LIN, W.-L. Thermal models of bioheat transfer equations in living tissue and thermal dose equivalence due to hyperthermia. *Biomedical Engineering: Applications, Basis and Communications 14*, 02 (2002), 86–96.

[106] SHRESTHA, D. C., ACHARYA, S., ET AL. Mathematical modeling on thermoregulation in sarcopenia. In *Neural Networks, Machine Learning, and Image Processing*. CRC Press, 2022, pp. 3–19.

[107] SHRESTHA, D. C., ACHARYA, S., AND GURUNG, D. B. A finite element approach to evaluate thermoregulation in the human body due to the effects of sweat evaporation during cooking, cleaning, and walking. *Mathematical Problems in Engineering 2021* (2021).

[108] Shrestha, D. C., Acharya, S., Gurung, D. B., et al. Modeling on metabolic rate and thermoregulation in three layered human skin during carpentering, swimming and marathon. *Applied Mathematics 11*, 08 (2020), 753.

[109] Shrestha, S., Gokul, K., and Gurung, D. B. Transient bioheat equation in breast tissue: Effect of tumor size and location. *Journal of Advances in Applied Mathematics 5*, 1 (2020).

[110] Slavinec, M., Repnik, R., and Klemencic, E. The impact of moisture on thermal conductivity of fabrics. *Anali Pazu 6*, 1/2 (2016), 8–12.

[111] Szasz, A., Szasz, O., and Szasz, N. Physical background and technical realizations of hyperthermia. In *Hyperthermia in cancer treatment: A primer.* Springer, 2006, pp. 27–59.

[112] Valvano, J. W. Bioheat transfer. *Encyclopedia of Medical Devices and Instrumentation 1* (2006), 188–97.

[113] van Hoof, J., Kort, H., and Hensen, J. Thermal comfort and hvac design for people with dementia. In *Proceedings of the International Federation on Ageing 9th global conference on aging. Montreal, Canada* (2008), pp. 1–18.

[114] Voelker, C., Hoffmann, S., Kornadt, O., Arens, E., Zhang, H., and Huizenga, C. Heat and moisture transfer through clothing.

[115] Wang, F., Ji, E., Zhou, X., and Wang, S. Empirical equations for intrinsic and effective evaporative resistances of multilayer clothing ensembles. *Ind Text 61* (2010), 176–180.

[116] Wang, S. *Analysis of boundary and interface closures for finite difference methods for the wave equation.* PhD thesis, Uppsala University, 2015.

[117] Weinbaum, S., and Jiji, L. A new simplified bioheat equation for the effect of blood flow on local average tissue temperature.

[118] Williams, J. T. *Textiles for cold weather apparel.* Elsevier, 2009.

[119] Wissler, E. H. Pennes' 1948 paper revisited. *Journal of applied physiology 85*, 1 (1998), 35–41.

[120] Wulff, W. The energy conservation equation for living tissue. *IEEE transactions on biomedical engineering*, 6 (1974), 494–495.

[121] Wust, P., Stein, U., and Ghadjar, P. Non-thermal membrane effects of electromagnetic fields and therapeutic applications in oncology. *International Journal of Hyperthermia 38*, 1 (2021), 715–731.

[122] Yu, H. *A high-order finite difference method for solving bioheat transfer equations in three-dimensional triple-layered skin structure.* Louisiana Tech University, 2004.

[123] Yue, K., Zhang, X., and Yu, F. An analytic solution of one-dimensional steady-state pennes' bioheat transfer equation in cylindrical coordinates. *Journal of thermal Science 13*, 3 (2004), 255–258.

[124] Zhao, J. J., Zhang, J., Kang, N., and Yang, F. A two level finite difference scheme for one dimensional pennes' bioheat equation. *Applied Mathematics and Computation 171*, 1 (2005), 320–331.

[125] Zhu, L. Heat transfer applications in biological systems. *Biomedical engineering & design handbook 1* (2009), 2–33.

[126] Zomordikhani, Z., Attar, M., Jahangiri, A., and Barati, F. Analysis of nonlinear bioheat transfer equation in magnetic fluid hyperthermia. *Journal of Mechanical Science and Technology 34*, 9 (2020), 3911–3918.

Appendix

Publications

1. Luitel K., Gurung D.B, Khanal H., and Uprety K.N., Stability and Convergence of Implicit Finite Difference Scheme for Bioheat Transfer Equation with Clothing Effect in Human Thermal Comfort, *Structural Integrity and Life*, Vol.21, Special Issue (2021), pp.21−28. http://divk.inovacionicentar.rs/ivk/ivk21 /023-IVKSpecialIssue-2021-KL-DBG-HK- KNU.pdf

2. Luitel K.,Gurung D.B, Khanal H., and Uprety K.N., Bio Heat Transfer Equation with Protective Layer, *Mathematical Problems in Engineering*, Hindawi, Vol. 2021, pp. 1-12, 2021, https://doi.org/10.1155/2021/6639550

3. Luitel K.,Gurung D.B, Khanal H., and Uprety K.N., Role of Clothing Insulation for Thermal Comfort: A Numerical Study Using Bio-Heat Transfer Model", *Journal of Mathematics and Statistics*, Vol.16, pp.224-232, 2020. https://thescipub.com/jmss, DOI:10.3844/jmssp.2020.224.232

4. Luitel K.,Gurung D.B, Khanal H., and Uprety K.N., Numerical Study of Transient Heat Transfer Model with Heat Transfer Coefficient and Conduction Effect in Cylindrical Living Tissue", *The Nepali Mathematical S Sciences Report*, Vol. 36, No. 1 & 2, pp.17-26, 2019. https://doi.org/10.3126/nmsr.v36i1-2.29967

5. Luitel K.,Gurung D.B, and Uprety K.N., Effect of Various Parameters for Temperature Distribution in Human Body: An Analytic Approach, *Special Issue on Recent Advances in Engineering System Journal*, Vol. 3, No.5, pp. 421–426,2018. www.astesj.com, DOI: 10.25046/aj030548

Paper Presentation

1. Luitel K., Gurung D.B, Khanal H., and Uprety K.N., "Axisymmetric Bioheat Transfer Model in Clothing System for Sweating and Metabolic Effect During Physical Exercise", National Conference on Mathematics and its Applications (NCMA-2022) organized by *Nepal Mathematical Society (NMS)* on June 11-13, 2022, Illam, Nepal.

2. Luitel K., Gurung D.B, Khanal H., and Uprety K.N., "Application of Bio Heat equation in Human Thermal Comfort with and without Clothing", International

Conference on Analysis and its Applications (ICAA_NEPAL _2021) organized by *Nepal Mathematical Society (NMS) in collaboration with TU, KU, SAU, NSU, and ANMA* on April 9-11, 2021.

3. Luitel K., Gurung D.B, Khanal H., and Uprety K.N., "Bioheat equation and Human Thermal Comfort", a talk in the occasion of International Day of Mathematics (πDay) organized by *Nepal Mathematical Society (NMS)* on 14 March 2021.

4. Luitel K., Gurung D.B, Khanal H., and Uprety K.N., "Stability and Convergence of Implicit Finite Difference Scheme for Bioheat Transfer Equation with Clothing Effect in Human Thermal Comfort", 2nd International Conference on Mathematical Modeling, Computational Intelligence Techniques and Renewable Energy (MMCITRE2021), *Pandit Deendayal Petroleum University*, Raisan-382007, Gandhinagar, India 06- 08 February 2021. (Paper ID. 032/MM-CITRE2021).

5. Luitel K., Gurung D.B, Khanal H., and Uprety K.N., "Mathematical Study of The Role of Clothing Insulation and Efficiency factor in Human Body with Protective Clothing System", a talk in the WoNiMS day Celebration and Empowering Women in Mathematics, organized by *Women of Neal in Mathematical Science (WoNimS)*, December 29, 2019, Nova Collage, Kathmandu, Nepal.

6. Luitel K., Gurung D.B, Khanal H., and Uprety K.N., "The Study of Numerical Method for Transient Heat Transfer in Cylindrical Living Tissue", 39th Southeastern Atlantic Regional Conference on Differential Equation (SEARCDE),organized by *Department of Mathematics, Embry-Riddle Aeronoutical University*, October 26 - 27, 2019, Daytona Beach, Florida, USA.

7. Luitel K., Gurung D.B, Khanal H., and Uprety K.N., "Numerical Study of Heat Transfer in Human Body with Protective Layer", 2nd International Conference on Application of Mathematics to non-Linear Sciences (AMNS-2019), organized by *Association of Nealise Mathematician in America (ANMA)*, June 27- 30, Pokhara, Nepal.

8. Luitel K., Gurung D.B, Khanal H., and Uprety K.N., "Finite Difference Approach to Study the Heat Transfer in Human Body with Clothes", *Indian Women and Mathematics* Annual Conference (IWM-2019), June 10-12, 2019, IIT, Bombay, India.

9. Luitel K., Gurung D.B, Khanal H., and Uprety K.N., "Analytical Study of the Effect of Ambient Temperature and Metabolism for Temperature Distribution on Cylindrical Living Tissue during Perspiration", National Conference on Mathematics and its Application, organized by *Nepal Mathematical Society (NMS)*, Butwal, Nepal, January 12 - 15, 2019.

10. Luitel K., Gurung D.B, Khanal H., and Uprety K.N., "Temperature Distribution on Cylindrical Living Tissue due to Perspiration," 2nd International Conference on Advances in Computational Mathematics (ICACM- 2018) jointly organized by *Central Department of Mathematics, Tribhuvan University (TU) Nepal and South Asian University (SAU)*, December 23- 24, 2018, Kathmandu, Nepal.

11. Luitel K., Gurung D.B, Khanal H., and Uprety K.N., "Sensible and Insensible Perspiration for Temperature Distribution in Cylindrical Living Tissue", International Conference on New Frontiers in Mathematics and Symposia on I-function and its Applications and Mathematics in Data Science, jointly organized by *School of Mathematics and Allied Sciences (ICNFM-SIAMDS-2018)*, December 11 – 13, 2018, Jiwaji University, Gwalior, India.

Poster Presentation

1. Luitel K., Gurung D.B, Khanal H., and Uprety K.N., "Mathematical Model for Bioheat Transfer with Protective Layer", *International Conference-Kathmandu Humboldkolleg 2022: Interdisciplinary Collaboration for Strengthening Science and Culture*, October 16-19, 2022, Kathmandu, Nepal

2. "HIV Within-Host Dynamic Incorporating Cell to Cell Virus Transmission", a project work in group on CIMPA Summer School in Mathematical Biology, *presented in the poster session on 2nd International Conference on Application of Mathematics to non-Linear Sciences (AMNS-2019)*, a group work, June 27-30, 2019, Pokhara, Nepal.

Participations in Conferences/Workshops

1. "CIMPA Summer School in Mathematical Biology", organized by *Association of Nepali Mathematicians in America (ANMA)*, June 17-26, 2019, Tribhuvan University, Nepal.

2. "Summer School on Mathematical Modeling and Scientific Computing with Python (SSMMSC- 2019)", June 03-07, 2019, *Kathmandu University,* Nepal.

3. "CIMPA-Nepal Research School on Aspects of Dynamical System", Organized by *Central Department of Mathematics, Tribhuvan University*, Kathmandu, Oct. 25 – Nov. 6, 2018.

4. "The Seminar-Workshop on Graph Theory and Optimization with Application in Industry and Society (Linear, Integer and Multi-criteria Optimization)", Organized by *Department of Mathematics University of Kaiserslautern, Germany, Central Department of Mathematics, Institute of Science and Technology, TU, Nepal, Department of Mathematics and Statistics Mindanao State University-Iligan Institute of Technology, The Philippines in collaboration with The German Academic Exchange Service (DAAD)*, March 12- 23, 2018.

Participations in Virtual Conferences/Workshops

1. "The International Congress of Mathematicians 2022 (ICM 2022)", *International Mathematical Union (IMU)*, fully virtual event, July 6–14 2022.

2. " World Meeting for Women in Mathematics (WM^2)" online, *Commettee for women in Mathematics (CWM)*, July 1-2 2022.

3. "Lecture Series in Mathematical Research" organized by *Association of Bangladeshi Women in Mathematics (ABWM)*, October 2, 2021.

4. One day National Seminar on Applications of FEM in Sciences and Engineering organized by the *Department of Mathematics, IISHLS, Indus University*, February 24, 2021.

5. "International E-Conference on "Recent Advances in Biomathematics" organized by *Bangladesh Society for Mathematical Biology (BSMB)*, December 18 – 19, 2020.

6. "One Week Online Short-term Course on "Computational Methods in Engineering Science" Organized by *Department of Mathematics, Govt. Women Engineering College, Ajmer and Department of Chemical Engineering, National Institute of Technology Jalandhar, Punjab*, October 24 –28, 2020.

7. The Webinar on "Applications of Nature Inspired Optimization Technique for Solving Real Life Problems" Conducted by *Department of Mathematics, KPI Institute of Engineering and Technology*, October 8, 2020.

8. Talk program on topic "Design and development of Intelligent Diagnostic System" organized by *Nepal Mathematical Society, Chapter-2, Nepal*, August 20, 2020.

9. Two-day international webinar on "Recent Advances in Mathematics & Covid-19" organized by the *Departments of Mathematics and Statistics & IQAC, St. Joseph's College for Women(A), Visakhapatnam, Andhra Pradesh in association with UASMS & SMSMS* , June 15- 16, 2020.
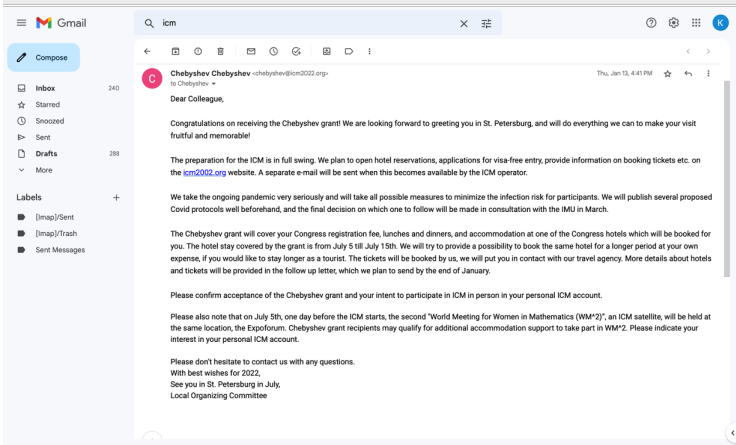
Research Article

Bioheat Transfer Equation with Protective Layer

Kabita Luitel [ID],[1] Dil Bahadur Gurung,[2] Harihar Khanal,[3] and Kedar Nath Uprety[4]

[1]*Department of Mathematics, Bhaktapur Multiple Campus, Bhaktapur, Nepal*
[2]*Department of Mathematics, Kathmandu University, Kavre, Dhulikhel, Nepal*
[3]*Department of Mathematics, Embry-Riddle Aeronautical University, Daytona Beach, FL, USA*
[4]*Central Department of Mathematics, Tribhuvan University, Kritipur, Nepal*

Correspondence should be addressed to Kabita Luitel; kabi123luitel@gmail.com

The human thermal comfort is the state of mind, which is affected not only by the physical and body's internal physiological phenomena but also by the clothing properties such as thermal resistance of clothing, clothing insulation, clothing area factor, air insulation, and relative humidity. In this work, we extend the one-dimensional Pennes' bioheat transfer equation by adding the protective clothing layer. The transient temperature profile with the clothing layer at the different time steps has been carried out using a fully implicit Finite Difference (FD) Scheme with interface condition between body and clothes. Numerically computed results are bound to agree that the clothing insulation and air insulation provide better comfort and keep the body at the thermal equilibrium position. The graphical representation of the results also verifies the effectiveness and utility of the proposed model.

1. Introduction

The study of thermal comfort in the complex vascular geometry of the human body with a protective clothing system is not only the subjective domain but also the physiological factors inside the body. According to the American Society of Heating, Refrigerating, and Air Conditioning Engineers (ASHRAE), thermal comfort is the state of the mind when one can feel and express the satisfaction with the thermal environment [1]. Thermoregulation is the process of controlling the internal body temperature through the hypothalamus heat production and heat loss center. The body also uses other processes of thermodynamical systems that constantly produce energy by metabolic activity together with dilating or constricting blood vessels, shivering, and sweating [2, 3].

The presence of clothes, on the other hand, plays a vital role for maintaining the thermal comfort at the equilibrium condition of heat production and heat loss by the body. Clothing, the interface between the skin surface and the environment, works as an insulator and also transports the heat from the body to the outer environment around us. The key factors affecting thermal comfort are categorized as

(1) Personal factors

(2) Environmental factors

1.1. The Personal Factors. Metabolism, determined by age, sex, health, etc., is one of the human personal factors which makes a difference in thermal comfort. Besides, another major factor which affects thermal comfort is clothing. A significant difference in thermal comfort can be caused by small changes in clothing layers. In the winter season, wearing a sweater and socks makes better comfort, whereas in summer, wearing light clothes makes better comfort in the workplace.

1.2. Environmental Factors. Air temperature, moving air, radiant temperature, and relative humidity are the environmental factors that help to maintain thermal comfort by keeping the room comfortable. The radiation heat flux, on the other hand, penetrates a certain depth passing entirely through the fabric, depending on the fabric structure and radiative wavelength. In contrast, the convection portion of the heat source could reach the fabric surface only [4].

Usually, heat transfer in the body through the garment occurs from heat conduction and heat radiation; then, the temperature rises and transfers into the air gap. Suitable clothing along with these environmental factors, therefore, maintains better comfort at home and workplace (business, office, study room, etc.).

2. Role of Clothing

2.1. Thermal Resistance and Clothing Insulation. The ratio of temperature difference between two faces of material to the rate of heat flow per unit area is defined as thermal resistance. In the study of thermal insulation of clothing, thermal resistance is a very important parameter defined as the function of thickness and thermal conductivity of clothes. Thermal Resistance R_{th} m^2 · (°C/W) is given by [5]

$$R_{th} = \frac{\Delta T}{q} = \frac{L}{k}, \tag{1}$$

where L is the thickness of cloth (m), ΔT is the temperature difference (°C), and q is the heat flow rate (W/m^2). Though the heat transfer in the clothed body consists of conduction and radiation, the primary determinant of the insulation is the thickness of clothes on which the insulation is very much dependent. The limbs of human body with insulation parameters can be seen in Figure 1.

Thermal insulation, together with the air gap, does not only provides comfort at the skin surface and body from a cold environment but also protects from burn injuries. While sitting by the fire, the air gap provides thermal insulation that limits heat transfer to skin and protects the skin from excessive heat.

2.1.1. Clo Unit. Clo unit is the measure of thermal resistance and includes the insulation provided by any layer of trapped air between skin and the insulation value of clothing itself. 1 Clo is defined as the insulation of the clothing system that requires maintaining a sitting-resting average male comfortable in a normally ventilated room. Clo is the thermal insulation of overall clothing worn by a person. It has 0.1 m/s air velocity at air temperature 21°C and relative humidity less than 50%. Among the total heat produced by the metabolic reaction, 24% heat is lost through evaporation and respiration. As 1 met = 50 kcal/m^{2}h, the evaporative and respiratory heat loss = 1 met × 24% = 50 × 0.24 = 12 kcal/m^{2}h. Remaining 38 kcal/m^{2}h is transmitted through the clothing system by conduction, convection, and radiation. The comfortable skin temperature is 33°C, so the total insulation of clothing and air layer $(I_T = I_{cl} + I_a)$ is given by [8]

$$I = \frac{33 - 21}{38} = 0.32,$$

$$I_a = 0.14 \text{m}^2 \cdot {}^{\circ}\text{C (h/kcal)},$$

$$(I_{cl} = 0.32 - 0.14)\text{m}^2 \cdot {}^{\circ}\text{C (h/kcal)} = 0.18 \text{ m}^2 \cdot {}^{\circ}\text{C (h/kcal)}, \tag{2}$$

where I_a is the insulation of air and I_{cl} is the insulation cloth.
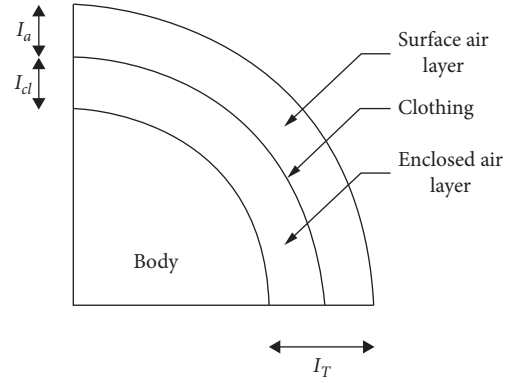

Figure 1: A cylindrical model with clothing and air insulation [6, 7].

Since 1 kcal/h = 1.163 watt (W), so 1 Clo unit is defined as

$$0.18 \text{ m}^2 \cdot {}^{\circ}\text{C} = \frac{0.18}{1.163} \equiv 0.155 \text{ m}^2 \cdot ({}^{\circ}\text{C/W}). \tag{3}$$

2.2. Convective and Radiative Heat Transfer. Clothing works as the mediator of heat exchange through convection as well as radiation. The standard measurement condition in ISO 9920, four different manikins in three different laboratories, were used and determined the male and female clothing thermal insulation values of 52 nonwestern clothing configuration [9]. If h_c (m^2 · (°C/W)) and h_r (m^2 · (°C/W)) are the heat exchange due to convection radiation, respectively, then the convective and radiative heat exchange is defined in [7, 9] by

$$h_c + h_r = \frac{\Delta T}{I_{cl}}. \tag{4}$$

2.3. Clothing Area Factor. The dimensionless parameter, clothing area factor f_{cl}, is the ratio between the surface area of clothed human body A_b (m^2) and the surface area of nude human body A_b (m^2) which is given by

$$f_{cl} = \frac{A_{cl}}{A_b}. \tag{5}$$

The prediction equation for clothing area factor f_{cl}, based on western clothing and listed in ISO Standard 9920-2009 (ISO 2009), can also be found in various publications. The equation for f_{cl} is given [1, 9, 10] as

$$\text{In Clo, } f_{cl} = 1 + 0.31 I_{cl},$$
$$\text{In } (\text{m}^2 \cdot ({}^{\circ}\text{C/W})), f_{cl} = 1 + 1.97 I_{cl}. \tag{6}$$

2.4. Clothing Efficiency Factor. The clothing efficiency factor(dimensionless) depends upon the air insulation I_{cl} (m^2 · (°C/W)) and the thermal insulation of overall clothing, not only the particular garment but also the entire garment, including tops, bottoms, innerwear, and everything

(including even socks and gloves). The total clothing insulation ($I_T = I_{cl} = \sum_i I_{cli}$) (where I_{cli} is the insulation of each fabric item) for a person in summer and winter is given in Table 1. So, the clothing efficiency factor F_{cl} (dimensionless) is provided by [4, 7, 8]

$$F_{cl} = \frac{I_a}{I_{cl} + (I_a/f_{cl})}. \tag{7}$$

Pennes [11], a famous researcher, established a bioheat transfer model in 1948 based on experimental observation incorporating the blood perfusion term for heat flow within tissue. Various methods related to the biological model using Pennes' equation is tackled by many researchers one after another. Zhao et al. [12] developed a two-level finite difference scheme for one-dimensional Pennes' bioheat equation and established the stability and convergence condition taking only one initial condition. Gurung and Saxena [13], Luitel et al. [2, 14, 15], Agrawal et al. [3], Acharya et al. [16], and Parsons [17] used Pennes' model for steady-state and unsteady-state temperature distribution within the human dermal part using finite element and finite difference methods.

So far as the study of clothing is concerned, a number of research studies [1, 4, 9, 10, 18] have turned significant stones in regards of thermal comfort in the human body under the protective clothing by taking the dry and evaporative heat loss with the significant clothing area factor within the different human manikins only by the experimental method taking the equation only in the clothing part. Havenith et al. [9] published a database of static clothing thermal insulation and vapor permeability values' nonwestern ensembles for ASHARE standard 55, ISO-7730 (International Organization for Standardization), and ISO-9920.

Gurung and Saxena [13] studied the transient temperature distribution in the human dermal part with a protective layer at low atmospheric temperature, considering the bioheat equation to observe only the effect of thickness

and mass of the protective layer. So, the mathematical study of the bioheat equation along with the impact of clothing insulation, air insulation, and clothing area factor is still lacking and is one of our research interests.

On the contrary, in the cold environment, the cold receptor becomes active and vasoconstriction of blood vessel takes place. Shivering of muscle also appears in this case. If the body core temperature goes down around 30°C, then one goes in the unconscious condition, and, if the body temperature goes down up to 27°C, his/her heart beating stops. Similarly, in the hot climatic condition, the hot receptor becomes active and vasodilation takes place and sweating occurs. The increment in body temperature up to 42°C causes hyperthermia [14–16, 19]. To overcome all these unusual conditions, the human body needs proper well-designed protective clothing because only the internal physiological conditions cannot cope up with such extreme cold and hot climatic condition without wearing sufficient clothing in winter and putting on only light clothing in summer. So, this study, heat transfer in the human body with protective clothing, is indispensable for proper management of clothing to keep the body highly comfortable condition.

The heat transfer in the human body with a protective clothing system is a heterogeneous phenomenon. The analytical solution of such material is not an easy task. So, the study of the numerical approach for getting an approximation solution is essential for this purpose. The recent paper aims to extend one-dimensional Pennes' bioheat equation with unconditionally stable state and convergence which incorporates various personal and environmental factors on the one hand and protective clothing on the other hand. The graphical representation of convergence for the FD scheme will be shown for the use of the model.

3. Mathematical Formulation of the Model

The bioheat transfer equation with the protective clothing system is given by

$$\rho c \frac{\partial T}{\partial t} = k\left(\frac{\partial^2 T}{\partial x^2} + \frac{\partial^2 T}{\partial y^2} + \frac{\partial^2 T}{\partial z^2}\right) + w_b c_b (T_a - T) + q_m + P(T_{sk} - T_{cl}), \tag{8}$$

where ρ is tissue density (kg/m³), c is tissue specific heat (J/kg°C), k is thermal conductivity (W/m°C), W_b is blood perfusion rate (kg/m²·s), c_b is blood specific heat (J/kg°C), T_a is arterial blood temperature (°C), q_m is metabolic heat generation (W/m³), and the symbol P in the last term is given by

$$P = \frac{k_{cl}}{A_{cl}}\left(\frac{W}{m^3 \cdot °C}\right), \tag{9}$$

where $A_{cl} = A_b f_{cl}$, k_{cl} is thermal conductivity of clothes (W/m·°C), T_{sk} is the skin temperature (°C), and (T_{cl}) is the cloth temperature (°C).

The bioheat equation (8) is the extension of the equation suggested by Pennes' in 1948. The left-hand side is the total heat storage; the first, second, and third terms of right-hand side are diffusion, perfusion, and metabolic heat generation. respectively. The extra term $P(T_{sk} - T_{cl})$, with clothing parameters, is the heat transfer from the skin to clothing layer.

One-dimensional unsteady-state temperature profiles in the cylindrical shape of the human body with the clothing system and the bioheat equation (8) in radial direction are performed and given below:

TABLE 1: Total insulation of clothes in Clo unit 8, 10.

Cloth item (summer)	(I_{cli}) Clo value	Cloth item (winter)	(I_{cli}) Clo value
Half shirt	0.19	Full shirt	0.28
Underwear	0.04	Underwear	0.04
Pants	0.11	Pants/trousers	0.24
Socks	0.02	Socks	0.03
Shoes	0.02	Shoes	0.04
—	—	Suit jacket	0.48
Total	0.38	Total	1.11

$$\rho c \frac{\partial T}{\partial t} = k \left(\frac{\partial^2 T}{\partial r^2} + \frac{1}{r} \frac{\partial T}{\partial r} \right) + w_b c_b (T_a - T) + q_m + P (T_{sk} - T_{cl}), \tag{10}$$

where r is radial distance from the center of core towards skin surface (m).

The study of heat transfer in such a nonhomogeneous phenomenon, the human body, and the protective clothing system is really cumbrous. So, we decouple equation (10) first and then combine by using the interface condition between the body and clothing part.

3.1. Heat Transfer Equation for Body.
As $P = 0$ in the body part so the bioheat equation for the body part is given by

$$\rho c \frac{\partial T_t}{\partial t} = k_t \left(\frac{\partial^2 T_t}{\partial r^2} + \frac{1}{r} \frac{\partial T_t}{\partial r} \right) + w_b c_b (T_a - T_t) + q_m. \tag{11}$$

3.2. Heat Transfer Equation for Clothing.
The heat equation for clothing with $W_b = 0$ and $q_m = 0$ is therefore given by

$$\rho c \frac{\partial T_{cl}}{\partial t} = k_{cl} \left(\frac{\partial^2 T_{cl}}{\partial r^2} + \frac{1}{r} \frac{\partial T_{cl}}{\partial r} \right) + P (T_{sk} - T_{cl}). \tag{12}$$

3.3. Boundary Conditions.
The inner boundary condition of the living tissue is considered uniform and taken as

$$\text{at } r = 0, \quad \frac{\partial T_t}{\partial r} = 0. \tag{13}$$

There is continuous heat flux between clothing surface and atmospheric environment as the outer surface of clothes is exposed to external environment [7, 17]. In this case, heat loss from the body via clothes is caused by convection and radiation. The Robin boundary condition due to convection condition is guided by Newton's law of cooling, and the term due to radiation is guided by the Stefan Boltzmann law and is given as

$$\text{at } r = R, \quad -k_{cl} \frac{\partial T_{cl}}{\partial r} = F_{cl} \left[h_c (T_{cl} - T_\infty) + \epsilon \sigma (T_{cl}^4 - T_\infty^4) \right], \tag{14}$$

where F_{cl} is the effective clothing area factor given in equation (14), h_c is the heat transfer coefficient due to convection, ϵ, the emissivity that lies between 0 to 1, $\sigma = 5.67 \times 10^{-8}$ is Stefan Boltzmann constant, and T_∞ is the atmospheric temperature.

The bioheat problem becomes nonlinear when the nonlinear radiation term in the boundary condition appears. In this case, it becomes difficult to formulate. To avoid such complexity, we apply the simplified form of boundary condition as

$$\begin{aligned} -k_{cl} \frac{\partial T_{cl}}{\partial r} &= F_{cl} \left[h_c (T_{cl} - T_\infty) + \epsilon \sigma (T_{cl} - T_\infty)(T_{cl} + T_\infty)(T_{cl}^2 - T_\infty^2) \right], \\ &= F_{cl} (T_{cl} - T_\infty) \left[h_c + \epsilon \sigma (T_{cl} + T_\infty)(T_{cl}^2 - T_\infty^2) \right], \\ &= F_{cl} (h_c + h_r)(T_{cl} - T_\infty), \\ &= h_A (T_{cl} - T_\infty). \end{aligned} \tag{15}$$

3.4. Initial Condition.
For the time dependent boundary value problem, the initial condition is given by

$$T(r, 0) = T_0(r), \text{ where, } T = T(T_t, T_{cl}). \tag{16}$$

4. Solution of the Model

For the solution of model (10), we perform the following steps:

(1) Construction of the Finite Difference (FD) scheme for models (11) and (12)

(2) Getting solution of (11)

(3) Using the solution of (11) to get the solution of (12) and applying the interface and boundary conditions

(4) Representing the combined results in graph by computer algebraic software

4.1. Construction of FD Scheme.
One-dimensional form of cylindrical tissue for the body part is divided into N discrete points uniquely specified by spatial indices, $r_i = i\Delta r$, in the radial direction. The discretization of circular cross-section of peripheral human limb, where the temperature flow in axial direction is uniform, is shown in Figure 2.

In the time discretization, Δt is denoted by the discrete time step size, and the total time to evaluate the temperature is $t^n = n\Delta t$.

4.2. FD Scheme for the Nodes in Body Part.
We use FD scheme by writing equation (11) using implicit finite difference (central difference) scheme for right-hand terms and forward difference for left-hand term.

4.2.1. FD Scheme at Boundary $r = 0$ (Body Core).
The cylindrical thickness r is measured from body core, as shown in Figure 2. At the body core, both r and the heat flux $(\partial T_t/\partial r)$ are zero; then, $(1/r)(\partial T/\partial r)$ approaches to indeterminate form $(0/0)$ as $r \longrightarrow 0$.

The use of Hospital rule then gives

$$\frac{1}{r} \frac{\partial T_t}{\partial r}\Big|_{r=0} = \frac{(\partial/\partial r)(\partial T_t/\partial r)}{(\partial/\partial r)(r)}\Big|_{r=0} = \frac{\partial^2 T_t}{\partial r^2}\Big|_{r=0}. \tag{17}$$

Now, equation (11) becomes

$$\rho c \frac{\partial T_t}{\partial t} = 2D\left(\frac{\partial^2 T_t}{\partial r^2}\right) + M(T_a - T_t) + S, \tag{18}$$

$$E_0 T_0^{n+1} - 4\alpha T_1^{n+1} - F = T_0^n, \tag{19}$$

where $D = (k_t/\rho c)$, $\alpha = (D\Delta t/\Delta r^2)$, $M = (w_b c_b/\rho c)$, $S = (q_m/\rho c)$, and $F = \Delta t(MT_a + S)$.

As shown in Figure 2, we solve the problem in two phase body part and clothing part. For the body part, we take the interior nodes from $i = 1, 2, \ldots N - 1$, and the FD scheme of equation (11) is given by

$$D_i T_{i-1}^{n+1} + E_i T_i^{n+1} + B_i T_1^{n+1} - F = T_i^n, \tag{20}$$

where $D_i = (-\alpha + (\alpha/2i))$, $E_i = (1 + 2\alpha + M\Delta t)$, and $B_i = (-\alpha - (\alpha/2i))$.

The construction in (20) implies that FD schemes have a truncation error in the order $O(\Delta r^2 + \Delta t)$ for each interior point (t^n, r_i), $n \geq 1$, $0 < i < N$.

At $i = N$, the skin surface is the interface between body and clothes. So, the FD scheme at $i = N$ is

$$D_N T_{N-1}^{n+1} + E_N T_N^{n+1} + B_N T_{N+1}^{n+1} - F = T_N^n. \tag{21}$$

4.2.2. Interface Condition at $i = N$ (at Skin Surface).
The interface temperature between the skin surface and clothes at $i = N$. The right-most Dirichlet boundary at this point is

$$T_t|_{i=N} = T_{cl}|_{i=N} = T_{\text{int}}. \tag{22}$$

FD scheme, at $i = N$, is

$$D_N T_{N-1}^{n+1} + E_N T_N^{n+1} + B_N T_{\text{int}}^{n+1} - F = T_N^n. \tag{23}$$

This construction implies that FD schemes have an error in the order $O(\Delta r^2 + \Delta t)$ for the gride point (t^n, r_N), at $i = N$.

The system of equations (19), (20), and (23) can be written in the matrix form as

$$A_1 T_t^{n+1} = T_t^n + B_1, \tag{24}$$

where $T_t^n = [T_0^n, T_1^n, T_3^n, \ldots, T_N^n]'$.

A_1 is the corresponding tridiagonal matrix of order $(N + 1) \times (N + 1)$ and T_t^{n+1} and B_1 are of column vectors of $(N + 1) \times 1$. A_1 matrix is diagonally dominant since the absolute value of each leading diagonal element satisfies the relation:

$$|a_{jj}| \geq \sum_{i=0, i\neq j}^{N} |a_{ij}|. \tag{25}$$

4.3. FD Scheme for Clothing Part.
As we have mentioned above, the skin surface is the interface between the body and clothing part at $i = N$; the FD scheme for (12) yields

$$D_N T_{N-1}^{n+1} + E_N T_N^{n+1} + B_N T_{N+1}^{n+1} = T_N^n, \tag{26}$$

where $E_N = E_{N+1} = E_{N+2} = \cdots = E_R = (1 + 2\alpha + P_1)$.

4.3.1. Interface Condition at $i = N$ (between Skin and Cloth).
Before taking the interface temperature between skin surface and clothes, it is necessary to evaluate the interface thermal conductivity K. The nonhomogeneous material such as body and clothes which consists different physiological properties, has nonuniform thermal conductivity. Thus, the proper formulation for nonuniform K is highly desirable. The interface conductivity K is to assume a linear variation of K between two points N and $N + 1$ is given by [20]

$$K = f_N k_t + (1 - f_N)k_{cl}, \tag{27}$$

where f_N is the interpolation factor defined by $f_N = (\Delta r_c/\Delta r)$ and Δr_c is the mesh size in protective layer.

For the interface grid point N, we consider the control volume surrounding N is filled with the uniform conductivity k_t of body tissue, one around $N + 1$ with a conductivity k_{cl} of clothes. The good representation for a heat flux over the composite domain between N and $N + 1$ leads to
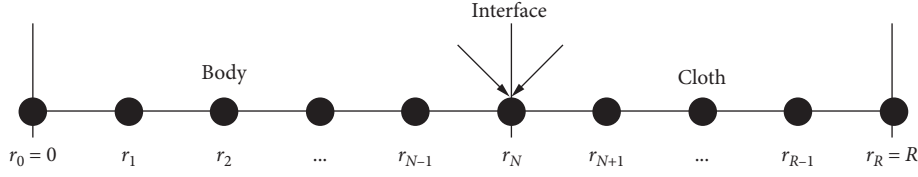
FIGURE 2: Discretization in radial direction with interface.

$$q_N = \frac{T_{N+1}^{n+1} - T_N^{n+1}}{((\Delta r/k_t) + (\Delta r_c/k_{cl}))}. \tag{28}$$

4.3.2. Interface Conditions at $i = N$ (Left Boundary for Cloth Part). The heat flux occurs at the skin surface, and the left most boundary of clothes at $i = N$ is given by

$$-k_t \frac{\partial T}{\partial r} = q_N. \tag{29}$$

FD formulation for (29):

$$\frac{T_{N+1}^{n+1} - T_{N-1}^{n+1}}{2\,\partial r} = -K\frac{T_{N+1}^{n+1} - T_N^{n+1}}{((\Delta r/k_t) + (\Delta r_c/k_{cl}))}, \tag{30}$$

$$T_{N-1}^{n+1} = T_{N+1}^{n+1} - 2R_c q_N.$$

Now, equation (26) with left boundary condition can be written as

$$D_N T_{N-1}^{n+1} + (2\alpha_1 - P_1)T_{N+1}^{n+1} - F_N = T_N^n, \tag{31}$$

where $F_N = 2D_N R_c q_N$.

FD scheme for each interior gride point (t^n, r_i), $n \geq 1$, $N < i < R$ in the clothing part with a truncation error of the order $O(\Delta r^2 + \Delta t)$ is given by

$$D_i T_{i-1}^{n+1} + E_i T_i^{n+1} + B_i T_1^{n+1} - F = T_i^n, \tag{32}$$

where $D_i = (-\alpha_1 + (\alpha_1/2i))$, $E_i = (1 + 2\alpha_1 + M\Delta t)$, $B_i = (-\alpha_1 - (\alpha_1/2i))$, and $\alpha_1 = (D_{cl}\Delta t/(\Delta r_c)^2)$.

4.3.3. Boundary Conditions at $i = R$ (at the Surface of the Cloth). The heat flux occurs at the outer surface of the right-most boundary of clothes at $i = R$ which is given by

$$-k_{cl}\frac{\partial T_{cl}}{\partial r_c} = h_A(T_{cl} - T_\infty), \tag{33}$$

$$T_{R+1}^{n+1} = T_{R-1}^{n+1} - 2h_A R_c(T_{cl} - T_\infty).$$

FD scheme at $i = R$ is now given by

$$(-2\alpha_1 - P_1)T_{R-1}^{n+1} + (E_R - 2B_R h_A R_c)T_R^{n+1} - F_R = T_R^n. \tag{34}$$

The system of equations (31), (32), and (34) can be written in the matrix form as

$$A_2 T_{cl}^{n+1} = T_{cl}^n + B_2, \tag{35}$$

where $T_{cl}^n = [T_N^n, T_{N+1}^n, T_{N+2}^n, \dots, T_{R-1}^n, T_R^n]'$.

A_2 is the corresponding tridiagonal matrix of order $(R - N) \times (R - N)$, and T_{cl}^{n+1} and B_2 are of column vectors of order $(R - N) \times 1$.

A_2 is diagonally dominant matrix since the absolute value of each leading diagonal element of A_2 satisfies the relation:

$$|a_{jj}| \geq \sum_{i=N, i\neq j}^{R} |a_{ij}|. \tag{36}$$

Since each matrices A_1 and A_2 are diagonally dominant, so A_1^{-1} and A_2^{-1} exist and systems (24) and (35) are separately solvable.

The constructed FD scheme (20) and (31) in our model has truncation error $\tau(\Delta r, \Delta t) = O(\Delta r^2 + \Delta t)$. So, as Δr, $\Delta t \longrightarrow 0$ as $\tau(\Delta r, \Delta t) \longrightarrow 0$ separately for body part $(0 \leq i \leq N)$ and clothes part $(N \leq i \leq R)$, hence, the model is consistent.

The notion of the second matrix norms of invertible matrices $\|A_1\|_2$, $\|A_2\|_2$ and their inverses $\|A_1^{-1}\|_2$, $\|A_2^{-1}\|_2$ together with Gregorian Theorem [12] imply the relation

$$\|E^{n+1}\|_2 \leq \|E^0\|_2 \tag{37}$$

where $E^{n+1} = \begin{cases} T_t^{(n+1)} - T_t^{*\,(n+1)}, \\ T_{cl}^{(n+1)} - T_{cl}^{*(n+1)}. \end{cases}$

$T_t^{*\,(n+1)}$ and $T_{cl}^{*(n+1)}$ are small perturb in $T_t^{(n+1)}$ and $T_{cl}^{(n+1)}$, respectively.

Then, by Lax–Richtmyer theorem, one can claim that the model is unconditionally stable with respect to initial data. Finally, the stability and consistent imply the convergence. Hence, the model is unconditionally convergent.

5. Numerical Results and Discussion

The numerical solution of heat transfer in human body with a protective clothing layer is obtained from the bioheat equation (10) by decoupling it into equations (11) and (12) and applying finite difference scheme separately. The temperature obtained from the system of (11) (skin surface) is used in equation (12) to calculate the temperature for clothes layer on the body. For the numerical experiment, the following parametric values in Tables 2 and 3 are chosen.

5.1. Graphical Representation. The effects of different parameters mentioned in Tables 1–3 have been investigated for heat transfer in a cylindrical-shaped clothed human body. Different mesh sizes are taken to demonstrate the validity and applicability of the developed numerical FD schemes (20) and (32). The tests of the combined solution of systems

TABLE 2: Thermophysical parameters related to the body part 15, 21.

Parameters	Symbols	Values	Units
Thermal conductivities	k_t	0.48	W/m°C
Blood specific heat	c_b	3850	J/kg°C
Blood density	ρ_b	1000	kg/m^3
Blood perfusion rate	W_b	3	kg/s·m^3
Metabolism	q_m	1085	W/m^3
Arterial temperature	T_a	37	°C
Thickness of tissue (domain)	N	0.03	M
Temperature at right boundary	T_b	24	°C

TABLE 3: Physical parameters related to clothing properties.

| Parameters	Symbols	Values	Units	References for the values
Thermal conductivities	k_{cl}	0.305	W/m°C	Abbas et al. [22]
Thickness of clothes	L_{cl}	0.0050	m	Gurung and Saxena [13]
Total thickness (tissue and cloth)	R	0.035	m	—
Density of clothes	ρ_{cl}	1550	kg/m^3	Holmer et al. [4]
Specific heat of clothes	c_{cl}	1340	J/kg°C	Holmer et al. [4]
Clothing insulation	I_{cl}	0.17	m$^2 \cdot$ (°C/W)	Holmer et al. [4], Havenith et al. [9]
Air insulation	I_a	0.0992	m$^2 \cdot$ (°C/W)	Havenith et al. [9]
Area of nude body	A_b	1.7	(m^2)	http://www.medicinenet.com
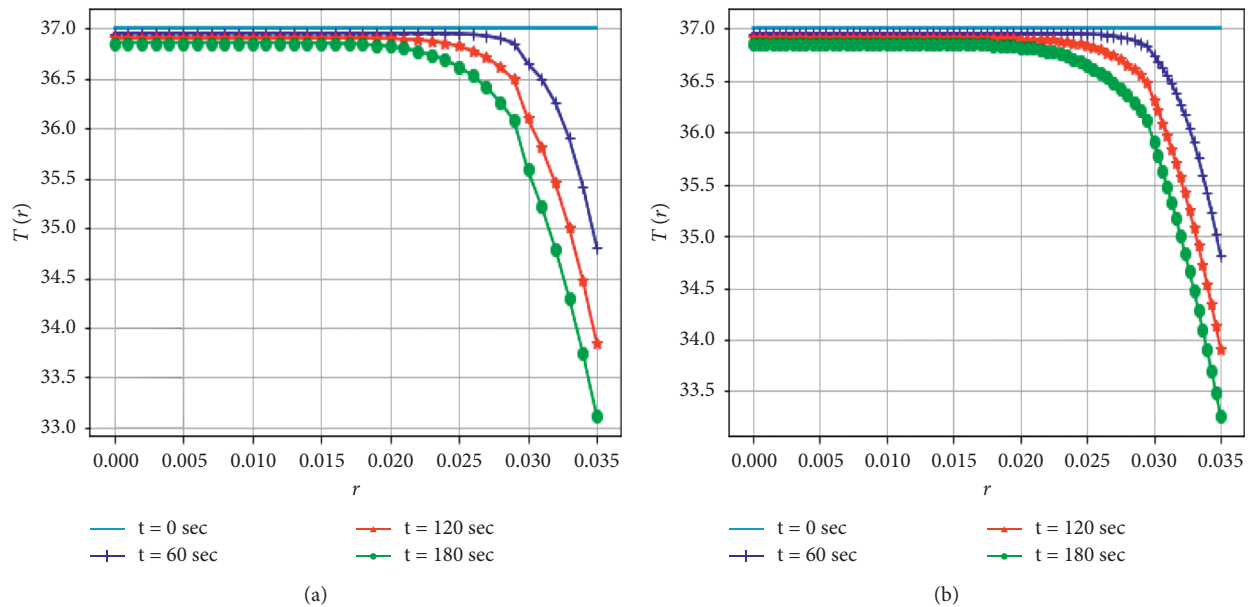
FIGURE 3: Continued.

(c)
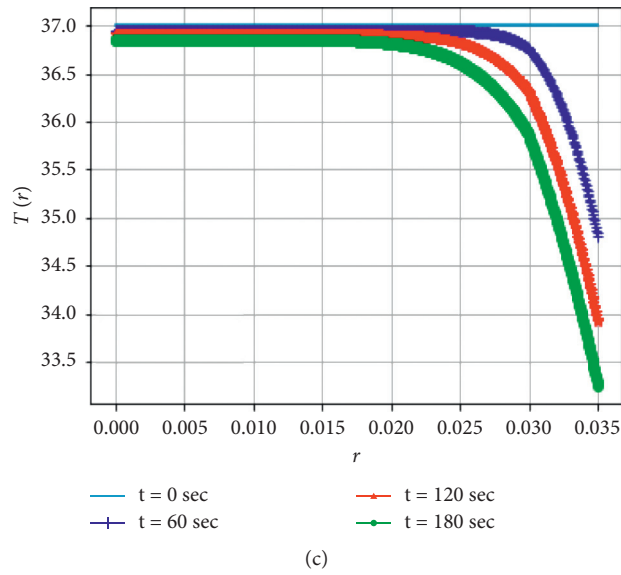
FIGURE 3: Temperature profile with various mesh sizes at time step $\Delta t = 0.01$ sec. (a) Mesh size $\Delta r = 0.001$ m, $\Delta t = 0.01\, s$. (b) Mesh size $\Delta r = 0.0005$ m, $\Delta t = 0.01\, s$. (c) Mesh size $\Delta r = 0.00005$ m, $\Delta t = 0.01\, s$.
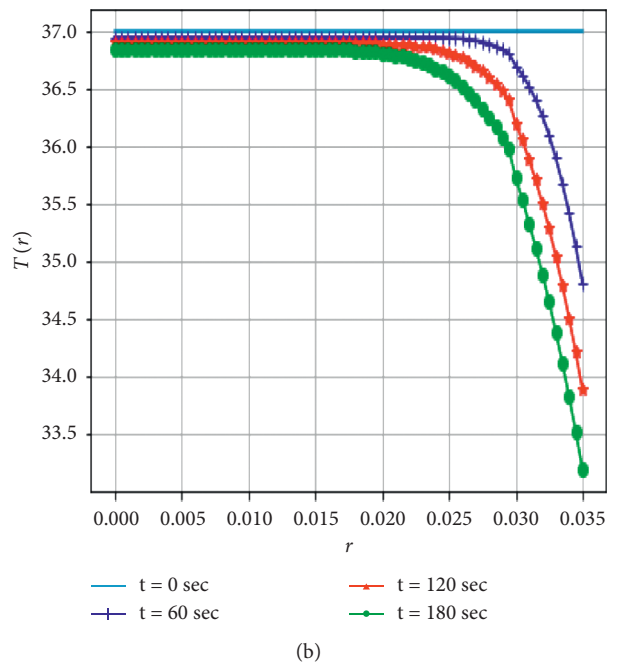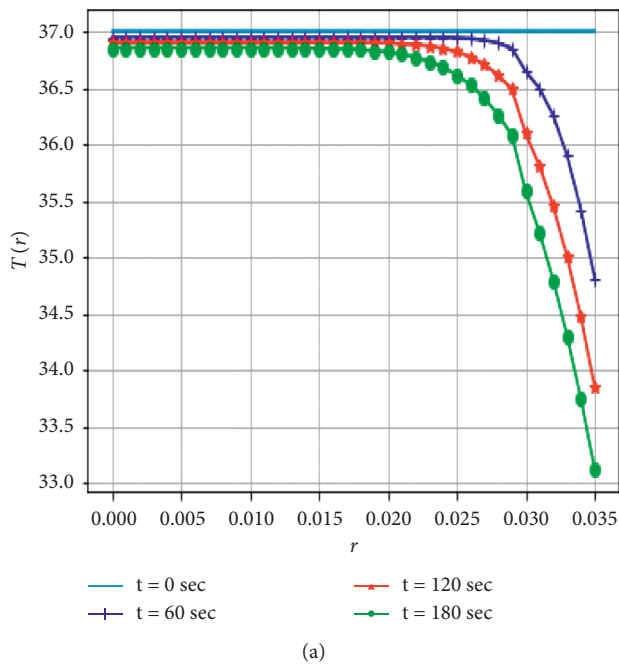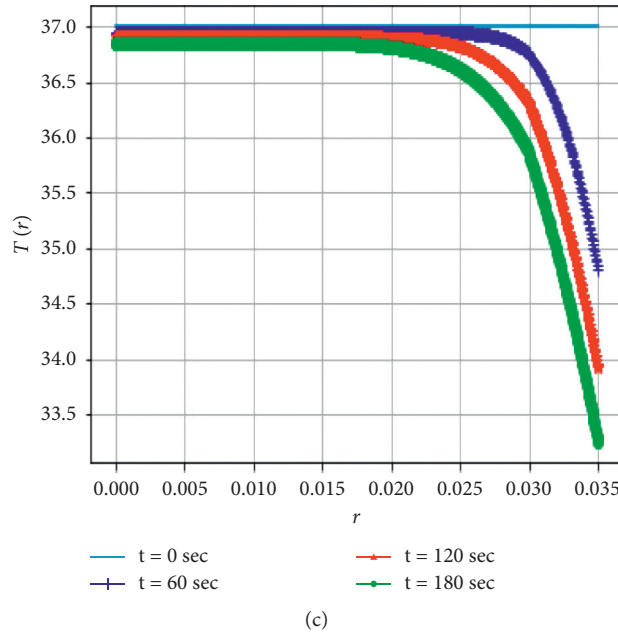

(a)

(b)

FIGURE 4: Continued.

(c)

Figure 4: Temperature profile with various mesh sizes at time step $\Delta t = 0.4$ sec. (a) Mesh size $\Delta r = 0.001$ m, $\Delta t = 0.4$ s. (b) Mesh size $\Delta r = 0.0005$ m, $\Delta t = 0.4$ s. (c) Mesh size $\Delta r = 0.00005$ m, $\Delta t = 0.4$ s.

Table 4: Temperature profile at the interface (skin surface) when $\Delta t = 0.01$ s.

Δr (m)	Temperature in 60 (s)	Temperature in 120 (s)	Temperature in 180 (s)
0.001	36.76374598	36.30866076	35.85715129
0.0001	36.76037207	36.30920285	35.86597663
0.00005	36.7602856	36.309688591	35.86747444

Table 5: Temperature profile at the interface (skin surface) when $\Delta t = 0.4$ sec.
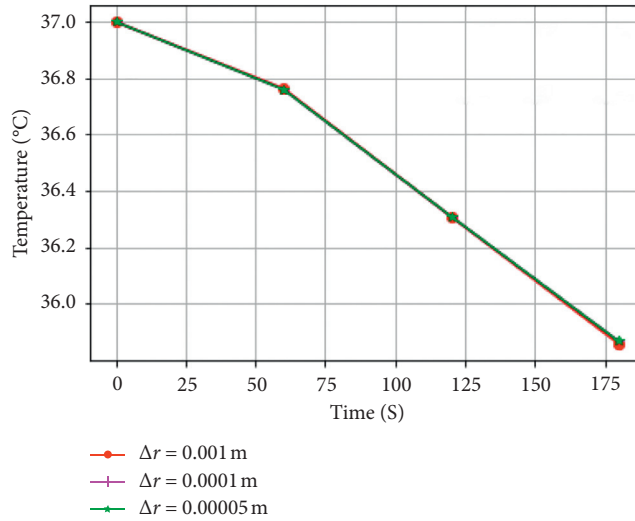
Δr (m)	Temperature in 60 (s)	Temperature in 120 (s)	Temperature in 180 (s)
0.001	36.75829838	36.30752624	35.85570826
0.0001	36.76037207	36.30920285	35.86597663
0.00005	36.7582809	36.30809916	35.866122888

(24) and (35) have been performed and tabulated in (a–c) of Figure 3 in time step $\Delta t = 0.01$ sec and (a–c) of Figure 4 in time step $\Delta t = 0.4$ sec with different mesh sizes 0.001 m, 0.0005 m, and 0.00005 m respectively.

In Figures 3(a) and 4(a), the curves are slightly deviated when $r_N = N\Delta r_N = 0.030$ m at the skin surface due to the interface condition between two materials having nonhomogeneous behavior. The curves in Figures 3(b) and 4(b) are less deviated than Figures 3(a) and 4(a), while the graphs in Figure 3(c) and Figure 4(c) are smoother than in previous four Figures. On the one hand, the comparison in graphs concerns that the increment in numbers of grid points makes the graphs smoother, more accurate, and reliable; on the other hand, the graphs are independent of mesh sizes. All the graphs in Figures 3 and 4 indicate that the temperature remains steady up to certain distance (0.02 m) from the body core, then decreases towards the skin surface and further then towards clothes. The temperature profile obtained in 60 seconds, in 120 seconds, and in 180 seconds are, respectively, the same no matter the mesh sizes are how small and large. The interface temperature (skin surface temperature) obtained from results having different mesh sizes at time steps 0.01 second and 0.4 second are, respectively, shown in Tables 4 and 5 and graphically shown in Figures 5(a) and 5(b). Similarly, the temperature in Tables 6 and 7 and Figures 6(a) and 6(b) represent these results exactly same way as in the previous case at the skin surface. As the graphs presented in Figure 7 and obtained temperature profile in Table 6 for body part and in Table 7 for clothes coincide, respectively, it can be concluded that the numerical solution of the model is stable and convergence with respect to the grid.

The temperatures in Table 8 and graphs in Figure 7 at time steps $\Delta t = 0.05$ s, $\Delta t = 0.1$ s, $\Delta t = 0.4$ s, and $\Delta t = 0.5$ s with $\Delta r = 0.0005$ m, respectively, coincide. So, all graphs are

(a)
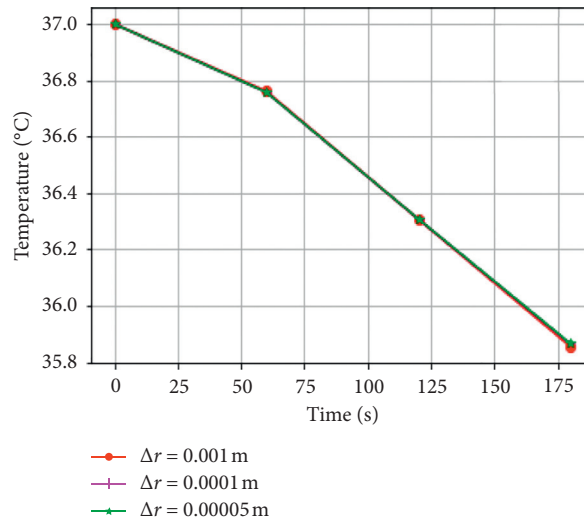
(b)

FIGURE 5: (a) Temperature profile at the interface (skin surface) at $\Delta t = 0.01$ s. (b) Temperature profile at the interface (skin surface) at $\Delta t = 0.4$ s.

TABLE 6: Temperature profile when $\Delta t = 0.01$ s.

Δr(m)	Temperature in 60 (s)	Temperature in 120 (s)	Temperature in 180 (s)
0.001	34.8052701	33.88093058	33.19336681
0.0001	34.80522479	33.9068697	33.25005773
0.00005	34.80551148	33.91018652	33.25706422

TABLE 7: Temperature profile when $\Delta t = 0.4$ sec.

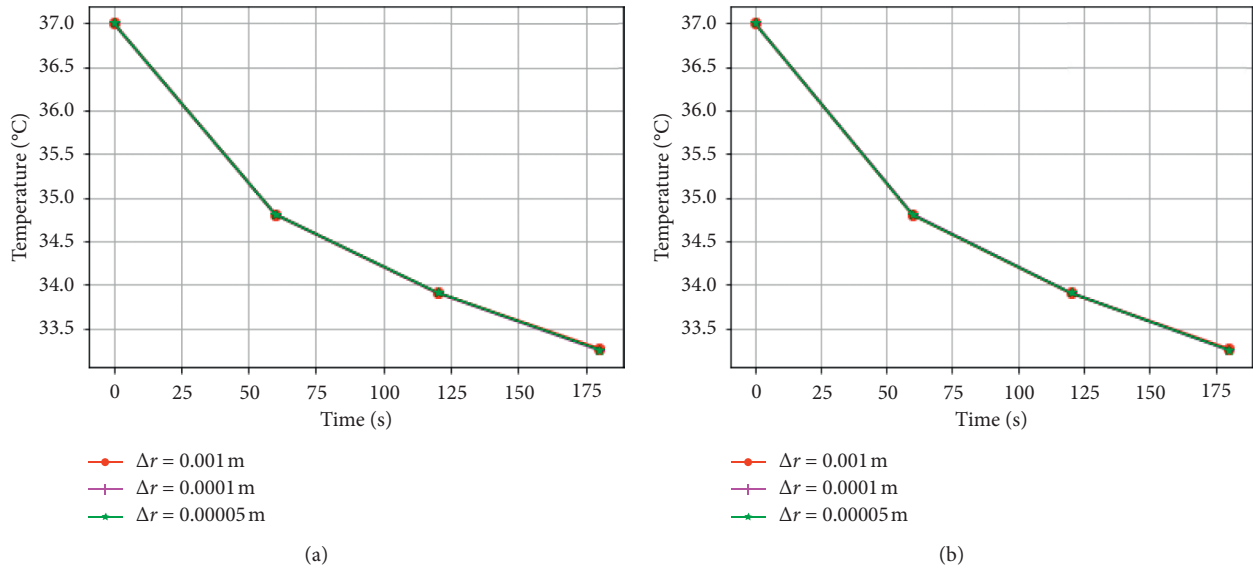| Δr (m)	Temperature in 60 (s)	Temperature in 120 (s)	Temperature in 180 (s)
0.001	34.79948362	33.87632483	33.18921782
0.0001	34.80522479	33.9068697	33.25005773
0.00005	34.79994767	33.90584859	33.25312605

(a)

(b)

FIGURE 6: (a) Temperature profile at the interface (skin surface) at $\Delta t = 0.01$ s. (b) Temperature profile at the interface (skin surface) at $\Delta t = 0.4$ s.
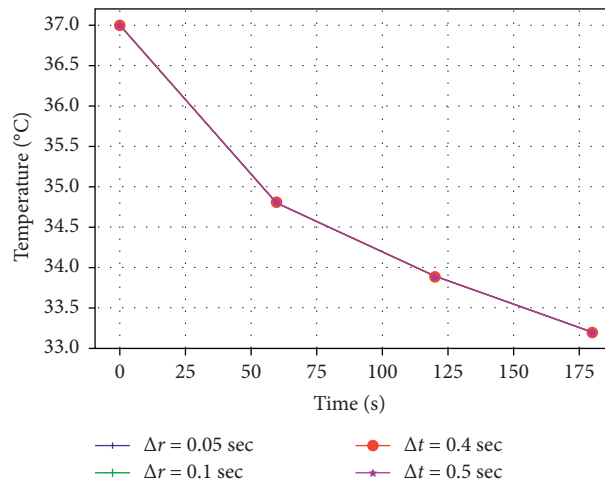

FIGURE 7: Temperature profile when $\Delta r = 0.0005$ m at different time steps.

TABLE 8: Temperature profile when $\Delta r = 0.0005$ m at different time steps.

Δt (s)	Temperature in 60 (s)	Temperature in 120 (s)	Temperature in 180 (s)
0.05	34.80467674	33.8804583	33.19294127
0.1	34.803935	33.87986792	33.19240934
0.4	34.79948362	33.87632483	33.18921782
0.5	34.79799948	33.8751435	33.18815399

independent of the time step sizes as well. These results help to verify the stability and convergence of the FD scheme for the model.

6. Conclusion

A one-dimensional time dependent bioheat transfer model with a protective clothing system has been established and solved using the fully implicit, unconditionally stable finite difference method. Because of the heterogeneous domain having two distinct physiological and physical behaviors of body and clothes, the differential equation models for two distinct parts (body and clothes) are solved separately using implicit scheme and then combined by using interface condition. The model is the extension of Pennes' bioheat equation with nonlinear Robin's boundary condition. The

developed model with the clothing phenomena is stable, consistent, and convergent on the basis of grid points as well as time step sizes. The numerical verification of the convergence and stability of the model has also been represented graphically. The result shows that suitable management of clothing, in cold and hot climatic condition, keeps the body in a highly satisfactory and comfortable level. The numerical computational results in this paper seem to agree with the similar values of clothing parameters which are experimentally verified in [1, 9]. The proposed model may be useful for the clothing and environmental designers as well as biomedical researchers.

Future work should include extension of the model to higher dimensions and use of fractional derivatives as studied in [23–25].

Data Availability

The data used for supporting the findings of this study are included within the article.

Conflicts of Interest

The authors declare that there are no conflicts of interest.

Acknowledgments

References

[1] ANSI/ASHRAE Standard 55-2017, *Thermal Environmental Condition for Human Occupancy*, ASHRAE, Atlanta, GA, USA, 2017.

[2] K. Luitel, D. B. Gurung, and K. N. Uprety, "Effect of various parameters for temperature distribution in human body: an analytical approach," *Advances in Science Technology and Engineering Systems Journal*, vol. 3, no. 5, pp. 421–426, 2018.

[3] M. Agrawal, N. Adlakha, and K. Pardasani, "Seminumerical model to study temperature distribution in peripheral layers of elliptical and tapered shaped human limbs," *Journal of Mechanics in Medicine and Biology*, vol. 10, no. 1, pp. 57–72, 2010.

[4] I. Holmer, "Protective clothing and heat stress," *Ergonomic*, vol. 38, no. 1, pp. 166–182, 1995.

[5] A. C. Guyton and J. E. Hall, *A Textbook of Medical Physiology*, Elsevier, Amsterdam, Netherlands, 2016.

[6] G. Havenith, I. Holmér, and K. Parsons, "Personal factors in thermal comfort assessment: clothing properties and metabolic heat production," *Energy and Buildings*, vol. 34, no. 6, pp. 581–591, 2002.

[7] K. Luitel, D. B. Gurung, H. Khanal, and K. N. Uprety, "Role of clothing insulation for thermal comfort: a numerical study using bio-heat transfer model," *Journal of Mathematics and Statistics*, vol. 16, no. 1, pp. 224–232, 2020.

[8] A. Das, "Clothing comfort related to thermal transmission, lecture-26," 2019, https://freevideolectures.com/course/4357/nptel-science-clothing-comfort/26.

[9] G. Havenith, K. Kuklane, J. Fan et al., "A database of static clothing thermal insulation and vapor permeability values of non-western ensembels for use in ASHARE standard 55, ISO 7733 and ISO 9920," *ASHARE Transaction*, vol. 121, pp. 197–215, 2015.

[10] C. Voelker, S. Hoffman, O. Konrad, E. Arens, and H. Zhang, "Heat and moisture transfer through clothing," in *Proceedings of theEleventh International IBPSA Conference*, Glasgow, Scotland, July 2009.

[11] H. H. Pennes, "Analysis of tissue and arterial blood temperatures in the resting human forearm," *Journal of Applied Physiology*, vol. 1, no. 2, pp. 93–122, 1948.

[12] J. J. Zhao, J. Zhang, N. Kang, and F. Yang, "A two level finite difference scheme for one dimensional Pennes' bioheat equation," *Applied Mathematics and Computation*, vol. 171, no. 1, pp. 320–331, 2005.

[13] D. B. Gurung and V. P. Saxena, "Transient temperature distribution in human dermal part with protective layer at low atmospheric temperature," *International Journal of Biomathematics*, vol. 3, no. 4, pp. 439–451, 2010.

[14] K. Luitel, "Mathematical model for temperature distribution in cylindrical human body," in *Proceedings of the 2nd International Conference on Man and Machine Interfacing (MAMI)*, IEEE, Bhubaneswar, India, December 2017.

[15] K. Luitel, D. B. Gurung, H. Khanal, and K. N. Uprety, "Numerical study of transient heat transfer model with heat transfer coefficient and conduction effect in cylindrical living tissue," *The Nepali Mathematical Sciences Report*, vol. 34, no. 1-2, pp. 17–26, 2019.

[16] S. Acharya, D. Gurung, and V. Saxena, "Mathematical modeling of sex related differences in the sensitivity of the sweating heat responses to change in body temperature," *British Journal of Mathematics & Computer Science*, vol. 12, no. 4, pp. 1–11, 2016.

[17] K. C. Parsons, "Protective clothing: heat exchange and physiological objects," *Ergonomics*, vol. 31, no. 7, pp. 997–1007, 1988.

[18] R. P. Sawant and S. B. Mhetra, "Human thermal comfort and role of clothing in it," *Journal of the Textile Association*, vol. 73, pp. 158–162, 2012.

[19] V. P. Saxena and J. S. Bindra, "Pseudo-analytic finite partition approach to temperature distribution problem in human limbs," *International Journal of Mathematics and Mathematical Sciences*, vol. 12, no. 2, pp. 403–408, 1989.

[20] S. V. Patankar, *Numerical Heat Transfer and Fluid Flow*, CRC Press, Boca Raton, FL, USA, 1980.

[21] Y. Kai, Z. Xinxin, and Y. Fan, "An analytical solution od one-dimensional steady-state Pennes bio-heat transfer equation in cylindrical coordinates," *Journal of Thermal Science*, vol. 13, no. 3, pp. 255–258, 2004.

[22] A. Abbas, Y. Zhao, J. Zhou, X. Wang, and L. Tong, "Improving thermal conductivity of cotton fabrics using composite coatings containing graphene, multiwall carbon nanotube or boron nitride fine particles," *Fibers and Polymers*, vol. 14, no. 10, pp. 1641–1649, 2013.

[23] S. Qureshi and A. Yusuf, "Fractional derivatives applied to MSEIR problems: comparative study with real world data," *The European Physical Journal Plus*, vol. 134, no. 4, p. 171, 2019.

[24] A. Yusuf, S. Qureshi, and S. F. Shah, "Mathematical analysis for an autonomous financial dynamical system via classical and modern fractional operators," *Chaos, Solitons & Fractals*, vol. 132, Article ID 109552, 2020.

[25] A. Yusuf, M. Inc, A. Isa Aliyu, and D. Baleanu, "Efficiency of the new fractional derivative with nonsingular Mittag-Leffler kernel to some nonlinear partial differential equations," *Chaos, Solitons & Fractals*, vol. 116, pp. 220–226, 2018.

Kabita Luitel[1], Dil Bahadur Gurung[2], Harihar Khanal[3], Kedar Nath Uprety[4]*

STABILITY AND CONVERGENCE OF IMPLICIT FINITE DIFFERENCE SCHEME FOR BIOHEAT TRANSFER EQUATION WITH CLOTHING EFFECT IN HUMAN THERMAL COMFORT

STABILNOST I KONVERGENCIJA IMPLICITNE SHEME KONAČNIH RAZLIKA ZA JEDNAČINU PRENOSA BIO-TOPLOTE SA UTICAJEM ODEĆE NA TERMIČKU UGODNOST

Adresa autora / Author's address:
[1)] Bhaktapur Multiple Campus, Tribhuvan University, Nepal
[2)] School of Science, Kathmandu University, Nepal
[3)] Embry-Riddle Aeronautical University, Beach, Florida, USA
[4)] Central Department of Mathematics, Tribhuvan University, Nepal   email: kabi123luitel@gmail.com

Keywords
- bioheat transfer
- clothing effect
- finite difference (FD) scheme
- effective clothing area factor

Ključne reči
- prenos bio-toplote
- uticaj odeće
- shema konačnih razlika (FD)
- faktor efikasnosti površine odeće

Abstract

   This paper studies the stability and convergence of implicit Finite Difference (FD) scheme of the bioheat transfer model of Pennes' type with the clothing effect at the boundary node. Robin's boundary condition, in this study, incorporates the clothing insulation, effective clothing area factor in the combined heat transfer coefficient and observes their effects for the thermal comfort in the human body. Lemma and theorems for consistency, stability and convergence of FD scheme are established and the numerical results are graphically presented for validation of the model.

INTRODUCTION

   The knowledge of temperature as well as heat transfer is essential for the treatment of cancer hyperthermia, cryosurgery, brain hypothermia and burn injury. A number of therapeutic and clinical applications of bioheat transfer models in the current century, including /1-3/, can be found in the field of biomathematics. The first and most popular bioheat transfer model based on the classical Fourier law was developed by H. Pennes /2/ in 1948 by incorporating the volumetry blood flow rate in tissue. Though many researchers /3-6/ have developed a bioheat transfer model, Pennes' model is still famous and widely used to study the human thermoregulatory system with the equilibrium human body temperature. Dai and Zhang /7/ developed and proved a three-level unconditionally stable and convergence of FD scheme for solving 1D Pennes' bioheat equation in a triple-layered skin structure by using discrete energy method. Zhao et al. /3/ developed two-level FD scheme for 1D Pennes' bioheat equation and proved unconditionally stable and convergence. Tuzikiewicz and Duda /8/ discussed on the stability of explicit scheme of bioheat transfer equation by Von Neumann approach. The physical and physiological factors along with clothing resistance are equally important phenomena for the thermoregulatory systems of the human body. Suitable management of clothes, on the other hand, provides better insulation and keeps a person in comfort position. Previously established models by Dai and Zhang /7/ and Zhao et

Izvod

   U radu je proučena stabilnost i konvergencija implicitne sheme konačnih razlika (FD) prenosa bio-toplote prema modelu tipa Penesa, sa uticajem odeće u graničnim čvorovima. Ovde Robinov granični uslov sadrži izolaciju odeće i faktor efikasnosti površine odeće u okviru kombinovanog koeficijenta prenosa toplote, i posmatraju se njihovi uticaji na termičku ugodnost tela čoveka. Definisane su Leme i teoreme za konzistentnost, stabilnost i konvergenciju sheme FD, a numerički rezultati su predstavljeni grafički radi provere modela.

al. /3/ have ignored the Robin's type boundary condition and also did not mention the effect of clothing resistance and insulation. These quantities cannot be neglected in the real-life situation. So, this paper focuses to study the mathematical model by incorporating the heat flux with clothing resistance, clothing area factor, and air insulation on the boundary. We construct the implicit finite difference scheme, establish and prove the theorems to show the FD scheme of our model is unconditionally stable and convergence having the same order of accuracy.

Role of clothes

   The amount or rate of heat resists being transferred through clothes is defined as the clothing heat resistance. For thermal conductivity of clothes (W/m°C), / 9/,

$$k_{cl} = q \frac{L_{cl}}{\Delta T},$$

where: L_{cl} is the thickness of cloth (m); ΔT the temperature difference (°C); q is heat flow rate (W/m²). The thermal resistance R_{cl} (m²°C/W) is given by, /9/,

$$R_{cl} = \frac{\Delta T}{q} = \frac{L_{cl}}{k_{cl}}.$$

MATHEMATICAL MODEL

   1D Pennes bioheat equation in cylindrical form is given by /2/ as

INTEGRITET I VEK KONSTRUKCIJA
Vol. 21, Specijalno izdanje (2021), str. S23–S28

S23

STRUCTURAL INTEGRITY AND LIFE
Vol. 21, Special Issue (2021), pp. S23–S28

$$\rho c \frac{\partial T}{\partial t} = \frac{1}{r}\left(kr \frac{\partial T}{\partial r} \right) + w_b c_b (T_a - T) + q_m , \qquad (1)$$

where: ρ is density (kg/m³); c specific heat (J/g°C); k thermal conductivity of tissue (W/m°C); w_b rate of blood perfusion (kg/m³s); c_b specific heat of blood (J/kg°C); T_a arterial temperature (°C); q_m metabolic heat production (W/m³).

The distance from the body core towards skin surface is denoted by r (m). The bioheat Eq.(1) with the clothing parameter P (W/m³), /9/, is written as

$$\rho c \frac{\partial T}{\partial t} = k\left(\frac{\partial^2 T}{\partial r^2} + \frac{1}{r}\frac{\partial T}{\partial r} \right) + w_b c_b (T_a - T) + q_m + P , \quad (2)$$

where: $P = P_{cl}(T_{sk} - T_{cl})$; and $P_{cl} = k_{cl}/A_{cl}$ (W/m³°C); A_{cl} is the surface area of clothed human body (m²).

Left boundary condition at r = 0 (body core)

The boundary condition for the interior part of the living tissue is considered uniform as

$$\text{at} \quad r = 0, \quad \frac{\partial T_t}{\partial t} = 0 . \qquad (3)$$

Right boundary condition at the clothes surface

The right side is fitted with clothes and directly exposed to the atmospheric environment, so boundary condition of the Robin type is

$$\text{at} \quad r = R, \quad -k_{cl}\frac{\partial T_{cl}}{\partial r_{cl}} = h_A(T_{cl} - T_\infty) , \qquad (4)$$

where: r_{cl} is thickness of clothes; h_c the convective heat transfer coefficient (W/m²°C); h_r radiative heat transfer coefficient (W/m²°C); T_{cl} clothes temperature (°C); T_∞ atmospheric temperature (°C). The clothing efficiency factor F_{cl} (dimensionless) is given by, /9-12/,

$$F_{cl} = \frac{I_a}{I_T} = \frac{I_a}{I_{cl} + I_a / f_{cl}} ,$$

where: I_{cl} is the clothing insulation (m²°C/W); I_a (m²°C/W) air insulation (m). The dimensionless clothing factor is the ratio of clothed surface and naked body surface area, $f_{cl} = A_{cl}/A_b$.

METHODOLOGY

Finite difference (FD) scheme is used as the numerical method. The main assumptions in this study are heat flows from body core toward the skin surface in radial direction, $(R - 1)$-th node is the interface between the skin surface and clothes. Clothing appears in the boundary, the R-th node is the clothes surface exposed to the environment. So, we use the boundary condition Eq.(4). The domain discretization can be seen in the circular limb of the body in Fig. 1.
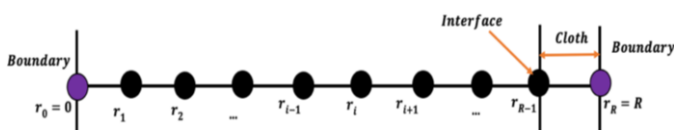

Figure 1. Discretization of mesh in radial direction.

Finite difference (FD) scheme

We consider the cylindrical coordinate system covered by the cylindrical differential mesh with step size Δr in

radial direction. In this case we also take n, $n + 1$ as two successive time level with time step Δt. Taking the implicit FD scheme for the internal i-th node with $i = 1, 2, 3,…, R\text{-}1$ is given by

$$\rho c \frac{T_i^{n+1} - T_i^n}{\Delta t} = k_t \frac{T_{i-1}^{n+1} - 2T_i^{n+1} + T_{i+1}^{n+1}}{\Delta r^2} + \frac{k_t}{2i\Delta r} \times$$
$$\times \left(T_{i+1}^{n+1} - T_{i-1}^{n+1} \right) + w_b \left(T_a - T_i^{n+1} \right) + q_m . \qquad (5)$$

The construction of FD scheme in Eq.(5) has truncation error of order $0(\Delta r^2 + \Delta t)$ for (t^n, r_i) on each interior grid point $n \geq 1$, $0 < i < R\text{-}1$.

When, $D = k_t/\rho c$, $\alpha = D\Delta t/\Delta r^2$, $M = w_b c_b/\rho c$, $S = q_m/\rho c$, and $F = \Delta t(MT_a + S)$. Rewriting the above Eq.(5), we have for $0 < i < R\text{-}1$,

$$D_i T_{i-1}^{n+1} + E_i T_i^{n+1} + B_i T_1^{n+1} - F = T_i^n , \qquad (6)$$

where: $D_i = \left(-\alpha + \frac{\alpha}{2i} \right)$; $E_i = (1 + 2\alpha + M\Delta t)$; $B_i = \left(-\alpha - \frac{\alpha}{2i} \right)$.

FD scheme for left boundary condition at i = 0

Due to the constant temperature at the core, when $r = 0$, then $\frac{1}{r}\frac{\partial T_t}{\partial r} \to 0$. In this situation we use L'Hospital rule to remove this indeterminate form at the left boundary node and get the equation at $i = 0$ as

$$\rho c \frac{\partial T_t}{\partial t} = 2D\left(\frac{\partial^2 T_t}{\partial r^2} \right) + M(T_a - T_t) + S . \qquad (7)$$

FD scheme at $i = 0$ with the help of boundary condition given in Eq.(3) is

$$E_0 T_0^{n+1} - 4\alpha T_1^{n+1} - F = T_0^n . \qquad (8)$$

FD scheme for skin surface at the interface at i = R - 1

$$D_{R-1} T_{R-2}^{n+1} + E_{R-1} T_{R-1}^{n+1} + B_{R-1} T_R^{n+1} - F = T_{R-1}^n . \qquad (9)$$

Equation (9) is FD scheme at R - 1, the system is taken as tight fitting or negligible air gap between body and clothes at $i = R\text{-}1$, the contact point between skin and clothes.

The interface thermal conductivity in /13/ is

$$k_t = k_{cl} = \frac{k_t k_{cl}(\Delta r + \Delta r_{cl})}{k_{cl}\Delta r + k_t \Delta r_{cl}} . \qquad (10)$$

The continuity and interface condition is given by /13/

at $i = R\text{-}1$, $k_t \frac{\partial T_{sk}}{\partial r} = k_{cl}\frac{\partial T_{cl}}{\partial r_{cl}}$, $k_t \frac{T_R^{n+1} - T_{R-1}^{n+1}}{\Delta r} = k_{cl}\frac{T_R^{n+1} - T_{R-2}^{n+1}}{\Delta r + \Delta r_{cl}}$.

From Eq.(10) we get, $k_t k_{cl} \frac{T_R^{n+1} - T_{R-2}^{n+1}}{k_T} = k_{cl}\frac{T_R^{n+1} - T_{R-1}^{n+1}}{\Delta r_{cl}}$,

where: Δr_{cl} is thickness of clothes; Δr is mesh size for body part; and $k_T = k_{cl}\Delta r + k_t\Delta r_{cl}$.

Now, suppose $\beta = k_t \Delta r_{cl}/k_T$, then

$$T_R^{n+1} = T_{R-1}^{n+1} + \beta\left(T_R^{n+1} - T_{R-2}^{n+1} \right) . \qquad (11)$$

With the help of Eq.(11), Eq.(9) can be written as

INTEGRITET I VEK KONSTRUKCIJA
Vol. 21, Specijalno izdanje (2021), str. S23–S28

S24

STRUCTURAL INTEGRITY AND LIFE
Vol. 21, Special Issue (2021), pp. S23–S28

$$D_{R-1}T_{R-2}^{n+1} + E_{R-1}T_{R-1}^{n+1} + B_{R-1}\left[T_{R-1}^{n+1} + \beta\left(T_R^{n+1} - T_{R-2}^{n+1}\right)\right] - F = T_{R-1}^n,$$

$$(D_{R-1} - \beta B_{R-1})T_{R-2}^{n+1} - (E_{R-1} + E_{R-1})T_{R-1}^{n+1} + BT_{R-1}^{n+1} - F = T_{R-1}^n. \tag{12}$$

Now, at $r = R$, $M = 0$, $S = 0$, the Eq.(6) for clothing part is given in FD scheme as

$$\left(-\alpha_1 + \frac{\alpha_1}{2R} - P_1\right)D_{R-1}T_{R-1}^{n+1} + (1 + 2\alpha_1 + P_1)T_R^{n+1} +$$

$$+ \left(-\alpha_1 + \frac{\alpha_1}{2R}\right)T_{R+1}^{n+1} = T_R^n, \tag{13}$$

where: $\alpha_1 = \dfrac{k_{cl}\Delta t}{\rho_{cl}c_{cl}(\Delta r_{cl})^2}$; $P_1 = \dfrac{P\Delta t}{\rho_{cl}c_{cl}}$.

Boundary condition at the clothing surface at $i = R$

The right boundary condition at the clothing surface in Eq.(4) is

at $r = R$ $-k_{cl}\dfrac{\partial T_{cl}}{\partial r_{cl}} = h_A(T_{cl} - T_\infty)$.

FD scheme for boundary condition is

$$T_{R+1}^{n+1} = T_{R-1}^{n+1} - 2h_A(T_{cl} - T_\infty). \tag{14}$$

From Eqs.(13) and (14), the FD scheme for the right boundary node is

$$(-2\alpha_1 - P_1)T_{R-1}^{n+1} + \left[(1 + 2\alpha_1 + P_1) + \alpha_1 + \frac{\alpha_1}{2R}\right]T_R^{n+1} +$$

$$+ 2h_A R_{cl}T_\infty\left(-\alpha_1 - \frac{\alpha_1}{2R}\right) = T_R^n,$$

$$D_{Rcl}T_{R-1}^{n+1} + [E_{Rcl} - 2h_A R_{cl}T_\infty B_{Rcl}]T_R^{n+1} +$$

$$+ 2h_A R_{cl}\left(-\alpha_1 - \frac{\alpha_1}{2R}\right) = T_R^n. \tag{15}$$

$$D_{Rcl} = (-2\alpha_1 - P_1), \quad E_{Rcl} = (1 + 2\alpha_1 + P_1),$$

$$B_{Rcl} = \left(-\alpha_1 - \frac{\alpha_1}{2R}\right), \quad F_R = 2h_A R_{cl}\left(-\alpha_1 - \frac{\alpha_1}{2R}\right).$$

The systems Eqs.(8), (6) and (15) together can be written as the matrix equation of the form

$$AT^{n+1} = T^n + B, \tag{16}$$

where: A is $(R+1)\times(R+1)$ tridiagonal square matrix; B is the column vector of size $(R+1)\times 1$ and

$$T^n = \begin{cases} T_t^n & \text{for } 1 \le i \le R-1 \\ T_{cl}^n & \text{for } i = R \end{cases} \tag{17}$$

ANALYSIS OF THE MODEL

To prove solvability and stability of Eq.(2), we introduce a column vector of size $(R+1)\times 1$ representing the numerical solution at time step t^n as $T^n = [T_0^n, T_1^n, \ldots, T_i^n, \ldots, T_R^n]$.

Theorem 1 (solvability of the model): for each time step n, Eq.(16) is unconditionally solvable.

Proof. To show solvability of Eq.(16), it is sufficient to prove that the matrix A is invertible, i.e. the matrix A is diagonally dominant, where the absolute value of diagonal element of each row of the coefficient matrix A in Eq.(16)

is greater than the sum of the absolute value of remaining elements in corresponding row of matrix A. Then we have

R_1 (1st row): $|a_{jj}| \ge \Sigma|a_{ij}|$ since $|1 + 4\alpha + M\Delta t| > |-4\alpha|$

R_i (i-th row): $|a_{jj}| \ge \sum\limits_{i=2, i \ne j}^{R-2}|a_{ij}|$.

Since $E_i = |1 + 2\alpha + M\Delta t|$, $|D_i| = \left|-\alpha + \dfrac{\alpha}{2i}\right|$, $|B_i| = \left|-\alpha - \dfrac{\alpha}{2i}\right|$,

So, $\left|1 + 2\alpha + M\Delta t\right| > \left|-\alpha + \dfrac{\alpha}{2i}\right| + \left|-\alpha - \dfrac{\alpha}{2i}\right| = |-2\alpha|$,

R_{R-1} (R-1)-th row: $|a_{jj}| \ge \Sigma|a_{ij}|$

Since $|E_{R-1} + B_{R-1}| = \left|(1 + 2\alpha + P_1) + \left(-\alpha - \dfrac{\alpha}{2(R-1)}\right)\right|$

$$|E_{R-1} + B_{R-1}| = \left|(1 + P_1) + \left(\alpha - \dfrac{\alpha}{2(R-1)}\right)\right|$$

on the other hand, $|D_{R-1} - \beta B_{R-1}| + |\beta B_{R-1}| \ge |D_{R-1}| =$

$$= \left|-\left(\alpha - \dfrac{\alpha}{2(R-1)}\right)\right| = \left(\alpha - \dfrac{\alpha}{2(R-1)}\right).$$

So $|E_{R-1} + B_{R-1}| > |D_{R-1} - \beta B_{R-1}| + |\beta B_{R-1}|$.

R_R R-th row: $|a_{jj}| \ge \Sigma|a_{jj}|$
Since $|E_{Rcl} - B_{Rcl}| > |D_{Rcl}|$

$$\Rightarrow \left|(1 + 2\alpha + P_1) + 2h_A R_{cl}\left(\alpha_1 + \frac{\alpha_1}{2R}\right)\right| > |-2\alpha_1 - P_1| = |2\alpha_1 + P_1|.$$

Clearly, each row is also diagonally dominant. So, matrix A is invertible. Hence Eq.(16) is unconditionally solvable.

Lemma 1. If λ_i for $i = 0, 1, 2, \ldots, R$ represents the eigenvalues of the square matrix A and '$\|\ \|_2$' represents the second matrix norm (i.e. $\|A\|_2 = \max\limits_i|\lambda_i|$, then we have the following results

(i) $$|\lambda_i| = \begin{cases} 1 + M\Delta t & \text{for } 1 \le i \le R-1 \\ 1 + P_1 & \text{for } i = R \end{cases}$$

(ii) $$\|A^{-1}\|_2 \ge \begin{cases} \dfrac{1}{1 + M\Delta t} \le 1 & \text{for } 1 \le i \le R-1 \\ \dfrac{1}{1 + P_1} \le 1 & \text{for } i = R \end{cases}$$

Theorem 2 (consistency): a finite difference (FD) scheme of Eq.(2) with truncation error $\tau(\Delta r, \Delta t)$ is consistent if

$$\tau(\Delta r, \Delta t) \to 0 \quad \text{as} \quad \Delta r, \Delta t \to 0.$$

It can be easily said that we have approximated our model Eq.(2) by FD scheme in Eqs.(8), (6), (12) and (13), which has truncation error $\tau(\Delta r, \Delta t) = O((\Delta r)^2 + \Delta t)$.

So, $\lim\limits_{\Delta r, \Delta t \to 0} \tau(\Delta r, \Delta t) = 0$.

Hence, the FD scheme of our model Eq.(2) is consistent.

Theorem 3 (stability): The FD scheme of Eq.(2) is unconditionally stable with respect to initial data if

INTEGRITET I VEK KONSTRUKCIJA
Vol. 21, Specijalno izdanje (2021), str. S23–S28

S25

STRUCTURAL INTEGRITY AND LIFE
Vol. 21, Special Issue (2021), pp. S23–S28

$$\left\| E^{n+1} \right\|_2 \leq \left\| E^0 \right\|_2,$$

where: $E^{n+1} = T^{n+1} - T^{*(n+1)}$ is an error equation; $T^{*(n+1)}$ is the small perturb in T^{n+1}.

Proof. Operating Eq.(17) by A^{-1} we obtain

$$T^{n+1} = A^{-1}T^n + A^{-1}B. \tag{I}$$

Take $T^{*(n+1)}$ be small perturb in T^{n+1}, then

$$AT^{*(n+1)} = T^{*(n)} + B.$$
$$T^{*(n+1)} = A^{-1}T^{*(n)} + A^{-1}B \tag{II}$$

Assume that

$E^{n+1} = T^{n+1} - T^{*(n+1)}$ be the error equation, then from Eq.(I) and Eq.(II) we get

$$E^{n+1} = (A^{-1}T^n + A^{-1}B) - (A^{-1}T^{*(n)} + A^{-1}B)$$

$$E^{n+1} = A^{-1}(T^n - T^{*(n)}) = A^{-1}E^n = A^{-1}(A^{-1}E^{n-1}) =$$

$$= (A^{-1})^2 E^{n-1} = (A^{-1})^2(A^{-1}E^{n-2}) = (A^{-1})^3 E^{n-2} =$$

$$= \ldots = (A^{-1})^n E^0 \quad \text{for} \quad n = 1, 2, \ldots, n.$$

So, we have, $E^{n+1} = (A^{-1})^n E^0$ for $n = 1, 2, \ldots, n$.

With respect to second norm, $\left\| E^{n+1} \right\|_2 \leq \left\| A^{-1} \right\|_2 \left\| E^0 \right\|_2$.

From Lemma 1, we apply $\left\| A^{-1} \right\|_2 \leq 1$, which implies

$$\left\| E^{n+1} \right\|_2 \leq \left\| E^0 \right\|_2.$$

Hence, by Lax-Ritchtmyer's Theorem the FD scheme of the extended bioheat equation with clothing system is unconditionally stable with respect to initial data.

Theorem 4 (convergence): FD scheme of Eq.(2) is unconditionally convergent.

Proof. Let

$$T^n = [T(r_0, t^n), T(r_1, t^n), \ldots, T(r_i, t^n), \ldots, T(r_R, t^n)]' \quad \text{of size}$$

$(R + 1) \times 1$ be the exact solution at time step t^n such that

$$AT^{n+1} = T^n + B + \tau^{n+1}, \tag{18}$$

where: τ^{n+1} be the truncation error vector at level t^n. We have the numerical solution in T in Eq.(16) based on the discretization schemes.

If $E^{n+1} = T^{n+1} - T^{n+1}$ is an error equation, then Eq.(16) and Eq.(18) yield

$$AE^{n+1} = E + \tau^{n+1}$$

$$E^{n+1} = A^{-1}E^n + A^{-1}\tau^{n+1} =$$

$$= A^{-1}(A^{-1}E^{n-1} + A^{-1}\tau^n) + A^{-1}\tau^{n+1} =$$

$$= (A^{-1})^2(A^{-1}E^{n-2} + A^{-1}\tau^{n-1}) + (A^{-1})^2\tau^n + A^{-1}\tau^{n+1} =$$

$$= (A^{-1})^3 E^{n-2} + (A^{-1})^3\tau^{n-1} + (A^{-1})^3\tau^n + A^{-1}\tau^{n+1} =$$

$$= \ldots = (A^{-1})^2 E^0 + \sum_{k}^{n} (A^{-1})^k \tau^{n-k}$$

$$E^{n+1} = (A^{-1})^2 E^0 + \sum_{k}^{n} (A^{-1})^k \tau^{n-k}. \tag{19}$$

Initially we take $T^0 = 0$, since initially no error occurs at $t = 0$. So, $E^0 = 0$, and taking norm on both sides of Eq.(19) gives the following result,

$$\left\| E^{n+1} \right\|_2 \leq \left\| A^{-1} \right\|_2^2 \left\| E^0 \right\|_2 + \left(\sum_{k=0}^{n} \left\| A^{-1} \right\|_2^k \right) \max_{1 \leq k \leq R} \left\| \tau^k \right\|_2$$

Since $E^0 = 0$ and from Lemma 1 we have $\left\| A^{-1} \right\|_2 \leq 1$,

$$\left\| E^{n+1} \right\|_2 \leq \left\| E^0 \right\|_2 + \left(\sum_{k=0}^{n} \left\| A^{-1} \right\|_2^k \right) \max_{1 \leq k \leq R} \left\| \tau^k \right\|_2.$$

By the construction of $\tau(\Delta r + \Delta t)$, we have

$$\left\| \tau^k \right\|_2 \to 0 \quad \text{as} \quad \Delta r \to 0, \Delta t \to 0.$$

This implies

$$\lim_{\Delta r, \Delta t \to 0} \left\| E^{n+1} \right\|_2 = 0 \quad \text{for} \quad 1 \leq k \leq R.$$

Hence the system is unconditionally convergent.

NUMERICAL VERIFICATIONS

One dimensional Pennes bioheat equation given in Eq.(2) is numerically discretized in Eq.(6) with Backward Scheme in Time and Central Difference Scheme in Space (BTCS). The tissue thickness of the human cylindrical limb in this model is taken $R = 0.03$ m /5, 14/ from body core to skin surface. So far the clothes effect is concerned, the thickness of clothes 0.005 m /4/ is added to tissue thickness and the results are calculated with the new thickness $R = 0.03 + 0.005$. Other various physical and physiological parameters from Table 1 (for human body) and Table 2 (for clothing parameters) are chosen for the numerical experiments.

Table 1. Thermophysical parameters /6, 14, 15/.

Parameters		value	unit
Thermal conductivity	k_t	0.48	W/m°C
Specific heat of blood	c_b	3850	J/kg°C
Blood density	ρ_b	1000	kg/m³
Blood perfusion rate	w_b	3	kg/s·m³
Metabolism	q_m	1085	W/m³
Arterial temperature	T_a	37	°C
Convectional heat transfer coefficient	h_c	10.023	W/m²·°C
Environmental temperature	T_s	28	°C

Table 2. Thermophysical parameters /9, 10, 12, 16/.

Parameters		value	unit
Thermal conductivities of clothes	k_{cl}	2.0462	W/m°C
Thickness of clothes	L_{cl}	0.010	m
Density of clothes	ρ_{cl}	1550	kg/m³
Specific heat of clothes	c_{cl}	1340	J/kg°C
Clothing Insulation	I_{cl}	1.34	m²·°C/W
Air insulation	I_a	0.025	m²·°C/W
Area of nude body	A_b	1.6	m²
Clothing area factor	f_{cl}	1.75	-

GRAPHICAL REPRESENTATION

The stability of the developed FD scheme Eq.(16) for cylindrical shape of the body with protective clothing system at the boundary node and its effects has also been verified by considering different parameters mentioned in Tables 1 and 2.

Different mesh sizes 25, 40, and 55, as well as mesh sizes 100, 500 and 1000 in both non-clothing and clothing cases are taken for the validity and applicability of the numerical (implicit FD) scheme Eq.(16) at time $\Delta t = 0.01$ s.

This numerical verification has been performed in Fig. 2 and Fig. 3 with three different meshes of 25, 40 and 55 with the time increment $\Delta t = 0.01$ s for non-clothing and clothing system of the body. In Fig. 2, the temperature of nude body at skin is 28 °C. In clothing state, on the other hand, the temperature becomes 32 °C in Fig. 3 which is because of the effect of clothing insulation and other parameters related to clothes. Similar results can be seen in Figs. 4 and 5 with mesh sizes 100, 500 and 1000 at time step $\Delta t = 0.01$ s in 180 seconds. The temperatures obtained in Figs. 2 and 4 almost coincide on the same curve even though the mesh sizes are different for the non-clothing case (nude body).
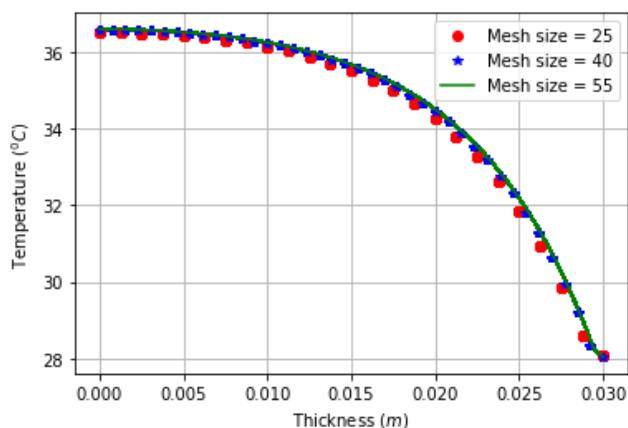
Figure 2. Radial temperature profile in 180 s.
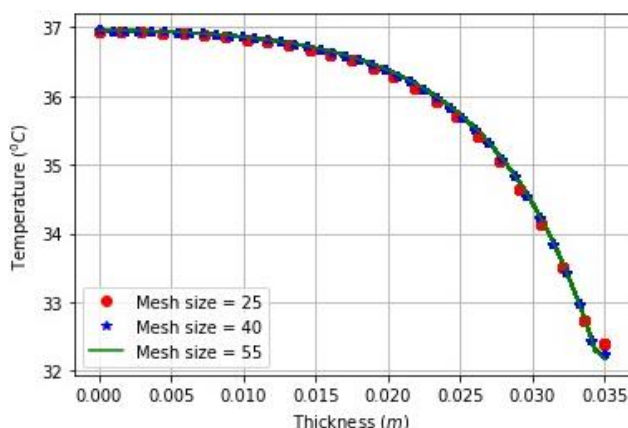
Figure 3. Radial temperature profile with clothing in 180 s.
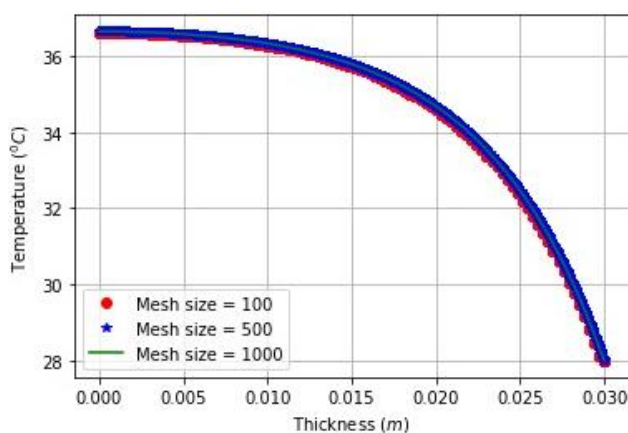
Figure 4. Radial temperature profile in 180 s.
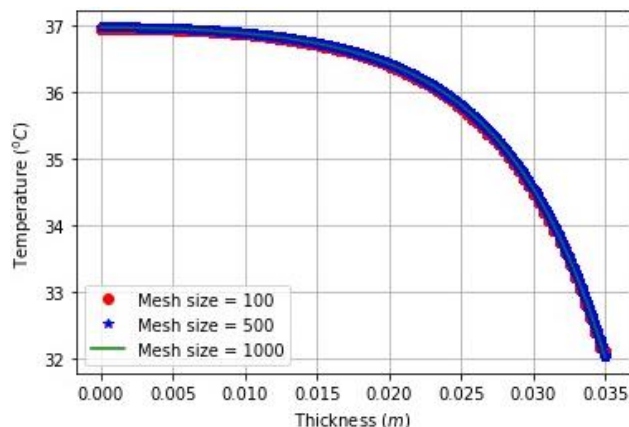
Figure 5. Radial temperature profile with clothing in 180 s.

The results in Figs. 3 and 5 in the clothing system are almost the same. In both cases, the figures are independent no matter what the mesh sizes are. These results verify the stability of implicit FD scheme for newly developed model.

CONCLUSION

In this study, an Implicit Finite Difference (FD) scheme, for one-dimensional transient bioheat transfer model with protective clothing at the boundary node of cylindrical body has been developed. The theorems are established and proven for analysing solvability, consistency, unconditionally stable and convergence of the model.

Also, the numerical verification of the model is represented graphically showing its stability and validity on one hand, and the presence of clothes of significant effect for thermal comfort of the person, on the other. The developed model fosters the advanced clothing system to achieve the comfort state of the human body.

ACKNOWLEDGEMENT

REFERENCES

1. Gurung, D.B., Luitel, K. (2012), *Development of bio-heat equation and its application*, In: Proc. Nepal Math. Soc. 2012, pp. 85-94.
2. Pennes, H.H. (1948), *Analysis of tissue and arterial blood temperatures in resting human forearm*, J Appl. Physiol. 1(2): 93-122. doi: 10.1152/jappl.1948.1.2.93
3. Zhao, J.J., Zhang, J., Kang, N., Yang, F. (2005), *A two level finite difference scheme for one dimensional Pennes' bioheat equation*, Appl. Math. Comp. 171(1): 320-331. doi: 10.1016/j.amc.2005.01.052
4. Gurung, D.B., Saxena, V.P. (2010), *Transient temperature distribution in human dermal part with protective layer at low atmospheric temperature*, Int. J Biomath. 3(4): 439-451. doi: 10.1142/S1793524510001070
5. Luitel, K. (2017), *Mathematical model for temperature distribution in cylindrical human body*, 2nd Int. Conf. on Man and Machine Interfacing (MAMI), Bhubaneswar, IEEE, 2017, pp. 1-5. doi: 10.1109/MAMI.2017.8307886
6. Luitel, K., Gurung, D.B., Uprety, K.N. (2018), *Effect of various parameters for temperature distribution in human body: An ana-*

INTEGRITET I VEK KONSTRUKCIJA
Vol. 21, Specijalno izdanje (2021), str. S23–S28

S27

STRUCTURAL INTEGRITY AND LIFE
Vol. 21, Special Issue (2021), pp. S23–S28

lytic approach, Spec. Issue Recent Adv. Eng. Syst. J (ASTESJ), 3(5): 421-426. doi: 10.25046/aj030548

7. Dai, W.Z., Zhang, J. (2002), *A three level finite difference scheme for solving the Pennes bioheat transfer in a triple-layered skin structure*, Tech. Rep. No.343-02, Department of Computer Science, University of Kentucky, 2002, pp.1-12.

8. Tuzikiewicz, W., Duda, M. (2015), *Bioheat transfer equation. The problem of FDM explicit scheme stability*, J Appl. Math. Comp. Mech. 14(4): 139-144. doi: 10.17512/jamcm.2015.4.14

9. Luitel, K., Gurung, D.B., Khanal, H., Uprety, K.N. (2021), *Bio-heat transfer equation with protective layer*, Math. Problems Eng., Vol.2021, Art. ID 6639550. doi: 10.1155/2021/6639550

10. Luitel, K., Gurung, D.B., Khanal, H., Uprety, K.N. (2020), *Role of clothing insulation for thermal comfort: A numerical study using bio-heat transfer model*, J Math. Statist. 16(1): 224-232. doi: 10.3844/jmssp.2020.224.232

11. Havenith, G., Holmer, I., Parsons, K. (2002), *Personal factors in thermal comfort assessment: clothing properties and metabolic heat production*, Energy Build. 34(6): 581-591. doi: 10.1016/S0378-7788(02)00008-7

12. Havenith, G., Kuklane, K., Fan, J., et al. (2015), *A database of static clothing thermal insulation and vapor permeability values of non-western ensembles for use in ASHRAE standard 55, ISO 7733 and ISO 9920*, ASHRAE Trans. 121(1): 197-215.

13. Patankar, S.V., Numerical Heat Transfer and Fluid Flow, CRC Press, Boca Raton, 1980. doi: 10.1201/9781482234213

14. Yue, K., Zhang, X., Yu, F. (2004), *An analytic solution of one-dimensional steady-state Pennes' bioheat transfer equation in cylindrical coordinates*, J Therm. Sci. 13(3): 255-258. doi: 10.1007/s11630-004-0039-y

15. Luitel, K., Gurung, D.B., Khanal, H., Uprety, K.N. (2019), *Numerical study of transient bio-heat transfer model with heat transfer coefficient and conduction effect in cylindrical living tissue*, The Nepali Math. Sci. Report, 36(1-2): 17-26. doi: 10.3126/nmsr.v36i1-2.29967

16. Voelker, C., Hoffmann, S., Kornadt, O., et al. (2009), *Heat and moisture transfer through clothing*, IPSA Building Simulation 2009, University of Strathclyde, Glasgow, Scotland, 2009. p.1-7. https://escholarship.org/uc/item/8qk6h840

• · · · · · ● ● ● ● · ·

New Elsevier Book Titles – Woodhead Publishing – Academic Press – Butterworth-Heinemann – …

Fretting Wear and Fretting Fatigue, 1st Edition, Fundamental Principles and Applications
Tomasz Liskiewicz Daniele Dini (Eds.)
Elsevier, Jan 2022
ISBN: 9780128240960

Forsthoffer's Proven Guidelines for Rotating Machinery Excellence
1st Edition
William Forsthoffer
Butterworth-Heinemann, Aug 2021
ISBN: 9780323854337
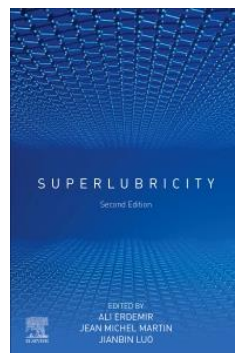
Superlubricity
2nd Edition.
Ali Erdemir Jean-Michel Martin Jianbin Luo Jianbin Luo (Eds.)
Elsevier, Sep 2020
ISBN: 9780444643131
EISBN: 9780444643148
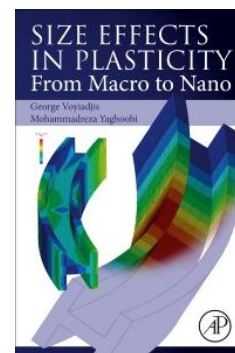
Size Effects in Plasticity
1st Edition, From Macro to Nano
George Voyiadjis Mohammadreza Yaghoobi
Academic Press, Aug 2019
ISBN: 9780128122365
EISBN: 9780128135136

Handbook of Data Science Approaches for Biomedical Engineering
1st Edition
Valentina Balas Vijender Solanki Raghvendra Kumar Manju Khari (Eds.)
Academic Press, Nov 2019
ISBN: 9780128183182
EISBN: 9780128183199
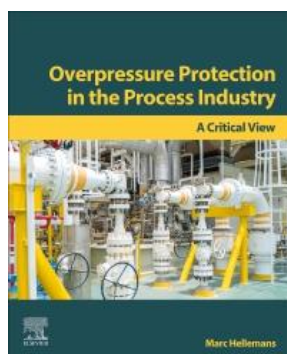
Overpressure Protection in the Process Industry, 1st Edition, A Critical View
Marc Hellemans
Elsevier, Jan 2022
ISBN: 9780323909563
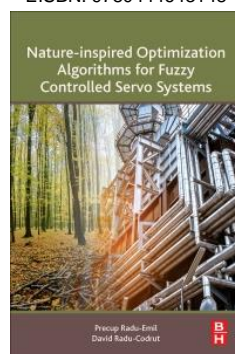
Nature-Inspired Optimization Algorithms for Fuzzy Controlled Servo Systems, 1st Edition
Radu-Emil Precup Radu-Codrut David
Butterworth-Heinemann, Apr 2019
ISBN: 9780128163580
EISBN: 9780128166062
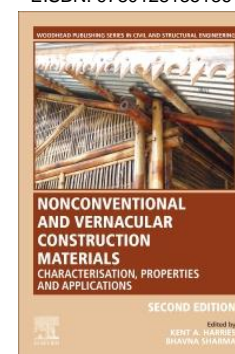
Nonconventional and Vernacular Construction Materials, 2nd Edition, Characterisation, Properties and Applications
Kent Harries Bhavna Sharma (Eds.)
Woodhead Publishing, Nov 2019
ISBN: 9780081027042
EISBN: 9780081027059

Original Research Paper

Role of Clothing Insulation for Thermal Comfort: A Numerical Study using Bio-Heat Transfer Model

[1]Kabita Luitel, [2]Dil Bahadur Gurung, [3]Harihar Khanal and [4]Kedar Nath Uprety

[1]*Department of Mathematics, Bhaktapur Multiple Campus, Nepal*
[2]*Department of Mathematics, Kathmandu University, Kavre, Dhulikhel, Nepal*
[3]*Department of Mathematics, Embry-Riddle Aeronautical University, Daytona Beach, Florida, USA*
[4]*Central Department of Mathematics, Tribhuvan University, Kirtipur, Nepal*

Abstract: Clothing plays a major role in protecting the human body from cold and hot environment by working as an insulator. The physical factors such as conduction, convection, radiation, evaporation and the physiological factors such as blood flow and metabolism within the body together with clothing system help to maintain human thermal comfort and the human thermoregulatory system. On the other hand, body is continuously losing a small amount of heat from the air gap between skin surface and protective clothes. This paper studies the role and effect of the insulations of clothes and air for dry heat loss and the moisture transfer due to air velocity along with walking speed and observes how they work together for temperature distribution in human body. Pennes' bioheat equation is taken as a model and Backward in Time and Central in Space (BTCS) scheme is used for obtaining the solution of the model. Clothing parameters, wind speed and walking speed have been added in the boundary condition in Pennes's model among them the clothing insulation helps prevent the heat loss whereas air velocity escalate heat loss from the body. The numerical results are implemented in Python.

Keywords: Thermal Comfort, Thermoregulatory System, Bioheat Transfer, Clothing and Air Insulation, Air Velocity

Introduction

Human's thermal comfort is not only the state of mind for satisfaction with environmental condition, but also balancing the body's core temperature 37°C (within the range ±0.6°C.) and thermoregulatory system. Body's internal physical and physiological phenomena such as conduction, convection, radiation, sweat evaporation, blood flow and metabolism in addition with the insulation of clothes and air and clothing area factors are the key thermal properties for balancing the uniform body temperature (Hall and Hall, 2020; Özişik *et al*., 2017; Luitel *et al*., 2018). These important components of the heat balance under the transient condition, the thermal energy generated by metabolism or transferred from solar radiation to the body part may go to alter the amount storage inside it.

Thermal comfort is one of the physiological concepts that effects by the human personal and environmental factors. Metabolism and clothes are the personal factors, if they change in little amount, the person's thermal comfort also changes. Radiant temperature, air temperature, long-wave radiation and radiation exchange with environment and short-wave absorption of solar radiation, on the other hand, can be categorized as the environmental factors (Holmér, 1995).

Human body continuously produces heat through metabolism, which is the rate of energy with time, therefore, has unit Watt(W). During the estimation of metabolic heat production rate of a specific activity, the value is generally related to the body volume (Pennes, 1948). So, the unit W/m^3 is used for the metabolic heat generation in the internal body temperature in bioheat transfer equations whereas (Voelker *et al*., 2009; Havenith *et al*., 2002; Holmér, 1995; Oğulata, 2007) used this metabolic heat generation rate in W/m^2 in relation with body surface area. *MET* is sometimes used for metabolic rate where the metabolic rate of seated person is given by:

$$1 MET = 50 kcal / m.h = 58.2 W / m$$

Body temperature may fall or rise according to the changes in external environment, internal physical and physiological parameters. Persons can minimize and keep the temperature balance by engaging themselves in exercise and using the comfort clothes during cold and sweating during hot environment (Havenith, 1999).

The heat exchange between human and surrounding can be written in the heat balance equation per unit body surface area as (Havenith, 1999; Luitel *et al*., 2019; Oğulata, 2007):

$$M - W_e = C + R + E_s + (C_r + E_r) + C_k \qquad (1)$$

Nomenclature

A_b	Surface area of nude body (m^2)
A_{cl}	Surface area of clothed body (m^2)
C	Heat loss through convection (W/m^2)
c	Tissue specific heat ($j/kg°C$)
c_b	Blood specific heat ($j/kg°C$)
C_k	Heat loss through thermal conduction (W/m^2)
c_r	heat loss through respiration (W/m^2)
E_a	Heat loss through evaporation (W/m^2)
E_r	Respiratory evaporative heat loss (W/m^2)
F_{cl}	Clothing efficiency factor (dimensionless)
f_{cl}	Clothing area factor (dimensionless)
h_A	Combined heat transfer coefficient ($W/m^2.°C$)
h_c	Convective heat transfer coefficient ($W/m^2.°C$)
I_a	Insulation of air ($m^2.°C/W$)
I_{cl}	Insulation of clothes ($m^2.°C/W$)
k	Thermal conductivity of body ($W/m.°C$)
q_m	Metabolic heat generation (W/m^3)
r	Radial distance (m)
ρ	Tissue density (W/m^2)
T_a	Arterial temperature($°C$)
T	Tissue (body) temperature ($°C$)
T_∞	Surrounding temperature($°C$)
v_a	Velocity of air (m/s)
v_{air}	Relative air velocity (m/s)
W_b	Relative air velocity (kg/m^3)
W_e	External work (W)
W_s	Walking speed (m/s)

Heat Transfer at the Skin Surface Due to Clothing

The skin releases the amount of latent heat which is caused either by the hot climatic condition or by the high physical exercise and secondly, the human body's evaporation is limited to the surrounding vapor pressure (Voelker *et al*., 2009; Parsons, 1988). Thirdly, fabric structure having different level of porosity, has different amount of entrapped air in the fabric. Tightly woven fabric having less permeability to air prevents heat loss.

Thermal Insulation of Clothes

The thermal resistance and the insulation provided by any layer of trapped air and the insulation value of clothes whose measurement is generally taken in Clo unit. The standard measurement of insulation in ASHARE Standard 55, ISO 7730 and ISO-9920 (Havenith *et al*., 2015) measured the clothing surface area and insulation which is based on the photographic method on the cylindrical limb of manikin. Some of these experimentally finding values of insulation for the non-western ensembles, are used in this study. The thermal resistance and the insulation provided by any layer of trapped air and the insulation value of clothes whose measurement is generally taken in Clo unit.

1 Clo is defined as the insulation of clothing system that requires to a comfortably sitting-resting average male in a normally ventilated room. It is the thermal insulation of overall clothing worn by the person not only the particular garment in 0.1 m/s air velocity at air temperature 21°C and relative humidity less than 50%. Among the total heat produced by metabolic reaction, 24% heat is lost through evaporation and respiration. The limbs of human body with insulation parameters can be seen in Fig. 1.

Clothing Efficiency Factor and the Convective Heat Transfer Coefficient

The ratio of clothed human body surface area A_{cl} and nude body surface area A_b is defined as the clothing area factor. The average body surface area of man is nearly 1.8 m^2. ISO-9920 (Voelker *et al*., 2009; Havenith *et al*., 2015) have calculated this factor f_{cl} as:
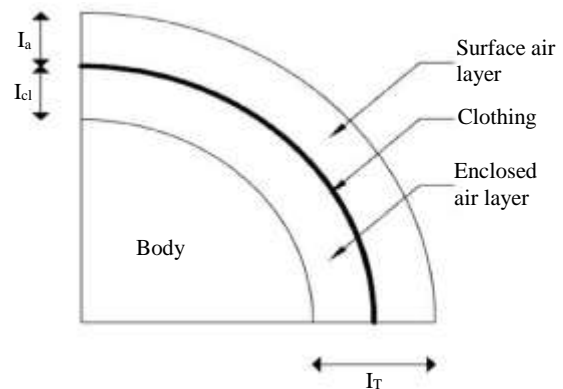
$$f_{cl} = \frac{A_{cl}}{A_b}$$

Fig. 1: Circular limb with clothing and air insulation (Havenith *et al*., 2015)

The equation for this f_{cl} in ISO-9922 is calculated as the function of clothing insulation I_{cl} in Clo value and given by:

$$f_{cl} = 1 + 0.31 I_{cl}$$

As 1 Clo = 0.155 $m^2.°C/W$, the same equation becomes:

$$f_{cl} = 1 + 1.97 I_{cl}$$

ASHARE standard 55 (Havenith *et al.*, 2015) prescribes the clothing efficiency factor without air velocity is given as:

$$F_{cl} = \frac{I_a}{I_T} = \frac{I_a}{I_{cl} + I_a / f_{cl}} \tag{2}$$

The total insulation of clothing and air $I_T = I_{cl} + I_a$ is the sum of surface air layer (insulation of air) I_a, enclosed air layer I_{cl} as shown Fig. 1, the cross-sectional cylindrical limb of clothed human body.

The human comfort system is the balanced condition between the heat produced by the internal metabolism and losing the heat from body by the means of conduction, convection and radiation. The heat transfer coefficient plays a vital role for maintaining this equilibrium position. The combined heat transfer coefficient h_C due to convection h_c and radiation h_r is given by (Havenith *et al.*, 2002):

$$h_C = F_{cl}(h_c + h_r)(T_{sk} - T_\infty) = \frac{T_{cl} - T_\infty}{I_a/f_{cl}} = \frac{T_{sk} - T_\infty}{I_T}$$

The convective heat transfer according to ISO-7933 on the other hand, depends upon the relative air velocity v_{air} and walking speed given as (Oğulata, 2007; Holmér, 1995; Havenith *et al.*, 2002):

$$h_c = 8.7 v_{air}^{0.6} \quad and \quad v_{air} = v_a + W_s$$

and:

$$W_s = 0.0052(M - 58).$$

The convective heat exchange h_C (Oğulata, 2007) in heat balance equation in Equation 1 is determined by:

$$h_C = h_c f_{cl}(T_{cl} - T_\infty)$$

During last few decades various form of the heat transfer model in biological tissue with protective clothes are tackled by various researchers after (Pennes, 1948). Gurung and Saxena (2010) have used the finite element approach to investigate the one-dimensional transient temperature distribution in human dermal parts with protective clothing at low atmospheric temperature. Havenith (1999) has developed the heat balance wearing protective clothing. Further (Havenith *et al.*, 2002; 2015; Holmér, 1995; Van Hoof *et al.*, 2010; Parsons, 1988; Oğulata, 2007) have developed the model for heat and moisture transfer through clothes by considering various environmental factors and insulation properties.

Though many researchers have played a major role for significant turn into the thermal comfort through protective clothing by taking the heat balance equation and focused on the heat transfer only through clothing, there is still lacking for the study of energy and heat balance in internal human body part and clothing as well. It, therefore, led us to initiate the study of bioheat equation together with these types of clothing insulation properties and air velocity and walking speed.

If one understands the thermal behavior of clothing property as well as human thermo physiological behavior, s/he will be able to determine the thermal comfort. So, this study focuses on both thermal properties of human body and the clothing properties such as insulation of clothes and air, clothing area factor which deals with the heat transfer from skin to environment via clothing and maintain the comfort level.

Mathematical Model

The study is being carried out on the cylindrical shape of the human body. So, in this study we imply the cylindrical form of one dimensional transient bioheat equation developed by (Pennes, 1948) incorporating the blood perfusion term in heat equation, is given by:

$$\rho c \frac{\partial T}{\partial t} = k \left[\frac{1}{r} \frac{\partial}{\partial r} \left(r \frac{\partial T}{\partial r} \right) \right] + W_b c_b (T_a - T) + q_m \tag{3}$$

Boundary Conditions

The temperature at the body core of the living tissue is almost constant (approximately 37°C). So, the equation for boundary condition is given as:

$$at \ r = 0, \quad \frac{\partial T}{\partial r} = 0 \tag{4}$$

As skin is covered by the clothes and outside the cloth is exposed to the environment, there is continuous heat flux between the cloth surface and the environment. In this case heat loss from the body to clothes and then clothes to environment is caused by convection, radiation, evaporation and the clothes insulation factors.

The mixed boundary condition with the heat transfer coefficient in terms of clothing insulation and air insulation is given by:

$$at \ r = R, \ -k\frac{\partial T}{\partial r} = h_A\left(T - T_\infty\right) \tag{5}$$

The combined heat transfer coefficient h_A due to convection and radiation along with clothing area factor and clothing insulation properties F_{cl} in Eq. (2) is given by:

$$h_A = F_{cl}\left(h_c + h_r\right) \tag{6}$$

Initial Condition

The initial condition for the transient boundary value problem is given by:

$$T(r,0) = T_0\left(r\right) \tag{7}$$

Solution of the Model

While the analytical method is not feasible with non-homogeneous medium, numerical technique will be a strong tool to handle such type of complex problems. So, we perform the Finite Difference (FD) scheme as the numerical method where one dimensional form of cylindrical tissue is divided into $J + 1$ discrete points uniquely specified by spatial indices, r_j in the radial direction. The discretization of peripheral human limb where the temperature flow in radial direction is shown in Fig. 2.

In the time discretization, we use backward finite difference scheme. The discrete time step size is denoted by Δt and the total time to evaluate the temperature is:

$$t_{max} = n\Delta t.$$

The differential equation is approximately expressed in the system of difference equation in finite difference scheme by using Taylor's series expansion. Central difference schemes are used in the interior of the computational domain, while the special boundary stencils are needed near the boundary to make it as accurate as interior stencils. Writing Eq. 3 by using (BTCS) scheme for $j = 1, 2, \ldots, J\text{-}1$ we get:

$$\rho c \frac{\partial T}{\partial t} = \frac{\rho c}{\Delta t}\left(T_j^{n+1} - T_j^n\right)$$

$$k\left(\frac{\partial^2 T}{\partial r^2}\right) = k\left(\frac{T_{j-1}^{n+1} - 2T_j^{n+1} + T_{j+1}^{n+1}}{\left(\Delta r\right)^2}\right)$$

$$k\frac{1}{r}\left(\frac{\partial T}{\partial r}\right) = \frac{k}{r_j}\left(\frac{T_{j+1}^{n+1} - T_{j-1}^{n+1}}{2\Delta r}\right)$$

After plugging these terms into Eq. 3 with:

$$D = \frac{k}{\rho c}, \lambda = \frac{D\Delta t}{\Delta r^2}, \mu = \frac{D\Delta t}{\Delta r},$$

$$M = \frac{W_b c_b}{\rho c}, S = \frac{q_m}{\rho c} \ and \ F = \Delta t\left(MT_a + S\right)$$

the system converts into the form:

$$\left(-\lambda + \frac{\mu}{2r_j}\right)T_{j-1}^{n+1} + \left(1 + 2\lambda + M\Delta t\right)T_j^{n+1}$$
$$+ \left(-\lambda - \frac{\mu}{2r_j}\right)T_{j+1}^{n+1} - F = T_j^n \ \ with \ j = 1, 2, \cdots, J-1 \tag{8}$$

Equation 8 is Finite Difference (FD) approximation for interior nodes of the Eq. 3.

FD Scheme at Boundary (Body Core) r = 0

The thickness r is me assured from body core towards the skin surface in the cylindrical human body as shown in Fig. 2. At the body core, both r and the heat flux $\frac{\partial T}{\partial r}$, are zero, then $\frac{1}{r}\left(\frac{\partial T}{\partial r}\right)$ approaches to indeterminate form $\frac{0}{0}$ as $r \rightarrow 0$.
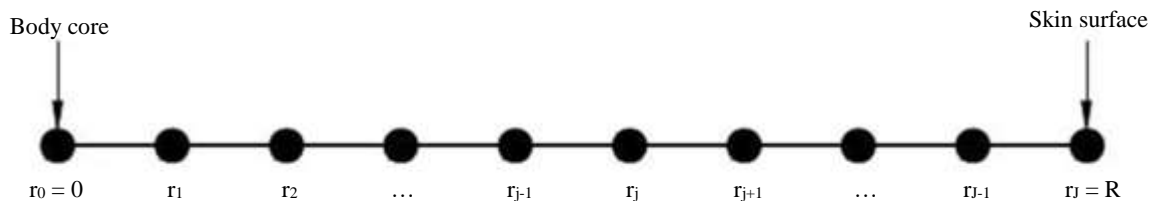

Fig. 2: Discretization in radial direction

The use of L'Hospital rule, then gives:

$$\frac{1}{r}\left(\frac{\partial T}{\partial r}\right)\bigg|_{r=0} = \frac{\left(\frac{\partial}{\partial r}\right)\left(\frac{\partial T}{\partial r}\right)}{\frac{\partial}{\partial r}(r)}\bigg|_{r=0} = \frac{\partial^2 T}{\partial r^2}\bigg|_{r=0}$$

Now Eq. 3 becomes:

$$\frac{\partial T}{\partial r} = \frac{2k}{\rho c}\left(\frac{\partial^2 T}{\partial r^2}\right) + \frac{W_b c_b}{\rho c}\left(T_a - T\right) + \frac{q_m}{\rho c} \quad (9)$$

FD approximation of Eq. 7 at $r = 0$ is:

$$-2\lambda T_{-1}^{n+1} + \left(1 + 4\lambda + M\Delta t\right)T_0^{n+1} - 2\lambda T_1^{n+1} - F = T_0^n \quad (10)$$

The FD scheme for $\frac{\partial T}{\partial r} = 0$ is:

$$T_{-1}^{n+1} = T_1^{n+1} \quad (11)$$

Using Eq. 11 in Eq. 10, we obtain:

$$\left(1 + 4\lambda + M\Delta t\right)T_0^{n+1} - 4\lambda T_1^{n+1} - F = T_0^n \quad (12)$$

FD Scheme at Boundary (Skin Surface) r = J

The central difference approximation of Eq. 5 gives:

$$T_{J+1}^{n+1} = T_{J-1}^{n+1} - \frac{2\Delta r h_A}{k}\left(T_J^{n+1} - T_\infty\right). \quad (13)$$

Then FD approximation at $r = J$ of Eq. 7 is:

$$-2\lambda T_{J-1}^{n+1} + \left[\left(1 + 2\lambda + M\Delta t\right) - \left(-\lambda - \frac{\mu}{2r_J}\right)\frac{2h_A\Delta r}{k}\right]T_J^{n+1}$$
$$+ F_J - F = T_J^n \quad (14)$$

where, $F_J = \frac{2\Delta r B_J}{k}\left(h_A T_\infty\right).$

Writing the Eq. 12, 8 and 14 in the matrix equation form:

$$AT^{n+1} = T^n + B, \quad (15)$$

were, $T^n = \begin{bmatrix} T_0^n & T_1^n & T_2^n & \cdots & T_J^n \end{bmatrix}',$

A is the corresponding tridiagonal matrix of order $(J + 1) \times (J + 1)$, T^{n+1} and B are of column vectors of order $(J + 1) \times 1$.

Results and Discussion

The heat and moisture transfer through clothes for living tissue depends upon the various biological, physiological, environmental as well as clothing properties. In this study the limb of cylindrical human body part is uniformly discretized into the number of small nodes. The heat flow in radial direction occurs from body core towards skin surface.

The role of effective clothing area factor with air insulation can be seen in dry heat transfer and the values of air velocity and walking speed for moisture transfer make changes in temperature of the human body as shown in Fig. 3-7. The values of parameter related to the body part are given in Table 1.

Effect of Clothing Insulation

The effect of clothing insulation and air insulation has been observed at the different time steps. The temperature profile with these effects is also compared with the temperature profile in the nude body. The tissue thickness 0.03 m is taken as the size of space domain. The values of parameters related to internal body parts have been assigned from Table 1. The solution of the system of Eq. 15 with these parametric values and the additional values (Havenith *et al.*, 2002; 2015). Figure 3 illustrates the graphs for the time dependent temperature profiles with clothing insulation I_{cl} and air insulation I_a. The parametric values from Table 1 without additional parameters, on the other, are used to obtain the graph of the temperature variation within the nude body in Fig. 4.

Normally surrounding air is cooler than the body's temperature. So, it flows from body core to outer environment as shown in Fig. 2. The cloth keeps the body warm and comfort by trapping a layer of air between person's skin and the fabric. This warmed up layer in Fig. 3 shows the rate of heat transfer from the body representing the temperature profiles at rest and different time steps. When a person removes clothing from her/his body, s/he starts to feel that the layer of trapped air dissipating and reacting to the cooler air around her/him. The rate of heat transfer from body in this situation is higher than that of clothing case. Except rest ($t = 0$) in both case (Clothed and Naked body), the temperature in skin from the body core with certain radial distance is uniform, i.e., steady state and then in Fig. 3 it goes down towards the skin surface and reaches 35.6°C in 60 sec, 35°C in 120 sec and 34.5°C in 180 sec. The results in this case, are the consequences of the insulation of clothes as well as air insulation.

On the other hand, the temperature at nude skin surface are 29°C in 60 sec, 26°C in 120 sec and 24°C in 180 sec respectively, represented in Fig. 4. Such a result is due to the absence of protective cloth in the body.
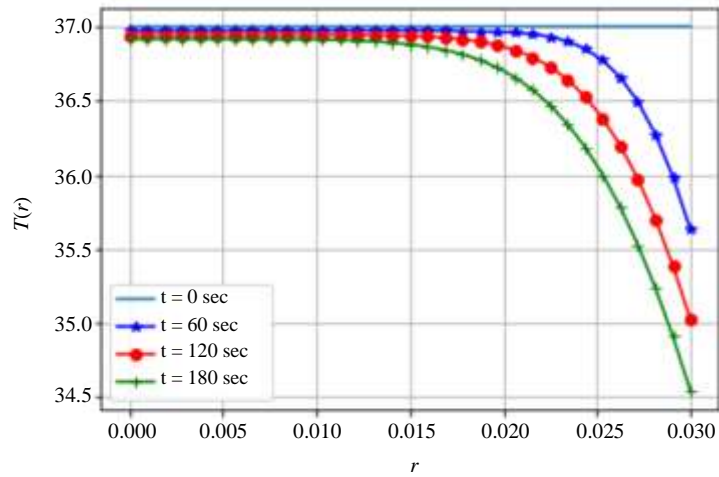
Fig. 3: Variation of skin surface temperature when $I_{cl} = 0.172$ m^2.°C/W, $I_a = 0.0992$ m^2.°C/W, $v_{air} = 0$ m/s and $W_s = 0$ m/s

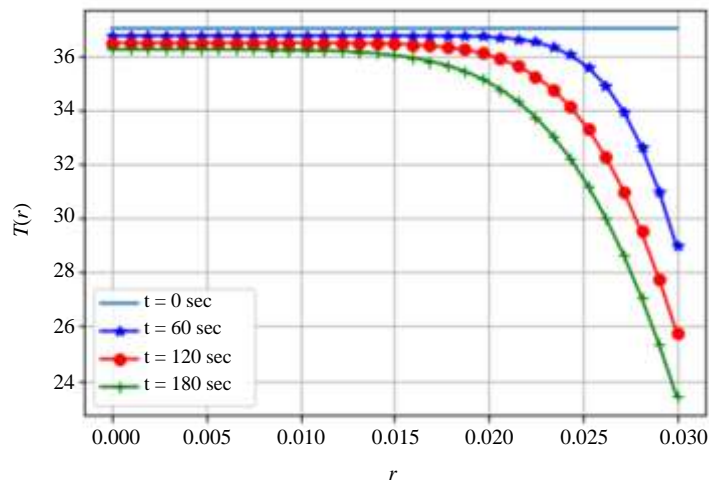**Fig. 4:** Radial temperature profile at nude body
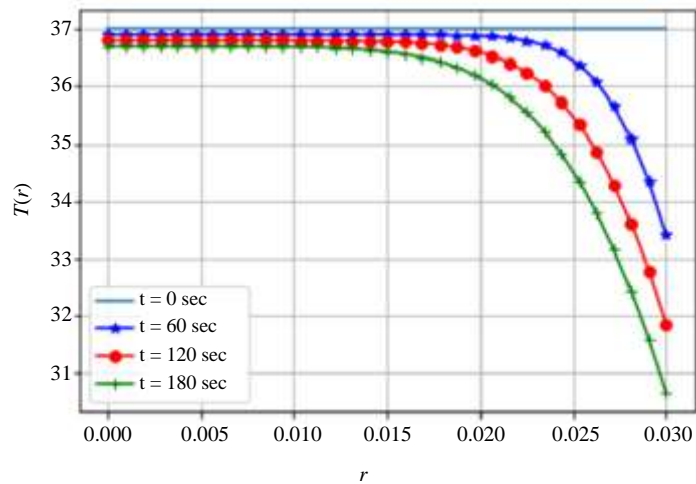
Fig. 5: Variation of skin surface temperature with $I_{cl} = 0.172$ m^2.°C/W, $I_a = 0.0992$ m^2.°C/W, $v_a = 4.1$ m/s and $W_s = 0.42$ m/s
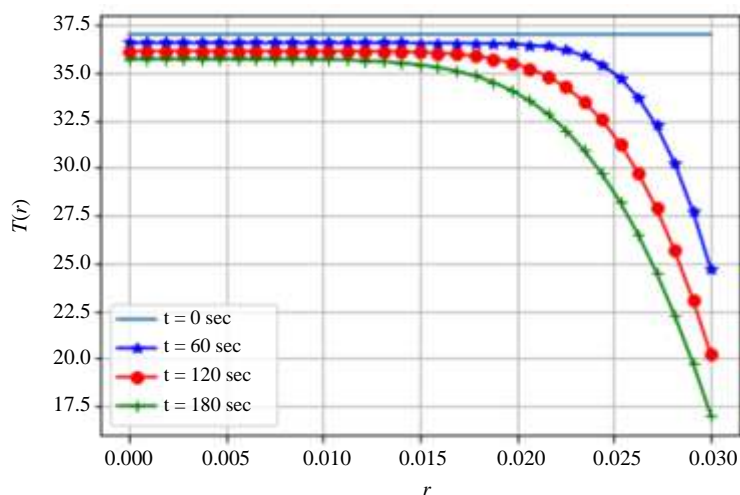
Fig. 6: Variation in temperature with $V_a = 4.1$ m/s and $W_s = 0.42$ m/s, $I_{cl} = 0$ m².°C/W and $I_a = 0$ m².°C/W
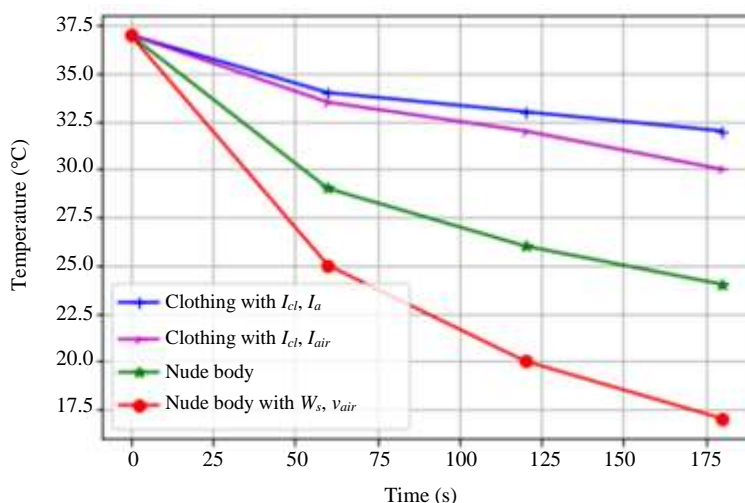

Fig. 7: Temperature profile at skin surface for nude body and clothed body, $R = 0.03$ m

Table 1: The body's internal and surrounding parametric values (Yue *et al*., 2004; Luitel, 2017)

Parameters	Symbols	Values	Units
Thermal conductivities	k	0.48	W/m°C
Blood specific heat	c_b	3850.00	j/Kg°C
Blood density	ρ_b	1000.00	kg/m³
Blood perfusion rate	w_b	3.00	kg/s.m³
Metabolism	q_m	1085.00	W/m³
Arterial temperature	T_a	36.98	°C
Tissue thickness	R	0.03	m
Environmental temperature	T_∞	30.00	°C
Nude body surface area	A_b	1.70	m²

Effect of Air Velocity and Walking Speed

The velocity of wind and person's walking speed have an important role for heat loss from the body. The values have been calculated and assigned from Table 1 along with all additional parametric values related to the air velocity and walking speed and clothing insulation (Havenith *et al*., 2002; Holmér, 1995) to observe the variation of temperature within the body.

The graphs in Fig. 5 stand for the temperature profile at the different time steps starting from 0 sec up to 180 sec. Even though the air velocity and walking

speed occur, there is only small variation in temperature at the skin surface than that of the temperatures in Fig. 3. This outcome is due to still occurrence of clothing insulation. Figure 6 brings out the effects of wind and walking speed while taking the values of parameters from (Havenith *et al.*, 2002; Holmér, 1995), where no insulation of clothing takes place. These significant variations in temperatures in Fig. 6 at skin surface in different time steps are upshot of the relative velocity of air.

Finally, the graphs in Fig. 7 display the significant variation in temperatures at the skin surface with and without clothing parameters at the time steps 0, 60, 120 and 180 sec. From all of these figures, there is no doubt that the clothing insulation helps decrease the rate of heat loss from the body whereas air velocity gives rise to heat loss from the body.

Conclusion

A cylindrical form of one dimensional Pennes' model for heat transfer through protective clothing is implicitly solved by using the finite difference method. The dry heat transfer and moisture transfer are studied in the microclimate region (between naked and clothed skin environment). Dry heat exchange due to thermal insulation of clothes and the air and moisture transfer due to air velocity with walking speed are compared and analyzed at the different time steps. In this study, the mixed boundary condition incorporating convective heat transfer coefficients with clothing parameters for dry heat exchange and air velocity and walking speed for moisture transfer is added in the in the Pennes' bioheat model. The result shows that the presence of cloth makes major difference in the human thermal comfort level. This paper may helpful for the biomedical researchers as well as environmental designers. They can get benefit from the knowledge of microclimate temperature and accordingly they can design workplace and functional clothing so that people can feel comfort for better performance.

Acknowledgement

Author's Contributions

Kabita Luitel: Preparation of initial manuscript with numerical solution of transient temperature profile.

Dil Bahadur Gurung: Contribution in developing the model and solution procedure.

Harihar Khanal: Contribution in developing a program and refining the model.

Kedar Nath Uprety: Contribution in developing and refining the model.

Ethics

There is no any ethical issue regarding to publication of the article. This work is original and has not been submitted and published in any other journal.

References

Gurung, D. B., & Saxena, V. P. (2010). Transient temperature distribution in human dermal part with protective layer at low atmospheric temperature. International Journal of Biomathematics, 3(04), 439-451.

Hall, J. E., & Hall, M. E. (2020). Guyton and Hall textbook of medical physiology e-Book. Elsevier Health Sciences.

Havenith, G. (1999). Heat balance when wearing protective clothing. Annals of occupational Hygiene, 43(5), 289-296.

Havenith, G., Holmér, I., & Parsons, K. (2002). Personal factors in thermal comfort assessment: clothing properties and metabolic heat production. Energy and buildings, 34(6), 581-591.

Havenith, G., Kuklane, K., Fan, J., Hodder, S., Ouzzahra, Y., Lundgren, K., ... & Loveday, D. (2015). A database of static clothing thermal insulation and vapor permeability values of non-Western ensembles for use in ASHRAE standard 55, ISO 7730 and ISO 9920. ASHRAE Trans, 121(1), 197-215.

Holmér, I. (1995). Protective clothing and heat stress. Ergonomics, 38(1), 166-182.

Luitel, K. (2017, December). Mathematical model for temperature distribution in cylindrical human body. In 2017 2nd International Conference on Man and Machine Interfacing (MAMI) (pp. 1-5). IEEE.

Luitel, K., Gurung, D. B., & Uprety, K. N. (2018). Effect of various parameters for temperature distribution in human body: An analytic approach. Advances in Science, Technology and Engineering Systems Journal, Special issue on Recent Advances in Engineering Systems Journal, 3(5), 421-426.

Luitel, K., Khanal, H., & Uprety, K. N. (2019). Numerical Study of Transient Bio-Heat Transfer Model with Heat Transfer Coefficient and Conduction Effect in Cylindrical Living Tissue. The Nepali Mathematical Sciences Report, 36(1-2), 17-26.

Oğulata, R. T. (2007). The effect of thermal insulation of clothing on human thermal comfort. Fibres & Textiles in Eastern Europe, 15(2), 61.

Özişik, M. N., Orlande, H. R., Colaço, M. J., & Cotta, R. M. (2017). Finite difference methods in heat transfer. CRC press.

Parsons, K. C. (1988). Protective clothing: heat exchange and physiological objectives. Ergonomics, 31(7), 991-1007.

Pennes, H. H. (1948). Analysis of tissue and arterial blood temperatures in the resting human forearm. Journal of applied physiology, 1(2), 93-122.

Van Hoof, J., Mazej, M., & Hensen, J. L. (2010). Thermal comfort: research and practice. Frontiers in Bioscience, 15(2), 765-788.

Voelker, C., Hoffmann, S., Kornadt, O., Arens, E., Zhang, H., & Huizenga, C. (2009). Heat and moisture transfer through clothing.

Yue, K., Zhang, X., & Yu, F. (2004). An analytic solution of one-dimensional steady-state Pennes' bioheat transfer equation in cylindrical coordinates. Journal of thermal Science, 13(3), 255-258.

NUMERICAL STUDY OF TRANSIENT BIO-HEAT TRANSFER MODEL WITH HEAT TRANSFER COEFFICIENT AND CONDUCTION EFFECT IN CYLINDRICAL LIVING TISSUE

Article · January 2019

5 authors, including:

Kabita Luitel
Tribhuvan University
3 PUBLICATIONS   **2** CITATIONS

Some of the authors of this publication are also working on these related projects:

Project   Mathematical study of the heat transfer in human body. View project

NUMERICAL STUDY OF TRANSIENT BIO-HEAT TRANSFER MODEL WITH HEAT TRANSFER COEFFICIENT AND CONDUCTION EFFECT IN CYLINDRICAL LIVING TISSUE

KABITA LUITEL [1] , DIL BAHADUR GURUNG[2], HARIHAR KHANAL[3] AND KEDAR NATH UPRETY [4]

[1] *Department of Mathematics, Bhaktapur Multiple Campus, Nepal*
[2] *Department of Mathematics, Kathmandu University, Kavre, Dhulikhel, Nepal*
[3] *Department of Mathematics, Embre-Riddle Aeronautical University, Dayotana Beach, Florida,USA*
[4] *Central Department of Mathematics, Tribhuvan University, Kirtipur, Nepal*

Abstract: The human thermal comfort is affected by the bodys heat exchange mechanism conduction, convection, radiation, and evaporation. The mode of heat transfer between the body and environment depends upon the human internal physiological phenomena, together with the boundary conditions. The present paper provides the comprehensive overview of the thermoregulatory system of human body and studies the numerical solution of unsteady-state one dimensional Pennes bio-heat equation with appropriate boundary conditions. The solution is used to observe the temperature profiles at different thermal conductivities, and different heat transfer coefficients in the living tissue at the various time steps. Various physical and physiological factors across the cylindrical living tissue have been incorporated in the model.

Key Words: Thermoregulatory control, Heat exchange mechanism, Unsteady - state, Cylindrical living Tissue

AMS (MOS) Subject Classification. 92C35 80A20

1. INTRODUCTION

Human body has the complex vascular geometry involving the multiple physical and physiological phenomena such as conduction, convection, radiation, sweat evaporation, blood flow and metabolism. Heat produced by human body may either preserved or transmitted to the environment. When the internal body core temperature is nearly 37^0C, human feels better comfort. So this temperature is considered as the normal temperature which is as the result of heat generation and the heat loss by the body[11]. According to Report of WHO, published in 1969, It is not recommended that body core temperature exceeds 38^0C for a daily exposure to heavy work." The fluctuation in this uniform body temperature so far above and below causes the disturbance in thermoregulatory system. So one should always try to keep balance the body temperature around 37^0C within the range $\pm 0.6^0C$.

.

Thermoregulation is the process controlling the internal body temperature through the hypothalamus heat production and heat loss center. The body also uses other processes like dilating or constricting blood vessels, sweating and shivering.

Metabolism, the major source of heat generation which differs from layer to layer with the highest heat generation in brain almost $13400\,w/m^3$ and in contrast, no heat production in bone $0\,w/m^3$[23]. In this study heat is assumed to be generated uniformly by metabolic and chemical reactions through the cylindrical living tissue. On the other hand, arterial and venous including the small blood vessels located in tissues also play a vital role for heat transfer between blood capillaries, and the tissues. The assumption and calculation made here is based on the Fick's law of perfusion. These important components of the heat balance under the transient condition, the thermal energy generated or transferred to the body part may go to alter the amount storage inside it.

The physical process of several mechanisms such as conduction, convection, sweat evaporation and radiation are the causes for the heat loss from the body. Though convection is the major part for heat loss from the body, in hotter environment heat loss depends more on evaporation. The heat exchange between skin surface and environment is determined by the amount of body area expose to outer environment [4, 20]. Evaluation of these physical and physiological parameters is a major task for the analysis of the heat transfer, and the thermoregulatory control.

Sweating is an essential process to regulate homeostasis in the human body. The brain, and body work within a delicate balance to ensure that the person's temperature is neither too high nor too low. At a constant core temperature, the sweating rate is proportional to the skin temperature and vice versa [20]. The weighted mean value of body, and skin temperature is taken to calculate sweat rate which is given by the valid equation [11].

$$E = \left[8.47 \times 10^-5(0.1 \times T_s + 0.9 \times T_a) - 36.6^0C \right] (kg/m^2.s)$$

where, T_s = skin surface temperature, and T_a = body core temperature.

Since last few decades the study of bioheat transfer problems became emerging area for research. Various models related to the heat transfer in biological tissue using Pennes' bioheat equations are handled by several researchers after the Pennes' model in 1948 [9]. Gurung and Saxena [5], have used the Finite Element Approach to invistigate the one dimensional steady-state temperature distribution in the dermal parts with quadratic shape function. Saxena and Bindra [21] have used Pseudo-Analytical Finite Partition Approach to the temperature distribution problem. In [20], Gurung and Acharya have simulated numerically the sex-related differences in the sensivity of the sweating heat response to change in body temperature. Khandey and Hussian [14] have investigated about the human peripheral tissue temperature during exposure to serve cold stress. They have used explicit formula of finite difference method for simulation. Gurung and Saxena [4] have studied about the transient temperature distribution in human dermal part with protective layer at low atmospheric temperature. Recently Roohi et al. [19] have developed the comprehensive model for the numerical study of space-time fractional bioheat equation. They have used

fractional-order Legendre function in their study.

As human body has the complex vascular distribution pattern embedded inside the tissue, the study of heat transfer in such living biological tissue is really a cumbrous phenomena. Bioheat transfer processes in living tissues are affected by various physical and physiological parameters, surrounding environments, initial and boundary conditions along with temperature-dependent metabolic heat generation [20].

As the body temperature may fall or rise according to the changes in external environment and other above mentioned physical and physiological parameters, one can be minimize and keep the temperature balance by engaging himself in exercise during cold and sweating during hot environment[6]. The heat balance given in the relation is

$$Heat \text{ Store } = \text{ Heat Production - Heat Loss}$$

Here,

$$\text{Heat Production : Metabolic Heat Generation,}$$

and

$$\text{Heat Loss: Conduction + convection + Radiation + Evaporation}$$

$$+ \text{Evaporation + Respiration}$$

Negative heat storage shows the more heat loss than production and in this case body starts cooling whereas positive heat storage shows the metabolic rate is higher than the sum of all heat losses and the body temperature rises.

The transient temperature profiles in the human body may helpful for the medical persons who monitor the temperature fluctuations in the tissue during the hyperthermia treatment against cancer .

The present paper focuses the study of transient solution of one dimensional bioheat transfer model and apply it to estimate the effect of higher and lower thermal conductivities in cylindrical living tissue. The model, Pennes' bioheat equation is solved by using finite difference technique with appropriate boundary conditions at the various time steps. Temperature profiles at various heat transfer coefficients and the metabolic heat generations have also been observed.

2. MODEL FOR HEAT TRANSFER

One dimensional time dependent governing differential equation is used as the basic mathematical model for the heat transfer which is given by

$$(2.1) \qquad \rho c \frac{\partial T}{\partial t} = k \frac{\partial^2 T}{\partial x^2} + W_b c_b (T_a - T) + q_m$$

This bioheat equation (2.1) is suggested by H. Pennes' in 1948. The left hand side is the total heat storage; and the first and second terms of right hand side are, respectively guided by Fick's laws of diffusion and perfusion whereas the third term is the rate of metabolic heat generation.

As the recent paper aims the study of temperature profiles in cylindrical shape of the human body. The cylindrical form of this bio heat equation in radial direction is performed here.

$$(2.2) \qquad \rho c \frac{\partial T}{\partial t} = k \left[\frac{1}{r} \frac{\partial}{\partial r} \left(r \frac{\partial T}{\partial r} \right) \right] + W_b c_b (T_a - T) + q_m$$

Where, ρ: tissue density(kg/m^3), c: tissue specific heat (j/kg^0C)
k: thermal conductivity (w/m^0C), W_b: blood perfusion rate $(kg/m^3.s)$
c_b : tissue specific heat(j/kg^0C), T_a: arterial blood temperature (^0C).
q_m: metabolic heat generation(w/m^3), r: radial distance from centre of core towards skin surface(m)

2.1. **Boundary Conditions:** The inner boundary condition of the living tissue is considered uniform and taken as;

$$(2.3) \qquad \text{at } r = 0, \qquad \frac{\partial T}{\partial r} = 0$$

There is continuous heat flux between the skin surface and atmospheric environment as outer surface of skin is exposed to external environment [17]. In this case heat loss from the body is caused by convection, radiation and evaporation. The Robin boundary condition guided by Newton's law of cooling is given by

$$(2.4) \qquad \text{at } r = R, \qquad -k \frac{\partial T}{\partial r} = h_c (T - T_\infty) + LE$$

Where, h_c: combined heat transfer coefficient due to convection and radiation
L: latent heat, E: sweat evaporation, T_∞: Environmental temperature

2.2. **Initial Condition:** For the time dependent boundary value problem, the initial condition is given by

$$(2.5) \qquad T(r, 0) = T_0(r)$$

3. Finite Difference Scheme for Solution of The Model

One dimensional form of cylindrical tissue is divided into $R+1$ discrete points uniquely specified by spatial indices, $r_i = i \Delta r'$ in the radial direction The discretization of circular cross section of peripheral human limb where the temperature flow in axial direction is uniform as shown in figure 1

In the time discretization, Δt is denoted by the discrete time step size, and the total time to evaluate the temperature is $t^n = n \Delta t$.
In finite difference scheme the differential equation with continuous derivative is approximately expressed in the system of difference equation by using Taylor's series expansion.
Writing equation (2.2) by using implicit finite difference scheme for RHS terms, and forward
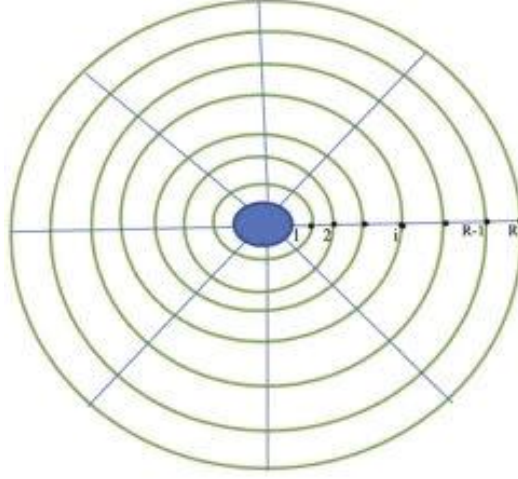
FIGURE 1. Circular cross section of peripheral human limb

difference for the term in left side we get,

$$\frac{\rho c}{\Delta t}\left[T_i^{n+1} - T_i^n\right] = k\left[\frac{T_{i-1}^{n+1} - 2T_i^{n+1} + T_{i+1}^{n+1}}{(\Delta r)^2}\right] + \frac{k}{r_i}\left[\frac{T_{i+1}^{n+1} - T_{i-1}^{n+1}}{2\Delta r}\right]$$

(3.1)
$$+ W_b c_b\left(T_a - T_i^{n+1}\right) + q_m \qquad i = 1, 2\cdots, R-1$$

For $D = \dfrac{k}{\rho c}, \lambda = \dfrac{D\Delta t}{\Delta r^2}, \mu = \dfrac{D\Delta t}{\Delta r,} M = \dfrac{W_b c_b}{\rho c}, S = \dfrac{q_m}{\rho c}, F = \Delta t\left(MT_a + S\right)$

we have,

$$\left(-\lambda + \frac{\mu}{2r_i}\right)T_{i-1}^{n+1} + (1 + 2\lambda + M)T_i^{n+1} + \left(-\lambda - \frac{\mu}{2r_i}\right)T_{i+1}^{n+1} - F = T_i^n$$

(3.2)
$$D_i T_{i-1}^{n+1} + E_i T_i^{n+1} + B_i T_{i+1}^{n+1} - F = T_i^n$$

with $i = 1, 2\cdots, R-1$

where, $E_i = (1 + 2\lambda + M), D_i = (-\lambda + \dfrac{\mu}{2r_i})$ and $B_i = (-\lambda - \dfrac{\mu}{2r_i})$

for, $i = 1, 2, \ldots, R$

The equation (3.2) is Finite difference scheme for interior nodes of the equation (2.2).

3.1. **FD Scheme at Boundary** $r = 0$**:** The cylindrical thickness r is measured from body core as shown in figure 2. At the body core, both r and the heat flux $\frac{\partial T}{\partial r}$, are zero, then $\frac{1}{r}(\frac{\partial T}{\partial r})$ approaches to indeterminate form $\frac{0}{0}$ as r $\to$ 0.
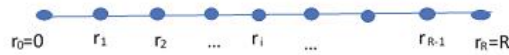

FIGURE 2. Discretization in radial direction

The use of L'Hospital rule, then gives

$$\frac{1}{r}\frac{\partial T}{\partial r}\Big|_{r=0} = \frac{(\frac{\partial}{\partial r})(\frac{\partial T}{\partial r})}{\frac{\partial}{\partial r}(r)} = \frac{\partial^2 T}{\partial r^2}\Big|_{r=0}$$

Now equation (2.2) becomes,

$$\text{(3.3)} \qquad \frac{\partial T}{\partial t} = \frac{2k}{\rho c}\left(\frac{\partial^2 T}{\partial r^2}\right) + \frac{W_b c_b}{\rho c}(T_a - T) + \frac{q_m}{\rho c}$$

The finite different scheme of equation (3.3) at $r = 0$ is

$$\text{(3.4)} \qquad -2\lambda T_{-1}^{n+1} + (1 + 4\lambda + M)\,T_0^{n+1} - 2\lambda T_1^{n+1} - F = T_0^n$$

The FD scheme for $\frac{\partial T}{\partial r} = 0$ is

$$\text{(3.5)} \qquad T_{-1}^{n+1} = T_1^{n+1}$$

Using equation (3.5) in equation (3.4), we obtain

$$\text{(3.6)} \qquad E_0 T_0^{n+1} - 4\lambda T_1^{n+1} - F = T_0^n$$

where, $E_0 = (1 + 4\lambda + M)$

3.2. **FD Scheme at Boundary** $r = R$**:** The central difference approximation is,

$$\text{(3.7)} \qquad T_{R+1}^{n+1} = T_{R-1}^{n+1} - \frac{2\Delta r h_c}{k}\left(T_R{}^{n+1} - T_\infty\right) - \frac{2\Delta r LE}{k}$$

Then FD equation at $r = R$ of equation (2.2) is

$$\text{(3.8)} \qquad -2\lambda T_{R-1}^{n+1} + (E_R - 2\Delta r h_c B_R/k)\,T_R^{n+1} + F_R - F = T_R^n$$

where, $F_R = \frac{2\Delta r B_R}{k}\left(h_c T_\infty - LE\right)$

Writing the equations (3.6), (3.2), and (3.8) in the matrix equation form

$$\text{(3.9)} \qquad AT^{n+1} = T^n + B$$

where, $\qquad T^n = \begin{bmatrix} T_0^n & T_1^n & T_2^n & \dots & T_r^n \end{bmatrix}'$

$$A = \begin{bmatrix} E_0 & -4\lambda & 0 & 0 & \dots & & 0 \\ D_1 & E_1 & B_1 & 0 & \dots & & 0 \\ 0 & D_2 & E_2 & B_2 & \dots & & 0 \\ \vdots & \vdots & \vdots & \ddots & \ddots & & \vdots \\ 0 & 0 & \dots & \dots & -2\lambda & \left(E_R - B_R\frac{2h_c\Delta r}{k}\right) \end{bmatrix}$$

$$T^{n+1} = \begin{bmatrix} T_0^{n+1} \\ T_1^{n+1} \\ T_2^{n+1} \\ \vdots \\ T_R^{n+1} \end{bmatrix} \qquad \text{and} \qquad B = \begin{bmatrix} F \\ F \\ F \\ \vdots \\ F \\ F - F_R \end{bmatrix}$$

4. Results and Discussion

The heat transfer model in living tissue depends upon the various biological properties as well as thermophysical parameters. In this study the cylindrical limb is uniformly discretized into the number of nodes in the radial direction where the heat flow is started from the core of the body towards skin surface as already shown in the figure 2.
The effect of various values of heat teansfer coefficients and thermal conductivities are shown in figures 3 and 4 respectively. The graphs in these figures are obtained by using the computer software Python.

4.1. **Effect of Heat Transfer Coefficient:** Temperature profiles in the case of a high and low heat transfer coefficients has been observed at the different time steps. The size of space domain (tissue thickness) R has been taken 0.03 m. In this case, the values of parameters have been assigned as follows [11].

$k = 0.48\,w/m^0C$, $c_b = 1000\,j/kg\,^0C$, $W_b = 3.5\,kg/m^3.s$, $T_a = 37^0C$,
$L = 24 \times 10^5\,j/kg$, $E = 4 \times 10^{-5}\,kg/m^2.s$, and $T_\infty = 22^0C$.

The system of equation (3.9) with these parametric values gives the graphs in figure 3(a), and figure 3(b) for the time dependent temperature profiles when the heat transfer coefficients h_c are $10.023\,w/m^2.^0C$ and $30.23\,w/m^2.^0C$ respectively [11]. The nude human body
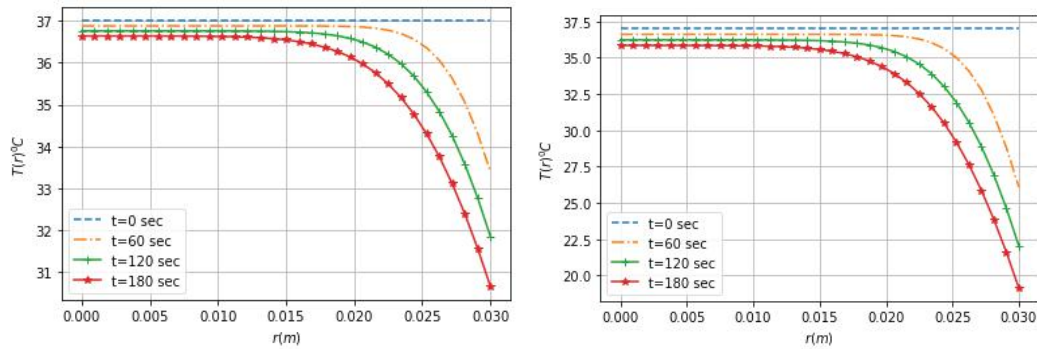
FIGURE 3. Radial Temperature profile at(a) $h_c = 10.023\,w/m^2.^0C$ (b) $h_c = 30.023\,w/m^2.^0C$

surface is directly affected by the outer environmental condition where the convection and radiation heat transfer coefficient appears. Figure 3(a) represents the temperature profiles at rest, 60, 120, and 180 seconds. Except rest (t = 0) the temperature in skin from the body core with certain radial distance is uniform, i.e. steady state and then it goes down slowly towards the skin surface. The temperature at skin surface is 33.5^0C in 60 second, 32^0C in 120 second, and 29^0C in 180 second. On the other hand, in figure 3(b), the temperature in the skin from body core from the core of body towards the skin surface slows sharply down. In 60 second, the temperature reaches 26^0C, in 120 second 22^0C, and in 180 second it reaches to 18^0C. This is due to higher heat transfer coefficient. Thus higher heat transfer coefficient has more capacity to reduce the body surface temperature than that of the lower heat transfer coefficient.

4.2. **Effect of Thermal Conductivities:** Heat loss through the lower and higher thermal conductivities have been calculated by assigning the following parametric values [11].

$h_c = 20.023 \, w/m^2.^0C$, $T_\infty = 22^0C$, $c_b = 1000 \, j/kg^0C$, $W_b = 3.5 \, kg/s.m^3$,
$T_a = 37^0C$, $L = 24 \times 10^5 \, j/kg$, and $E = 4 \times 10^{-5} \, kg/m^2.s$,

The system of equation (3.9) gives the graph in figure 4(a) and figure 4(b) for time dependent temperature profiles at the values of thermal conductivities k are $0.24 \, w/m^0C$ and $0.72 \, w/m^0C$ respectively [11].

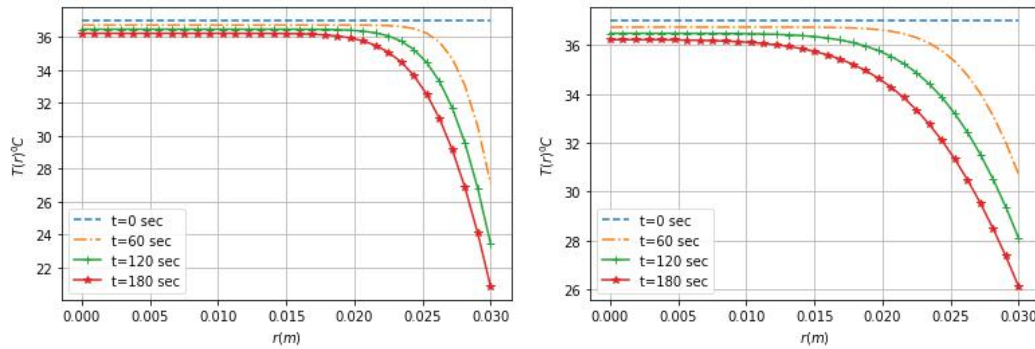From Figure 4(a), we observe that except rest, the temperature in the skin from body

FIGURE 4. Radial Temperature profile at (a) $k = 0.24 \, w/m.^0C$ (b)$k = 0.72 \, w/m.^0C$

core upto certain radial distance is uniform as in the case of heat transfer coefficients, i.e. steady state. After then the temperature decreases rapidly towards the skin surface and the temperature at skin surface is 27^0C in 60 second, 23^0C in 120 second, and 21^0C in 180 second. On the other hand, in figure 4(b), it is found that the temperature profile in the skin from the body core towards the skin surface decreases smoothly down. In 60 second, the temperature reaches 31^0C, in 120 second 28^0C, and in 180 second it reaches up to 26^0C. Thus higher thermal conductivities causes to rise in the skin surface temperature than the lower thermal conductivity.

5. CONCLUSION

A time dependent bioheat transfer model is solved using the implicit finite difference method for analyzing the heat transfer coefficient and conduction effect in the cylindrical shape of human body. The result shows that the temperature at the skin surface decreases significantly on the increase of heat transfer coefficient in the different time steps. While increasing in thermal conductivity the temperature on the skin surface increases. On one hand the graphs show the role of convection and conduction for heat loss from skin surface, on the other hand, this paper provides the knowledge of prevention of physiological disturbance due to several phenomena and the important and comprehensive overview of the thermoregulatory system of human body. There is inverse relation in time and temperature if $T_\infty < 37^0C$. This paper is bound to be helpful for those who involve themselves

in the medical field, such as hyperthermia treatment against cancer and the biomedical researcher for further investigation in thermal disturbance. This paper can be extended in annular, and axial direction by incorporating the clothing effect in thermoregulatory system.

Acknowledgment

REFERENCES

[1] ANSI/ASHRAE Standard 55-2017, Thermal Environmental Condition for Human Occupacy.

[2] Babita Kumari and Neeru Adlakha, Two Dimensional Finite Difference Model to Study Temperature Distribution in SST Region of Human Limbs Immediately after Physical Exercise in Cold Environment, *International Journal of Computational Materials Science and Enginnering*, Vol.4 N0. 1, pp 1550002-15500012, 2015.

[3] C. Guyton and E.Hall, A Textbook of Medical Physiology, *Elesvier*, 2016.

[4] D.B. Gurung, V.P. Saxena, Transient Temperature Distribution in Human Dermal Part with Protective Layer at Low Atmospheric Temperature, *International Journal of Biomathematics*, Vol.3, No. 4, pp 439- 451, 2010.

[5] D.B. Gurung, V.P Saxena, and P.R Adhikari, Finite Element approach to The one-dimensional Steady-state Temperature Distribution in the Dermal parts with Quadratic Shape Function, *J.Appl. Math and information*, Vol. 27, pp 301 - 313, 2009.

[6] George Havenith, Heat Balance Wearing Protective Clothing, *J Ann. Occup. Hyg.*, Vol. 43, NO. 5, pp 289-296, 1999.

[7] Gokul K. C., D. B. Gurung, Mathematical Model: Thermal Effects of Two Wheeler Rider's Speed in His/Her Eye, *Journal of Mathematical Sciences and Modelling*, Vol. 121, No. 31 pp 143 - 154, 2019.

[8] H. Arkin., Lx Xu, and K.R Holms, Recent Developments in Modeling, Heat transfer in blood Perfused Tissue, IEEE Transactions on Biomedical Engineering, 41, 97 - 107, 1994. *IEEE Transactions on Biomedical Engineering*, Vol. 29, pp 285-310, 1983.

[9] H.H. Pennes, Analysis of Tissue and Arterial Blood Temperatures in Resting human forearm, *Journal of Applied Physiol*, Vol. 1, pp 93 - 122, 1948.

[10] https://www.biology-online.org.

[11] Kabita Luitel, Dil Bahadur Gurung and Kedar Nath Uprety, Effect of Various Parameters for Temperature Distribution in Human Body: An Analytical Approach, *Special Issue on Recent Advances in Engineering System Journal www.astesj.com*, Vol. 3, No. 5, pp 421 -426, 2018.

[12] Kabita Luitel, "Mathematical Model for Temperature Distribution in Cylindrical Human Body" *IEEE 2017, 2nd International Conference on Man and Machine Interfacing (MAMI), IEEE*, pp 1-5 2017.

[13] Li- Na Zhai, Jan Li, Prediction Methods of skin Burn for Performance evaluation of Thermal Protective clothing, *www.Science direct.com, www.elesvier.com/locate/burns.*, http:/dx.doi.org/10.1016/j.burns.2015.02.019.

[14] M. A. Khandey, Fida Hussian, Explicit Formula of Finite Difference Method to Estimate Human Peripheral Tissue Temperature During Exposure to Serve Cold Stress,*Journal of Thermal Biology*,Vol. 48, pp 51 - 55, 2015.

[15] Mamta Agrawal, Neeru Adlakha and Kamalraj Pardasani, Seminumerical Model to Study Temperature Distribution in Peripheral Layers of Elliptical and Tapered Shaped Human Limbs, *Journal of Mechanics in Medicine and Biology*, Vol. 10, N0. 01, pp 57 - 72, 2010.

[16] Malgorzata A. Jankowska and Grazyna Sypniewska-Kaminska, An Interval Finite Difference Method for The Bioheat Transfer Problem Described by The Pennes Equation with Uncertain Parameters, *Mechanics and Control* Vol. 31 No. 2 , 2012, Doi: http://dx.doi.0rg/10.7494/mech.2012.31.2.77

[17] Mir Ajir and Javid Gani Dar, Mathematical Analysis of Bioheat Equation for the Study of Thermal Stress on Human Brain, *Applied Mathematics and Information Sciences Letters, An International Journal*, Vol. 5 No.1, pp 33-39, 2017. http://dx.doi.0rg/10.18576/amisl/050106

[18] Randall J. Leveque, Finite Difference Methods for Ordinary and Partial Differencial Equation, *Siam Society for Industrial and Applied Mathematics*, Philadelpha, 2007.

[19] R. Roohi, M.H. Heydari, M.Aslami, and M. R. Mahmoudi, A Comprehensive Numerical Study of Space-Time Fractional Bioheat Equation Using Fractional -Order Legendre Functions, *The European physical Journal PLus,* Doi: 10.1140/epjp/i2018-12204-x,

[20] Saraswati Acharya, D.B. Gurung, V. P. Saxena, Mathematical Modeling of Sex-Related Differences in the Sensitivity of the Sweating Heat Responses to Change in Body Temperature, *British Journal of Mathematics and Computer Science, www.sciencedomain.or.com*, Vol. 12 No. 4, 1 -11, 2016.

[21] V.P Saxena and J.S. Bindra, Psudo-Analytic Finite Partition Approach to Temperature Distribution Problem in Human Limbs, Vol. 12, No. 2, pp 403 - 408, 1989.

[22] Yas Kuno, The physiology of Human Perspiration, *J.and A. Churchil LtI*, Vol. 40, Glucester Place Portman Square, London, 1934.

[23] Yidirim, Eda Diden, A Mathematical Model of The Himan Thermal System, *Master Degree Thesis*, 2005.

ASTES

Effect of Various Parameters for Temperature Distribution in Human Body: An Analytic Approach

Kabita Luitel[*,2], Dil Bahadur Gurung[1], Kedar Nath Uprety[2]

[1]*Department of Mathematics, School of Science, Kathmandu University, 45210, Nepal*

[2]*Central Department of Mathematics, Tribhuvan University, 44618, Nepal*

A R T I C L E I N F O	A B S T R A C T
	This paper is the extension of the work originally presented in 2nd International Conference on Man and Machine Interfacing (MAMI 2017) and the paper of Yue et al. The present study aims at observing the effect of various parameters on temperature distribution profiles at various environmental temperature, tissue thermal conductivities, metabolic rates, blood perfusion rates, and heat transfer coefficients. The analytic solution of Pennes' bioheat equation in the steady-state case is obtained by using the Modified Bessel's equation incorporating the effect of sweating and non-sweating state of the body. From the study, it was observed that the variation of atmospheric temperature and heat transfer coefficients have a significant effect for the temperature distribution in the body towards the skin surface.

1. Introduction

Heat transfer plays a very important role in the living system. This is the complex process, which includes not only some physical factors—conduction, convection, radiation, evaporation but also the physiological factors—blood flow and metabolism. These physical and physiological factors help maintain the constant human body temperature around 37^0C which is the equilibrium point of the production of heat and loss of heat by the body. The extreme temperatures from the normal body temperature influence the function of biological tissue and the whole system of the body. Death may occur if the body temperature is 27^0C and below and if 42^0C and above. So we should maintain the body temperature around 37^0C. The heat transfer in the blood vessel also helps to maintain uniform body core temperature regardless of changes in environmental temperature. Metabolism, another important source of heat gain is the chemical process that occurs in the living organism to grow and produce, maintain their structure, and respond to their respective environment [1, 2, 3].

Sweat evaporation is one of the effective parameters in the thermoregulatory process, which is the only way to lose heat when the ambient temperature is higher than the normal body (36.1^0C - 37.2^0C) temperature. Due to the sweat evaporation, 22% of heat losses from the body. Evaporative heat exchange also involves the loss of heat through the evaporation of sweat from the skin surface. We generally calculate the rate of sweat evaporation as the weighted mean value of the body core and skin temperature. The reasonable equation for the sweat rate is [4, 5].

$$E = 8.47 \times 10^{-5}\{(0.1 \times T_{sk} + 0.9 \times T_b) - 36.6°C\}Kg/m^2/sec$$

Where $T_{sk} = $ skin surface temperature

and $T_a = 37°C$ (body core temperature)

It has been proved that the transfer of latent heat from the living being to its environment is often estimated by multiplying the loss in weight attributable to evaporation by the latent heat vaporization of water 'L' which decreases from 2501J/g at 0^0C to 2406 J/g at 40^0C[6]. Havenith et al.[7] however, have mentioned the values for 'L' ranging from 2,398 J/g to 2,595J/ g. and finally suggested the latent heat of evaporation is only dependent on temperature giving a number of 2,430J/g at 30^0C.

Acharya et al. [5] used variational finite element (FEM) method to prepare one dimensional heat transfer model for the comparative study of temperature profiles of human male and

*Corresponding author: Kabita Luitel, Department of Mathematics, Bhaktapur Multiple Campus, TU, Nepal, E-mail: kabi123luitel@gmail.com

temperature profiles of female luteal and follicular phases of the menstrual cycle.

Havenith et al. [7] studied experimentally by using thermal manikin to determine the effective cooling power of moisture evaporation. They measured both heat loss and mass loss independently by allowing a direct calculation of an effective latent heat of evaporation.

The knowledge of heat transfer is equally important in the field of biomedical research as well as in the treatment of cancer, now a great threat to the existence of humanity. Bioheat transfer models have therapeutic and clinical importance. These models are helpful for the more effective treatment of cancer than it is now. As per Arkin et al., the effect of hyperthermia treatment depends on the temperature and duration of heating. If a constant temperature could be maintained, the duration of heating would be a reasonable way of expressing thermal dose [8].

Over a hundred years' time, the effects of the blood flow have been examined on the heat transfer of living tissue. After Bernard came up with an experimental study in 1876, physicians, physiologists, and engineers are interested in the mathematical modeling of the complex thermal interaction between the vascular systems of the body.

In 1948 pennes' H.H. [9] proposed the simple linear mathematical model based on experimental observation for describing heat flow within the tissue. Many other researchers, one after another, have developed alternative models for describing the perfusion rate and difference between the arterial blood temperature and the local tissue temperature. But Pennes' model still has an acceptable result to predict the transient temperature due to its simplicity and flexibility [1].

Previous researchers such as Acharya et al. [5], Khandey and Saxena [10], Gurung and Saxena [11], Aijar and Dar [12], Nadel [13] observed the effect of latent heat of sweat evaporation for temperature variation in the human body only by using numerical (Specially FEM) techniques. Numerical methods give the approximation result whereas if the analytic solutions of these equations are attainable, they will give the exact result. Even though the analytical method was used by Yue et al.[2] to solve the model, but this model has not incorporated the effect of Latent heat and sweat evaporation. The analytical approach for the study of such problems is still lacking. So the present study focuses on a mathematical model of the body temperature based on the Pennes' bioheat equation due to the sweat evaporation. The temperature at various physical and physiological conditions in the sweating case in comparison with the non-sweating case will be observed in the study

2. Mathematical Model

The governing differential equation used in the model is given by [9].

$$\rho c \frac{\partial T}{\partial t} = \nabla \cdot (K \nabla T) + M(T_a - T) + S \qquad (1)$$

Where, ρ = density of tissue (kg/m^3), c = specific heat (J/Kg. ^{0}C), K = thermal conductivity (W/m^{0}C), ρ_b = density of blood (Kg/m^3), w_b = blood perfusion rate per unit volume (m^3/s.m^3), c_b = blood specific heat (J/kg.^{0}C), M = $\rho_b w_b c_b$ (W/m^3.^{0}C), S = metabolic

heat generation (W/m^3), T_a = temperature of arterial blood (^{0}C), T = tissue temperature (^{0}C).

2.1. Boundary Conditions

Heat loss takes place from the surface of the human body due to convection, radiation, and evaporation because the human body surface is exposed to the environment. So the boundary conditions used in this study is given by

$$R = 0, \qquad \frac{dT}{dr} = 0 \qquad (2)$$

$$R = r, \qquad -K\frac{dT}{dr} = h_C(T - T_\infty) + LE \qquad (3)$$

Where R is the radius of concerned tissue (m), h_C is the coefficient of heat transfer on the surface of the tissue (W/m^2.^{0}C), T_∞ is atmospheric temperature (^{0}C), L is the latent heat (J/Kg) and E denotes the evaporation rate (Kg /m^2.sec).

3. Analytic Solution

Being human body cylinder in shape, equation (1) has been converted into the cylindrical form. The one dimensional steady–state equation in the radial direction is expressed as,

$$\frac{1}{r}\frac{d}{dr}\left(r\frac{dT}{dr}\right) + \frac{M}{K}(T_a - T) + \frac{S}{K} = 0 \qquad (4)$$

To perform the non-dimensionalization of (4) with boundary conditions (2) and (3), we introduce the following characteristic quantities and dimensionless parameters,

$$\tilde{r} = \frac{r}{R}, \text{ and } \tilde{T} = \frac{T - T_\infty}{T_a - T_\infty}, \qquad (5)$$

$$\widetilde{M} = \frac{MR^2}{K}, \tilde{S} = \frac{SR^2}{K(T_a - T_\infty)}, \qquad (6a)$$

$$\widetilde{h_C} = \frac{h_C R}{K}, \qquad \widetilde{N} = \frac{LER}{K(T_a - T_\infty)} \qquad (6b)$$

Differentiating **(5)** with respect to 'r' then, substituting in (4) we get

$$\frac{1}{\tilde{r}}\frac{d}{d\tilde{r}}\left(\tilde{r}\frac{d\tilde{T}}{d\tilde{r}}\right) + \frac{R^2 M(1 - \tilde{T})}{K} + \frac{SR^2}{K(T_a - T_\infty)} = 0 \qquad (7)$$

With the use of **(6a)** and **(6b)**, **(7)** reduces after calculating to

$$\frac{1}{\tilde{r}}\frac{d}{d\tilde{r}}\left(\tilde{r}\frac{d\tilde{T}}{d\tilde{r}}\right) - \widetilde{M}\tilde{T} + \left(\widetilde{M} + \widetilde{N}\right) = 0 \qquad (8)$$

For computational simplicity, again we put

$$\boldsymbol{M} + \boldsymbol{N} = \mathrm{U}$$

$$\widetilde{\boldsymbol{M}} = \mathrm{V}$$

$$\emptyset = \mathrm{U} - \mathrm{V}T$$

And get the **(9)** as follows

$$\tilde{r}^2 \frac{d^2\emptyset}{d\tilde{r}^2} + \tilde{r}\frac{d\emptyset}{d\tilde{r}} - V\tilde{r}^2\emptyset = 0 \qquad (9)$$

This equation is the Modified Bessel's equation of zero order and comparing it with Modified Bessel equation

$$\begin{bmatrix} x^2 \frac{d^2y}{dx^2} + x \frac{dy}{dx} - (\beta^2 x^2 + p^2)y = 0 \\ Whose\ solution\ is\ given\ by \\ y = AI_p(\beta x) + BK_p(\beta x) \end{bmatrix}$$

The solution of equation (9) for $\emptyset$ can be written as

$$\emptyset = c_1 I_0(\sqrt{V}\tilde{r}) + c_2 K_0(\sqrt{V}\tilde{r})$$

Where c_1 and c_2 are arbitrary constants.

After differentiating $\emptyset$ with respect to $\tilde{r}$, calculating and substituting the corresponding values with boundary conditions, the solution for $\tilde{T}$ and then the solution for T can be written as in (10) and (11).

$$\tilde{T} = \frac{U}{V} - \frac{1}{V}\left[\left\{\frac{\widetilde{h_c}U + \widetilde{N}V)I_0(\sqrt{V}\tilde{r})}{\widetilde{h_c}I_0(\sqrt{V}\tilde{r}) + \sqrt{V}I_1(\sqrt{V}\tilde{r})}\right\}\right] \qquad (10)$$

$$T = T_\infty + (T_a - T_\infty)\left[\frac{U}{V} - \frac{1}{V}\left\{\frac{(\widetilde{h_c}U + V\widetilde{N})I_0((\sqrt{V}\tilde{r}))}{\widetilde{h_c}I_0(\sqrt{V}\tilde{r}) + \sqrt{V}I_1(\sqrt{V}\tilde{r})}\right\}\right] \qquad (11)$$

Table 1: Thermo-physical parameters [1, 14]

Parameters	Symbols	Values	Unit
Thermal conductivity	K	0.48	W/m^{0}C
Blood specific heat	c_b	3850	J/Kg^{0}C
Blood density	ρ_b	1000	Kg/m^3
Perfusion rate	w_b	3	Kg/s.m^3
Metabolism	S	1085	W/m^3
Arterial temperature	T_a	36.98	^{0}C
Tissue thickness	R	0.03	M
Heat transfer coefficient	h_C	10.023	W/m^2.^{0}C
Latent heat	L	2400000	J/Kg
Evaporation rate	E	0.00004	Kg/m^2.sec
Environmental temperature	T_∞	30	^{0}C

The effect at various temperature profiles based on the above parameters values are presented graphically and discussed below.

4. Results and Discussions

The analytical solution of the bioheat equation for the cylindrical body and its respective results of physical properties depends on various factors. So the following values of parameters from table 1 have been used in equation (11) to observe the effect of different atmospheric temperature, thermal conductivities, blood perfusion rates, metabolic heat generation, and heat transfer coefficients.

4.1. Effect of Atmospheric Temperature

The temperature profiles at a various atmospheric temperature below 37^0C (normal body temperature) at $T_\infty = 25^0C$, 28^0C, 31^0C and 34^0C, and above 37^0C at $T_\infty = 38^0C$, 41^0C, 44^0C and 47^0C, are considered and shown respectively in Figures 1(a), 1(b) and 1(c), 1(d).

Although the graphs in both Figures 1(a) and 1(b) show that the body temperature decreases from the core of the body towards the skin surface if the atmospheric temperature is less than the body core temperature, the graphs in Figure 1(b) show that the body temperature decreases more quickly towards the skin surface than in Figure 1(a). This is due to the evaporation effect. On the other hand, if the atmospheric temperature is higher than the body core temperature, the body temperature increases from the core of the body towards the skin surface, which can be seen in Figures 1(c) and 1(d). Moreover, the graphs in Figure 1(d) show that the temperature increases more slowly towards the skin surface than in the graphs in Figure 1(c) due to sweat evaporation, which helps to cool down the body temperature.
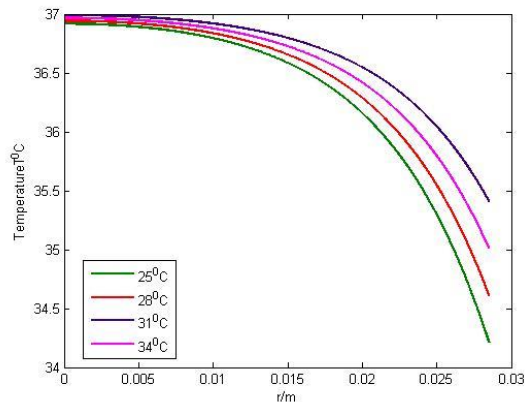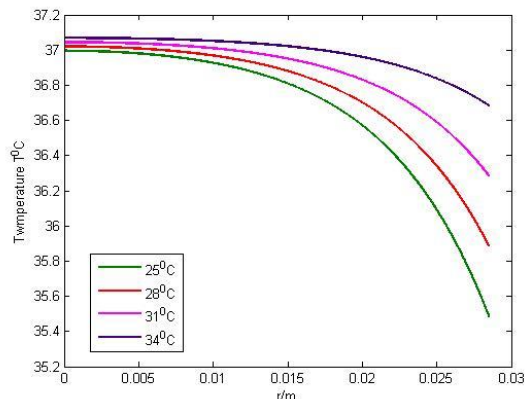

Figure 1(a): Effect of $T_\infty < 37^0$C when $E= 0$

Figure 1(b): Effect of $T_\infty < 37^0$C with LE
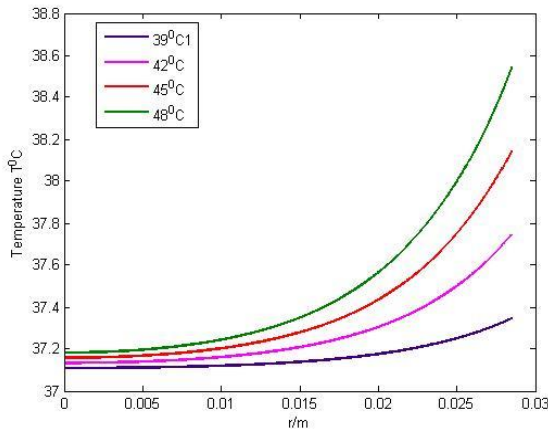
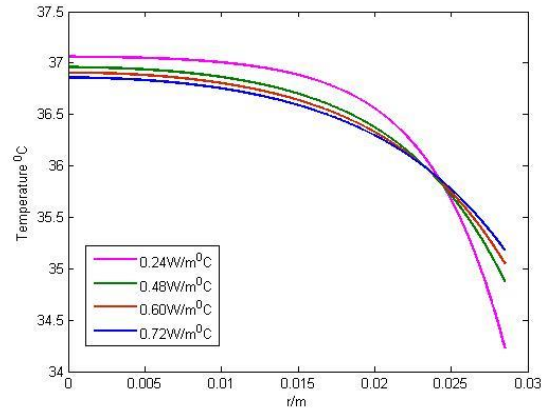Figure 1(c): Effect of $T_\infty > 37^0$C when $E= 0$

Figure 2(b): Effect of thermal Conductivities with *LE*

4.3. Effect of Blood Perfusion

The various values of blood perfusion are taken as w_b = 1.5 Kg/s.m^3, 2 Kg/s.m^3, 2.5 Kg/s.m^3 and 3 Kg/s.m^3 to observe their effect on the temperature of the body. The graphs in Figures 3(a) and 3(b) indicate that the gradient temperature variation in radial direction decreases with the increase of the blood perfusion. Figure 3(b) shows that the temperature falls more sharply towards the surface of the body than in Figure 3(a) because of the evaporation effect together with the blood perfusion.
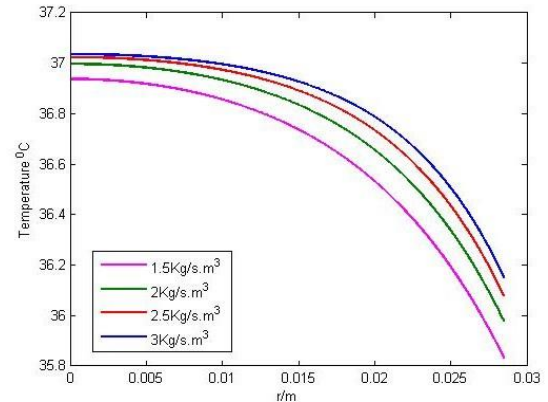

Figure 1(d): Effect of $T_\infty > 37^0$C with *LE*

4.2. Effects of Thermal Conductivities

The temperature profiles at various thermal conductivities K = 0.24W/m^{0}C, 0.48W/m^{0}C, 0.60W/m^{0}C and 0.72W/m^{0}C are shown graphically in Figures 2(a) and 2(b). With the increase in thermal conductivities, the inner part of body temperature increases but the temperature on the body surface decreases sharply as the thermal conductivities increase. It happens due to the conduction process at the body surface.

Figure 3(a): Effect of blood perfusion when $E= 0$

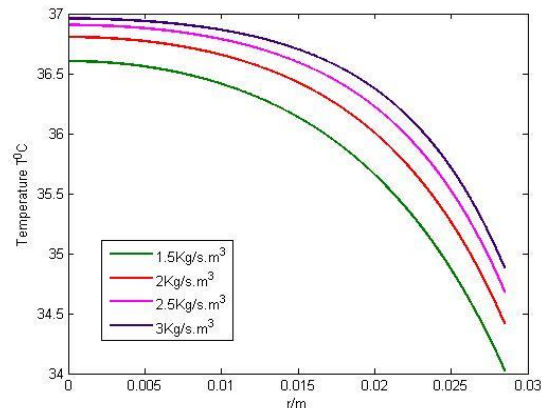Figure 2(a): Effect of thermal Conductivities when $E= 0$

Figure 3(b): Effect of blood perfusion with *LE*

4.4. Effect of Metabolic Heat Generation

The various values of metabolic heat generation q_m = 141.05 W/m³, 271.25 W/m³, 542W/m³ and 1085 W/m³ are taken. Graphs in Figures 4(a) and 4(b) show that the values of metabolic heat generation have a very small effect on temperature distribution in the human body. The change in metabolic heat from 542W/m³ to 1085 W/m³ make the small change in body temperature almost 0.1⁰C whereas its effect on the skin surface is negligible. This happens due to the negligible concentration of blood vessels towards the skin surface. In the case when sweat evaporation is present (Figure 4(b)), the effect of metabolic heat is almost negligible.
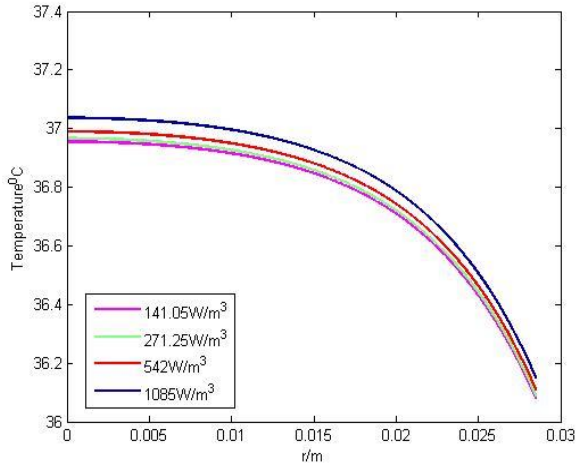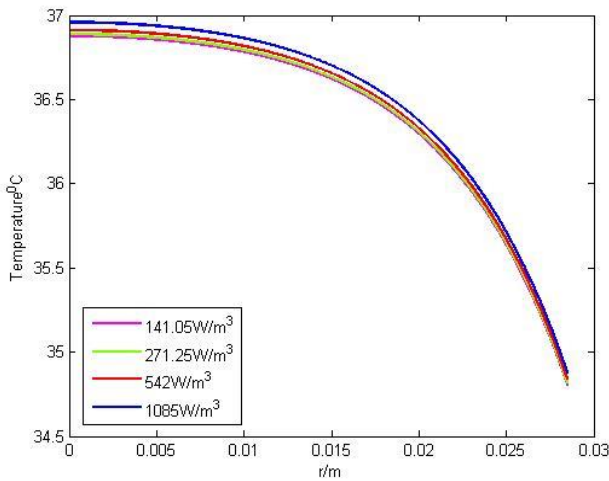

Figure 4(a): Effect of metabolism when *E = 0*

Figure 4(b): Effect of metabolism with *LE*

4.5. Effect of Heat Transfer Coefficients

The various values of heat transfer coefficients are considered at h_C = 5.023 W/m².⁰C, 10.023 W/m².⁰C, 15.023 W/m².⁰C and 20.023 W/m².⁰C. The significant effect of the heat transfer coefficient can be seen in Figures 5(a) and 5(b). The curves in these figures indicate that the gradient temperature in the radial direction decreases with the increase of the heat transfer coefficients.
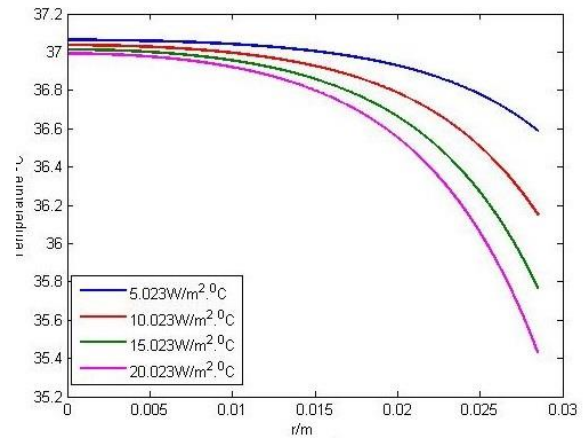

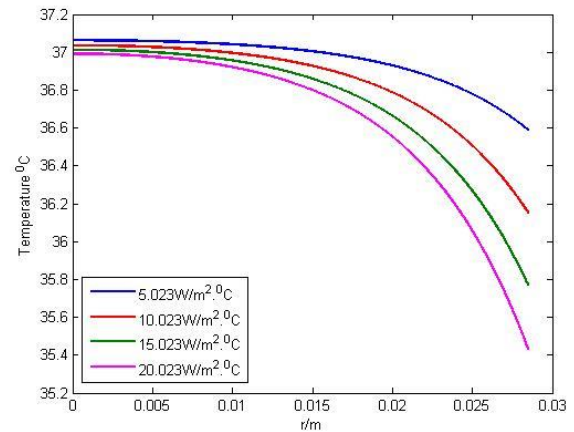Figure 5(a): Effect of h_C when *E= 0*

Figure 5(b): Effect of h_C with *LE*

5. Conclusion

In the present study, the analytical solution of the cylindrical form of Pennes' bioheat equation with boundary conditions including the latent heat of sweat evaporation in the one-dimensional steady-state case is obtained. The effect of the temperature changes in various atmospheric temperature, thermal conductivities, metabolic heat generation rates, blood perfusion rates, and heat exchange coefficients has been observed by using the solution obtained from this model. The study reveals that the atmospheric temperature, blood perfusions, and the heat transfer coefficients have a more significant effect on the temperature variation on the skin surface than in the body core. The gradient temperature in the radial direction decreases with the increase of the ambient temperature, the blood perfusion rates, and the heat transfer coefficients. There is a slight variation in body core temperature even an increase in metabolic heat generation. Its effect on the skin surface is negligible. The various parameters used in this model have certainly a more remarkable effect on the temperature distribution in the human body than the case suggested in [1, 2]. Such a model may be useful for the researcher as well as thermal diagnosis and hyperthermia treatment of cancer. The analytic solution obtained in this paper can also be extended in the axial and angular direction as well as unsteady state case.

Conflict of Interest

The authors make it sure that there is no conflict of interest.

References

[1] Kabita Luitel, "Mathematical Model for Temperature Distribution in Cylindrical Human Body" IEEE 2017, 2nd International Conference on Man and Machine Interfacing (MAMI), IEEE 2017.

[2] Yue Kai Zhang, Fan You Xinxin, An Analytic Solution of One – dimensional Steady – state Pennes Bio-heat.Transfer Equation in Cylindrical Coordinates, Journal of Thermal Science, 13(3),52 - 54, 2004.

[3] Ahmed Lakhssassi, Kengne, and Emmanuel Semmaoui, Modified Pennes' equation modeling bio-heat transfer in living tissues: analytical and numerical analysis, Natural Sciences, B, 1375 - 1385, 2010.

[4] Hoppe PR., Heat Balancing modeling, Institute, and Outpatient Clinic for Occupational Medicine, Experientia. 49:741-746, 1993.

[5] Saraswati Acharya, D.B. Gurung, V. P. Saxena, Mathematical Modeling of Sex-Related Differences in the Sensitivity of the Sweating Heat Responses to Change in Body Temperature, British Journal of Mathematics & Computer Science, 12(4), 1 -11, 2016. www.sciencedomain.or.com

[6] Monteith JL., Latent Heat of Vaporization in Thermal Physiology, Nature New Biology 236: 1996, 1972.

[7] George Havenith, Peter Bröde, Emiel den Hartog, Kalev Kuklane, Ingvar Holmer, Rene M. Rossi, Mark Richards, Brian Farnworth, and Xiaoxin Wang, Evaporative cooling: the effective latent heat of evaporation in relation to evaporation distance from the skin, J Appl Physiol, 114, 778 - 785, 2013. doi:10.1152/japplphysiol.01271.2012.

[8] H Arkin., Lx Xu, and K.R Holms, Recent Developments in Modeling, Heat transfer in blood Perfused Tissue, IEEE Transactions on Biomedical Engineering, 41, 97 - 107, 1994.

[9] H.H. Pennes', Analysis of Tissue and Arterial Blood Temperatures in Resting human forearm, Journal of Applied Physiol, 1, 93 - 1948.

[10] M.A. Khandey and V. P. Saxena, FEM Estimation of One-dimensional Unsteady-State Heat Regulation in Human Head exposed to the Cold Environment, Journal of Biological system, 17, 853 -- 863, 2009.

[11] D.B Gurung, V.P Saxena, and P.R Adhikari, Finite Element approach to The one-dimensional Steady-state Temperature Distribution in the Dermal parts with Quadratic Shape Function, J.Appl. Math and information, 27, 301 - 313, 2009.

[12] Mir Aijar and Javid Gani Dar, Mathematical Analysis of Bioheat Equation for the Study of Thermal Stress on Human Brain, Applied Mathematics & Information Sciences and Letters An International Journal, 1 5(1), 33 - 39, 2017.

[13] ER Nadel, RW Bullard, JAJ Stolwijk. Importance of skin temperature in the regulation of sweating. J. Appl. Physiol., 46, 430 - 437, 1979.

[14] Lalif M. Jiji, Heat Conduction, 3rd Edition Springer, 52 – 54, 2009.

[15] W.J Minkowycz and E.M, Sparrow Advance in Numerical Heat Transfer Printed in the United States of America, (III), 2009.

[16] Kabita Luitel, D.B. Gurung, Mathematical Model for temperature Distribution in Cylindrical Human Body, The Nepali Mathematical Sciences Report, 3, (1&2), 19 - 28, 2012.

[17] Mir Aijar and M. A. Khanday, Temperature Distribution and Thermal Damage of Peripheral Tissue in Human Limbs During Heat Stress, A Mathematical Model, Journal of Mechanics in Medicine and Biology, 16(2), 16500--16517, 2016.

[18] Ying He, A Numerical coupling model to analyze the blood flow temperature and oxygen transport in Human Breast Tumor and laser irradiation, *Japanese Journal of Computers in Biology and Medicine,* (2006), 36, P.1336-1350.

[19] D.B Gurung, Saraswoti Acharya, Five Layered Temperature distribution in Human dermal Part. Nepali Mathematical Sciences Report, Central Department of Mathematics, Tribhuvan University, Kirtipur, Nepal, 2011.

[20] D.B Gurung, Kabita Luitel, Development of Bio-Heat Equation and its Application, Proceedings of Nepal Mathematical Society, 85 - 94, 2012.

[21] Mamata Agrawal, Neeru Adlakha, R.K Pardadsani, Modeling and Simulation of the thermal effect of Metastasis Timors in Human Limbs, International Symposium on Devices MEMS, Intelligent system and communication (ISDMISC), 24 - 29, 2011.

[22] Gokul K C, D.B. Gurung, and P. R. Adhikari, Thermal Effect of the eyelid in human eye temperature model, J. App. Math. & informatics 32(5-6), 649 - 663, 2014.

[23] Luisiana X. Cundin, William P. Roach, Nancy Millenbaugh, Empirical Comparison of Pennes' Bio-Heat Equation, Proc. Of SPINE, 7175, 717516-1 -- 717516-9.